

Electronic Thesis and Dissertation Repository

2-20-2018 3:00 PM

Examining the role of ganglioside homeostasis in neurodegeneration and aging using MALDI imaging mass spectrometry

Sarah Caughlin
The University of Western Ontario

Supervisor
Whitehead, Shawn N.
The University of Western Ontario Co-Supervisor
Cechetto, David F.
The University of Western Ontario

Graduate Program in Anatomy and Cell Biology
A thesis submitted in partial fulfillment of the requirements for the degree in Doctor of Philosophy
© Sarah Caughlin 2018

Follow this and additional works at: <https://ir.lib.uwo.ca/etd>



Part of the [Neurosciences Commons](#)

Recommended Citation

Caughlin, Sarah, "Examining the role of ganglioside homeostasis in neurodegeneration and aging using MALDI imaging mass spectrometry" (2018). *Electronic Thesis and Dissertation Repository*. 5236.
<https://ir.lib.uwo.ca/etd/5236>

This Dissertation/Thesis is brought to you for free and open access by Scholarship@Western. It has been accepted for inclusion in Electronic Thesis and Dissertation Repository by an authorized administrator of Scholarship@Western. For more information, please contact wlsadmin@uwo.ca.

Abstract

Gangliosides are a family of membrane lipids enriched in the central nervous system (CNS) that play an important role in cell signaling processes on the membrane. Alterations in the homeostatic distribution of the a-series family of gangliosides has been observed in both pre-clinical models and human patients with neurodegenerative diseases and injuries, such as Alzheimer's disease (AD) and strokes. Ganglioside dysregulation has been implicated as an important mechanisms driving pathology in the aging brain, yet there is little information on where and when these lipid changes occur as well as the role of dysregulation during neurodegeneration. Matrix-Assisted Laser Desorption/Ionization (MALDI) imaging mass spectrometry (IMS) is a novel imaging technique that can map the distribution of ionizable molecules on a sample in a 2-dimensional format, making it the ideal tool for analyzing gangliosides on post-mortem brain tissue sections. A comorbid rat model of stroke and A β toxicity, using an endothelin-1 (ET-1) induced unilateral striatal stroke together with intracerebralventricular (icv) injections of A β (25-35), was used to examine ganglioside dysregulation in response to neurodegenerative injuries of varying severity. Results indicated that ganglioside dysregulation was correlated with the severity of the neurodegenerative injury and showed a characteristic pattern of depleted protective complex gangliosides with accumulated toxic simple gangliosides at the site of injury. Transgenic (Tg) rats with a mutation in the Alzheimer's precursor protein (APP) demonstrated a similar characteristic shift in ganglioside distribution during aging compared to wild-type (Wt) rats in brain regions which are susceptible to damage in AD, such as the white matter and hippocampus. Finally, chloroquine (CQ), a pharmacological inhibitor of ganglioside catabolism, was used

as a treatment for ganglioside dysregulation after injury in the rat comorbid stroke model. CQ was found to prevent ganglioside dysregulation acutely after stroke and was correlated with reduced pathology and functional impairments. These results support the hypothesis of ganglioside dysregulation as an important mechanism of neurodegeneration in the aging and injured brain and highlights the benefits associated with the restoration of ganglioside homeostasis after stroke injury.

Keywords

Gangliosides, Neurodegeneration, GM3, GM2, GM1, GD1, Lipid homeostasis, Matrix-assisted laser desorption/ionization, MALDI, Imaging mass spectrometry, IMS, Ischemic stroke, Alzheimer's disease, Chloroquine.

Co-Authorship Statement

Chapter 2 of this thesis was published in PLoS One and co-authored by J. Hepburn, D. Park, K. Yeung, D. Cechetto, and S. Whitehead. I performed MALDI IMS experiments, data analysis, wrote and edited the manuscript. J. Hepburn performed surgical procedures on 4 animals used for MALDI IMS and completed all IHC experiments. D. Park performed MALDI IMS on 3 brain sections used for analysis. K. Yeung, D. Cechetto, and S. Whitehead edited the manuscript.

Chapter 3 of this thesis was published in Scientific Reports and co-authored by S. Maheshwari, N. Weishaupt, K. Yeung, D. Cechetto, and S. Whitehead. I performed all experiments with assistance in data analysis from S. Maheshwari and N. Weishaupt. I wrote and edited the manuscript with assistance from S. Whitehead, K. Yeung, and D. Cechetto.

Chapter 4 of this thesis was published in BBA General Subjects. It was co-authored by S. Maheshwari, K. Yeung, D. Cechetto, Y. Agca, C. Agca, K. Jurcic, A. Harris, and S. Whitehead. I completed all experiments with assistance in data analysis from S. Maheshwari. I wrote and edited the manuscript with assistance from K. Yeung, D. Cechetto, and S. Whitehead. Transgenic Fischer rats were provided by Y. Agca and C. Agca. K. Jurcic and A. Harris assisted in the completion of supplemental figure 1 which is provided as appendix iv in this work.

Chapter 5 of this thesis was submitted to Neuroimage for publication and was co-authored by J. Hepburn, L. Wang, K. Yeung, D. Cechetto, and S. Whitehead. I completed all MALDI IMS, *in vitro*, and behavioural experiments. L. Wang extracted and cultured all primary cortical neurons used in *in vitro* experiments. J. Hepburn performed all IHC experiments. I wrote and edited the manuscript with assistance from K. Yeung, D. Cechetto, and S. Whitehead.

Acknowledgments

Firstly, I would like to thank my supervisor Dr. Shawn Whitehead. I will never understand exactly what it was that you saw in me over 5 years ago that made you think I was the right person for this challenging project, but I am grateful to have had the opportunity to learn and grow under your tutelage. Thank you for seeing great potential in me and challenging me to achieve things I never thought possible.

To my co-supervisor Dr. David Cechetto, thank you for being exactly what I needed you to be. You were the unbiased voice of reason among chaos that was always able to set me back on the right path when I felt lost and defeated, for that I am eternally grateful. I would also like to thank Dr. Cechetto's staff on the Rwanda project for their friendship and support over the years, particularly Mrs. Nicole MacLeod for her wonderful sense of humour and kindness.

I am very grateful to Dr. Ken Yeung and the MALDI MS facility manager Mrs. Kristina Jurcic for all of their help and advice over the years, and without whom this work would not have been possible. Thank you for being so patient when explaining various basic analytical chemistry concepts to me and being willing to look at problems from my point of view, you have truly made this interdisciplinary collaboration a very positive experience.

I would like to thank all of the members of the Cechetto/Whitehead and Yeung labs, past and present, for being such amazingly talented and fun individuals to work with. In particular, I would like to thank Hayley, Jen, Jasmine, Mona, Kristina, Alex, Aaron, and Nadia. You all played a much larger role in getting me through grad school than you know and your friendship was, and continues to be a major source of strength for me moving forward.

Thank you to all the students of the Department of Anatomy and Cell Biology for supporting me. I feel honoured to have been a part of our wonderful student council as your representative for two years. I will cherish the memories we shared at social events, council meetings, TAsheps, volunteer activities, and random hall encounters. I feel so fortunate to have been a part of this family. The foundation of this family, of course, being the administrative and support staff I have had the pleasure of working with over the years

(Debbie, Shazia, Glenda, Tom, Micheal, Faye, and Jacqui) and the wonderful Chairs of the Department Dr. Kem Rogers and Dr. Allison Allan. Thank you for giving the students a strong voice in shaping the direction and policies of the Department.

Of course, I cannot finish this section without thanking Dr. Lynn Wang for being the glue that holds everything in the lab together. Your kindness, dedication, competence, and willingness to help anyone with anything goes far beyond the job title of “technician” and I am so fortunate to have had you with me from the very beginning to guide and teach me.

I would also like to thank the members of my advisory committee over the years: Dr. Ken Yeung, Dr. Raj Rajukumar, Dr. Vania Prado, and Dr. Brian Allman for all of their guidance and input on my various projects.

Finally, I would like to thank my family and friends. Parents, thank you for being patient, supportive, and understanding as I invested so much of my time and energy in school. I’m done now, I promise. To my brother Brian, thank you for always being the person I can turn to for help and for having a solution to every conceivable problem, you are the smartest and most caring person I know. To my best friend Meredith Rex, no one keeps me grounded like you do. Thank you for your understanding during the hard times, the home cooked meals, shared drinks, and the many creative distractions. I would like to thank Brad Shrum for asking if I would like to volunteer in the Mele lab so many years ago and setting me on the path that led to the completion of this PhD. Thank you for your patience, encouragement, and friendship over the years, I will always cherish our time together. To my better half, Greg, thank you for being the inspiration for the kind of grad student I wanted to be. Your dedication and passion for science has always pushed me to be my best self. Thanks for all the laughs, drinks, long-distance visits, and adventures, you are my kindred spirit and I certainly would have fallen apart many times without your support.

Table of Contents

Abstract	i
Co-Authorship Statement.....	iiii
Acknowledgments.....	iiv
Table of Contents	vi
List of Figures	xiii
List of Appendices	xv
List of Abbreviations	xvi
Chapter 1	1
1 Introduction.....	1
1.1 Ischemic stroke	1
1.2 Alzheimer’s disease	3
1.3 Comorbidity of AD and Stroke.....	6
1.4 Gangliosides.....	8
1.4.1 Ganglioside Structure.....	9
1.4.2 GM3	14
1.4.3 GM2	17
1.4.4 GM1	18
1.4.5 GD1a.....	20
1.4.6 Gangliosides in neurodevelopment and aging	21
1.4.7 Gangliosides in stroke.....	23
1.4.8 Gangliosides in neurodegenerative diseases: Parkinson’s disease, Huntington’s disease, Prion diseases	25
1.4.9 Gangliosides in neurodegenerative diseases: Alzheimer’s disease	27

1.5 Chloroquine.....	32
1.6 MALDI IMS	34
1.7 Rationale and objectives	37
1.8 References.....	39

Chapter 2 : Increased expression of simple ganglioside species GM2 and GM3 detected by MALDI Imaging mass spectrometry in a combined rat model of A β toxicity and stroke	61
2.1 Abstract.....	61
2.2 Introduction.....	62
2.3 Materials and Methods.....	68
2.3.1 <i>Animals Models</i>	68
2.3.2 <i>Euthanasia</i>	69
2.3.3 <i>Immunohistochemistry</i>	70
2.3.4 <i>Immunofluorescence</i>	70
2.3.5 <i>MALDI Imaging Mass Spectrometry</i>	71
2.3.6 <i>Data Analysis</i>	72
2.4 Results.....	73
2.4.1 <i>Increased GM3 expression within infarcted region of combined Aβ/ET-1 group persists as 21 d</i>	73
2.4.2 <i>GM3 accumulation is associated with increased neurodegeneration and decreased cell survival at 21 d at the site of injury</i>	75
2.4.3 <i>Elevated GM2 at 3 d remains elevated at 21 d only in combined Aβ/ET-1 group</i>	77
2.4.4 <i>Elevated GM1 expression in combined Aβ/ET-1 group.</i>	79
2.4.5 <i>Increased GD1a [Na⁺] expression at 3 d in combined Aβ/ET-1 group</i> ...	81
2.4.6 <i>Decreased expression of GD1a [K⁺] at 3 d in ET-1 alone group</i>	83
2.5 Discussion.....	85

2.6 References.....	88
---------------------	----

Chapter 3 : Age dependent and regional heterogeneity in the long-chain base of A-series gangliosides observed in the rat brain using MALDI

Imaging.....	92
3.1 Abstract	92
3.2 Introduction	93
3.3 Materials and Methods.....	97
3.3.1 <i>Animal model</i>	97
3.3.2 <i>MALDI IMS</i>	97
3.3.3 <i>Data Analysis</i>	99
3.4 Results.....	99
3.4.1 <i>LCB Genotype differences between Wt and Tg APP21 rats were restricted to GM3 within the peri-ventricular corpus callosum.</i>	99
3.4.2 <i>Significant anatomical heterogeneity throughout the rat life span within subcortical and basal ganglia structures for gangliosides GM1 and GM3</i>	102
3.4.3 <i>Cortical layers show regional heterogeneity in ganglioside of LCB length</i>	104
3.4.4 <i>Hippocampus: Age-dependent accumulation in d20:1/d18:1 species in the dentate gyrus molecular layer observed in complex gangliosides only.</i>	106
3.4.5 <i>Age-dependent increase in LCB ratio observed in the white matter for both complex gangliosides and simple ganglioside GM3.</i>	108
3.4.6 <i>Overall age effects</i>	111
3.5 Discussion.....	114
3.6 References.....	118

Chapter 4 : Membrane lipid homeostasis in a prodromal rat model of AD: Characteristic profiles in ganglioside distributions during aging detected using MALDI imaging mass spectrometry	123
4.1 Abstract.....	123
4.2 Introduction.....	124
4.3 Materials and Methods.....	127
4.3.1 <i>Animal Model</i>	127
4.3.2 <i>MALDI IMS</i>	128
4.3.3 <i>Data Analysis</i>	128
4.4 Results.....	131
4.4.1 <i>Increased proportion of simple gangliosides at 12 m in Tg APP21 rats across the brain</i>	131
4.4.2 <i>GD1 d18:1 is decreased in the gray matter of Tg APP21 rats with maintenance or increases in d20:1 species</i>	134
4.4.3 <i>GM1 increases with age but is less abundant in Tg APP21 rats than Wt</i>	137
4.4.4 <i>Decreased GM2 d20:1 levels in early life with significant transgene differences at old age in the hippocampus</i>	139
4.4.5 <i>Early increases in GM3 in Tg APP21 rats with transgene differences at 12 m</i>	141
4.4.6 <i>Age-dependent decrease in GD1 d18:1 in white matter regions with increases in simple species only in Tg APP21 rats</i>	144
4.5 Discussion.....	148
4.6 References.....	152
 Chapter 5 : Restoring ganglioside homeostasis after stroke using chloroquine is associated with pathological and functional improvements in Wistar rats.....	 156
5.1 Abstract.....	156
5.2 Introduction.....	157

5.3	Materials and Methods.....	161
5.3.1	<i>Stroke Model</i>	161
5.3.2	<i>Chloroquine Administration</i>	161
5.3.3	<i>Immunohistochemistry and Fluoro Jade B</i>	161
5.3.4	<i>Primary cortical neuron cultures</i>	162
5.3.5	<i>Fluorescence Microscopy</i>	162
5.3.6	<i>MALDI IMS</i>	162
5.3.7	<i>Ladder task – Motor assessment.</i>	163
5.3.8	<i>Novel Object Recognition – Short Term Memory Task</i>	164
5.3.9	<i>Data Analysis</i>	164
5.4	Results.....	165
5.4.1	<i>Pathological shift in ganglioside homeostasis prevented with CQ treatment at 3 d</i>	165
5.4.2	<i>Ganglioside homeostasis partially restored by CQ 21 d after comorbid stroke injury</i>	168
5.4.3	<i>Exogenous GM3 results in toxicity in primary cortical neurons which is protected by CQ treatment</i>	171
5.4.4	<i>Stroke-induced motor and cognitive impairments prevented by CQ treatment.</i>	173
5.4.5	<i>Reduced brain pathology at 21 d in CQ-treated stroke rats</i>	176
5.5	Discussion	178
5.6	References	180
Chapter 6 : Discussion		184
6.1	Summary of Objectives.....	187
6.2	Gangliosides and pathological inflammation.....	184
6.3	Ganglioside dysregulation	185

6.4 Role of the ceramide moiety in aging and neurodegeneration	186
6.5 CQ and ganglioside metabolism – limitations/benefits	188
6.6 Alternative approaches for modulation of ganglioside metabolism	189
6.7 Gangliosides and white matter.....	190
6.8 MALDI IMS – limitations and future directions	192
6.9 Significance of the research	193
6.10 References.....	194
Appendices.....	204
Curriculum Vitae	231

List of Figures

Figure 1.1: Ganglioside Structure.....	11
Figure 1.2: Diagram of a and b-series ganglioside structure and major metabolic enzymes.	133
Figure 2.1: Chemical Structure and Metabolic Pathways Involved in Ganglioside Synthesis and Catabolism.....	64
Figure 2.2: MALDI IMS Workflow.	67
Figure 2.3: Increased GM3 expression within infarcted region of combined A β /ET-1 group persists at 21 d.....	74
Figure 2.4: Effects of GM3 accumulation on neurodegeneration following stroke.	76
Figure 2.5: Elevated GM2 Expression at 3 d Remains Increased only in Combined A β /ET-1 Group.	78
Figure 2.6: Elevated GM1 Expression in Combined A β /ET-1 Group.	80
Figure 2.7: Increased GD1a [Na ⁺] Expression at 3 d in Combined A β /ET-1 Group	82
Figure 2.8: Decreased expression of GD1a [K ⁺] at 3 d in ET-1 alone group.	84
Figure 3.1: Ganglioside structure and detection using MALDI IMS.	96
Figure 3.2: Representative MALDI IMS images of each a-series ganglioside in all 4 tissue sections.....	98
Figure 3.3: Increased d20:1/d18:1 GM3 ratio in PVCC between birth and old age in TgAPP21 rats.....	101
Figure 3.4: Significant regional heterogeneity in ganglioside LCB ratio among sub-cortical structures.	103

Figure 3.5: LCB ratio highest in superficial layers of the cortex and shows opposite pattern during early development among complex and simple gangliosides.	105
Figure 3.6: Significant regional heterogeneity in d20:1/d18:1 ratio during aging among hippocampal layers.	107
Figure 3.7: Unique pattern of d20:1 LCB accumulation in the white matter for simple ganglioside GM3 as well as significant differences among white matter regions during aging.	110
Figure 3.8: Differential alterations in LCB during early brain development and adulthood in Fisher rats.	113
Figure 4.1: MALDI IMS Detection and visualization of a-series gangliosides across rat brain tissue.	130
Figure 4.2: The percentage distribution of simple gangliosides in various brain regions of Tg APP21 rats.	133
Figure 4.3: Distribution of the GD1 d18:1 and d20:1 species during aging.	136
Figure 4.4: Increase of GM1 during aging in various brain regions of Tg APP rats.	138
Figure 4.5: Shifts in GM2 expression during aging.	140
Figure 4.6: Increased GM3 in Tg APP21 rats.	143
Figure 4.7: Unique ganglioside alterations in white matter regions of the brain during aging.	146
Figure 5.1: Chloroquine and ganglioside catabolism.	160
Figure 5.2: Ganglioside homeostasis restored at 3 d in comorbid injured rats treated with CQ.	167
Figure 5.3: Partial restoration of complex ganglioside homeostasis observed at 21 d via MALDI IMS.	170

Figure 5.4: CQ increases cell viability and decreases apoptosis in response to toxic low and high dose GM3 administration..... 172

Figure 5.5: Reduced forelimb Motor and cognitive impairments in stroke rats treated with CQ..... 175

Figure 5.6: CQ treatment reduces brain pathology after stroke..... 177

List of Appendices

Appendix i: Effect of incubation time and freezing on spatial resolution of ganglioside GM1 in MALDI imaging of mouse brain tissue	200
Appendix ii: The evolution of the MALDI IMS protocol and improvements in signal intensity and spatial resolution over time	202
Appendix iii: Sublimation of DAN matrix for the detection and visualization of gangliosides in rat brain tissue for MALDI Imaging Mass Spectrometry.....	205
Appendix iv: MS/MS of gangliosides.....	227
Appendix v: GM3 species with varied carbon length increase in response to stroke injury and can be prevented using CQ treatment.....	229

List of Abbreviations

A β	Amyloid beta
AD	Alzheimer's disease
ALS	Amyotrophic lateral sclerosis
APO	Apolipoprotein
APP	Alzheimer precursor protein
BACE	Beta-secretase
BDNF	Brain-derived neurotrophic factor
β Gal	Beta-galactosidase
β Hex	Beta-hexosaminidase
BrdU	Bromodeoxyuridine
CAA	Cerebral amyloid angiopathy
CJD	Creutzfeldt-Jakob disease
CMBT	5-Chloro-3-mercaptopbenzothiazole
CNS	Central nervous system
CQ	Chloroquine
DAN	1-5-Diaminonaphthalene
DESI	Desorption electrospray ionization
EGF	Epidermal growth factor
ET-1	Endothelin-1

Gal	Galactose
GalNAc	N-acetyl-galactosamide
GBS	Guillain-barre syndrome
GD	Ganglio-disialio
GDNF	Glial-derived neurotrophic factor
GEM	Ganglioside-enriched microdomains
GFAP	Glial fibrillary acidic protein
Glc	Glucose
GM	Ganglio-monosialo
GT	Ganglio-trisialo
HD	Huntington's disease
HIF	Hypoxia inducible factor
HPTLC	High performance thin layer chromatography
icv	Intracerebroventricular
IHC	Immunohistochemistry
IL	Interleukin
IMS	Imaging Mass Spectrometry
KO	Knock-out
LacCer	Lactosylceramide
LAMP	Late endosomal/lysosomal marker

LCB	Long chain base
MALDI	Matrix-Assisted Laser Desorption/Ionization
MAG	Myelin associated glycoprotein
MCAO	Middle cerebral arterial occlusion
MCP	Monocyte chemoattractant protein
MIP	Macrophage inflammatory protein
mRNA	messenger ribonucleic acid
m/z	Mass-to-charge ratio
NDMA	N-methyl-D-aspartate
NFκB	Nuclear factor kappa B
PD	Parkinson's disease
PI	Propidium iodide
PSEN	Presenilin
PYR	Pyrimethamine
qPCR	Quantitative polymerase chain reaction
ROS	Reactive oxygen species
rtPA	Recombinant tissue plasminogen activator
SAM	Senescence-accelerated mice
SIMS	Secondary ion mass spectrometry
TBI	Traumatic brain injury

Tg	Transgenic
TNF	Tumor necrosis factor
TUNEL	Terminal deoxynucleotidyl transferase dUTP nick end labeling
VCI	Vascular cognitive impairment
VEGF	Vascular endothelial growth factor
Wt	Wild type

Chapter 1

1 Introduction

The following chapter contains a review of the literature pertaining to the topics discussed in this work. Ganglioside dysregulation was examined in the context of neurodegeneration and aging in rats using a novel imaging technique. Relevant background information on the pathogenesis of ischemic stroke, Alzheimer's disease (AD), and the co-morbidity of stroke and AD are presented, followed by a detailed description of gangliosides and their role during aging, injury, and neurodegenerative disease. Next, the MALDI imaging mass spectrometry technique used to examine the distribution of gangliosides in the brain is described. Finally, background information on a pharmacological compound used to prevent ganglioside dysregulation is provided.

1.1 Ischemic stroke

A stroke is the abrupt development of neurological deficits due to an interruption of blood supply, and thus oxygen, to the brain. These injuries can be either hemorrhagic or ischemic in nature. Ischemic strokes are most common, accounting for roughly 80% of all strokes, and occur as a result of blood vessel occlusion (Fluri, Schuhmann, & Kleinschnitz, 2015). The brain region surrounding the occlusion is starved of oxygen and energy, setting off a cascade of pathological events that can lead to irreversible tissue damage. Excitotoxicity in the early stages of the ischemic cascade is caused by a massive release of the excitatory neurotransmitter glutamate (Lai, Zhang, & Wang, 2014). Neural cells have a large number of glutamate receptors which makes the brain particularly susceptible to excitotoxic damage, and thus ischemic injuries (Lai et al., 2014). Glutamate stimulates N-methyl-D-aspartate (NMDA) receptors on the cell surface mediate the influx of calcium (Ca^{2+}) into the cell. The increased Ca^{2+} then triggers a secondary intracellular Ca^{2+} overload which promotes apoptotic cell death (Randall & Thayer, 1992; Szydlowska & Tymianski, 2010). When excessive intracellular Ca^{2+} is taken up by mitochondria, reactive oxygen species (ROS) and free radicals are produced leading to oxidative stress, further perpetuating neurodegeneration (Castilho, Ward, & Nicholls, 1999; Zoppo et al., 2000). The pathological events in the ischemic cascade are not linear, but rather circular in nature, with

one factor affecting downstream events and also feeding back to exacerbate the initial triggering event.

The region immediately surrounding the ischemic occlusion is termed the necrotic core, where irreversible cellular damage often occurs. The ischemic penumbra is a perilesion area surrounding the necrotic core which is vulnerable to damage but can also be prevented depending on a number of variables, such as autophagy and inflammation (C Iadecola & Anrather, 2011). Autophagy is a mechanism in which intracellular components are broken down and recycled and can be considered a pro-survival mechanism for the cell when it selectively degrades damaged or malfunctioning cellular components. However, prolonged exposure to stress, such as an ischemic stroke, can over-activate this process, leading to apoptotic cell death (Debnath, Baehrecke, & Kroemer, 2005; Mizushima, Levine, Cuervo, & Klionsky, 2009). Microglia and astrocytes, the brain's inflammatory cells, arrive at the site of injury, leading to an upregulation of pro-inflammatory cytokines, such as tumor necrosis factor (TNF)- α , interleukin (IL)-1 β , macrophage inflammatory protein (MIP)-1 α , and monocyte chemoattractant protein -1 (MCP-1) (Hawkins et al., 2017; C Iadecola & Anrather, 2011; Zoppo et al., 2000). When neuroinflammation spreads outside of the necrotic core, the upregulation of pro-inflammatory cytokines can become pathological, leading to phagocytic engulfment and pro-apoptotic/autophagic signaling of potentially viable cells (Hawkins et al., 2017).

Currently, the only effective treatment for stroke is recombinant tissue plasminogen activator (rtPA), an anti-clotting agent, which must be administered within a very narrow therapeutic window (within 3 hrs of stroke) and excludes individuals over the age of 80, those who take anti-coagulant medications, those with mild or recurring strokes, and those with comorbidities (Fluri et al., 2015; X. Liu et al., 2013; The National Institute of Neurological Disorders and Stroke rt-PA Stroke Study Group, 1995). A review of rtPA administration in 2165 stroke patients at a Canadian teaching hospital revealed that 73% of patients were excluded from treatment as they arrived at the hospital more than 3 hrs after stroke onset. Of the total patients with ischemic stroke who were present at the hospital within 3 hrs, only 26% received rtPA treatment once the exclusion criteria listed above was factored in (Barber, Zhang, Demchuk, & Hill, 2001). Patients who do receive this treatment

have a significantly decreased risk of severe neurological impairments but it is accompanied by a 10 fold increase in the risk of intracerebral hemorrhage (Liu et al., 2013; The National Institute of Neurological Disorders and Stroke rt-PA Stroke Study Group, 1995). Due to the multifactorial nature of the ischemic cascade, it is unlikely that a single target approach will be sufficient to temper the complex interaction of pathogenesis after stroke (Fisher, 1997; Liu et al., 2013). Thus, a better understanding of the key mediators of ischemic damage would allow for a more effective approach to treatment.

Ischemic stroke can be modelled in animals to study the mechanisms governing the pathogenesis and test possible therapeutic interventions. The most common animal model of stroke is middle cerebral artery occlusion (MCAO) (Fluri et al., 2015; Longa, Weinstein, Carlson, & Cummins, 1989; Tamura, Graham, McCulloch, & Teasdale, 1981). This technique involves sending a suture through the common carotid artery until the MCA is reached and occluded for a predetermined period (generally 60-120 min in rats), after which time the occlusion is released and reperfusion begins. Different strains of rats were found to have distinct responses to MCAO injuries, making the choice of rat strain an important variable to consider in experimental stroke research. For example, Sprague-Dawley rats were found to have considerable variability in stroke size in response to MCAO injuries while Wistar rats exhibited the most consistent results (Howells et al., 2010; Ström, Ingberg, Theodorsson, & Theodorsson, 2013). Injection of the potent vasoconstrictive peptide Endothelin-1 (ET-1) is another common model of ischemic stroke. It is less invasive and results in lower mortality rates than MCAO, and can be administered directly into discrete brain regions (Fluri et al., 2015). ET-1 is generally administered topically or to the desired brain region via a stereotaxic injection, where cerebral blood flow is reduced up to 90% in the surrounding focal region, followed by reperfusion over several hours (Bogaert, Scheller, Moonen, Sarre, & Smolders, 2000; Fuxe et al., 1997). Thus, the ET-1 stroke model can be used to simulate smaller, “lacunar” infarcts that are common in the human aging brain.

1.2 Alzheimer’s disease

Age-related dementia has emerged as one of the biggest health problems of our time, affecting roughly 35.6 million people world-wide, with that number expected to triple by

2050 (Costantino Iadecola, 2013; The World Health Organization, 2012). It presents a devastating societal burden for caregivers and taxpayers alike, as it has become more costly to manage than both cancer and heart disease in the US (Hurd, Martorell, Delavande, Mullen, & Langa, 2013). Alzheimer's disease (AD) is a neurodegenerative disease characterized by progressive cognitive decline and represents the most common form of dementia. Alois Alzheimer described four major neuropathological features of the disease including senile plaques, neurofibrillary tangles, hardening of arteries, and lipid granule accumulation (Chan et al., 2009; Foley, 2010; Iadecola, 2013). Patients with AD exhibit altered sensory perceptions most commonly manifesting as memory loss which progressively worsen leading to a wide array of behavioural deficits as the disease progresses. The cause of AD remains unclear; however, several genetic and non-genetic factors have been implicated.

The amyloid cascade hypothesis was one of the most prominent theories of AD pathogenesis. Generally, it states that the accumulation and deposition of amyloid beta ($A\beta$) plaques in the brain lead to neuronal dysfunction and cell death (Goate et al., 1991). This theory posited that $A\beta$ accumulation was the driving factor in the development of AD-related symptoms and associated pathologies such as neurofibrillary tangles, inflammation, neuronal loss, and cognitive decline (Hardy & Higgins, 1992). However, increasing evidence has countered this hypothesis as the total amyloid burden was not found to be correlated with cognitive decline or even the manifestation of AD symptoms (Haass & Selkoe, 2007; McLean et al., 1999; Snowdon et al., 1997). Although $A\beta$ is still considered an important factor in the pathogenesis of AD, attention has shifted from solid $A\beta$ plaques to soluble oligomers of $A\beta$, in conjunction with other predisposing factors, as a major driver of the disease (Ferreira, Vieira, & Felice, 2007; Li et al., 2009; Tomiyama et al., 2010).

AD can present in either an early onset form (familial) or late onset form (sporadic). Genetic factors are thought to be the main cause of familial AD cases. Mutations in several genes regulating the cleavage and processing of amyloid precursor protein (APP) have been shown to upregulate the production of $A\beta$. APP is cleaved by proteases, β - and γ -secretase, to form $A\beta$. Presenilin (PSEN) regulates the activity of γ -secretase to increase

the ratio of long chain A β 42 to A β 40, a toxic fragment of the A β protein. The presence of the apolipoprotein E4 (APOE4) gene has been found to increase the risk for familial AD and remains the most common genetic screening marker for individuals with a family history of early-onset AD (Bandaru et al., 2009; Carrieri, Bonafè, Luca, Rose, & Varcasia, 2001; Sanan et al., 1994). The main risk factor for the sporadic form of AD is age, which is hypothesized to interact with certain environmental and lifestyle factors along with existing conditions, such as stroke and diabetes, to initiate AD (Purnell, Gao, Callahan, & Hendrie, 2009; Reitz, 2012).

The vascular system of the brain is thought to play a major role in the development and progression of AD. Roughly 90% of AD patients present with cerebral amyloid angiopathy (CAA), which occurs when A β (mostly A β 40) deposits and accumulates in blood vessels, leading to narrowing of blood vessels and cognitive decline (Attems, Jellinger, Thal, & Van Nostrand, 2011). The narrowing of cerebral blood vessels increases the risk for ischemic stroke injuries and impedes the clearance of solutes from the brain (Jellinger, 2002; Soontornniyomkij et al., 2010). The occipital lobe is the most frequently and severely affected part of the brain for CAA, followed by the frontal lobe (Attems, Jellinger, & Lintner, 2005). As the disease progresses, accumulated A β leads to degeneration of vessel smooth muscle, leading to a thinning of vessel walls, making them more vulnerable to “mini aneurysms” and dysphoric, or structurally abnormal, vessel formation (Attems et al., 2011). Carriers of the APOE4 gene who develop late-onset dementia are at a higher risk of developing CAA (Trembath et al., 2007). Thus, the interaction of A β with the brain’s vasculature is a critical component of the pathogenesis of AD.

Vascular dementia is the second most common form of dementia. It is characterized by the presence of vascular lesions and is commonly associated with the appearance of white matter lesions which can accumulate over time in a condition referred to as leukoaraiosis (Hachinski & Potter, 1987; Iadecola, 2013). This form of dementia is highly associated with cardiovascular risk factors such as stroke, hypertension, diabetes, hyperlipidemia and smoking. Many of the symptoms of vascular dementia overlap with those of AD, often being differentiated solely on the severity or location of

neurodegenerative or vascular lesions. White matter lesions can grow over time and are correlated with the evolution of cognitive impairments (Maillard, Carmichael, Fletcher, & Reed, 2012). Indeed, vascular risk factors are known to play a major role in the initiation and progression of dementia (Hachinski, Bowler, & Loeb, 1993; Steingart, Hachinski, & Lau, 1987; Thiel, Cechetto, Heiss, Hachinski, & Whitehead, 2014).

1.3 Comorbidity of AD and Stroke

A number of variables have been shown to correlate and/or increase the risk of developing AD such as atherosclerotic disease, atrial fibrillation, hypertension and adult-onset diabetes mellitus (Cechetto, Hachinski, & Whitehead, 2008; Cifuentes et al., 2015). In fact, the incidence of “pure” dementia is relatively rare, while a mixed vascular-degenerative presentation is quite common (Dodge, Chang, Kamboh, & Ganguli, 2012; Iadecola, 2013). Epidemiological evidence is particularly strong pertaining to the relationship between the incidence of stroke and the development of dementia. Approximately 25% of stroke survivors develop dementia (Jin, Østbye, Feightner, Di Legge, & Hachinski, 2008). Patients with both minor cerebral infarcts and AD lesions are more likely to develop the clinical manifestations of dementia with synergistic effects on dementia related pathology (Hachinski & Munoz, 2000; Snowden et al., 1997). Elderly individuals are at a particularly high risk of “silent strokes”, or lacunar infarcts, which are ischemic lesions in small vessels that often do not produce observable deficits but can lead to accumulated damage over time (Masuda, Nabika, & Notsu, 2001). Patients with lacunar infarcts in the basal ganglia, thalamus, or white matter regions have demonstrated a high prevalence of dementia (Gold et al., 2005; Prins et al., 2004; Schmidt et al., 2005; Snowden et al., 1997), therefore, the location of stroke injury is also a determining factor in the development of subsequent dementia.

The interaction between stroke and AD has also been shown to be bidirectional, with increases in A β being associated with compromised vascular function (Grammas, Yamada, & Zlokovic, 2002). For example, A β plaques have been observed to accumulate around cerebral blood vessels leading to vascular degeneration (Kalaria, 2002). On the

other hand, APP protein has been observed to accumulate around the site of infarcts in rats (Kalaria et al., 1993). Additionally, hypoxia caused by hypoxia inducible factor 1 α (HIF-1 α) was associated with increased A β production and cleavage by β -secretase (BACE1), which the authors suggest may contribute to triggering the amyloid cascade (Zhang et al., 2007). Thus, a complex interaction exists between stroke and AD that can synergistically overlap to produce exacerbated pathology.

Clinical findings of interaction and synergism between stroke and AD have been recapitulated in a number of animal models which have been useful in teasing apart the mechanisms involved. Synergistic interactions of pathology have been observed in rats who have received both icv injections of the toxic A β peptide 25-35 in addition to a focal ET-1 induced striatal stroke (Amtul et al., 2014; Whitehead, Cheng, Hachinski, & Cechetto, 2007; Whitehead, Hachinski, & Cechetto, 2005). These rats displayed increased neuroinflammation, progressive increases in infarct size, and performed worse on cognitive memory tasks than rats with just ET-1 stroke or A β toxicity alone. Another study using transgenic (Tg) APP rats with or without ET-1 stroke injuries, demonstrated that Tg rats with increased A β production displayed increased cognitive inflexibility on an operant set shifting task compared to Tg rat without a stroke or wild type (Wt) rats with stroke, suggesting a synergistic effect on cognitive impairment in the comorbid rats (Levit et al., 2017).

A correlation has been observed between individuals who carry the APOE4 gene and cerebrovascular disease (Kalmijn, Feskens, Launer, & Kromhout, 1996). The Canadian Study of Health and Aging examined the joint effect of stroke and APOE4 in 954 participants and found that individuals who had both a stroke and were positive for the APOE4 gene displayed the highest prevalence of dementia (Jin et al., 2008). However, it was found that the effect of stroke on the incidence of dementia was not affected by the presence of the APOE4 gene, suggesting that stroke and APOE4 may increase the risk for dementia via independent mechanisms (Jin et al., 2008). Conversely, the PSEN1 gene has been shown to render neural cells vulnerable to hypoxia-induced apoptosis *in vitro* and was correlated with increased intracellular levels of Ca²⁺ (Mattson, Zhu, Yu, & Kindy, 2000). *In vivo*, PSEN1 knock-in mice display increased brain damage in response to a focal ischemic

reperfusion injury and worsened behavioural outcomes (Mattson et al., 2000). These studies suggest that the interaction between AD and stroke may be partially governed by specific genetic markers.

Common neuropathological features are present in both AD and stroke, with vascular dysfunction being the most prevalent. Vascular cognitive impairment (VCI), an umbrella term which encompasses all cognitive disorders associated with cerebrovascular disease and injury, is thought to occur primarily due to reduced cerebral blood flow and damage to myelin, leading to cerebral atrophy and dysfunctions in connectivity within the brain (Appelman et al., 2009; Dichgans & Leys, 2017; Lawrence et al., 2013). VCI is a very common feature of senile dementia, making up roughly 75% of cases (Gearing et al., 1995; Hachinski, 2008). Another common neuropathological feature is neuroinflammation. The activation and proliferation of microglia and astrocytes, increased ROS, upregulation of inflammatory cytokines and nuclear factor kappa B (NF κ B) are all neuroinflammatory events that are synergistically activated in the presence of both AD and stroke (Bales, Du, Holtzman, Cordell, & Paul, 2000; Cheng et al., 2006; Stoll, Jander, & Schroeter, 1998; S. N. Whitehead et al., 2005). The neuroinflammatory response after stroke is exacerbated by the presence of A β toxicity and is implicated as mechanism which can mediate the severity of cognitive impairments (Amtul et al., 2014; Li et al., 2011; Whitehead, Cheng, Hachinski, & Cechetto, 2007; Whitehead, Hachinski, & Cechetto, 2005). Indeed, anti-inflammatory treatment has shown beneficial effects in reducing the exacerbated neuroinflammatory response and cognitive impairments associated with stroke and A β comorbidity (Whitehead, Cheng, Hachinski, & Cechetto, 2005). However, anti-inflammatory agents alone are not sufficient to prevent the pathogenesis of either stroke or AD further investigate factors which may be mediating the synergistic interaction between stroke and AD.

1.4 Gangliosides

Over 60% of the mass of our brains are made up of lipids (Chang, Ke & Chen, 2009) yet their precise role in the development and pathogenesis of neurodegenerative diseases and injuries remains unclear. Changes in brain lipids are correlated with the progression of diseases, such as AD (Ariga, McDonald, & Yu, 2008). Indeed, lipid biomarkers may hold

the key to identifying individuals at risk of developing neurodegenerative diseases. Mapstone et al, used a lipidomics approach to identify several plasma phospholipids in peripheral blood samples that could predict, with 90% accuracy, the conversion from a cognitively normal phenotype to mild cognitive impairment or AD within a 2-3 year timeframe (Mapstone et al., 2014). These findings are particularly important given the disappointing results from biomarkers that target other AD-associated proteins in cerebral spinal fluid such as A β 42 and Tau (Irizarry, 2004). Thus, a better understanding of the role of lipids in the aging brain may reveal important mechanistic clues as to the development of neurodegenerative diseases and the brain's response to injury. One group of membrane lipids, called gangliosides, are of particular interest in the context of neurodegeneration as they have been shown to be altered in response to a number of neurodegenerative diseases and injuries. The following section provides background on ganglioside structure, function, as well as a review of the literature of their role in neurodegenerative diseases and injuries.

1.4.1 Ganglioside Structure

Gangliosides are part of a glycosphingolipid family that contain sialic acid residues. They have a wide variety of biological functions due to their location on the outer leaflet of plasma membranes (Lopez & Schnaar, 2009). They make up a crucial component of lipid rafts, or ganglioside-enriched microdomains (GEMs), where they effect the physical properties of the membrane as well as their function (Daniotti & Iglesias-Bartolomé, 2011; Sandro Sonnino & Prinetti, 2010). Lipid rafts are complexes made up of cholesterol, glycosphingolipids, and proteins which play an important role in signal transduction. The specific functions of lipid rafts varies depending on their composition which can lead to the segregation of rafts within the lipid bilayer based on, for example, the type of gangliosides present (Sonnino, Mauri, Ciampa, & Prinetti, 2013). Lipid rafts cluster molecules with similar properties together in order to facilitate the molecular interactions required for specialized cellular functions (Hooper, 1998). Gangliosides play an important role in stabilizing lipid rafts due to their physical structure, both within the phospholipid bilayer and on the outer leaflet of the membrane (Sonnino & Prinetti, 2010).

The hydrophobic portion of the ganglioside molecule is made up of the ceramide domain which contains a sphingosine moiety with a carbon chain of variable length attached to a fatty acid (**Fig. 1.1**). The ceramide domain acts to provide structural integrity on the membrane but is also suggested to play a more critical role in determining ganglioside function. Gangliosides with 18 carbons (d18:1) in their sphingosine moiety are most common in the CNS, however, gangliosides can also have shorter or longer carbon chains. The length of the carbon chain in the sphingosine moiety can alter the fluidic properties of the membrane which has functional consequences for glycoprotein interactions at the cell surface (Masserini, Palestini, & Freire, 1989; Sonnino & Chigorno, 2000). Indeed, gangliosides with varying carbon lengths are thought to have unique functional roles in the brain (Sonnino & Chigorno, 2000), however, technical challenges in detecting and visualizing gangliosides with varying carbon lengths has made it difficult to examine this hypothesis. Alterations in the length of the carbon chain in the ceramide domain are thought to occur during ganglioside degradation and recycling processes, however the precise mechanisms remain unclear (Palestini, Masserini, Sonnino, & Tettamanti, 1990).

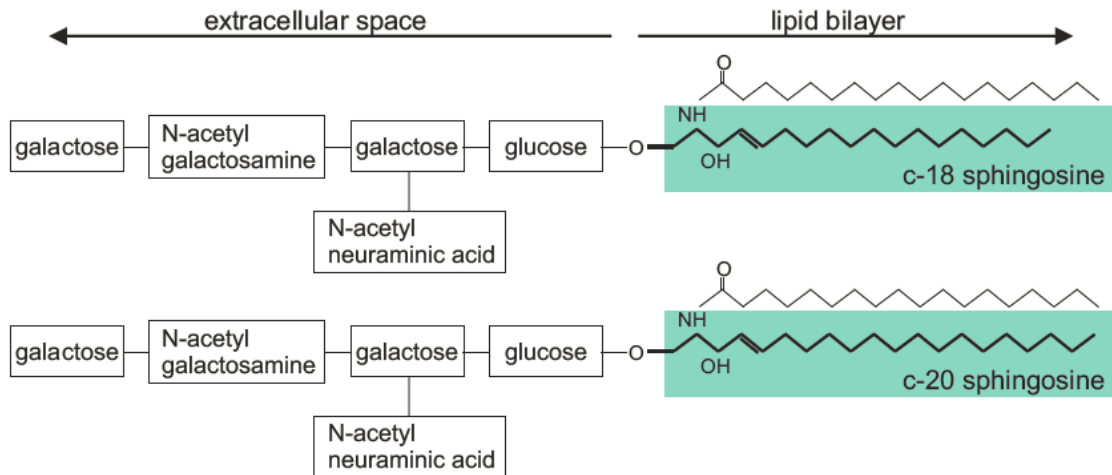


Figure 1.1: Ganglioside Structure. Gangliosides are composed of both a hydrophilic domain which extends into the extracellular space, and hydrophobic ceramide anchor (highlighted) embedded within the lipid bilayer. The hydrophilic portion contains an oligosaccharide chain of variable length which is composed of 3 types of sugar units (glucose, galactose, N-acetyl galactosamine) as well as sialic acid residues (NeuAc). The number and type of sugar units along with the number of sialic acid residues attached to galactose units determines the type of ganglioside (i.e. GM1, GM2, GM3). The hydrophobic portion of the molecule is made up of a fatty acid, usually stearic acid, and a sphingosine LCB tail with varying numbers of carbons. The most common form of ganglioside contains 18 carbons (d18:1) within the sphingosine moiety with the second most common form having a slightly longer carbon tail with 20 carbons (d20:1). Figure modified from Weishaupt et al., 2015.

Ceramide forms the hydrophobic backbone of the ganglioside molecule and is synthesized in the endoplasmic reticulum (Bisel, Pavone, & Calamai, 2014). The hydrophilic domain contains an oligosaccharide chain made up of a variable amount of glucose (Glc), galactose (Gal), and N-acetylgalactosamine (GalNAc), as well as one or more sialic acid residues. Glycosylation occurs in the golgi apparatus where only a limited number of oligosaccharides (Glc, Gal, GalNAc) are assembled to form gangliosides. The number and sequence of sugar units in the oligosaccharide domain act as a coding unit which are selective to specific glycoprotein interactions, giving each ganglioside species a unique regulatory function on the membrane (Ledeen & Wu, 2015). The combination of lactose and ceramide, or LacCer, forms the main lipid core of all gangliosides (Prokazova, Samovilova, Gracheva, & Golovanova, 2009). GM3 is produced when a sialic acid residue is added to LacCer by the enzyme GM3 synthase (also known as ST I, ST3Gal V, or CMP-NeuAC) (**Fig. 1.2**). This ganglioside forms the basis upon which all other gangliosides are synthesized. Oligosaccharide units and/or sialic acid residues are added to GM3 by various glycosyltransferases and sialyltransferase enzymes to produce the over 200 identified species of gangliosides (Bisel et al., 2014). Berselli et al., proposed that the activity of GM3 synthase may be related to the location within the golgi apparatus and can dictate assembly of either simple gangliosides, such as GM3 or GD3, or more complex gangliosides, such as GM1 and GD1a (Berselli et al., 2006).

Hydrolysis of sialic acids by Neu3 in lysosomes and on the plasma membrane is the first step of ganglioside degradation (Ha, Lee, Cho, Kim, & Kim, 2004; Prokazova et al., 2009). Gangliosides with a sialic acid residue on a terminal chain galactose unit or polysialic gangliosides are the first to be catabolized and can be degraded directly in the membrane, while gangliosides with a single sialic acid residue located on a middle chain galactose unit, such as GM1, are degraded only in the lysosome (Miyagi et al., 1999). Gangliosides are transported to endosomes and eventually lysosomes where they are sequentially degraded by hydrolytic enzymes such as sialidase, β -galactosidase (β Gal), and β -hexosaminidase (β Hex) (Bisel et al., 2014).

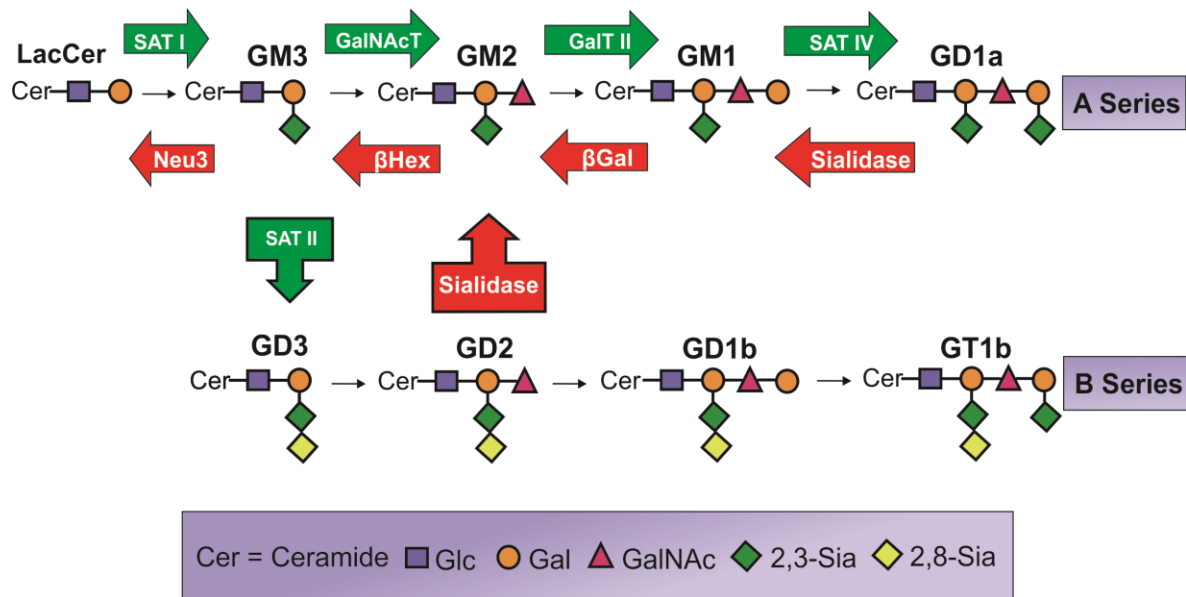


Figure 1.2: Schematic of A- and B-series ganglioside metabolism. Gangliosides are synthesized (green) from the conversion of Lactosylceramide (LacCer) to GM3 by the addition of a sialic acid residue to the galactose unit of LacCer by the SAT I enzyme (or GM3 synthase). Thus, GM3 is the structural precursor of all other ganglioside species with more complex species being synthesized from GM3 by various transferase enzymes that add sugar units (GalNAcT, GalT II) and sialic acids (SAT IV, SAT II). Gangliosides are catabolized (red) by sialidase as well as sugar cleaving enzymes β -Galactosidase (β Gal) and β -Hexosaminidase (β Hex). Catabolism of gangliosides generally occurs within endosomes and lysosomes, however, there are membrane-bound sialidases which can directly catabolize gangliosides with sialic acids on terminal galactose units, such as GD1a and GT1b, directly on the membrane. GM3 is catabolized by a specialized sialidase enzymes called Neu3, which can only break down GM3.

1.4.2 GM3

Ganglioside GM3 is the first and simplest member of the ganglioside family and is the metabolic precursor of more complex gangliosides and thus plays a determining role in the abundance of all upstream ganglioside species. GM3 is the main ganglioside in extra-neural tissues, but is present only in small amounts in the CNS (Dawson, Matalon, & Dorfman, 1972; Muthings & Cacic, 1997; Negroni, Chigorno, Tettamanti, & Sonnino, 1996; Nilsson & Svennerholm, 1982; Ohashi, 1978; Prokazova et al., 2009; Rauvala & Finne, 1980; Seyfried, Ando, & Yu, 1978). GM3 synthase, which synthesizes GM3 from LacCer, is a unique sialyltransferase enzyme that is specific only to the GM3 lipid substrate, whereas other sialyltransferases can sialylate various lipid substrates (Harduin-lepers, Mollicone, Delannoy, & Oriol, 2005). Therefore, GM3 plays an important regulatory role for the synthesis of all other downstream gangliosides.

GM3 was identified as a molecule that regulates cell growth leading to interest in its potential role in the field of oncology. Numerous mechanistic studies examining the effects of GM3 in various cancer-based *in vitro* cell lines and *in vivo* rodent tumor models have identified important regulatory functions of GM3 including the inhibition of cell growth, proliferation, migration, adhesion, cell motility, angiogenesis, as well as the upregulation of apoptotic pathways (Chung et al., 2014; Fujimoto et al., 2005). Additionally, GM3 accumulation can increase the expression of TNF- α , a pro-inflammatory cytokine which modulates immunity and apoptosis (Kabayama et al., 2005). Exogenous administration of GM3 to B16 cells and cultured mouse melanoma cells resulted in a drastic increase in TNF- α mRNA, while cells treated with D-1-threo-1-phenyl-2-decanoylamino-3-morpholino-1-propanol (D-PDMP), an inhibitor of GM3 synthesis, resulted in decreased TNF- α mRNA expression (Péguet-navarro et al., 2017; Prokazova et al., 2009; Wang et al., 2007). The ability of GM3 to modulate a major pro-inflammatory cytokine suggests that it may play a role in the development of pathological inflammation. Angiogenesis, a critical factor for tumor growth, is suppressed when GM3 levels are increased through autocrine and paracrine effects on vascular-endothelial growth factor (VEGF) and by blocking VEGF receptor 2 (Choi et al., 2006; Mukherjee et al., 2008; Seyfried & Mukherjee, 2010). However, when complex gangliosides GM1 and GD1a were increased as well,

angiogenesis was restored suggesting that the balance between GM3 and complex gangliosides was an important factor in determining GM3's anti-angiogenic properties (Abate, Mukherjee, & Seyfried, 2006). In the mouse brain, astrocytomas expressing high levels of GM3 were found to be less vascularized and grow slower than those expressing low levels of GM3 (Seyfried & Murkhejee, 2010). GM3's interaction with TNF- α and VEGF have also led to interest for researchers in the field of metabolic disease as GM3 accumulation is correlated with insulin resistance in type 2 diabetes (Inokuchi, 2007; Sasaki et al., 2003; Veillon et al., 2015; Vukovic, Bozic, Markotic, Ljubicic, & Kurir, 2015; Wang et al., 2013; Zador et al., 1993). TNF- α appears to have a bidirectional relationship with GM3, with increases in the pro-inflammatory cytokine also being linked to an increase in GM3 synthase in animal models of metabolic disease (Tagami et al., 2002). Indeed, increases in GM3 have been shown to play a pathological role in animal models of metabolic disease through suppression of insulin-sensitive glucose transport and impaired wound healing (Randeria et al., 2015; Tagami et al., 2002). Reducing GM3 levels was shown to improve wound healing by increasing angiogenesis when applied to the lesion site and was also associated with increased insulin sensitivity and glucose tolerance in the liver of mice (Randeria et al., 2015; Yoshizumi et al., 2007). Overall, GM3 accumulation appears to be tied to the inflammatory response and impairs healing by blocking angiogenesis.

In order to examine the function of GM3 within the CNS, several *in vitro* and *in vivo* knock-out models have been developed. Studies in GM2/GD2 and GM3 synthase single and double KO mice, which lack complex gangliosides and accumulate simple ganglioside GM3, have demonstrated severe behavioural deficits that are exacerbated with aging leading to increased neurodegeneration, severe white matter pathology, and disrupted axon-glia interactions (Niimi et al., 2011; Sugiura et al., 2005; Tajima et al., 2009; Yamashita et al., 2005). Single KO GM2/GD2 synthase mice, which lack complex gangliosides and accumulate both simple gangliosides GM3 and GD3 developed progressive behavioural neuropathies including deficits in reflexes, strength, coordination and balance (Chiavegatto, Sun, Nelson, & Schnaar, 2000). Sheik et al., used the same single KO mouse model and found that the KO mice had reduced expression of myelin-associated glycoprotein (MAG) along with severe deficits in white matter including

decreased central myelination, axonal degeneration in both the central and peripheral nervous system, and demyelination of peripheral nerves (Sheikh et al., 1999). These studies not only suggest that complex gangliosides are essential to maintain the integrity of the nervous system throughout life but also point to potential toxicity associated with GM3 accumulation in the brain.

A number of *in vitro* neural models have confirmed many of the findings from oncology-based studies with regards to the accumulation GM3. Sohn et al., examined the effect of glutamate toxicity on GM3 levels and GM3 toxicity in HT22 hippocampal cells and found that glutamate toxicity led to an increase in GM3 in a time dependent manner, as assessed by high performance thin layer chromatography (HPTLC). GM3, GD3, and GT1 were then exogenously administered to HT22 cells but only GM3 was found to significantly decrease cell viability (Sohn et al., 2006). HT22 cells transfected with GD3 synthase siRNA to increase GM3 levels showed similar results on cell viability, further supporting the hypothesis that GM3 accumulation leads to cell death. The authors suggest that GM3 may be directly connected to toxic events such as the production of ROS and Ca^{2+} influx by stimulating the oxidative pathway (Sohn et al., 2006). Nakatsuji & Miller administered GM3, GM1, and GD3 to rat primary astrocyte cultures and found that only GM3 administration resulted in a significant decrease in cell proliferation, as assessed by BrdU staining, and led to an increase in apoptosis, as measured by TUNEL staining (Nakatsuji & Miller, 2001). The authors further examined the effects of GM3 accumulation *in-vivo* through icv injections of GM3 into the right ventricle of Sprague-Dawley rats and examined cell proliferation and apoptosis. BrdU staining was decreased 30% in the lateral and dorsolateral ventricular regions in GM3 injected rats while there was an increase in TUNEL positive staining in the same regions in addition to the subventricular zone and striatum. The authors demonstrate that the inhibition of cell proliferation by exogenous GM3 is correlated with the increased expression of cell cycle inhibitor p27KIP1 and suggest that proliferating neural precursors may be more susceptible to GM3 toxicity than mature, non-proliferating cells (Nakatsuji & Miller, 2001). Thus, GM3 accumulation may play an important mechanistic role in the development and progression of neurodegeneration in the brain.

1.4.3 GM2

Ganglioside GM2 is a minor component of brain gangliosides. It is formed through the addition of a glucose sugar unit to the oligosaccharide chain of GM3 by GM2 synthase. There is little direct evidence detailing the functions of GM2. It is thought to be involved in the process of insulin resistance through interactions with insulin receptors, however, the precise function of GM2 remains unclear (Higashi et al., 2011). GM2, like GM3, has also been shown to play a role in oncogenesis. It has been suggested that GM2 plays a protective role and that its depletion is correlated with greater cancer malignancy (Bisel et al., 2014). Accumulations of GM2 have been observed in the brains of several pre-clinical and clinical manifestations of neurodegenerative diseases such as AD and Hunter's disease (Bisel et al., 2014; Dufresne et al., 2017; Pernber, Blennow, Bogdanovic, Månsson, & Blomqvist, 2012).

Studies of GM2 gangliosidosis, wherein an inherited genetic defect in the catabolic enzyme β Hex leads to an accumulation of GM2, have revealed important clues as to its role in the brain. Patients with GM2 gangliosidosis are characterized by progressive deterioration of motor, cerebral, and spinocerebellar function caused by a deficiency in lysosomal enzyme β Hex (Maegawa et al., 2007). β -Hex has two main gene variants, HexA, and HexB. Genetic mutations of a specific gene variant lead to the development of unique neuropathies. For example, mutation in the HexA gene variant leads to the development of Tay Sachs disease, while mutations in both HexA and HexB lead to Sandhoff's disease. The infantile versions of GM2 gangliosidosis are the most severe, and generally result in death during infancy. Late-onset forms include juvenile, sub-acute, adult, and chronic subtypes with the severity and progression being correlated with the level of HexA activity (Conzelmann & Sandhoff, 1983). Therefore, treatments aimed at increasing the activity of HexA, and subsequently β -Hex activity, should lead to functional benefits. Pyrimethamine (PYR), an anti-malarial compound, was found clinically to act as a pharmacological chaperone that increases HexA levels, thereby decreasing GM2 levels and restoring ganglioside homeostasis. PYR was administered to several human Tay Sachs and Sandhoff's disease cell lines which resulted in an increase of HexA levels (Maegawa et al., 2007). In 2011, a phase I/II clinical trial of PYR in patients with Tay Sachs or Sandhoff's

disease showed a 4-fold increase in HexA levels and is currently moving forward to further examine the clinical effects in patients (Clarke et al., 2011). These studies demonstrate the efficacy of targeting the ganglioside metabolic pathway as a treatment for ganglioside accumulation.

GM2 levels are transiently increased in response to neurodegenerative injuries such as stroke and traumatic brain injuries (Whitehead et al., 2011; Woods et al., 2013). In a crucial mechanistic study of a mouse model of fetal alcohol spectrum disorder, Saito et al., describe GM2's potential role in neurodegeneration. Mice were subcutaneously injected with ethanol on post-natal day 7, which led to a severe apoptotic neurodegenerative response. GM2 levels were increased in the brain following ethanol injection and peaked at 24 hrs, followed by a decrease at 72 hrs, similar to the GM2 response after a neurodegenerative injury. The authors examined the abundance of GM2, GM1, and GD1a using HPTLC and found accumulation patterns which suggest GM2 may be a degradation product of more complex species. GM2 accumulation was found to occur primarily in lysosomes, mitochondrial membranes, and activated microglia, and also co-localized with caspase-3 positive (apoptotic) neurons. The authors hypothesized, based on their results, that GM2 was involved in mitochondrial-mediated apoptosis and increased in microglia due to phagocytic functions, as GM2 staining in microglia partially overlapped with staining for a late endosomal/lysosomal marker LAMP1 (Saito et al., 2013). Overall, evidence from the literature suggests that GM2 accumulation is correlated with neurodegeneration and apoptosis.

1.4.4 GM1

GM1, along with GD1a/b and GT1a/b make up the main gangliosides found in the brain. GD1 and GT1 contain the same oligosaccharide units as GM1 but have additional sialic acid residues. These additional sialic acids are susceptible to degradation from membrane-bound sialidase enzymes, however, GM1 is resistant to most forms of sialidase (Miyagi et al., 1999; Sonnino et al., 2011). GM1 can be found throughout the CNS but has been

reported to be particularly enriched in the white matter (Vajn, Viljetic, Degmecic, Schnaar, & Heffer, 2013).

GM1 has numerous signaling and regulatory functions compared to other ganglioside species (Ledeen & Wu, 2015). It is involved in the maintenance of lipid raft integrity and modulation of calcium (Ca^{2+}), sodium (Na^+), and potassium (K^+) ions across the plasma membrane to maintain homeostasis and promote neurite outgrowth (Rodriguez, Piddini, Hasegawa, Miyagi, & Dotti, 2001; Suzuki et al., 2007; Gusheng Wu, Lu, Andre, Gabius, & Ledeen, 2016). Contrary to GM3's anti-angiogenic properties, complex gangliosides such as GM1 and GD1 are pro-angiogenic (Gullino, 2017; Margheri et al., 2015; Ziche, Alessandri, & Gullino, 1989). GM1 can also promote neuritogenesis by modulating the binding activity of several cell adhesion molecules including neural cell adhesion molecule, N-cadherin, and laminin which promotes Ca^{2+} influx and tropomyosin-related kinase A (TrkA) mediated activation of nerve growth receptors (Laitinen, Leppiinen, Merenmies, & Rauvala, 1987; Ledeen & Wu, 2015; Mutoh, Tokuda, & Miyadai, 1995; Walsh, Skaper, & Doherty, 1994). GM1 can further modulate neurotrophic factors through association with trkB receptors to promote the release of brain-derived neurotrophic factor (BDNF) and the Ret/GFR α complex to promote glial cell-line derived neurotrophic factor (GDNF), which functions to preserve the viability of catecholaminergic neurons (Pascual, Hidalgo-Figueroa, & Piruat, 2008; Pitto et al., 1998). Together, these functions highlight the crucial neuroprotective role of GM1 in the brain.

GM1 began gaining interest as a therapeutic for neurodegeneration after exogenous administration of mixed brain gangliosides were found to improve peripheral sympathetic regeneration and re-innervation in cats (Ceccarelli, Aporti, & Finesso, 1976). Since then, GM1 has demonstrated neuroprotective and restorative effects in a number of neurodegenerative disease and injury models, as well as in human clinical trials (discussed below). An important development in the use of GM1 as a therapeutic was the creation of semisynthetic analogs of GM1 called lysogangliosides (LIGAs) which have identical biological functions to GM1 but have demonstrated increased membrane permeability in some cases (Kharlamov et al., 1994; Ledeen & Wu, 2015). While the oligosaccharide domain and sphingosine moiety are identical in LIGAs to GM1, the fatty acid chain in the

ceramide domain is often modified to shorter versions to facilitate permeability across the blood brain barrier and cellular membranes.

Although there is ample evidence supporting the protective role of GM1 in the brain, an accumulation can be problematic as well, highlighting the importance of tight homeostatic regulation. Similar to GM2 gangliosidosis, a genetic defect in the β -Gal enzyme, which catabolizes GM1 to GM2, results in the accumulation of GM1 in the brain, a condition termed GM1 gangliosidosis. GM1 gangliosidosis is characterized by progressive psychomotor deterioration and seizures and has both a severe infantile version and several late-onset forms. A GM1-mediated mechanism that is thought to contribute to the symptoms of GM1 gangliosidosis is excessive neurite outgrowth leading to cellular abnormalities such as “ectopic” growth of dendritic spines and neuro-axonal dystrophy (Walkley, 2003). These structural abnormalities lead to impaired signal transduction. Overall, there is ample evidence supporting the neuroprotective functions of GM1, however, homeostasis appears to be a key factor in dictating its ability to carry out these functions.

1.4.5 GD1a

GD1a is formed by the addition of a sialic acid residue to the terminal galactose unit of the GM1 oligosaccharide chain by sialyltransferase. GD1a is highly abundant throughout the brain but has been reported to be particularly enriched in the olfactory bulb, neocortex, amygdala, substantia nigra, thalamic nuclei and in myelinated commissural fibers (Vajn et al., 2013).

GD1a is an endogenous ligand for myelin associated glycoprotein, or MAG, a ganglioside-binding protein expressed selectively on myelin membrane on axon surfaces which functions to maintain the long-term integrity of axons and myelin (Pan et al., 2005; Sheikh et al., 1999). MAG is known to be an inhibitor of axon outgrowth that can limit recovery after CNS injury, therefore, increasing GD1a is associated with inhibition of axon outgrowth and regeneration, a process which can be reversed through administration of sialidase or GM1 (Rubovitch, Zilbe, Chapman, Schreiber, & Pick, 2017; H. J. Yang et al.,

2011). Although increasing GD1a levels after CNS injury can inhibit regeneration, a depletion of GD1a can also have deleterious effects on recovery as it is essential in maintaining appropriate axon-myelin interactions and ensuring the long-term stability of axons (Suzuki et al., 2007). It is important to note that not all MAG receptors bind GD1a, therefore the degree of MAG modulation by GD1a may be brain region dependent (Schnaar, 2010).

Ganglioside GD1a also been extensively studied in the field of Oncology and has been shown to enhance VEGF induced cell proliferation and migration of endothelial cells (Lang, Guerrero, Li, & Ladisch, 2001; Mukherjee et al., 2008). Additionally, it has been observed to enhance epidermal growth factor (EGF) when upregulated in fibroblasts (Liu, Li, & Ladisch, 2004). Anti-GD1a antibodies are significantly elevated in motor neuron diseases and syndromes such as Guillain-Barre syndrome (GBS) and Amyotrophic lateral sclerosis (ALS) (Ho et al., 1999; Kaji et al., 2000; Pestronk et al., 1989). Interestingly, anti-GD1a antibodies were only found to be elevated in the axonal form of GBS and not the demyelinating form, pointing to the important role of GD1a in axon stability (Ho et al., 1999; Yuki, Yoshino, Sato, Shinozawa, & Miyatake, 1992).

Because of GD1a's susceptibility to membrane-bound sialidase, one of its hypothesized roles in the brain is to act as a reserve pool for GM1 (Riboni, Prinetti, Bassi, & Tettamanti, 1991). This has led many to believe that GD1a and GM1 act as one functional unit, in conjunction with membrane-bound sialidase, to maintain GM1 levels in the brain (Ledeen & Wu, 2015; Miyagi & Yamaguchi, 2012; Sonnino et al., 2011). Indeed, due to the many important neuroprotective functions of GM1 and the inhibitory role of GD1a in recovery from injury, the breakdown of GD1a on the membrane may be an essential neuroprotective mechanism.

1.4.6 Gangliosides in neurodevelopment and aging

During pre-natal development, GM3 and GD3 are highly abundant in the brain (Yu, Tsai, & Ariga, 2012). GD3 has been observed to be the major ganglioside in neural stem cells, making up about 80% of the total ganglioside content (Nakatani, Yanagisawa, Suzuki, &

Yu, 2010). This finding suggests that the activity of GD3 synthase, which convert GM3 to GD3, may be highly active during prenatal development. The tight regulation of gangliosides during development support the hypothesis that the abundance of each species is related to the unique functional roles they play during specific stages of development (Yu et al., 2012). Elevated GM3 and GD3 levels are observed during neural tube formation and neural cell differentiation (Yu, Nakatani, & Yanagisawa, 2009). GM3 has also been observed to increase during cell contact formation (Hakomori, 2002). Studies in mammalian brains have shown that GM1 and GD1 levels are low during the early phases of neuron migration and mitosis but are rapidly upregulated during process outgrowth, synaptogenesis, and myelination (Yu et al., 2009; Yu et al., 2012). Complex ganglioside content increases in postnatal development leading to a shift from structurally simple gangliosides to complex (Piccinini et al., 2010). Simple gangliosides GM3 and GM2 are downregulated, while complex species GM1, GD1 and GT1 are upregulated (Ngamukote, Yanagisawa, Ariga, Ando, & Yu, 2007; Yu, Macala, Taki, Weinfield, & Yu, 1988). This shift is correlated with an increase in expression of ganglioside synthase genes (Ishii et al., 2007). Mice lacking complex gangliosides through knock-out (KO) of GM1 synthase develop progressive, age-dependent neurodegeneration, particularly with regards to axon-myelin interactions (Allende & Proia, 2002; Yao et al., 2014). A rare human disorder has been identified which results in the congenital loss of function of GM3 synthase, and thus, of all gangliosides. The disorder is characterized by severe neuromuscular and cognitive impairments, blindness, and seizures (Simpson et al., 2004; Vajn et al., 2013). These findings point to the important role of complex gangliosides in maintaining the functional integrity of nervous tissues in the developed brain.

During aging, the physical and chemical properties of the membrane are altered resulting in a shift in the balance and/or changed ratios of many lipid species, including gangliosides (Ariga, McDonald, & Yu, 2008). Barrier et al., 2007 used HPTLC to examine ganglioside changes during aging in the cortex of mice and found an increase in GM3 between 12 and 24 months, a decrease in GM2 between 6 and 24 months, and a minor decrease in GD1a between 3 and 6 months (Barrier et al., 2007). Total ganglioside content has been reported to decrease with age (Aydin, Cengiz, Ag, & Han, 2000; Ohsawa & Shumiya, 1991). Interestingly, an increase in simple ganglioside GM3 has been found to be

correlated with cell senescence *in vitro* (Patschan et al., 2008), a finding which was recapitulated in a senescence-accelerated mouse model. Oshawa & Shumiya used senescence-accelerated mice (SAM-P/8), which show earlier onset of irreversible advancement of senescence, shorter life span, age-related deterioration in learning abilities, and spongi-form degeneration, and found that they had decreased levels of complex gangliosides GD1 and GT1 along with a progressive increase in GM3 levels compared to control mice, as measured by HPTLC (Ohsawa & Shumiya, 1991). These studies indicate that ganglioside dysregulation, resulting in the depletion of complex gangliosides and the accumulation of GM3, may occur during the natural aging process.

Interestingly, the ceramide moiety has also been shown to be altered during aging. Sugiura et al., found an increase in the proportion of d20:1 species of GD1 compared to d18:1 species in the molecular layer of the mouse hippocampus during aging (Sugiura, Shimma, Konishi, Yamada, & Setou, 2008). Indeed, previous evidence has also suggested that the accumulation of 20 carbon species of complex gangliosides is correlated with aging (Mansson, Vanier, & Svennerholm, 1977; Palestini, Masserini, Sonnino, & Tettamanti, 1990; Palestini, Masserini, Fiorilli, Calappi & Tettamanti, 1993). These studies also provide evidence that significant anatomical heterogeneity in the age-dependent accumulation of d20:1 species may be present, however, a comprehensive examination of these species across the brain during aging has yet to be completed.

1.4.7 Gangliosides in stroke

Ganglioside dysregulation has been observed in the murine brain following neurodegenerative injuries such as stroke and traumatic brain injuries (TBI). Following TBI, mice were found to have significant increases in simple ganglioside GM2 in periventricular, hippocampal, and thalamic brain regions 2 hrs after injury which peaked at 24 hr then returned to control levels by 72 hrs (Woods et al., 2013). A similar transient increase of simple gangliosides was observed in response to stroke damage. Whitehead et al., examined the abundance and distribution of both complex and simple gangliosides in a mouse model of MCAO ischemic stroke. Following MCAO, a significant increase in GM2

and GM3 species were observed in the ipsilateral hemisphere 3 d post-stroke, which peaked at 7 d then returned to control levels by 14 d (Whitehead et al., 2011). The authors further demonstrated that the degree of simple ganglioside accumulation varied depending on the anatomical brain region, with the striatum and hippocampus showing a more severe accumulation than the cerebral cortex. Taken together, these studies provide evidence that simple ganglioside accumulation may be involved in neurodegeneration after injury and that certain brain regions may be more susceptible than others to dysregulation.

Increasing GM1 levels has been examined as a potential treatment for stroke due to its neurotrophic and pro-angiogenic properties and was found to be effective in reducing stroke-induced pathology both pre-clinically and in human patients. Several functions of GM1 have been described as being particularly important in protecting neural cells from the damage caused by the ischemic cascade including: 1) protecting against excitotoxicity by regulating Ca^{2+} influx into the cell (Wu & Ledeen, 1994; Zhang et al., 2015), 2) protecting cellular membranes by maintaining ion balance (Na^+ - K^+) and reducing edema in neurons (Karpiak, Li, & Mahadik, 1987); 3) inhibiting nitric oxide production, lipid peroxidation, excessive activation of glutamate receptors, excitatory amino acids, and free radical production (Avrova et al., 1998; Carolei, Fieschi, & Bruno, 1991); 4) improving survival of neurons by increasing blood flow and axonal growth (Rabin, Bachis, & Mocchetti, 2002; Rong, Zhou, Xiao-Wen, Tao, & Tang, 2013); and 5) enhancing neurotrophic activity to strengthen neural remodeling and promote recovery after injury (Ferrari & Greene, 1996; Marconi et al., 2005). Another mechanism in which GM1 is thought to confer neuroprotection through inhibition of autophagy. Li et al., administered GM1 to rats for 3 consecutive days following MCAO and found that a dose of 50 mg/kg was associated with a decrease in infarct volume and increased neuro-behavioural scores. The authors found that GM1 treatment after MCAO led to a decrease in autophagy markers Beclin-1 and LC3-II, suggesting that GM1 may exert a neuroprotective effect through inhibition of excessive autophagy that would otherwise lead to cell death. Administration of tat-Beclin-1 to increase autophagy after MCAO in addition to GM1 treatment abolished in the protective effects of GM1 on infarct size and neuro-behavioural deficits, further supporting the existence of a neuroprotective GM1-mediated mechanism of autophagy inhibition (Li, Tian, Long, Chen, & Lu, 2016).

GM1 is a major component in cerebral white matter and increasing GM1 levels has been shown to reduce damage to white matter regions after a hypoxic injury. Rong et al., used a neonatal rat model of hypoxia-induced white matter damage to show that GM1 treatment for 5 consecutive days reduced structural damage in the brain (edema, apoptosis, and necrosis around the ventricles), protected against white matter damage (increased myelin basic protein staining while also decreasing APP and GFAP staining), and reduced behavioural impairments (Rong et al., 2013).

Despite very promising evidence of a potential GM1-derived treatment for stroke in pre-clinical models, results of human clinical trials have demonstrated mixed results. Several human clinical trials failed to demonstrate a significant therapeutic benefit of GM1 treatment in stroke patients (Braune, 1991; Candelise, 2002; Hoffbrand, Bungley, Oppenheimer, & Sheldon, 1988), while others have shown that significant neurological and pathological improvements were associated with the treatment (Argentino et al., 1989; Bassi, Albizzati, Sbacchi, Frattola, & Massarotti, 1984). More studies are needed which examine the role of ganglioside dysregulation in stroke to address the controversial findings of these studies.

1.4.8 Gangliosides in neurodegenerative diseases: Parkinson's disease, Huntington's disease, Prion diseases

The accumulation of GM3 and GM2 has been described as characteristic of diseased neurons (Walkley, 2003). Indeed, it is considered a central feature of diseases such as Niemann-Pick type C, Gaucher's disease, and Hunter's disease (Kreutz et al., 2013; Dufresne et al., 2017). Ganglioside dysregulation has also been reported in a number of neurodegenerative diseases including Parkinson's disease (PD), Huntington's disease (HD), Prion diseases, and AD. In each case, despite the varying mechanisms involved, a depletion of complex gangliosides in the brain is observed which is often accompanied by a concomitant increase in simple species. Ganglioside dysregulation has been linked to the abnormal aggregation of proteins that is a central hallmark of the aforementioned

neurodegenerative conditions: α -synuclein in PD, Huntington in HD, Prion protein in Creutzfeldt-Jakob disease, and A β in AD.

PD is characterized by the progressive loss of dopaminergic neurons in the substantia nigra pars compacta leading to impairments in motor function (Sulzer & Surmeier, 2013). Human patients were found to have a depletion of GM1 in the occipital cortex, an area that is generally thought to not be largely affected in the disease, as compared to age-matched controls, which the authors suggest could be indicative of a systemic deficit of GM1 (Wu, Lu, Kulkarni, & Ledeen, 2012). This was associated with lower levels of phosphorylation of proteins in glial cell line-derived neurotrophic factor (GDNF) receptors of nigral neurons, which are critical for the survival of catecholaminergic neurons. These findings were recapitulated by the same group in a mouse model lacking complex gangliosides which developed symptoms reminiscent of human PD patients including motor impairments, depletion of striatal dopamine, and aggregation of α -synuclein protein (Gusheng Wu et al., 2012). GDNF Signaling could be restored using the semisynthetic GM1 analog LIGA20 (Hadaczek et al., 2015; Gusheng Wu et al., 2012). Indeed, increasing GM1 levels in the brain through exogenous administration has shown great promise in pre-clinical PD mouse and primate models, which eventually led to human clinical trials (Herrero, Perez-Otan, Oset, Kastner, & Hirsch, 1993; Pope-Coleman, Tinker, & Schneider, 2000; Schneider, Kean, & DiStefano, 1995).

Ganglioside dysregulation in HD is characterized not only by a depletion of complex species but also by an increase in GD3. Simple ganglioside GD3 has, similar to GM3, been linked to toxicity through stimulation of reactive oxygen species, leading to apoptosis (Scorrano, Petronilli, Lisa, & Bernardi, 1999), and has been implicated as a mechanism of neurodegeneration in HD (Desplats et al., 2007). Desplats et al., 2007, used microarray analysis, qPCR, and Western blot to examine changes in lipid gene expression in a Tg mouse model of HD as well as human caudate post-mortem samples. The authors found a 38% reduction in GM1 content in the Tg HD mice as compared to Wt along with a significant upregulation the St8sial gene, which encodes GD3 synthase, in the caudate of human HD patients (Desplats et al., 2007). Di Pardo et al., examined two different models

of HD mice (YAC128 and R6/2) and found that both Tg mouse models had significant deficiencies in complex gangliosides GM1, GD1a, and GT1b in the corpus callosum. Importantly, the authors found that these changes in gangliosides could be detected in the early stages of the disease. Taken together, these results suggest that ganglioside dysregulation may play a mechanistic role in the development of neurodegenerative diseases, such as HD, and that the white matter may be particularly susceptible to damage (Di Pardo, Amico, & Maglione, 2016).

Prion diseases, or spongiform encephalopathies, such as Creukfeldt-Jakob's disease (CJD), are characterized by a shift in complex and simple gangliosides. In a guinea pig model of CJD, a marked decrease in total ganglioside content was observed in brain regions highly affected by the disease such as the cerebral cortex, basal ganglia and thalamus, and brain stem. When the abundance of each individual ganglioside species in the brain was quantified using TLC, an increase in simple gangliosides GM3, GD3, and GD2 were observed along with a decrease in GM1, GD1a, GD1b, and GT1b (Yu & Manuelidis, 1978). In human CJD patients, a similar trend is observed but with a more severe depletion of multisialylated complex species GD1a, GD1b, and GT1b along with a particularly high accumulation of simple ganglioside GD3 (Ando, Toyoda, Nagai, & Ikuta, 1984; Ohtani, Tamai, Ohnuki, & Miura, 1996; Tamai et al., 1979). Di Martino et al., found a similar shift in complex and simple gangliosides in a Scrapie-infected hamsters, another type of prion disease (Martino, Safar, Callegaro, Salem, & Gibbs, 1993). Overall ganglioside content is reduced in the brains of patients with neurodegenerative diseases, potentially owing to a shift in ganglioside content leading to neuronal loss in affected regions (Desplats et al., 2007).

1.4.9 Gangliosides in neurodegenerative diseases: Alzheimer's disease

The role of gangliosides in AD remains unclear as a number of studies point to seemingly contradictory results. For example, while there is a large amount of evidence implicating GM1 as major driver of toxic A β accumulation in the brain, there is also evidence demonstrating that GM1 acts in a protective manner against AD pathology (Fantini, Yahi,

& Garmy, 2013; Grimm et al., 2012; Kreutz et al., 2013; Yanagisawa, Odaka, Suzuki, & Ihara, 1995; Yang et al., 2013). Regardless of the precise function, ganglioside dysregulation has been identified as a hallmark of the disease (Ariga et al., 2008).

Proteolytic processing of APP is influenced by the lipid composition of cellular membranes, with gangliosides having an important role in interacting with A β in membrane rafts (Wolozin, 2004). In particular, gangliosides GM3 and GM1 have a high affinity for interaction with A β . Cholesterol has been shown to promote the binding of A β to GM1 enriched rafts to form what is termed ganglioside-bound A β (GA β), a structure hypothesized to act as a seed for toxic A β fibrillogenesis (Ariga et al., 2008; Fantini, Yahi, & Garmy, 2013; Yanagisawa, Odaka, Suzuki, & Ihara, 1995). Several studies have reported that the formation of GA β can induce conformational changes in A β from a random coiled structure to an ordered structure rich in β sheets when environmental factors, such as the pH, are favourable (Choo-Smith, Garzon-Rodriguez, Glabe, & Surewicz, 1997; Matsuzaki, Kato, & Yanagisawa, 2010; McLaurin & Chakrabartty, 1996, 1997). This process is thought to occur mostly in early endosomes and leads to increased aggregation of A β in the brain (Kimura & Yanagisawa, 2007; Yamamoto, Nostrand, & Yanagisawa, 2006; Yanagisawa et al., 1995). Toxic A β fibrillation has also been shown to be amplified through binding with GM3 enriched lipid rafts, leading to further dysregulation of ganglioside activity. In a study by Grimm et al., A β binding to GM3 led to a reduction in the activity of GD3 synthase, and thus decreased turnover from a to b-series gangliosides (Grimm et al., 2012)

Human AD patients, similar to patients with other neurodegenerative diseases, show a significant decrease in total ganglioside content as compared to controls which is suggested to be related to the loss of the more abundant complex gangliosides (Molander-melin, Blennow, Bogdanovic, Dellheden, & Fredman, 2005; Svennerholm & Gottfries, 1994). The degree and location of ganglioside loss varies depending on the time of onset, with early onset, or familial AD patients having demonstrated a 58-70% decrease compared to controls in grey matter regions and 81% in frontal white matter, while late-onset patients appeared to show severe depletions only in the temporal lobe, hippocampus, and frontal white matter (Ariga et al., 2008; Svennerholm & Gottfries, 1994). Accumulations of simple

gangliosides GM2 and GM3 have also been observed in brain regions highly susceptible to neurodegeneration in AD. In a study by Kracun et al., gangliosides were found to be perturbed in early-onset AD patients such that there was a decrease in complex gangliosides GM1 and GD1a in the frontal and temporal cortices of the brain. These same regions were found to have a significant increase in simple gangliosides GM3 and GM2 compared to control brains (Kracun, Kalanj, Talan-hranilovic, & Cosovic, 1992). Gottfries et al., found a similar ganglioside distribution pattern in the brains of early-onset AD patients (Gottfries, Jungbjer, Karlsson, & Svennerholm, 1996). Significant accumulations of GM3 were observed in the entorhinal cortex of late-onset AD patients, a brain region particularly susceptible to neurodegeneration in AD (Chan et al., 2012). These results point to the possibility of ganglioside degradation as a mechanism of pathology in AD brains. Indeed, Pitto et al., observed an upregulation of the GM1 catabolic enzyme β -Gal in cultured fibroblasts from AD patients compared to controls, leading to the accumulation of simple gangliosides GM2 and GM3 (Pitto et al., 2005). Overall, the severe depletion of complex gangliosides and accumulation of simple gangliosides in brain regions which are highly susceptible to neurodegeneration are consistent with the neuronal loss and cortical/hippocampal thinning considered the pathological hallmarks of the disease (Ariga et al., 2008).

Understanding the role of ganglioside dysregulation in AD may not be as straightforward as a simple shift in the homeostatic distribution, rather, the unique functional properties of each species may lead to specific interactions with certain types of A β that are more or less favorable depending on various environmental factors. Pre-clinical animal models of AD have revealed important mechanistic information on the interaction of gangliosides with A β and specific mutations of various genes involved in the pathogenesis of human AD. Yamamoto et al., showed that different species of gangliosides reacted to specific types of hereditary A β and led to their accumulation. For example, the authors report that GM1 interacted with the Arctic variant of A β , GD3 with the Flemish A β variant, and GM3 with the Dutch and Italian A β variants. Interestingly, GM3, and GM2 to a lesser extent, were found to be the major gangliosides in human cerebrovascular smooth muscle cells, which the authors suggest may contribute to the accumulation of the Dutch A β variant in vascular walls. The authors further proposed that this differential interaction

of gangliosides with various hereditary variants of A β may contribute to the region-specific deposition of A β fibrils in the brain (Yamamoto, Hirabayashi, Amari, & Yamaguchi, 2005). A follow up study by the same group used a Tg mouse model of AD with double Swedish/London mutations of the APP gene in addition to a knock out of the GM2 synthase gene, resulting in the accumulation of GM3 and a reduction in complex gangliosides. The authors found that the Tg KO mice developed a severe dyschoric-form amyloid angiopathy in which amyloid deposition extended from blood vessel walls into the surrounding parenchyma and suggests, according to the authors, an important role of GM3 in the development of vascular A β pathology in the brain (Oikawa et al., 2009). Barrier et al., examined several transgenic mouse models of AD and found that the degree and type of ganglioside perturbation observed was associated with the specific genetic modifications of the mice. Transgenic APP mice with Swedish and London mutations (APPSL) showed a significant decrease in all b-series gangliosides within the cortex at 24 m along with a 2-3 fold increase in simple a-series gangliosides GM2 and GM3 compared to controls. Double transgenic mice with APPSL and PS1 mutations showed a slightly different pattern at 24 m, with a less severe depletion of complex a and b-series gangliosides and an accumulation of simple ganglioside GD3. However, like the APPSL only mice, the APPSL/PS1 mice showed a significant increase in simple gangliosides GM3 and GM2 compared to age-matched controls. In the double Tg APPSL/PS1 mice, an accumulation of simple gangliosides could be observed as early as 3 m, which, the authors suggest, implicates ganglioside dysregulation as an early driver of pathology in AD (Barrier et al., 2007). Thus, ganglioside dysregulation resulting in the accumulation of toxic simple gangliosides along with a depletion of protective complex gangliosides is region-specific and is linked to the proteolytic processing of A β , making the restoration of ganglioside homeostasis a potentially critical point of intervention.

The ceramide domain of gangliosides may also play an important role in the development and progression of AD as ceramides with longer carbon chains have not only be observed to increase during the natural aging process, but also accumulate in brain regions susceptible to neurodegeneration in AD. Cutler et al., examined the distribution of several lipids in normal aging human subjects and AD patients. Long chain ceramides

(d24:1) were not only found to accumulate during normal aging in control subjects, but showed a significant increase in the middle frontal gyrus of AD patients compared to controls, an area highly susceptible to neurodegeneration. Examination of long chain ceramide levels in the cerebellum of AD patients, an area generally spared from neurodegenerative damage, showed no such increase in long chain ceramides, indicating that there are regional differences in long chain ceramide accumulation that may be correlated to neurodegeneration in AD. Additionally, the degree of accumulation of long chain ceramides was found to be correlated with the severity of AD pathology. The authors further examined the interaction of long chain ceramides with A β in hippocampal neurons and saw an increase in long chain ceramides in response to the exogenous administration of A β 1-42. The increase in long chain ceramides was correlated with an increase in oxidative stress, as measured by lipid peroxidation product 4-hydroxynonenal (HNE), further supporting the possibility of mechanistic interaction between long chain ceramides and neurodegeneration (Cutler et al., 2004). Overall, the accumulation of these ganglioside species represents a potential mechanism of toxicity in the AD brain and is worthy of further investigation.

Restoring ganglioside homeostasis in the early and later stages of AD progression is gaining interest as a therapeutic intervention for AD. Contrary to the hypothesized pathological role of GM1 in toxic A β fibril formation, exogenously administered GM1 has demonstrated therapeutic benefits both pre-clinically and clinically in AD. GM1 administration in the presence of A β 1-40 or A β 1-42 injected into the ventricles of rats led to reduced memory impairments on the novel object recognition (NOR) task and Morris water maze and was associated with a decrease in oxidative stress and the maintenance of K⁺-Na⁺ ATPase activity (Kreutz et al., 2013; Yang et al., 2013). In a human clinical trial, several AD patients were treated with GM1 through continual ventricular injections for a period of 12 m. The progression of neural deterioration ceased in treated patients while increases in cerebral blood flow were observed. GM1-treated patients showed improvements in motor skills and cognitive performance in reading, writing, and comprehension (Svennerholm et al., 2002). These studies highlight the potential therapeutic interactions of GM1 in AD. Treatments targeting the accumulation of simple gangliosides have also demonstrated promise in pre-clinical models of AD. When Dutch APP mice were

treated with a small molecule pharmacological chaperone that increases the activity of β -Hex, resulting in a decrease of GM2 levels, anxiety was reduced and learning behaviours improved on the novel object recognition task (NOR) which was associated with a reduction in GA β in the subiculum and perirhinal cortex (Knight et al., 2014). Thus, targeting ganglioside dysregulation has shown therapeutic benefits in AD models and is worthy of further investigation.

1.5 Chloroquine

The ideal intervention for the prevention of ganglioside dysregulation in the brain would block both the degradation of protective complex gangliosides and the accumulation of toxic simple gangliosides in the brain. While there is currently no known compound which can selectively accomplish this task, it is possible to transiently block lysosomal activity, thus disrupting ganglioside catabolism. N-(7-chloroquinolin-4-yl)-N,N-diethyl-pentane-1,4-diamine, or Chloroquine (CQ), is best known as an anti-malarial agent. Pharmacologically, CQ is a weak base leading to its accumulation in acidic cellular organelles, such as lysosomes. The accumulation of CQ in lysosomes leads to an increase in vacuolar pH and the subsequent disruption of acidic lysosomal enzymes (Poole & Ohkuma, 1981; Wang et al., 2016). CQ is characterized by its ability to inhibit autophagy, act as an anti-inflammatory agent, and alter lipid composition through disruption of metabolic enzymes.

The autophagy-blocking properties of CQ have demonstrated utility as a therapeutic agent in oncology, revealing another important function of the compound. CQ can improve sensitivity of tumours to chemotherapy and prevent metastasis (Zhang et al., 2015). One mechanism with which it has been shown to exert these effects is through stabilization and normalization of tumor vasculature by modulating Notch-1 activity, pointing to its vasculo-protective properties (Maes et al., 2014). Indeed, systemically-administered CQ has demonstrated a neuroprotective effect against damage to the blood brain barrier in mice (Mielke, Murphy, Maritz, Bengualid, & Ivy, 1997). These protective effects of CQ on the vasculature may be particularly useful as a therapeutic for vascular injuries, such as strokes.

The anti-inflammatory properties of CQ garnered interest in the compound as a therapeutic for inflammatory disorders including rheumatoid arthritis. A series of human clinical trials led to the conclusion that CQ acts as an effective anti-rheumatic compound in roughly 90% of patients, although treatment was most effective when paired with immunosuppressive medications (Ferraz et al., 1994; Freedman & Steinberg, 1960; Popert, Meijers, Sharp, & Bier, 1961). Pathological inflammation is also a hallmark of the ischemic cascade and CQ has been shown to downregulate pro-inflammatory cytokines and mediate inflammatory responses through inhibition of toll-like receptor (TLR)-3 after stroke (Cui et al., 2013). CQ further confers protection after a neurodegenerative injury by reducing ROS and inhibiting autophagy (Hirata et al., 2011). The inhibition of autophagy, as previously mentioned, is of particular relevance to stroke therapies due to prolonged environmental stressors which can promote the over-activation of autophagy pathways, leading to cell death (Li, Tian, Long, Chen, & Lu, 2016). Thus, CQ has a number of neuroprotective effects that make it a promising therapeutic intervention for strokes.

CQ also exhibits a strong interaction with lipids (Pfau et al., 1997) and has been used to inhibit the degradation of gangliosides both *in vitro* and *in vivo*, leading to the accumulation of complex gangliosides (Marchesini, Benaglia, Piccinotti, Bresciani, & Preti, 1998; Pfau et al., 1997). CQ disrupts the activity of lysosomal enzymes β -Gal and β -Hex leading to an increase in GM1 levels and a decrease in GM1 degradation products GM2 and GM3 (Riboni, Caminiti, Bassi, & Tettamanti, 1995; Yuyama, Yamamoto, & Yanagisawa, 2006). Pfau et al., administered a low dose of CQ both pre-natally and post-natally in rat pups in order to examine intrauterine effects of CQ on dendritic maturation in the hippocampus and found that CQ increased GM1 and decreased GM3 levels in pre-natal rats with an increase in GM1 levels also observed post-natally. Low dose CQ resulted in a significant elongation of apical and basilar dendrites of CA3 neurons and early formation of dendritic spines in the CA1 region of the hippocampus, however, the functional consequences of this altered dendritic architecture remains unclear (Pfau et al., 1997). Overall, CQ's ability to transiently block the degradation of complex gangliosides makes it a useful tool to examine the potential therapeutic benefits of preventing ganglioside dysregulation in stroke and AD.

1.6 MALDI IMS

Mass spectrometry (MS) is an analytical technique that detects the mass-to-charge ratio (m/z) of ionized molecules (Zaima, Hayasaka, Goto-Inoue, & Setou, 2010). The imaging component of MS technologies is a fairly recent development and has opened the door to previously unattainable spatial distribution information. This is particularly true in the area of lipidomics, where visualization of lipids in tissue sections previously relied upon techniques such as Immunohistochemistry (IHC). These techniques are especially problematic where membrane lipids are concerned due to their hydrophobic core being embedded within the plasma membrane and thus inaccessible for antibody-epitope binding. Antibodies for the various ganglioside species, if they exist, can only differentiate between ganglioside species based on their hydrophilic oligosaccharide domain. While this information may provide a general idea of ganglioside distribution patterns, it lacks the required specificity to reach meaningful biological conclusions on its own. Alternatively, ganglioside expression has been quantified using thin layer chromatography techniques, however these techniques require homogenization of tissue samples for lipid extraction which can be problematic when examining ganglioside distribution in discrete brain regions.

There are three main ionization platforms which can be paired with an imaging modality for imaging MS experiments, each with its own advantages and disadvantages (Barceló-coblijn & Fernández, 2015; Chaurand, 2012): Matrix-Assisted Laser Desorption/Ionization (MALDI) uses a laser to ablate laser-absorbing matrix-coated samples under vacuum to achieve ionization of intact analytes of a wide molecular weight range from metabolites to proteins, Secondary Ion Mass Spectrometry (SIMS) uses a primary ion beam to sputter the surface of the sample then collects and analyses secondary ions, producing primarily fragmented ions in most cases (Guerquin-Kern, Wu, Quintana, & Croisy, 2005), Desorption Electrospray Ionization (DESI) requires minimal sample preparation and takes place under atmospheric pressure but has diminished sensitivity for larger molecular weight analytes (Wiseman & Laughlin, 2005). Adaptations and evolution in technologies are leading to increasing variations and complementary pairings in

ionization sources to maximize the specific advantages of each and customize the technology to suit the desired experimental paradigm (Monroe et al., 2008; Trimpin & Deinzer, 2007; Zhang, Wang, Liu, Han, & Xiong, 2016). Most importantly, IMS technology is capable of simultaneously detecting and imaging the ionic distribution of numerous molecules in a label-free manner from a variety of biological samples such as animal and human tissues, plants, and bacteria. MALDI IMS can detect a wide range of molecules, from very small molecules ($m/z < 1000$) to large molecules ($m/z > 100$ kDa), making it very versatile in experimental applications (Svatos, 2010; Yates, 1998; Zaima et al., 2010). Because the mass range of a-series gangliosides falls within an m/z of 1000 – 2500 and high spatial resolution is required to examine discrete brain structures, MALDI IMS provides the ideal imaging platform for the detection and visualization of gangliosides in the brain.

Sample preparation, including tissue freezing, sectioning, matrix selection, and method of matrix deposition all play a critical role in determining the quality of MALDI IMS data (Chaurand, 2012). It is preferable that samples for MALDI IMS remain chemically unmodified for analysis, which is why flash freezing, using either dry ice or liquid nitrogen, are generally used during sample preparation as opposed to chemical fixation. Further, chemical fixation using formaldehyde is generally avoided due to cross-linking of proteins which can disrupt and/or distort MALDI data (Zaima et al., 2010). Ionization efficiency, which refers to the number of ions generated relative to the total number of molecules consumed, is a critical factor to consider during sample preparation and is influenced by the thickness of the tissue section (Murray et al., 2013; Sugiura, Shimma & Setou, 2006). Molecules with a lower molecular weight can be imaged from sections between 5 – 20 μm thick while it is recommended that thinner sections (2 – 5 μm) be used for molecules with a higher molecular weight (Zaima et al., 2010).

MALDI IMS requires the coating of a matrix to facilitate ionization of analytes in the sample. The matrix can have several important roles in MALDI IMS depending on the solvent system used including: 1) extraction of molecules from the sample based on their chemical properties, 2) absorbing laser energy and transferring of the energy to analyte molecules, and 3) influencing spatial imaging resolution. Homogenous deposition of the

matrix on the sample and minimization of analyte delocalization during matrix deposition are crucial for achieving high spatial resolution. Gangliosides have a negative charge due to the sialic acid residues on their structure, which means they are primarily imaged in negative polarity ion mode when analyzed via MALDI IMS. This negative charge also influences the types of matrices that will be used during sample preparation, as some matrix-solvent mixtures have a greater affinity for extracting negatively charged lipids than others (Thomas, Charbonneau, Fournaise, & Chaurand, 2012). The method of matrix deposition is a factor which is particularly important when imaging lipids, such as gangliosides. While wet matrix application techniques, wherein a solvent is used to dissolve a powdered matrix, are most common, they present an increased likelihood of large crystals forming on the surface of the sample as well as an increased risk of molecular delocalization, both of which can greatly reduce detection and imaging quality. Dry matrix application techniques, such as sublimation, can circumvent these limitations. Additional factors such as solvent rinses and incubation times may also lead to improvement in ganglioside signals at the expense of possible analyte delocalization (Angel, Spraggins, Baldwin, & Caprioli, 2012; **Appendix 1**).

Once in the MALDI MS instrument, MS spectra are acquired through a series of repetitive laser pulses at predefined x-y coordinates. Broadly, the sample surface is irradiated using laser energy wherein protonation or deprotonation of molecules leads to the formation of either positively or negatively charged ions. Time-of-flight (TOF) analyzers are most common for MALDI IMS applications and allow ions to separate based on their m/z ratio (Dreisewerd, 2003; Zaima et al, 2010). The ions are finally quantified by a detector and MALDI MS data is then represented as peaks on a mass spectrum that indicates the relative abundance of each ion within the sample. This analytical data is accompanied by a “molecular map” of the ionic distribution of each peak across the intact tissue section formed by the numerous laser acquisition points. Because of the variability that is inherent in the sample preparation process and run-to-run variation related to ionization efficiency and background matrix suppression, MALDI IMS is considered a semi-quantitative technique. Various normalization and statistical approaches can be implemented to reduce errors caused by between-scan variability in order to pool data from multiple imaging experiments.

MALDI IMS has already been used to address various fundamental questions regarding the localization and biological role of gangliosides in the brain, including in pre-clinical models of neurodegenerative disease and injury (Colsch, Jackson, Dutta, & Woods, 2011; Dufresne et al., 2017; Hirano-Sakamaki et al., 2015; Whitehead et al., 2011; Woods et al., 2013). For example, recent evidence using a combination of MALDI IMS and IHC examined ganglioside distribution in a Tg mouse model of AD. Tg Arc/Sw mice, which develop A β plaques, contained significantly increased levels of simple gangliosides GM2 d18:1 and GM3 d18:1 and d20:1, but not GM1 in cortical and hippocampal A β plaques (Kaya et al., 2017). The authors suggest that this increase in simple gangliosides are likely a result of complex ganglioside degradation or inhibition of lysosomal storage and degradation. Because of the semi-quantitative nature of MALDI IMS, pairing the technique with another form of ganglioside detection has become common and can aide in interpreting findings (Jones et al., 2017; Kaya et al., 2017).

1.7 Rationale and objectives

Gangliosides belong to a large family of glycosphingolipids enriched in the CNS that have important regulatory functions on the cell plasma membrane. Their abundance is tightly regulated by lysosomal enzymes in order for each species to carry out their unique functions (Yamamoto et al., 1996; Yu, Nakatani, & Yanagisawa, 2009). Alterations in ganglioside homeostasis is hypothesized to play an important role in the pathogenesis of neurodegenerative diseases and injuries (Ariga et al., 2013; Cutler et al., 2004; Whitehead et al., 2011; Woods et al., 2013), however, the nature of the relationship between neurodegeneration and ganglioside dysregulation remains unclear.

Novel imaging technologies, such as MALDI IMS, can be used to examine the distribution and abundance of gangliosides with greater sensitivity and specificity than traditional lipid imaging techniques, making it the ideal tool for a comprehensive and detailed analysis of a-series gangliosides in the brain.

The overarching hypothesis of these studies was that ganglioside dysregulation occurs in the aging brain and in response to neurodegenerative injuries and that restoring ganglioside homeostasis will result in functional benefits after injury in rats.

The main objectives of this study were: 1) Examine ganglioside dysregulation in response to neurodegenerative injuries of varying severity to determine if specific patterns of alteration are associated with the neurodegenerative response (Chapter 2); 2) Examine changes in the ganglioside long chain base throughout the brain during aging in a-series gangliosides (Chapter 3); 3) Determine if a-series gangliosides are altered differently in the normal aging rat brain versus a rat model of prodromal AD to identify specific patterns of dysregulation which may be tied to the development of neurodegeneration in the aging brain (Chapter 4) and; 4) Examine the potential pathological and functional benefits associated with preventing ganglioside dysregulation after stroke (Chapter 5).

In Chapter 2, the degree of toxic simple ganglioside accumulation was found to be correlated with the severity of the neurodegenerative insult, with the d20:1 species often showing a more severe alteration in response to the injury than the d18:1 species. Little is known on the role of d20:1 versus d18:1 species of gangliosides, however, the d20:1 species are hypothesized to accumulate in an age-dependent manner relative to the d18:1. In chapter 3, the ratio of d20:1 to d18:1 species of A-series gangliosides was examined during aging in Fischer rats. Interestingly, only complex gangliosides were observed to have an age-dependent increased in the d20:1/d18:1 ratio whereas this ratio decreased for simple gangliosides across the brain, with the exception of white matter regions. In chapter 4, A-series gangliosides were examined individually in Wt and Tg APP rats in order to better understand the age-dependent alterations of simple and complex gangliosides during normal aging and in the prodromal stages of AD. Interestingly, an age-dependent depletion of complex ganglioside GD1 d18:1 was observed in the white matter of the brain. Additionally, Tg APP21 rats were found to have increased levels of toxic ganglioside species GM2 and GM3 than their Wt counterparts, pointing to a toxic pattern of ganglioside dysregulation in Tg APP rats. Finally, in chapter 5, an intervention using a pharmacological compound (chloroquine) aimed at preventing ganglioside dysregulation was examined after a severe stroke injury. Restoration of ganglioside homeostasis after

stroke was associated with reduced motor and cognitive impairment in Wistar rats. This work highlights the important role of ganglioside dysregulation in the rat brain during aging and neurodegeneration and the therapeutic benefits associated with maintaining ganglioside homeostasis after stroke injury.

1.8 References

- Abate, L. E., Mukherjee, P., & Seyfried, T. N. (2006). Gene-linked shift in ganglioside distribution influences growth and vascularity in a mouse astrocytoma. *Journal of Neurochemistry*, *98*, 1973–1984.
- Allende, M. L., & Proia, R. L. (2002). Lubricating cell signaling pathways with gangliosides. *Current Opinion in Structural Biology*, *12*(5), 587–592.
- Amtul, Z., Nikolova, S., Gao, L., Keeley, R. J., Bechberger, J. F., Fisher, A. L., Whitehead, S.N. & Cechetto, D. F. (2014). Neurobiology of Aging Comorbid Ab toxicity and stroke : hippocampal atrophy , pathology , and cognitive deficit. *Neurobiology of Aging*, 1–10.
- Ando, S., Toyoda, Y., Nagai, Y., & Ikuta, F. (1984). Alterations in brain gangliosides and other lipids of patients with Creutzfeldt-Jakob disease and subacute sclerosing panencephalitis (SSPE). *The Japanese Journal of Experimental Medicine*, *54*(6), 229–234.
- Angel, P. M., Spraggins, J. M., Baldwin, H. S., & Caprioli, R. (2012). Enhanced Sensitivity for High Spatial Resolution Lipid Analysis by Negative Ion Mode Matrix Assisted Laser Desorption Ionization Imaging Mass Spectrometry. *Analytical Chemistry*, *84*, 1557–1564.
- Appelman, A. P. A., Exalto, G., Graaf, Y. Van Der, Biessels, G., Mali, W., & Geerlings, M. (2009). White Matter Lesions and Brain Atrophy : More than Shared Risk Factors? A systematic review. *Cerebrovasc Dis*, *28*, 227–242.
- Argentino, C., Sacchetti, M., Toni, D., Savoini, G., D’Arcangelo, E., Erminio, F., & Fieschi, C. (1989). GM1 Ganglioside Therapy in Acute Ischemic Stroke. *Stroke*, *20*(9), 1143–1149.
- Ariga, T., Itokazu, Y., McDonald, M. P., Hirabayashi, Y., Ando, S., & Yu, R. K. (2013). Brain gangliosides of a transgenic mouse model of Alzheimer’s disease with deficiency in GD3-synthase: expression of elevated levels of a cholinergic-specific ganglioside, GT1a α . *ASN Neuro*, *5*(2), 141–8. <https://doi.org/10.1042/AN20130006>
- Ariga, T., McDonald, M. P., & Yu, R. K. (2008). Role of ganglioside metabolism in the pathogenesis of Alzheimer’s disease--a review. *Journal of Lipid Research*, *49*(6), 1157–75.
- Attems, J., Jellinger, K. A., & Lintner, F. (2005). Alzheimer’s disease pathology influences

severity and topographical distribution of cerebral amyloid angiopathy. *Acta Neuropathologica*, 110(3), 222–231.

- Attems, J., Jellinger, K., Thal, D. R., & Van Nostrand, W. (2011). Review : Sporadic cerebral amyloid angiopathy. *Neuropathology and Applied Neurobiology*, 37, 75–93.
- Avrova, N. F., Victorov, I. V., Tyurin, V. A., Zakharova, I. O., Sokolova, T., Andreeva, N., ... Gonchar, V. (1998). Inhibition of glutamate-induced intensification of free radical reactions by gangliosides: possible role in their protective effect in rat cerebellar granule cells and brain synaptosomes. *Neurochemical Research*, 23(7), 945–952.
- Aydin, M., Cengiz, S., Ag, B., & Han, E. (2000). Age-related Changes in GM1 , GD1a , GT1b Components of Gangliosides in Wistar Albino Rats. *Cell Biochemistry and Function*, 45(March 1999), 41–45.
- Bales, K. R., Du, Y., Holtzman, D., Cordell, B., & Paul, S. (2000). Neuroinflammation and Alzheimer's disease: critical roles for cytokine/A β -induced glial activation, NF- κ B, and apolipoprotein E. *Neurobiology of Aging*, 21(3), 427–432.
- Bandaru, V., Troncoso, J., Wheeler, D., Pletnikova, O., Wang, J., Conant, K., & Haughey, N. (2009). ApoE4 disrupts sterol and sphingolipid metabolism in Alzheimer's but not normal brain. *Neurobiology of Aging*, 30(4), 591–599.
- Barber, P. A., Zhang, J., Demchuk, A. M., & Hill, M. D. (2001). Why are stroke patients excluded from TPA therapy? An analysis of patient eligibility. *Neurology*, 56(8), 1015–1020.
- Barceló-coblijn, G., & Fernández, J. A. (2015). Mass spectrometry coupled to imaging techniques : the better the view the greater the challenge. *Frontiers in Physiology*, 6(3), 1–7.
- Barrier, L., Ingrand, S., Damjanac, M., Rioux Bilan, A., Hugon, J., & Page, G. (2007). Genotype-related changes of ganglioside composition in brain regions of transgenic mouse models of Alzheimer's disease. *Neurobiology of Aging*, 28(12), 1863–72.
- Bassi, S., Albizzati, M. G., Sbacchi, M., Frattola, L., & Massarotti, M. (1984). Double-blind evaluation of monosialoganglioside (GM1) therapy in stroke. *Journal of Neuroscience Research*, 12(2–3), 493–498.
- Berselli, P., Zava, S., Sottocornola, E., Milani, S., Berra, B., & Colombo, I. (2006). Human GM 3 synthase : A new mRNA variant encodes an NH 2 -terminal extended form of the protein. *Biochimica et Biophysica Acta*, 1759, 348–358.
- Bisel, B., Pavone, F. S., & Calamai, M. (2014). GM1 and GM2 gangliosides : recent developments. *Biomol Concepts*, 5(1), 87–93.
- Bogaert, L., Scheller, D., Moonen, J., Sarre, S., & Smolders, I. (2000). Neurochemical changes and laser Doppler flowmetry in the endothelin-1 rat model for focal cerebral ischemia. *Brain Research*, 887(2), 266–275.
- Braune, S. (1991). Is ganglioside GM1 effective in the treatment of stroke? *Drugs & Aging*, 1(1), 57–66.

- Candelise, L. (2002). Gangliosides for Acute Ischemic Stroke. *Stroke*, 33(9), 2336–2336.
- Carolei, A., Fieschi, C., & Bruno, R. (1991). Monosialoganglioside GM1 in cerebral ischemia. *Cerebrovascular and Brain Metabolism Reviews*, 3(2), 134–157.
- Carrieri, G., Bonafè, M., Luca, D. M., Rose, G., & Varcasia, O. (2001). Mitochondrial DNA haplogroups and APOE4 allele are non-independent variables in sporadic Alzheimer's disease. *Human Genetics*, 108(3), 194–198.
- Castilho, R. F., Ward, M. W., & Nicholls, D. G. (1999). Oxidative Stress, Mitochondrial Function, and Acute Glutamate Excitotoxicity in Cultured Cerebellar Granule Cells. *Journal of Neurochemistry*, 72, 1394–1401.
- Caughey, G., Roughead, E. E., Pratt, N., Killer, G., & Gilbert, A. L. (2011). Stroke risk and NSAIDs: an Australian population-based study. *MJA*, 195(9), 525–529.
- Ceccarelli, B., Aporti, F., & Finesso, M. (1976). Effects of brain gangliosides on functional recovery in experimental regeneration and reinnervation. *Adv Exp Med Biol*.
- Cechetto, D. F., Hachinski, V., & Whitehead, S. N. (2008). Vascular risk factors and Alzheimer's disease. *Expert Review of Neurotherapeutics*, 8(5), 743–50.
- Chan, K., Lanthier, P., Liu, X., Sandhu, J. K., Stanimirovic, D., & Li, J. (2009). MALDI mass spectrometry imaging of gangliosides in mouse brain using ionic liquid matrix. *Analytica Chimica Acta*, 639(1–2), 57–61. <https://doi.org/10.1016/j.aca.2009.02.051>
- Chan, R. B., Oliveira, T. G., Cortes, E. P., Honig, L. S., Duff, K. E., Small, S. a, ... Di Paolo, G. (2012). Comparative lipidomic analysis of mouse and human brain with Alzheimer disease. *The Journal of Biological Chemistry*, 287(4), 2678–88.
- Chang, C.Y., Ke, D.S. & Chen, J.Y. (2009). Essential fatty acids and human brain. *Acta Neurol Taiwan*, 18(4), 231-241.
- Chaurand, P. (2012). Imaging mass spectrometry of thin tissue sections: a decade of collective efforts. *Journal of Proteomics*, 75(16), 4883–92.
- Cheng, Y., Wang, M., Yu, Y., Lawson, J., Funk, C. D., & Fitzgerald, G. A. (2006). Cyclooxygenases, microsomal prostaglandin E synthase-1, and cardiovascular function. *The Journal of Clinical Investigation*, 116(5).
- Chiavegatto, S., Sun, J., Nelson, R. J., & Schnaar, R. L. (2000). A functional role for complex gangliosides: motor deficits in GM2/GD2 synthase knockout mice. *Experimental Neurology*, 166(2), 227–34.
- Choi, H., Chung, T., Kang, S., Lee, Y., Ko, J., Kim, J., & Kim, C. (2006). Ganglioside GM3 modulates tumor suppressor PTEN-mediated cell cycle progression — transcriptional induction of p21 WAF1 and p27 kip1 by inhibition of PI-3K / AKT pathway. *Glycobiology*, 16(7), 573–583.
- Choo-Smith, L. P., Garzon-Rodriguez, W., Glabe, C., & Surewicz, W. (1997). Acceleration of amyloid fibril formation by specific binding of Aβ(1-40) peptide to ganglioside-containing membrane vesicles. *The Journal of Biological Chemistry*, 272(37), 22987–

22990.

- Chung, T.-W. W., Choi, H.-J. J., Kim, S.-J. J., Kwak, C.-H. H., Song, K.-H. H., Jin, U.-H. H., ... Kim, C.-H. H. (2014). The ganglioside GM3 is associated with cisplatin-induced apoptosis in human colon cancer cells. *PloS One*, *9*(5).
- Cifuentes, D., Poittevin, M., Dere, E., Broquères-you, D., Bonnin, P., Benessiano, J., ... Lévy, B. I. (2015). Hypertension Accelerates the Progression of Alzheimer-Like Pathology in a Mouse Model of the Disease. *Hypertension*, *65*, 218–224.
- Clarke, J. T. R., Mahuran, D. J., Sathe, S., Kolodny, E. H., Rigat, B. A., Raiman, J. A., & Tropak, M. B. (2011). An open-label Phase I / II clinical trial of pyrimethamine for the treatment of patients affected with chronic GM2 gangliosidosis (Tay – Sachs or Sandhoff variants). *Molecular Genetics and Metabolism*, *102*(1), 6–12.
- Colsch, B., Jackson, S. N., Dutta, S., & Woods, A. S. (2011). Molecular Microscopy of Brain Gangliosides: Illustrating their Distribution in Hippocampal Cell Layers. *ACS Chemical Neuroscience*, *2*(4), 213–222.
- Conzelmann, E., & Sandhoff, K. (1983). Partial enzyme deficiencies: residual activities and the development of neurological disorders. *Developmental Neuroscience*. Karger Publishers.
- Cui, G., Ye, X., Zuo, T., Zhao, H., Zhao, Q., Chen, W., & Hua, F. (2013). Chloroquine pretreatment inhibits toll-like receptor 3 signaling after stroke. *Neuroscience Letters*, *548*, 101–104.
- Cutler, R. G., Kelly, J., Storie, K., Pedersen, W. A., Tammara, A., Hatanpaa, K., ... Mattson, M. P. (2004). Involvement of oxidative stress-induced abnormalities in ceramide and cholesterol metabolism in brain aging and Alzheimer’s disease. *Proc.Natl.Acad.Sci.U.S.A*, *101*(7), 2070–2075.
- Daniotti, J. L., & Iglesias-Bartolomé, R. (2011). Metabolic pathways and intracellular trafficking of gangliosides. *IUBMB Life*, *63*(7), 513–520.
- Dawson, G., Matalon, R., & Dorfman, A. (1972). Glycosphingolipids in Cultured Human Skin Fibroblasts. *The Journal of Biological Chemistry*, *247*(18), 5944–5950.
- Debnath, J., Baehrecke, E. H., & Kroemer, G. (2005). Does Autophagy Contribute to Cell Death? *Autophagy*, *1*(2), 66–74.
- Desplats, P. A., Denny, C. A., Kass, K. E., Gilmartin, T., Head, S. R., Sutcliffe, J. G., ... Thomas, E. A. (2007). Glycolipid and ganglioside metabolism imbalances in Huntington’s disease. *Neurobiology of Disease*, *27*(3), 265–277.
- Di Pardo, A., Amico, E., & Maglione, V. (2016). Impaired levels of gangliosides in the corpus callosum of Huntington disease animal models. *Frontiers in Neuroscience*, *10*, 1–8.
- Dichgans, M., & Leys, D. (2017). Vascular Cognitive Impairment. *Circulation Research*, *120*(3), 573–591.

- Dodge, H., Chang, C., Kamboh, I., & Ganguli, M. (2012). Risk of Alzheimer's disease incidence attributable to vascular disease in the population. *Alzheimers Dement*, 7(3), 356–360.
- Dreisewerd, K. (2003). The Desorption Process in MALDI. *Chemical Reviews*, 103(2), 395–426.
- Dufresne, M., Guneyesu, D., Patterson, N. H., Marcinkiewicz, M. M., Regina, A., Demeule, M., & Chaurand, P. (2017). Multimodal detection of GM2 and GM3 lipid species in the brain of mucopolysaccharidosis type II mouse by serial imaging mass spectrometry and immunohistochemistry. *Analytical and Bioanalytical Chemistry*, 409, 1425–1433.
- Fantini, J., Yahi, N., & Garmy, N. (2013). Cholesterol accelerates the binding of Alzheimer's β -amyloid peptide to ganglioside GM1 through a universal hydrogen-bond-dependent sterol tuning of glycolipid conformation. *Frontiers in Physiology*, 4(120), 1–10.
- Ferrari, G., & Greene, L. A. (1996). Prevention of neuronal apoptotic death by neurotrophic agents and ganglioside GM1: insights and speculations regarding a common mechanism. *Perspectives on Developmental Neurobiology*, 3(2), 93–100.
- Ferraz, M. B., Pinheiro, G. R. C., Helfenstein, M., Albequerque, E., Rezende, C., & Roimicher, L. (1994). Combination therapy with methotrexate and chloroquine in rheumatoid arthritis: A multicenter randomized placebo-controlled trial. *Scandinavian Journal of Rheumatology*, 23(5), 231–236. 1
- Ferreira, S. T., Vieira, M. N. N., & Felice, F. G. De. (2007). Critical Review Soluble Protein Oligomers as Emerging Toxins in Alzheimer's and Other Amyloid Diseases. *IUBMB Life*, 59(4–5), 332–345.
- Fisher, M. (1997). Characterizing the target of acute stroke therapy. *Stroke*, 28, 866–872.
- Fluri, F., Schuhmann, M. K., & Kleinschnitz, C. (2015). Animal models of ischemic stroke and their application in clinical research. *Drug Design, Development and Therapy*, 9, 3445–3454.
- Foley, P. (2010). Lipids in Alzheimer's disease: A century-old story. *Biochimica et Biophysica Acta (BBA)-Molecular and Cellular Biology*, 1801(8), 750–753.
- Freedman, A., & Steinberg, V. L. (1960). Chloroquine in rheumatoid arthritis: A double blindfold trial of treatment for one year. *Ann Rheum Dis*, 19, 243–250.
- Fujimoto, Y., Izumoto, S., Suzuki, T., Kinoshita, M., Kagawa, N., & Wada, K. (2005). Ganglioside GM3 inhibits proliferation and invasion of glioma. *Journal of Neuro-Oncology*, 71, 99–106.
- Fuxe, K., Bjelke, B., Andbjør, B., Grahn, H., Rimondini, R., & Agnati, L. F. (1997). Endothelin 1 induced lesions of the frontoparietal cortex of the rat. A possible model of focal cortical ischemia. *Neuroreport*. LWW.
- Gearing, M., Mirra, S. S., Hedreen, J. C., Sumi, S. M., Hanson, L., & Heyman, A. (1995).

- The Consortium to Establish a Registry for Alzheimer's Disease (CERAD). Part X. Neuropathology confirmation of the clinical diagnosis of Alzheimer's disease. *Neurology*, 45(3), 451–466.
- Goate, A., Chartier-Harlin, M-C., Mullan, M., Brown, J., Crawford, F., Fidani, L., Giuffra, L., ... & Hardy, J. (1991). Segregation of a missense mutation in the amyloid precursor protein gene with familial Alzheimer's disease. *Nature*, 349, 704-706. doi:10.1038/349704a0
- Gold, G., Herrmann, R., Canuto, A., Hof, P. R., Michel, J., Bouras, C., & Giannakopoulos, P. (2005). Cognitive Consequences of Thalamic , Basal Ganglia , and Deep White Matter Lacunes in Brain Aging and Dementia. *Stroke*, 1184–1189. <https://doi.org/10.1161/01.STR.0000166052.89772.b5>
- Gottfries, C., Jungbjer, B., Karlsson, I., & Svennerholm, L. (1996). Reductions in membrane proteins and lipids in basal ganglia of classic Alzheimer disease patients. *Alzheimer Dis Assoc Disord*, 10(2), 77–81.
- Grammas, P., Yamada, M., & Zlokovic, B. (2002). The cerebrovasculature: a key player in the pathogenesis of Alzheimer's disease. *Journal of Alzheimer's Disease*, 4(3), 217–223.
- Grimm, M. O. W., Zinser, E. G., Grösgen, S., Hundsdörfer, B., Rothhaar, T. L., Burg, V. K., ... Hartmann, T. (2012). Amyloid precursor protein (APP) mediated regulation of ganglioside homeostasis linking Alzheimer's disease pathology with ganglioside metabolism. *PloS One*, 7(3), e34095.
- Guerquin-Kern, J. L., Wu, T. D., Quintana, C., & Croisy, A. (2005). Progress in analytical imaging of the cell by dynamic secondary ion mass spectrometry (SIMS microscopy). *Biochimica et Biophysica Acta: General Subjects*, 1724(3), 228–238.
- Gullino, P. M. (2017). Prostaglandins and Gangliosides of Tumor Microenvironment : Their Role in Angiogenesis. *Acta Oncologica*, 34(3), 439–441.
- Ha, K.-T. T., Lee, Y. C., Cho, S.-H., Kim, J.-K., & Kim, C. H. (2004). Molecular characterization of membrane type and ganglioside-specific sialidase (Neu3) expressed in E. coli. *Molecules and Cells*, 17(2), 267–273.
- Haass, C., & Selkoe, D. J. (2007). Soluble protein oligomers in neurodegeneration: lessons from the Alzheimer's amyloid β -peptide. *Nature Reviews Molecular Cell Biology*, 8, 101–112.
- Hachinski, V. (2008). Shifts in Thinking About Dementia. *JAMA*, 300(18), 2172–2173.
- Hachinski, V. C., Bowler, J. V., & Loeb, C. (1993). Vascular dementia. *Neurology*, 43(10), 2159–2160.
- Hachinski, V. C., & Potter, P. (1987). Leuko-araiosis. *Archives of Neurology*, 44(1), 21–23.
- Hachinski, V., & Munoz, D. (2000). Vascular factors in cognitive impairment--where are we now? *Annals of the New York Academy of Sciences*, 903(519), 1–5.

- Hadaczek, P., Wu, G., Sharma, N., Ciesielska, A., Bankiewicz, K., Davidow, A. L., ... Ledeen, R. W. (2015). GDNF signaling implemented by GM1 ganglioside; failure in Parkinson's disease and GM1-deficient murine model. *Experimental Neurology*, 263, 177–189.
- Hakomori, S. (2002). The glycosynapse. *Proceedings of the National Academy of Sciences*, 99(5), 225–232.
- Harduin-lepers, A., Mollicone, R., Delannoy, P., & Oriol, R. (2005). The animal sialyltransferases and sialyltransferase-related genes : a phylogenetic approach. *Glycobiology*, 15(8), 805–817.
- Hardy, J. & Higgins, G. (1992). Alzheimer's disease: The amyloid cascade hypothesis. *Science*, 256(5054)
- Hawkins, K. E., Demars, K. M., Alexander, J. C., Leon, L. G. De, Pacheco, S. C., Graves, C., ... Febo, M. (2017). Targeting resolution of neuroinflammation after ischemic stroke with a lipoxin A 4 analog : Protective mechanisms and term effects on neurological recovery. *Brain and Behavior*, 7, e00688. 8
- Herrero, M. T., Perez-Otan, I., Oset, C., Kastner, A., & Hirsch, E. C. (1993). GM-1 ganglioside promotes the recovery of surviving midbrain dopaminergic neurons in MPTP-treated monkeys. *Neuroscience*, 56(4), 965–972.
- Higashi, K., Kubo, H., Watanabe, H., Fujimori, K., Mikami, T., & Kaneko, H. (2011). Adipokine ganglioside GM2 activator protein stimulates insulin secretion. *FEBS Letters*, 585(16), 2587–2591.
- Hirano-Sakamaki, W., Sugiyama, E., Hayasaka, T., Ravid, R., Setou, M., & Taki, T. (2015). Alzheimer's disease is associated with disordered localization of ganglioside GM1 molecular species in the human dentate gyrus. *FEBS Letters*, 589(23), 3611–3616.
- Hirata, Y., Yamamoto, H., Shukry Moursy Atta, M., Mahmoud, S., Oh-hashii, K., & Kiuchi, K. (2011). Chloroquine inhibits glutamate-induced death of a neuronal cell line by reducing reactive oxygen species through sigma-1 receptor. *Journal of Neurochemistry*, 119, 839–847.
- Ho, T. W., Willison, H. J., Nachamkin, I., Li, C. Y., Veitch, J., Ung, H., ... McKhaan, J. (1999). Anti-GD1a antibody is associated with axonal but not demyelinating forms of Guillain-Barre syndrome. *Annals of Neurology*, 45(2), 168–173.
- Hoffbrand, B., Bungley, P., Oppenheimer, S., & Sheldon, C. (1988). Short report Trial of ganglioside GM 1 in acute stroke. *Journal of Neurology, Neurosurgery, and Psychiatry*, 51, 1213–1214.
- Hooper, N. M. (1998). Membrane biology : Do glycolipid microdomains really exist ? *Current Biology*, 8(4), 114–116.
- Howells, D. W., Porritt, M. J., Rewell, S. S. J., Collins, V. O., Sena, E. S., Worp, H. B. Van Der, ... Macleod, M. R. (2010). Different strokes for different folks : the rich diversity of animal models of focal cerebral ischemia. *Journal of Cerebral Blood Flow &*

Metabolism, 30(8), 1412–1431.

- Hurd, M., Martorell, P., Delavande, A., Mullen, K. J., & Langa, K. M. (2013). Monetary Costs of Dementia in the United States. *The New England Journal of Medicine*, 368, 1326–1334.
- Iadecola, C. (2013). Review The Pathobiology of Vascular Dementia. *Neuron*, 80(4), 844–866.
- Iadecola, C., & Anrather, J. (2011). The immunology of stroke: from mechanisms to translation. *Nature Medicine*, 17, 796–808.
- Inokuchi, J. (2007). Insulin Resistance as a Membrane Microdomain Disorder. *Yakugaku Zasshi*, 127(4), 579–586.
- Irizarry, M. C. (2004). Biomarkers of Alzheimer disease in plasma. *NeuroRx*, 1(2), 226–234.
- Ishii, A., Ikeda, T., Hitoshi, S., Fujimoto, I., Torii, T., Sakuma, K., ... Ikenaka, K. (2007). Developmental changes in the expression of glycogenes and the content of N-glycans in the mouse cerebral cortex. *Glycobiology*, 17(3), 261–276.
- Jellinger, K. (2002). Alzheimer disease and cerebrovascular pathology: an update. *Journal of Neural Transmission*, 109(5–6), 813–836.
- Jin, Y. P., Østbye, T., Feightner, J. W., Di Legge, S., & Hachinski, V. (2008). Joint effect of stroke and APOE 4 on dementia risk: the Canadian Study of Health and Aging. *Neurology*, 70(1), 9–16.
- Jones, E. E., Zhang, W., Zhao, X., Quiason, C., Dale, S., Shahidi-Latham, S., ... Sun, Y. (2017). Tissue Localization of Glycosphingolipid Accumulation in a Gaucher Disease Mouse Brain by LC-ESI-MS/MS and High-Resolution MALDI Imaging Mass Spectrometry. *SLAS Discovery*, 22(10).
- Kabayama, K., Sato, T., Kitamura, F., Uemura, S., Kang, B. W., Igarashi, Y., & Inokuchi, J.-I. (2005). TNF α -induced insulin resistance in adipocytes as a membrane microdomain disorder: involvement of ganglioside GM3. *Glycobiology*, 15(1), 21–29.
- Kaji, R., Kusunoki, S., Mizutani, K., Oka, N., Kojima, Y., Kohora, N., & Kimura, J. (2000). Chronic motor axonal neuropathy associated with antibodies monospecific for n-acetylgalactosaminyl GD1a. *Muscle & Nerve*, 23(5), 702–706.
- Kalaria, R. N., Bhatti, S. U., Palatinsky, E. A., Pennington, D., Shelton, E., Chan, H., & Lust, W. (1993). Accumulation of the [beta] amyloid precursor protein at sites of ischemic injury in rat brain. *Neuroreport*.
- Kalmijn, S., Feskens, E. J., Launer, L. J., & Kromhout, D. (1996). Cerebrovascular disease, the apolipoprotein e4 allele, and cognitive decline in a community-based study of elderly men. *Stroke*, 27(12), 2230–2235.
- Karpiak, S., Li, Y., & Mahadik, S. (1987). Gangliosides (GM1 and AGF2) reduce mortality due to ischemia: Protection of membrane function. *Stroke*, 184–187.

- Kaya, I., Brinet, D., Michno, W., Syvanen, S., Sehlin, D., Zetterberg, H., ... Hanrieder, J. (2017). Delineating Amyloid Plaque Associated Neuronal Sphingolipids in Transgenic Alzheimer's Disease Mice (tgArcSwe) Using MALDI Imaging Mass Spectrometry. *ACS Chemical Neuroscience*, 8, 347–355.
- Kharlamov, a, Zivkovic, I., Polo, a, Armstrong, D. M., Costa, E., & Guidotti, a. (1994). LIGA20, a lyso derivative of ganglioside GM1, given orally after cortical thrombosis reduces infarct size and associated cognition deficit. *Proceedings of the National Academy of Sciences of the United States of America*, 91(14), 6303–7.
- Kimura, N., & Yanagisawa, K. (2007). Endosomal accumulation of GM1 ganglioside-bound amyloid β -protein in neurons of aged monkey brains. *Neuroreport*, 18(16), 1669–1673.
- Knight, E. M., Williams, H. N., Stevens, A. C., Kim, S. H., Kottwitz, J. C., Morant, A. D., ... Boyd, R. E. (2014). Evidence that small molecule enhancement of β -hexosaminidase activity corrects the behavioral phenotype in Dutch APP E693Q mice through reduction of ganglioside-bound A β . *Neuroreport*, 20(1), 109–117.
- Kracun, I., Kalanj, S., Talan-hranilovic, I. J., & Cosovic, C. (1992). Cortical distribution of gangliosides in Alzheimer's disease. *Neurochemistry International*, 20(3), 433–438.
- Kreutz, F., Petry, S., Camassola, M., Schein, V., Guma, F. C. R., Beyer, N., ... Trindade, T. (2013). Alterations of membrane lipids and in gene expression of ganglioside metabolism in different brain structures in a mouse model of mucopolysaccharidosis type I (MPS I). *Gene*, 527(1), 109–114.
- Lai, T. W., Zhang, S., & Wang, Y. T. (2014). Excitotoxicity and stroke : Identifying novel targets for neuroprotection. *Progress in Neurobiology*, 115, 157–188.
- Laitinen, J., Leppiinen, R., Merenmies, J., & Rauvala, H. (1987). Binding of laminin to brain gangliosides and inhibition of laminin-neuron interaction by the gangliosid. *FEBS Letters*, 217(1), 94–100.
- Lang, Z., Guerrero, M., Li, R., & Ladisch, S. (2001). Ganglioside GD1a enhances VEGF-induced endothelial cell proliferation and migration. *Biochemical and Biophysical Research*, 282(4), 1031–1037.
- Lawrence, A. J., Patel, B., Morris, R. G., Mackinnon, A. D., Rich, P. M., Barrick, T. R., & Markus, H. S. (2013). Mechanisms of Cognitive Impairment in Cerebral Small Vessel Disease : Multimodal MRI Results from the St George's Cognition and Neuroimaging in Stroke (SCANS) Study. *PloS One*, 8(4), e61014.
- Ledeer, R. W., & Wu, G. (2015). The multi-tasked life of GM1 ganglioside, a true factotum of nature. *Trends in Biochemical Sciences*, 40(7), 407–418.
- Levit, A., Regis, A. M., Garabon, J. R., Oh, S., Desai, S. J., Rajakumar, N., ... Allman, B. L. (2017). Behavioural inflexibility in a comorbid rat model of striatal ischemic injury and mutant hAPP overexpression. *Behavioural Brain Research*, 333(March), 267–275.
- Li, C., Zhao, R., Gao, K., Wei, Z., Yaoyao, M., Ting, L., ... Cheung, Y. (2011). Astrocytes:

- implications for neuroinflammatory pathogenesis of Alzheimer's disease. *Current Alzheimer Research*, 8(1), 67–80.
- Li, L., Tian, J., Long, M. K., Chen, Y., & Lu, J. (2016). Protection against Experimental Stroke by Ganglioside GM1 Is Associated with the Inhibition of Autophagy. *PloS One*, 11(1), 1–13.
- Li, S., Hong, S., Shepardson, N. E., Walsh, D. M., Shankar, G. M., & Selkoe, D. (2009). Article Soluble Oligomers of Amyloid b Protein Facilitate Hippocampal Long-Term Depression by Disrupting Neuronal Glutamate Uptake. *Neuron*, 62(6), 788–801.
- Liu, X., Ide, J. L., Norton, I., Marchionni, M. A., Ebling, M. C., Wang, L. Y., ... Agar, N. Y. R. (2013). through the blood-brain barrier with MALDI mass spectrometry imaging. *Scientific Reports*, 3(2859), 1–7.
- Liu, Y., Li, R., & Ladisch, S. (2004). Exogenous Ganglioside G D1a Enhances Epidermal Growth Factor Receptor Binding and Dimerization. *The Journal of Biological Chemistry*, 279(35), 36481–36489.
- Longa, E., Weinstein, P., Carlson, S., & Cummins, R. (1989). Reversible Middle Cerebral Artery Occlusion Without Craniectomy in Rats. *Stroke*, 20(1), 84–91.
- Lopez, P. H. H., & Schnaar, R. L. (2009). Gangliosides in cell recognition and membrane protein regulation. *Current Opinion in Structural Biology*, 19, 549–557.
- Maegawa, G. H. B., Tropak, M., Buttner, J., Stockley, T., Kok, F., Clarke, J. T. R., & Mahuran, D. J. (2007). Pyrimethamine as a Potential Pharmacological Chaperone for Late-onset Forms of GM2 Gangliosidosis. *The Journal of Biological Chemistry*, 282(12), 9150–9161.
- Maes, H., Kuchnio, A., Peric, A., Moens, S., Nys, K., Bock, K. De, ... Agostinis, P. (2014). Article Tumor Vessel Normalization by Chloroquine Independent of Autophagy. *Cancer Cell*, 26, 190–206.
- Maillard, P., Carmichael, O., Fletcher, E., & Reed, B. (2012). Coevolution of white matter hyperintensities and cognition in the elderly. *Neurology*, 79(5).
- Mansson, J. E., Vanier, M. T., & Svennerholm, L. (1977). Changes in the fatty acid and sphingosine composition of the major gangliosides of human brain with age. *Short Communications*, (July), 159–161.
- Mapstone, M., Cheema, A. K., Fiandaca, M. S., Zhong, X., Mhyre, T. R., Macarthur, L. H., ... Federoff, H. J. (2014). Plasma phospholipids identify antecedent memory impairment in older adults. *Nature Medicine*, 20(4), 415–418.
- Marchesini, S., Benaglia, G., Piccinotti, A., Bresciani, R., & Preti, A. (1998). Ganglioside GM2 is substrate for a sialidase in MDCK cells. *FEBS Letters*, 428, 115–117.
- Marconi, S., Toni, L. De, Lovato, L., Tedeschi, E., Gaetti, L., Acler, M., & Bonetti, B. (2005). Expression of gangliosides on glial and neuronal cells in normal and pathological adult human brain. *Journal of Neuroimmunology*, 170, 115–121.

- Margheri, F., Papucci, L., Schiavone, N., Agostino, R. D., Trigari, S., Serrati, S., ... Fibbi, G. (2015). Differential uPAR recruitment in caveolar-lipid rafts by GM1 and GM3 gangliosides regulates endothelial progenitor cells angiogenesis. *J Cell Mol Med*, *19*(1), 113–123.
- Martino, A. Di, Safar, J., Callegaro, L., Salem, N., & Gibbs, C. J. (1993). Ganglioside Composition Changes in Spongiform Encephalopathies : Analyses of 263K Scrapie-Infected Hamster Brains. *Neurochemical Research*, *18*(8), 907–913.
- Masserini, M., Palestini, P., & Freire, E. (1989). Influence of glycolipid oligosaccharide and long-chain base composition on the thermotropic properties of dipalmitoylphosphatidylcholine large unilamellar vesicles containing gangliosides. *Biochemistry*, *28*(12), 5029–5034.
- Masuda, J., Nabika, T., & Notsu, Y. (2001). Silent stroke: pathogenesis, genetic factors and clinical implications as a risk factor. *Current Opinion in Neurology*, *14*(1), 77–82.
- Matsuzaki, K., Kato, K., & Yanagisawa, K. (2010). Abeta polymerization through interaction with membrane gangliosides. *Biochimica et Biophysica Acta*, *1801*(8), 868–77. <https://doi.org/10.1016/j.bbali.2010.01.008>
- Mattson, M. P., Zhu, H., Yu, J., & Kindy, M. S. (2000). Presenilin-1 Mutation Increases Neuronal Vulnerability to Focal Ischemia In Vivo and to Hypoxia and Glucose Deprivation in Cell Culture : Involvement of Perturbed Calcium Homeostasis. *The Journal of Neuroscience*, *20*(4), 1358–1364.
- Mclaurin, J., & Chakrabarty, A. (1996). Membrane Disruption by Alzheimer b-Amyloid Peptides Mediated through Specific Binding to Either Phospholipids or Gangliosides. *The Journal of Biological Chemistry*, *271*(43), 26482–26489.
- Mclaurin, J., & Chakrabarty, A. (1997). Characterization of the interactions of Alzheimer P-amyloid peptides with phospholipid membranes. *Eur J Biochem*, *245*, 355–363.
- McLean, C. A., Cherny, R. A., Fraser, F. W., Fuller, S., Smith, M., Vbeyreuther, K., ... Masters, C. (1999). Soluble pool of A β amyloid as a determinant of severity of neurodegeneration in Alzheimer's disease. *Annals of Neurology*, *46*(6), 860–866.
- Mielke, J. G., Murphy, M. P., Maritz, J., Bengualid, K. M., & Ivy, G. O. (1997). Chloroquine administration in mice increases beta-amyloid immunoreactivity and attenuates kainate-induced blood-brain barrier dysfunction. *Neuroscience Letters*, *227*(3), 169–172.
- Miyagi, T., Wada, T., Iwamatsu, A., Hata, K., Yoshikawa, Y., Tokuyama, S., & Sawada, M. (1999). Molecular Cloning and Characterization of a Plasma Membrane-associated Sialidase Specific for Gangliosides *. *The Journal of Biological Chemistry*, *274*(8), 5004–5011.
- Miyagi, T., & Yamaguchi, K. (2012). Mammalian sialidases : Physiological and pathological roles in cellular functions. *Glycobiology*, *22*(7), 880–896.
- Mizushima, N., Levine, B., Cuervo, A. M., & Klionsky, D. J. (2009). Autophagy fights disease through cellular self-digestion. *Nature*, *451*(7182), 1069–1075.

- Molander-melin, M., Blennow, K., Bogdanovic, N., Dellheden, B., & Fredman, P. (2005). Structural membrane alterations in Alzheimer brains found to be associated with regional disease development ; increased density of gangliosides GM1 and GM2 and loss of cholesterol in detergent- resistant membrane domains. *Journal of Neurochemistry*, *92*, 171–182.
- Monroe, E. B., Jurchen, J. C., Koszczuk, B. A., Losh, J. L., Stanislav, S., & Sweedler, J. V. (2008). Massively parallel sample preparation for the MALDI MS analyses of tissues. *Analytical Chemistry*, *78*(19), 6826–6832.
- Mukherjee, P., Faber, A. C., Shelton, L. M., Baek, R. C., Chiles, T. C., & Seyfried, T. N. (2008). Ganglioside GM3 suppresses the proangiogenic effects of vascular endothelial growth factor and ganglioside GD1a. *Journal Of Lipid Research*, *49*, 929–938.
- Muthings, J., & Cacic, M. (1997). Glycosphingolipid expression in human skeletal and heart muscle assessed by immunostaining thin-layer chromatography. *Glycoconjugate Journal*, *14*, 19–28.
- Mutoh, T., Tokuda, A., & Miyadai, T. (1995). Ganglioside GM1 binds to the Trk protein and regulates receptor function. *Proceedings of the National Academy of Sciences*.
- Nakatani, Y., Yanagisawa, M., Suzuki, Y., & Yu, R. K. (2010). Characterization of GD3 ganglioside as a novel biomarker of mouse neural stem cells. *Glycobiology*, *20*(1), 78–86.
- Nakatsuji, Y., & Miller, R. H. (2001). Selective cell-cycle arrest and induction of apoptosis in proliferating neural cells by ganglioside GM3. *Experimental Neurology*, *168*(2), 290–9.
- Negrone, E., Chigorno, V., Tettamanti, G., & Sonnino, S. (1996). Evaluation of the efficiency of an assay procedure for gangliosides in human serum. *Glycoconjugate Journal*, *13*, 347–352.
- Ngamukote, S., Yanagisawa, M., Ariga, T., Ando, S., & Yu, R. K. (2007). Developmental changes of glycosphingolipids and expression of glycoconjugates in mouse brains. *Journal of Neurochemistry*, *102*, 2327–2341.
- Niimi, K., Nishioka, C., Miyamoto, T., Takahashi, E., Miyoshi, I., & Itakura, C. (2011). Biochemical and Biophysical Research Communications Impairment of neuropsychological behaviors in ganglioside GM3-knockout mice. *Biochemical and Biophysical Research Communications*, *406*(4), 524–528. 1
- Nilsson, O., & Svennerholm, L. (1982). Accumulation of glucosylceramide and glucosylsphingosine (psychosine) in cerebrum and cerebellum in infantile and juvenile Gaucher disease. *Journal of Neurochemistry*, *39*(3), 709–718.
- Ohashi, M. (1978). A Comparison of the Ganglioside Distributions of Fat Tissues in Various Animals by Two-Dimensional Thin Layer Chromatography. *Lipids*, *14*(1), 52–57.
- Ohsawa, T., & Shumiya, S. (1991). Age-related alteration of brain gangliosides in senescence-accelerated mouse (SAM)-P/8. *Mechanisms of Ageing and Development*,

59, 263–274.

- Ohtani, Y., Tamai, Y., Ohnuki, Y., & Miura, S. (1996). Ganglioside alterations in the central and peripheral nervous systems of patients with Creutzfeldt-Jakob disease. *Neurodegeneration*, *5*(4), 331–338.
- Oikawa, N., Yamaguchi, H., Ogino, K., Taki, T., Yuyama, K., Yamamoto, N., ... Yanagisawa, K. (2009). Gangliosides determine the amyloid pathology of Alzheimer's disease. *Neuroreport*, *20*(12), 1043–1046.
- Palestini, P., Masserini, M., Fiorilli, A., Calappi, E., & Tettamanti, G. (1993). Age-Related Changes in the Ceramide Composition of the Major Gangliosides Present in Rat Brain Subcellular Fractions Enriched in Plasma Membranes of Neuronal and Myelin Origin. *Journal of Neurochemistry*, *61*(3), 955–960.
- Palestini, P., Masserini, M., Sonnino, S., & Tettamanti, G. (1990). Changes in the ceramide composition of rat forebrain gangliosides with age. *Journal of Neurochemistry*, *54*(1), 230–235.
- Pan, B., Fromholt, S. E., Hess, E. J., Crawford, T. O., Griffin, J., Sheik, K., & Schnaar, R. (2005). Myelin-associated glycoprotein and complementary axonal ligands, gangliosides, mediate axon stability in the CNS and PNS: neuropathology and behavioral deficits in single and double-null mice. *Experimental Neurology*, *95*(1), 208–217.
- Pascual, A., Hidalgo-Figueroa, M., & Piruat, J. I. (2008). Absolute requirement of GDNF for adult catecholaminergic neuron survival. *Nature Neuroscience*, *11*, 755–761.
- Patschan, S., Chen, J., Gealekman, O., Krupincza, K., Wang, M., Shu, L., ... Ms, G. (2008). Mapping mechanisms and charting the time course of premature cell senescence and apoptosis : lysosomal dysfunction and ganglioside accumulation in endothelial cells. *Am J Physiol Renal Physiol*, *294*, 100–109.
- Péguet-navarro, J., Sportouch, M., Popa, I., Berthier, O., Schmitt, D., & Portoukalian, J. (2017). Gangliosides from Human Melanoma Tumors Impair Dendritic Cell Differentiation from Monocytes and Induce Their Apoptosis. *The Journal of Immunology*, *170*, 3488–3494.
- Pernber, Z., Blennow, K., Bogdanovic, N., Månsson, J.-E., & Blomqvist, M. (2012). Altered distribution of the gangliosides GM1 and GM2 in Alzheimer's disease. *Dementia and Geriatric Cognitive Disorders*, *33*(2–3), 174–88.
- Pestronk, A., Adams, R. N., Cornblath, D., Kuncl, R. W., Drachman, D. B., & Rn, L. C. (1989). Patterns of serum IgM antibodies to GM1 and GD1a gangliosides in amyotrophic lateral sclerosis. *Annals of Neurology*, *25*(1), 98–102.
- Pfau, G., Westphal, S., Dietzmann, K., Bossanyi, P., Augustin, W., & Verlag, G. F. (1997). Chloroquine effects on intrauterine and postnatal dendritic maturation of hippocampal neurons and on lipid composition of the developing rat brain. *Experimental and Toxicologic Pathology*, *49*(5), 361–367.
- Piccinini, M., Scandroglio, F., Prioni, S., Buccinnà, B., Loberto, N., Aureli, M., ... Prinetti,

- A. (2010). Deregulated sphingolipid metabolism and membrane organization in neurodegenerative disorders. *Molecular Neurobiology*, *41*(2–3), 314–340.
- Pitto, M., Mutoh, T., Kuriyama, M., Ferraretto, A., Palestini, P., & Y, M. M. (1998). Influence of endogenous GM1 ganglioside on TrkB activity , in cultured neurons. *FEBS Letters*, *439*, 93–96.
- Pitto, M., Raimondo, F., Zoia, C., Brighina, L., Ferrarese, C., & Masserini, M. (2005). Enhanced GM1 ganglioside catabolism in cultured fibroblasts from Alzheimer patients. *Neurobiology of Aging*, *26*(6), 833–838.
- Poole, B., & Ohkuma, S. (1981). Effect of Weak Bases on the Intralysosomal pH in Mouse Peritoneal Macrophages. *The Journal of Cell Biology*, *90*, 665–669.
- Pope-Coleman, A., Tinker, J. P., & Schneider, J. S. (2000). Effects of GM1 ganglioside treatment on pre-and postsynaptic dopaminergic markers in the striatum of parkinsonian monkeys. *Synapse*, *36*(2), 120–128.
- Popert, A. J., Meijers, K. A. E., Sharp, J., & Bier, F. (1961). Chloroquine diphosphate in rheumatoid arthritis. A controlled trial. *Ann Rheum Dis*, *20*, 18–35.
- Prins, N., van Dijk, E., Heijer, T., Vermeer, S., Koudstaal, P., Oudkerk, M., ... Breteler, M. (2004). Cerebral White Matter Lesions and the Risk of Dementia. *Archives of Neurology*, *61*, 1531–1534.
- Prokazova, N. V, Samovilova, N. N., Gracheva, E. V, & Golovanova, N. K. (2009). Ganglioside GM3 and its biological functions. *Biochemistry. Biokhimiia*, *74*(3), 235–249.
- Purnell, C., Gao, S., Callahan, C. M., & Hendrie, H. (2009). Cardiovascular Risk Factors and Incident Alzheimer Disease. *Alzheimer Dis Assoc Disord*, *23*(1), 1–10.
- Rabin, S. J., Bachis, A., & Mocchetti, I. (2002). Gangliosides activate Trk receptors by inducing the release of neurotrophins. *Journal of Biological Chemistry*, *277*(51), 49466–49472.
- Randall, R. D., & Thayer, S. (1992). Glutamate-induced calcium transient triggers delayed calcium overload and neurotoxicity in rat hippocampal neurons. *Journal of Neuroscience*.
- Randeria, P. S., Seeger, M. A., Wang, X., Wilson, H., Shipp, D., & Mirkin, C. A. (2015). siRNA-based spherical nucleic acids reverse impaired wound healing in diabetic mice by ganglioside GM3 synthase knockdown. *Proceedings of the National Academy of Sciences*, *112*(18), 5573–5578.
- Rauvala, H., & Finne, J. (1980). Gangliosides of brain and of extraneural tissues: structural relationship to protein-linked glycans. In *Structure and Function of Gangliosides* (pp. 185–198).
- Reitz, C. (2012). Alzheimer's disease and the amyloid cascade hypothesis: a critical review. *International Journal of Alzheimer's Disease*, *2012*, 11.

- Riboni, L., Caminiti, A., Bassi, R., & Tettamanti, G. (1995). The degradative pathway of gangliosides GM1 and GM2 in Neuro2a cells by sialidase. TL - 64. *Journal of Neurochemistry*, 64 VN-readcube.com(1), 451–454.
- Riboni, L., Prinetti, A., Bassi, R., & Tettamanti, G. (1991). Cerebellar granule cells in culture exhibit a ganglioside-sialidase presumably linked to the plasma membrane. *FEBS*, 287(1,2), 42–46.
- Rodriguez, J. A., Piddini, E., Hasegawa, T., Miyagi, T., & Dotti, C. G. (2001). and Regeneration in Hippocampal Neurons in Culture. *The Journal of Neuroscience*, 21(21), 8387–8395.
- Rong, X., Zhou, W., Xiao-Wen, C., Tao, L., & Tang, J. (2013). Ganglioside GM1 reduces white matter damage in neonatal rats. *Acta Neurobiologiae Experimentalis*, 73(3), 379–86.
- Rubovitch, V., Zilbe, Y., Chapman, J., Schreiber, S., & Pick, C. G. (2017). Restoring GM1 ganglioside expression ameliorates axonal outgrowth inhibition and cognitive impairments induced by blast traumatic brain injury. *Scientific Reports*, (December 2016), 1–12.
- Saito, M., Chakraborty, G., Shah, R., Mao, R., Kumar, A., Yang, S., ... Saito, M. (2013). Elevation of GM2 ganglioside during ethanol-induced apoptotic neurodegeneration in the developing mouse brain. *Journal of Neurochemistry*, 121(4), 649–661.
- Sanan, D. A., Weisgraber, K. H., Russell, S. J., Mahley, R. W., Huang, D., Saunders, A., ... Strittmatter, W. J. (1994). Rapid Publication Apolipoprotein E Associates with p3 Amyloid Peptide of Alzheimer's Disease to Form Novel Monofibrils. *Journal of Clinical Investigation*, 94(August), 860–869.
- Sasaki, A., Hata, K., Suzuki, S., Sawada, M., Wada, T., Yamaguchi, K., ... Miyagi, T. (2003). Overexpression of Plasma Membrane-associated Sialidase Attenuates Insulin Signaling in Transgenic Mice. *The Journal of Biological Chemistry*, 278(30), 27896–27902.
- Scharf, S., Mander, A., Ugoni, A., Vajda, F., & Christophidis, N. (1999). A double-blind, placebo-controlled trial of diclofenac/misoprostol in Alzheimer's disease. *Neurology*, 53(1).
- Schmidt, R., Ropele, S., Enzinger, C., Petrovic, K., DePhil, S., Schmidt, H., ... Frazekas, F. (2005). White matter lesion progression, brain atrophy, and cognitive decline: the Austrian stroke prevention study. *Annals of Neurology*, 58(4), 610–616.
- Schnaar, R. L. (2010). Brain gangliosides in axon – myelin stability and axon regeneration. *FEBS Letters*, 584(9), 1741–1747.
- Schneider, J. S., Kean, A., & DiStefano, L. (1995). GM1 ganglioside rescues substantia nigra pars compacta neurons and increases dopamine synthesis in residual nigrostriatal dopaminergic neurons in MPTP-treated *Journal of Neuroscience Research*, 42(1), 117–123.
- Scorrano, L., Petronilli, V., Lisa, F. Di, & Bernardi, P. (1999). Commitment to Apoptosis

- by GD3 Ganglioside Depends on Opening of the Mitochondrial Permeability Transition Pore. *The Journal of Biological Chemistry*, 274(32), 22581–22585.
- Seyfried, T. N., Ando, S., & Yu, R. K. (1978). Isolation and characterization of human liver hematoside. *Journal Of Lipid Research*, 19, 538–543.
- Seyfried, T. N., & Mukherjee, P. (2010). Ganglioside GM3 Is Antiangiogenic in Malignant Brain Cancer. *Journal of Oncology*, 2010.
- Sheikh, K. a, Sun, J., Liu, Y., Kawai, H., Crawford, T. O., Proia, R. L., ... Schnaar, R. L. (1999). Mice lacking complex gangliosides develop Wallerian degeneration and myelination defects. *Proceedings of the National Academy of Sciences of the United States of America*, 96(13), 7532–7.
- Simpson, M. A., Cross, H., Proukakis, C., Priestman, D. A., Neville, D. C. A., Reinkensmeier, G., ... Crosby, A. H. (2004). Infantile-onset symptomatic epilepsy syndrome caused by a homozygous loss-of-function mutation of GM3 synthase. *Nature Genetics*, 36(11), 1225–1229.
- Snowdon, D. A., Greiner, L. H., Mortimer, J. A., Riley, K. P., Greiner, P. A., & Markesbery, W. R. (1997). Brain Infarction and the Clinical Expression of Alzheimer Disease: The Nun Study. *JAMA*, 277(10), 813–817.
- Sohn, H., Kim, Y. S., Kim, H. T., Kim, C. H., Cho, E. W., Kang, H. Y., ... Ko, J. H. (2006). Ganglioside GM3 is involved in neuronal cell death. *The FASEB Journal : Official Publication of the Federation of American Societies for Experimental Biology*, 20(8), 1248–1250.
- Sonnino, S., & Chigorno, V. (2000). Ganglioside molecular species containing C18- and C20-sphingosine in mammalian nervous tissues and neuronal cell cultures. *Biochimica et Biophysica Acta - Reviews on Biomembranes*, 1469(2), 63–77.
- Sonnino, S., Chigorno, V., Aureli, M., Masilamani, A., Valsecchi, M., Loberto, N., ... Prinetti, A. (2011). Role of gangliosides and plasma membrane-associated sialidase in the process of cell membrane organization. In *The molecular immunology of complex carbohydrates* (pp. 297–316).
- Sonnino, S., Mauri, L., Ciampa, M. G., & Prinetti, A. (2013). Gangliosides as regulators of cell signaling: Ganglioside-protein interactions or ganglioside-driven membrane organization? *Journal of Neurochemistry*, 124(4), 432–435.
- Sonnino, S., & Prinetti, A. (2010). Gangliosides as Regulators of Cell Membrane Organization and Functions. In *Sphingolipids as signalling and regulatory molecules* (pp. 165–184).
- Soontornniyomkij, V., Lynch, M. D., Mermash, S., Pomakian, J., Badkoobehi, H., Clare, R., & Vinters, H. (2010). Cerebral Microinfarcts Associated with Severe Cerebral β -Amyloid Angiopathy. *Brain Pathology*, 20(2), 459–467.
- Steingart, A., Hachinski, V. C., & Lau, C. (1987). Cognitive and neurologic findings in subjects with diffuse white matter lucencies on computed tomographic scan (leukoaraiosis). *Archives of Neurology*, 44(1), 32–35.

- Stoll, G., Jander, S., & Schroeter, M. (1998). Inflammation and glial responses in ischemic brain lesions. *Progress in Neurobiology*. Elsevier.
- Ström, J. O., Ingberg, E., Theodorsson, A., & Theodorsson, E. (2013). Method parameters' impact on mortality and variability in rat stroke experiments : a meta-analysis. *BMC Neuroscience*, *14*(41), 1471–2202.
- Sugiura, Y., Furukawa, K., Tajima, O., Mii, S., Honda, T., & Furukawa, K. (2005). Sensory nerve-dominant nerve degeneration and remodeling in the mutant mice lacking complex gangliosides. *Neuroscience*, *135*(4), 1167–1178.
- Sugiura, Y., Shimma, S., Konishi, Y., Yamada, M. K., & Setou, M. (2008). Imaging mass spectrometry technology and application on ganglioside study; visualization of age-dependent accumulation of C20-ganglioside molecular species in the mouse hippocampus. *PLoS One*, *3*(9), e3232.
- Sulzer, D., & Surmeier, D. J. (2013). Neuronal vulnerability, pathogenesis, and Parkinson's disease. *Movement Disorders*, *28*(6), 715–723.
- Suzuki, Y., Ichinomiya, S., Kurosawa, M., Ohkubo, M., Watanabe, H., Iwasaki, H., ... Brady, R. (2007). Chemical chaperone therapy: clinical effect in murine GM1-gangliosidosis. *Annals of Neurology*, *62*(6), 671–675.
- Svatos, A. (2010). Mass spectrometric imaging of small molecules. *Trends in Biotechnology*, *28*(8), 425–434.
- Svennerholm, I., & Gottfries, C. (1994). Membrane Lipids , Selectively Diminished in Alzheimer Brains , Suggest Synapse Loss as a Primary Event in Early-Onset Form (Type I) and Demyelination in Late-Onset Form (Type II). *Journal of Mass Spectrometry : JMS*, *62*, 1039–1047.
- Svennerholm, L., Bråne, G., Karlsson, I., Lekman, A., Ramstrom, I., & Wikkelso, C. (2002). Alzheimer disease—effect of continuous intracerebroventricular treatment with GM1 ganglioside and a systematic activation programme. *Dementia and Geriatric Cognitive Disorders*, *14*, 128–136.
- Szydłowska, K., & Tymianski, M. (2010). Calcium, ischemia and excitotoxicity. *Cell Calcium*, *47*(2), 122–129.
- Tagami, S., Inokuchi, J., Kabayama, K., Yoshimura, H., Kitamura, F., Uemura, S., ... Igarashi, Y. (2002). Ganglioside GM3 Participates in the Pathological Conditions of Insulin Resistance. *The Journal of Biological Chemistry*, *277*(5), 3085–3092.
- Tajima, O., Egashira, N., Ohmi, Y., Fukue, Y., Mishima, K., Iwasaki, K., ... Furukawa, K. (2009). Reduced motor and sensory functions and emotional response in GM3-only mice: Emergence from early stage of life and exacerbation with aging. *Behavioural Brain Research*, *198*(1), 74–82.
- Tamai, Y., Ohtani, Y., Miura, S., Narita, Y., Iwata, T., Kaiya, H., & Namba, M. (1979). Creutzfeldt-Jakob disease--alteration in ganglioside sphingosine in the brain of a patient. *Neuroscience Letters*, *11*(1), 81–86.

- Tamura, A., Graham, D., McCulloch, J., & Teasdale, G. (1981). Focal Cerebral Ischaemia in the Rat : 1 . Description of Technique and Early Neuropathological Consequences Following Middle Cerebral Artery Occlusion. *Journal of Cerebral Blood Flow and Metabolism*, *1*, 53–60.
- The National Institute of Neurological Disorders and Stroke rt-PA Stroke Study Group, N. (1995). Tissue plasminogen activator for acute ischemic stroke. *The New England Journal of Medicine*, *333*(24), 1581–1587.
- The World Health Organization. (2012). Dementia: A public health priority.
- Thiel, A., Cechetto, D. F., Heiss, W., Hachinski, V., & Whitehead, S. N. (2014). Amyloid burden, neuroinflammation, and links to cognitive decline after ischemic stroke. *Stroke*, *45*, 2825–2829.
- Thomas, A., Charbonneau, J. L., Fournaise, E., & Chaurand, P. (2012). Sublimation of New Matrix Candidates for High Spatial Resolution Imaging Mass Spectrometry of Lipids: Enhanced Information in Both Positive and Negative Polarities after 1,5-Diaminonaphthalene Deposition. *Analytical Chemistry*, *84*, 2048–2054.
- Tomiyama, T., Matsuyama, S., Iso, H., Umeda, T., Takuma, H., Ohnishi, K., ... Mori, H. (2010). A Mouse Model of Amyloid ^β Oligomers : Their Contribution to Synaptic Alteration , Abnormal Tau Phosphorylation , Glial Activation , and Neuronal Loss In Vivo. *Neurobiology of Disease*, *30*(14), 4845–4856.
- Trembath, D., Ervin, J. F., Broom, L., Szymanski, M., Welsh-Bohmer, K., Pieper, C., & Hulette, C. M. (2007). The distribution of cerebrovascular amyloid in Alzheimer's disease varies with ApoE genotype. *Acta Neuropathologica*, *113*(1), 23–31.
- Trimpin, S., & Deinzer, M. L. (2007). Solvent-free MALDI-MS for the analysis of beta-amyloid peptides via the mini-ball mill approach: qualitative and quantitative advances. *Journal of the American Society for Mass Spectrometry*, *18*(8), 1533–43.
- Vajn, K., Viljetic, B., Degmecic, I., Schnaar, R., & Heffer, M. (2013). Differential Distribution of Major Brain Gangliosides in the Adult Mouse Central Nervous System. *PloS One*, *8*(9), 1–11.
- Veillon, L., Go, S., Matsuyama, W., Suzuki, A., Nagasaki, M., Yatomi, Y., & Inokuchi, J. (2015). Identification of Ganglioside GM3 Molecular Species in Human Serum Associated with Risk Factors of Metabolic Syndrome. *PloS One*, *10*(6), e0129645.
- Vukovic, I., Bozic, J., Markotic, A., Ljubovic, S., & Kurir, T. (2015). The Missing Link - Likely Pathogenetic Role of GM3 and Other Gangliosides in the Development of Diabetic Nephropathy. *Kidney and Blood Pressure Research*, *40*, 306–314.
- Walkley, S. U. (2003). and cellular pathogenesis of glycolipid Neurobiology storage diseases. *The Royal Society*, *358*, 893–904.
- Walsh, F. S., Skaper, S. D., & Doherty, P. (1994). Cell adhesion molecule (NCAM and N-cadherin)-dependent neurite outgrowth is modulated by gangliosides. *Progress in Brain Research*, *101*, 113–118.

- Wang, C., Zhao, T., Li, Y., Huang, G., White, M. A., & Gao, J. (2016). Investigation of endosome and lysosome biology by ultra pH-sensitive nanoprobe. *Advanced Drug Delivery Reviews*, 1–10.
- Wang, H., Isaji, T., Satoh, M., Li, D., Arai, Y., & Gu, J. (2013). Antitumor Effects of Exogenous Ganglioside GM3 on Bladder Cancer in an Orthotopic Cancer Model. *Urology*, 81(1).
- Wang, P., Wu, P., Zhang, J., Sato, T., Yamagata, S., & Yamagata, T. (2007). Positive regulation of tumor necrosis factor- α by ganglioside GM3 through Akt in mouse melanoma B16 cells. *Biochemical and Biophysical Research Communications*, 356, 438–443.
- Whitehead, S., Cheng, G., Hachinski, V., & Cechetto, D. F. (2005). Interaction Between a Rat Model of Cerebral Ischemia and β -amyloid toxicity: II. Effects of triflusal. *Stroke*, 36, 1782–1789.
- Whitehead, S. N., Chan, K. H. N., Gangaraju, S., Slinn, J., Li, J., & Hou, S. T. (2011). Imaging mass spectrometry detection of gangliosides species in the mouse brain following transient focal cerebral ischemia and long-term recovery. *PloS One*, 6(6), e20808.
- Whitehead, S. N., Cheng, G., Hachinski, V. C., & Cechetto, D. F. (2007). Progressive increase in infarct size, neuroinflammation, and cognitive deficits in the presence of high levels of amyloid. *Stroke; a Journal of Cerebral Circulation*, 38(12), 3245–50.
- Whitehead, S. N., Hachinski, V. C., & Cechetto, D. F. (2005). Interaction between a rat model of cerebral ischemia and beta-amyloid toxicity: inflammatory responses. *Stroke; a Journal of Cerebral Circulation*, 36(1), 107–12.
- Wiseman, J. M., & Laughlin, B. C. (2005). Desorption Electrospray Ionization (DESI) Mass Spectrometry: *Current Separations and Drug Development*, 11–14.
- Wolozin, B. (2004). Cholesterol and the Biology of Alzheimer's Disease. *Neuron*, 41, 7–10.
- Woods, A. S., Colsch, B., Jackson, S. N., Post, J., Baldwin, K., Roux, A., ... Balaban, C. (2013). Gangliosides and ceramides change in a mouse model of blast induced traumatic brain injury. *ACS Chemical Neuroscience*, 4(4), 594–600.
- Wu, G., & Ledeen, R. W. (1994). Gangliosides as modulators of neuronal calcium. *Progress in Brain Research*, 101, 101–112.
- Wu, G., Lu, Z., Andre, S., Gabius, H., & Ledeen, R. W. (2016). Functional interplay between ganglioside GM1 and cross-linking galectin-1 induces axon-like neurogenesis via integrin-based signaling and TRPC5-dependent Ca influx. *Journal of Neurochemistry*, 136(3), 550–563.
- Wu, G., Lu, Z., Kulkarni, N., & Ledeen, R. W. (2012). Deficiency of Ganglioside GM1 Correlates With Parkinson's Disease in Mice and Humans. *Journal of Neuroscience Research*, 90, 1997–2008.

- Yamamoto, A., Haraguchi, M., Yamashiro, S., Fukumoto, S., Furukawa, K., Takamiya, K., ... Furukawa, K. (1996). Heterogeneity in the expression pattern of two ganglioside synthase genes during mouse brain development. *J. Neurochem.*, *66*(1), 26–34.
- Yamamoto, N., Hirabayashi, Y., Amari, M., & Yamaguchi, H. (2005). Assembly of hereditary amyloid b -protein variants in the presence of favorable gangliosides. *FEBS Letters*, *579*, 2185–2190.
- Yamamoto, N., Nostrand, W. E. Van, & Yanagisawa, K. (2006). Further evidence of local ganglioside-dependent amyloid b -protein assembly in brain. *Neuroreport*, *17*(16), 16–18.
- Yamashita, T., Wu, Y., Sandhoff, R., Werth, N., Mizukami, H., Ellis, J. M., ... Proia, R. L. (2005). Interruption of ganglioside synthesis produces central nervous system degeneration and altered axon – glial interactions. *Proceedings of the National Academy of Sciences*, *102*(8), 2725–2730.
- Yanagisawa, K., Odaka, A., Suzuki, N., & Ihara, Y. (1995). GM1 ganglioside-bound amyloid β -protein (A β): A possible form of preamyloid in Alzheimer's disease. *Nature Medicine*, *1*, 1062–1066.
- Yang, H. J., Jung, K. Y., Kwak, D. H., Lee, S., Ryu, J., Kim, J., ... Lee, J. W. (2011). Inhibition of ganglioside GD1a synthesis suppresses the differentiation of human mesenchymal stem cells into osteoblasts. *Develop Growth Differ*, *53*, 323–332.
- Yang, M., Cao, L., Xie, M., Yu, Y., Kang, R., Yang, L., ... Tang, D. (2013). Chloroquine inhibits HMGB1 inflammatory signaling and protects mice from lethal sepsis. *Biochemical Pharmacology*, *86*(3), 410–418.
- Yang, R., Wang, Q., Min, L., Sui, R., Li, J., & Liu, X. (2013). Monosialoanglioside improves memory deficits and relieves oxidative stress in the hippocampus of rat model of Alzheimer's disease. *Neurological Sciences*, *34*(8), 1447–1451.
- Yao, D., Mcgonigal, R., Barrie, J. A., Cappell, J., Cunningham, M. E., Meehan, G. R., ... Willison, H. J. (2014). Neuronal Expression of GalNAc Transferase Is Sufficient to Prevent the Age-Related Neurodegenerative Phenotype of Complex Ganglioside-Deficient Mice. *The Journal of Neuroscience*, *34*(3), 880–891.
- Yates, J. R. (1998). Mass spectrometry and the age of the proteome. *Journal of Mass Spectrometry*, *33*(1), 1–19.
- Yoshizumi, S., Suzuki, S., Hirai, M., Hinokio, Y., Yamada, T., Yamada, T., ... Oka, Y. (2007). Increased hepatic expression of ganglioside-specific sialidase, NEU3, improves insulin sensitivity and glucose tolerance in mice. *Metabolism: Clinical and Experimental*, *56*(3), 420–429.
- Yu, R. K., Macala, L. J., Taki, T., Weinfield, H. M., & Yu, F. S. (1988). Developmental changes in ganglioside composition and synthesis in embryonic rat brain. *Journal of Neurochemistry*, *50*(6), 1825–1829.
- Yu, R. K., & Manuelidis, E. E. (1978). Ganglioside alterations in guinea pig brains at end stages of experimental Creutzfeldt-Jakob disease. *Journal of the Neurological*

Sciences, 35(1), 15–23.

- Yu, R. K., Nakatani, Y., & Yanagisawa, M. (2009). The role of glycosphingolipid metabolism in the developing brain. *Journal of Lipid Research*, 50 Suppl, S440–S445.
- Yu, R. K., Tsai, Y. T., & Ariga, T. (2012). Functional roles of gangliosides in Neurodevelopment: An overview of recent advances. *Neurochemical Research*, 37(6), 1230–1244.
- Yuki, N., Yoshino, H., Sato, S., Shinozawa, K., & Miyatake, T. (1992). Severe acute axonal form of Guillain–Barré syndrome associated with IgG anti-GD1a antibodies. *Muscle & Nerve*, 15(8), 899–903.
- Yuyama, K., Yamamoto, N., & Yanagisawa, K. (2006). Chloroquine-induced endocytic pathway abnormalities : Cellular model of GM1 ganglioside-induced A β fibrillogenesis in Alzheimer ' s disease. *FEBS Letters*, 580, 6972–6976.
- Zador, I., Deshmukh, G., Kunkel, R., Johnson, K., Radin, N., & Shayman, J. (1993). A Role for Glycosphingolipid Accumulation in the Renal Hypertrophy. *Journal of Clinical Investigation*, 91, 797–803.
- Zaima, N., Hayasaka, T., Goto-Inoue, N., & Setou, M. (2010). Matrix-assisted laser desorption/ionization imaging mass spectrometry. *International Journal of Molecular Sciences*, 11(12), 5040–55.
- Zhang, J., Fang, X., Zhou, Y., Deng, X., Lu, Y., Li, J., ... Xu, R. (2015). The Possible Damaged Mechanism and the Preventive Effect of Monosialotetrahexosylganglioside in a Rat Model of Cerebral Ischemia-Reperfusion Injury. *Journal of Stroke and Cerebrovascular Disease*, 24(7), 1471–1478.
- Zhang, X., Zhou, K., Wang, R., Cui, J., Lipton, S. A., Liao, F., ... Zhang, Y. (2007). Hypoxia-inducible Factor 1 a (HIF-1a) -mediated Hypoxia Increases BACE1 Expression and b-Amyloid Generation. *The Journal of Biological Chemistry*, 282(15), 10873–10880.
- Zhang, Y., Wang, J., Liu, J., Han, J., & Xiong, S. (2016). Combination of ESI and MALDI mass spectrometry for qualitative , semi-quantitative and in situ analysis of gangliosides in brain. *Scientific Reports*, 6, 1–11.
- Ziche, M., Alessandri, G., & Gullino, P. M. (1989). Gangliosides promote the angiogenic response. *Laboratory Investigation; a Journal of Technical Methods and Pathology*, 61(6), 629–634.
- Zoppo, G., Ginis, I., John, M., Iadecola, C., Wang, X., & Feuerstein, G. Z. (2000). Inflammation and Stroke : Putative Role for Cytokines , Adhesion Molecules and iNOS in Brain Response to Ischemia. *Brain Pathology*, 10, 95–112.

Chapter 2 : Increased expression of simple ganglioside species GM2 and GM3 detected by MALDI Imaging mass spectrometry in a combined rat model of A β toxicity and stroke

2.1 Abstract

The aging brain is often characterized by the presence of multiple comorbidities resulting in synergistic damaging effects in the brain as demonstrated through the interaction of Alzheimer's disease (AD) and stroke. Gangliosides, a family of membrane lipids enriched in the central nervous system, may have a mechanistic role in mediating the brain's response to injury as their expression is altered in a number of disease and injury states. Matrix-Assisted Laser Desorption Ionization (MALDI) Imaging Mass Spectrometry (IMS) was used to study the expression of a-series ganglioside species GD1a, GM1, GM2, and GM3 to determine alteration of their expression profiles in the presence of beta-amyloid (A β) toxicity in addition to ischemic injury. To model a stroke, rats received a unilateral striatal injection of endothelin-1 (ET-1) (stroke alone group). To model A β toxicity, rats received intracerebralventricular (icv) injections of the toxic 25-35 fragment of the A β peptide (A β alone group). To model the combination of A β toxicity with stroke, rats received both the unilateral ET-1 injection and the bilateral icv injections of A β ₂₅₋₃₅ (combined A β /ET-1 group). By 3 d, a significant increase in the simple ganglioside species GM2 was observed in the ischemic brain region of rats who received a stroke (ET-1), with or without A β . By 21 d, GM2 levels only remained elevated in the combined A β /ET-1 group. GM3 levels however demonstrated a different pattern of expression. By 3 d GM3 was elevated in the ischemic brain region only in the combined A β /ET-1 group. By 21 d, GM3 was elevated in the ischemic brain region in both stroke alone and A β /ET-1 groups. Overall, results indicate that the accumulation of simple ganglioside species GM2 and GM3 may be indicative of a mechanism of interaction between AD and stroke.

2.2 Introduction

As we age, our brains become more vulnerable to diseases and injuries. Elderly patients often simultaneously experience two or more medical conditions which complicates the study of age-related neurodegenerative diseases such as Alzheimer's disease (AD). When multiple conditions are present simultaneously (comorbidity), synergistic effects on pathology and cognitive outcomes can be observed as demonstrated in the case of AD and stroke. A key study which examined the incidence of dementia among a group of elderly nuns diagnosed with AD found that only 57% of those diagnosed with AD developed dementia, while 93% of those who had suffered small subcortical infarcts plus a pathological diagnosis of AD developed dementia (Snowdon et al., 1997). AD and stroke comorbidity has also been observed in carriers of the APOE4 gene. Data from the Canadian Study of Health and Aging (CSHA) showed that prevalence of dementia was increased among those who had a history of stroke and were also APOE4 carriers (Jin et al., 2008). Furthermore, another study demonstrated that APOE4 carriers with a history of stroke were five times more likely to develop dementia than APOE4 carriers without such a history (Jonston et al., 2000). Although the clinical evidence for the interaction between AD and stroke has been well documented, the mechanism(s) for this interaction remains unclear. A potential mediator for this interaction may lie within a family of cellular membrane lipids known as gangliosides.

Gangliosides are glycosphingolipids characterized by the presence of sialic acid residues. Being embedded within the plasma membrane, gangliosides perform a wide variety of biological functions by interacting with signaling molecules both within and outside of the cell. Some of these biological functions include cell signaling, proliferation, differentiation, embryogenesis, oncogenesis, neurodegeneration, and apoptosis (Prokazova et al., 2009; Yu, Suzuki & Yanagisawa, 2010). Ganglioside metabolism is controlled by the activities of several enzymes, which can add or remove sialic acid residues and/or oligosaccharide units to form the various derivatives that make up the ganglioside molecules. A-series gangliosides are the first, structurally simplest group of gangliosides derived from the addition of a sialic acid residue to lactosylceramide and contain the most abundant ganglioside species in the mammalian central nervous system, GM1, as well as

GD1a, GM2, and GM3 (Ando, Chang & Yu, 1978) (Fig 2.1). Every form of ganglioside is hypothesized to have unique functions within the cell and a normal homeostatic distribution of each species is maintained within healthy organisms (Yamamoto et al., 1996; Yu, Nakatani & Yanagisawa, 2009; Sekigawa et al., 2011). Complex gangliosides GM1 and GD1a are more abundant in the brain than the simple species GM2 and GM3 and have been shown to be beneficial for recovery when exogenously administered in a number of in vitro, animal, and human disease and injury studies (Schneider et al., 2013; Kreutz et al. 2011).

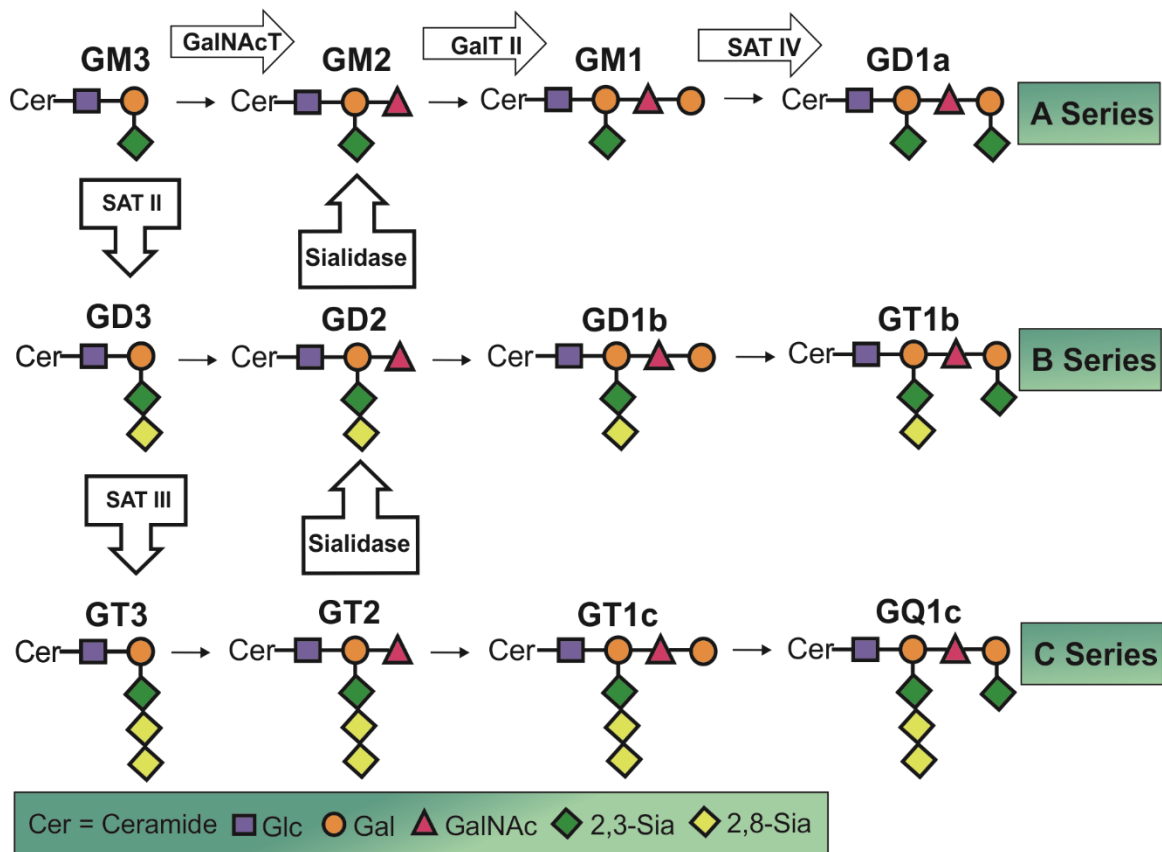


Figure 2.1: Chemical Structure and Metabolic Pathways Involved in Ganglioside Synthesis and Catabolism. Gangliosides are composed of a hydrophobic domain called ceramide (Cer) and a hydrophilic domain made up of a series of sugar units (glucose – Glc, galactose – Gal, and N-acetylgalactosimine –GalNAc) with a sialic acid residue (Sia) attached to a galactose sugar unit. The number and type of sugar units and sialic acids present in the hydrophilic domain determines the type of ganglioside species (GM3, GM2, etc.). A group of transferase enzymes adds either a sugar unit (GalNAcT, GalT) or a sialic acid residue (sialyltransferase - SAT) to synthesize different ganglioside species. A different set of catabolic enzymes within the lysosome can also break down these components, thus a homeostatic abundance of each ganglioside species is maintained in a healthy organism.

Little is known of the functions of ganglioside GM2 in the adult mammalian brain. However, GM2 gangliosidosis, a group of autosomal recessive disorders caused by dysfunction in enzyme metabolic pathways, such as Tay Sachs and Sandhoff's disease, can lead to accumulation of GM2 in neuronal cells resulting in a broad spectrum of neurological disorders (Bley et al., 2011). More recently, GM2 expression has been found to be elevated within the mouse brain at the injury site after a focal brain injury such as a traumatic brain injury or stroke (Whitehead et al., 2011; Woods et al., 2013). GM3, an essential component of the plasma membrane and lipid rafts (Prokazova et al., 2009), is structurally the simplest member of the ganglioside family and acts as a metabolic precursor to the other more complex ganglioside species (Fig 2.1). As such, GM3 plays a crucial role in regulating the level of expression of all other ganglioside species in cells. Although GM3 is one of the main gangliosides expressed in extra-neural tissues of vertebrates, it is generally expressed only in very small quantities in the healthy adult mammalian brain (Prokazova et al., 2009). Accumulation of GM3 in neural tissue has been shown to lead to toxic effects and apoptosis (Nakatsuji & Miller, 2001; Prokazova et al., 2009; Sohn et al., 2006). GM3 has been successfully used as a treatment for tumors due to its potent anti-angiogenic and apoptotic effects (Abate, Mukherjee & Seyfried, 2006; Chung et al., 2009; Seyfried & Mukherjee, 2010). An increase in GM3 expression has also been observed in both human and animal models of AD (Chan et al., 2012), as well as in mouse models of stroke—reperfusion injury (Whitehead et al., 2011). Finally, additional to the sugar chains, the functions of gangliosides may also be determined by ceramides. In particular, certain gangliosides differ only by the length of their sphingosine backbone, d18:1 and d20:1 (18 carbon and 20 carbon species), and have been suggested to have unique roles within the cell (Angel, Spraggins, Baldwin & Caprioli, 2012; Kotani et al., 1994; Whitehead et al., 2011; Woods et al., 2013).

Labelling and visualizing gangliosides within tissue using immunohistochemistry (IHC) is a commonly used technique for identifying different species of gangliosides. However, the efficacy of antibody labelling on lipids in general is controversial and the availability of specific ganglioside antibodies for certain species can be very limited or non-existent (Richards et al., 2012). Moreover, immunolabelling is also incapable of distinguishing between the d18:1 and d20:1 species as the ceramides are hidden within the

cell membrane, inaccessible to antibodies for labelling. An alternative approach is the detection of gangliosides based on their molecular mass through spectrometry. Matrix-Assisted Laser Desorption/Ionization Imaging Mass Spectrometry (MALDI IMS) can detect ganglioside molecules directly within tissue sections without any kind of immunological labelling. The masses and intensities of all ganglioside ions are recorded simultaneously within an anatomical reference point (Fig 2.2).

Figure 2. Schematic depiction of MALDI IMS protocol.

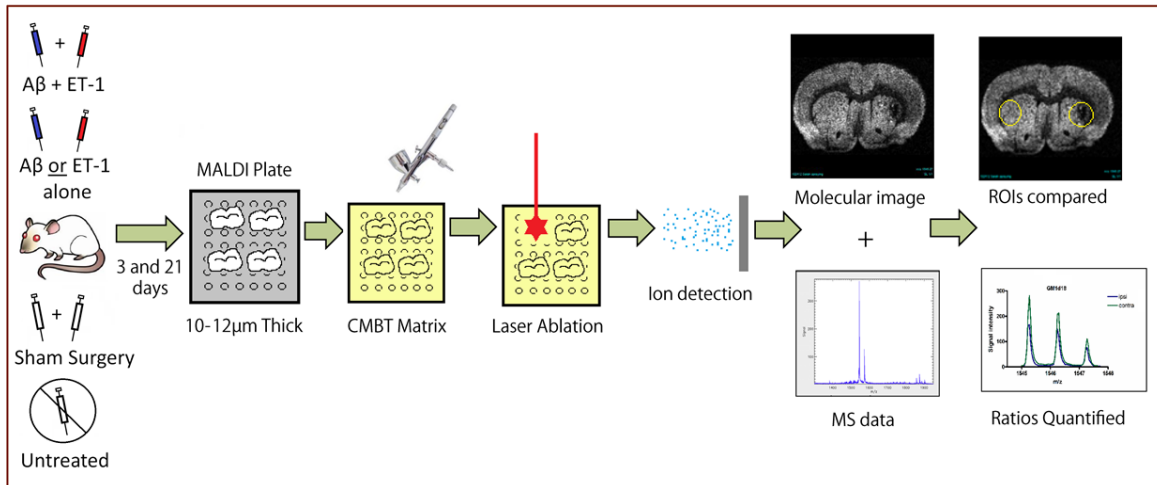


Figure 2.2: MALDI IMS Workflow. Following surgery, rats are euthanized via anesthetic overdose and decapitated. Fresh brains are isolated and sectioned at 10µm on a cryostat onto MALDI plates. Sections sprayed with CMBT matrix using an airbrush are processed on a MALDI mass spectrometer (Sciex 4700). Regions of interest (ROIs) are chosen with reference to the rat brain atlas by Paxinos and Watson. Stroke regions are identified and mass spectra are averaged from the infarct as well as from the corresponding non-injured striatum on the contralateral hemisphere. Mass spectra are generated from each ROI, and the peak height for the species of interest is calculated. Quantified data are represented as the ratio of the peak height between the ipsilateral (stroke) and contralateral ROIs.

Perturbations in the normal homeostatic expression of gangliosides have been observed in several models of neurodegeneration such as AD (Barrier et al., 2007; Svennerholm & Gottfries, 1994), Huntington's disease (Desplats et al., 2007), Parkinson's disease (Schneider et al., 2013), and prion diseases (Martino et al., 1993); however, this has not yet been reported within the context of comorbidities. Previous work using the same animal model as this study, has demonstrated that a synergistic relationship exists between animal models of stroke and AD both pathologically and behaviourally (Cechetto, Hachinski & Whitehead, 2008; Whitehead, Cheng, Hachinski & Cechetto, 2007), however the mechanism of this interaction remains unclear. This study utilizes both the novel MALDI IMS technique and, where possible, traditional IHC to examine changes in a-series ganglioside expression in rats who underwent either surgical striatal endothelin-1 (ET-1) injection (stroke alone group), bilateral icv injections of beta-amyloid (A β 25–35) (A β alone group), or ET-1 with bilateral icv injections A β 25–35 (combined A β /ET-1 group). The ET-1 subcortical stroke model was chosen as it produces subcortical lacunar type infarcts that resemble those typically seen in patients who, upon post-mortem examination, have been identified as having pathological correlates of both AD and stroke (Snowdon et al., 1997). In addition, previous studies have demonstrated that targeted injections of ET-1 produced a transient focal ischemia-reperfusion injury in rats (Jiwa, Garrad & Hainsworth, 2010; Whitehead, Hachinski & Cechetto, 2005; Whitehead, Cheng, Hachinski, & Cechetto, 2005).

2.3 Materials and Methods

2.3.1 *Animals Models*

Rats were weighed before being anaesthetized in a Harvard anesthesia box with 3% isoflurane in 2 L/min oxygen and placed in a Kopf stereotaxic apparatus. Using an operating microscope, an incision was made in the scalp and the skull was exposed. Bregma was used as a reference point for all injection sites: Injections were administered with a Hamilton glass syringe at a rate of 1 μ L over 30 sec. The syringe was left in place for 3 min after each injection then slowly removed. Rat body temperature was maintained at 37°C on a heating pad during the surgical and recovery periods before being returned to a cage. To induce A β toxicity, rats received 15 μ L bilateral icv injections of the toxic A β

fragment, A β 25–35 (50 nmol), at coordinates -0.8 mm (anterior/posterior), \pm 1.4 mm (medial/lateral) and -4.0 mm (dorsal/ventral). A β 25–35 (Sigma-Aldrich Co., St. Louis, USA) was dissolved in saline and stored at -80°C in 30 μ L aliquots and kept on dry ice prior to injection to prevent aggregation and allow better diffusion throughout the ventricles (Whitehead, Hachinski & Cechetto, 2005; Whitehead, Cheng, Hachinski, & Cechetto, 2005). To induce stroke, rats received a 3 μ L unilateral injection of the potent vasoconstrictor ET-1 (60 pmol) into the right striatum, at coordinates +0.5 mm (anterior/posterior), -3.0 mm (medial/lateral) and -5.0 mm (dorsal/ventral). ET-1 (Sigma-Aldrich Co., St. Louis, USA) was dissolved in sterile water and stored at -80°C in 8 μ L aliquots and kept on dry ice prior to injection. To induce the comorbid A β /ET-1 model, rats received bilateral icv injections of A β 25–35 followed by a unilateral ET-1 injection into the striatum at the same concentrations and coordinates as above. Sham surgery group animals underwent the same surgical procedure as the combined A β /ET-1 group rats but did not receive any chemical injections, only needle insertion to the appropriate brain regions. The mortality rate was slightly (but not statistically significantly) higher in ET-1 groups but was less than 10% of the total animals used and was attributed to the effects of the interaction between ET-1 and anesthesia.

2.3.2 *Euthanasia*

For histochemical and IHC analysis, rats were euthanized at 3 or 21 d post-surgery via Euthanyl overdose (0.5 mL, i.p.). Animals were then perfused transcardially with 0.01 M phosphate buffered saline (PBS) (pH 7.4) followed by 4% paraformaldehyde (PFA) (pH 7.4). Brains were removed and kept in the same PFA solution for 24 hr, then cryoprotected in 30% sucrose until they were fully submerged. Brains were sectioned coronally on a Cryo3 Cryostat (TissueTek, Dublin, USA) into 35 μ m thick sections and were stored in cryoprotectant at 4°C until used for immunohistochemistry. For MALDI IMS analysis, rats were euthanized via Euthanyl overdose (0.5 mL i.p.) at either 3 or 21 d post-surgery. Rats were decapitated and fresh whole brains were carefully removed and immediately frozen on dry ice. Frozen brains were stored at -80°C until used for MALDI IMS analysis.

2.3.3 *Immunohistochemistry*

Sections from each experimental group were processed simultaneously to reduce variability between groups. Sections were washed in 0.1 M PBS (3 x 15 min each), then quenched for 15 min in 1.5% hydrogen peroxide. Sections were washed in PBS (3 x 5 min each), then blocked in 1.5% bovine serum albumin (BSA) (Serological Research Institute, Richmond, USA) diluted in PBS with Triton-X (PBST) for 30 min. Sections were incubated with primary antibodies diluted in 1.5% BSA (PBST) for 48 hr at 4°C on a shaker. IHC procedure was similar for: mouse anti-rat OX-6 (1:1000, BD Biosciences, Mississauga, Canada), NeuN (1:1000, EMD Millipore, Billerica, USA), GFAP (1:1000, EMD Millipore, Billerica, USA) GM3 (1:500, Seikagaku Corporation, Tokyo, Japan), GM1 and GD1b (1:500, Ronald Schnaar, Johns Hopkins University, USA); however Triton-X was not used for GM3, GM1 or GD1b staining due to its membrane delocalizing effects (Lopez & Schnaar, 2009). Sections were then washed in PBS (3x 15 min each) then incubated with HRP-conjugated secondary antibodies diluted in 1.5% BSA (PBST) for 1 hr. HRP-conjugated (anti-mouse IgG) (1:200, Vector Laboratories, Burlington, Canada) and anti-rabbit IgG secondary antibodies (1:200, Vector Laboratories, Burlington, Canada) were used for the appropriate primary antibodies. Sections were washed in PBS (3 x 15 min each) then incubated in avidin-biotinylated complex (ABC) reagent (Vector Laboratories, Burlington, Canada) for 1 hr. Sections were then washed in PBS (3 x 5 min each) and developed in fresh 0.001% diaminobenzidine (DAB) (Vector Laboratories, Burlington, Canada) at 10 mg in 20 mL PBS with 300 µL 3% H₂O₂, Sigma for 5 min. Sections were washed in PBS (3 x 15 min each) then mounted onto VWR microscope slides coated in 0.3% gelatin, dehydrated, cleared with xylene and then cover-slipped with Depex (Fisher Scientific).

2.3.4 *Immunofluorescence*

Free-floating sections were washed in PBS (3 x 10 min) then blocked in 1.5% BSA for 1 hr at room temperature. Sections were incubated with antibodies to GM3 [1:500] and either NeuN (1:1000, Millipore, Billerica, USA), GFAP (1:1000, Millipore, Billerica, USA) or IBA-1 for activated microglia/macrophages (1:1000, Santa Cruz Biotechnology Inc., Santa Cruz, USA) in 1.5% BSA for 48 hrs at 4°C. Sections were washed in PBS (3 x 10 min

each) then incubated with FITC conjugated anti-mouse IgG (1:300, Santa Cruz Biotechnology Inc., Santa Cruz, USA) and TR-conjugated anti-rabbit IgG (1:300, Santa Cruz Biotechnology Inc., Santa Cruz, USA) for 1 hr at room temperature in the dark. Sections were washed in PBS (3 x 10 min) and mounted onto microscope glass slides and cover-slipped with Fluoroshield mounting media (Sigma-Aldrich, Toronto, Canada).

Fluoro Jade B. FJB is commonly used as a marker of neurodegeneration in the brain. Sections were washed in PBS (6 x 10 min each) then mounted onto microscope slides with 0.3% gelatin and allowed to dry overnight. Slides were placed in 1% sodium hydroxide and in 80% ethanol for 5 min. Slides were then rehydrated in 95% ethanol for 3 min; 70% ethanol for 3 min; 50% ethanol for 2 min, and finally distilled water (3 x 1 min each). Slides were then incubated in 0.06% potassium permanganate (KMnO₄) for 15 min on a shaker, in the dark. Slides were washed in distilled water (3 x 1 min each), then placed in fresh 0.0004% FJB (Millipore, Billerica, USA) in 0.1% acetic acid for 20 min on a shaker in the dark. Slides were washed in distilled water (3 x 1 min each) then allowed to dry in the fume hood before a xylene clearance step (1 min) and cover-slipped with Depex.

Microscopy Imaging. Images were taken on a Leica DC300 (Leica Microsystems, Concord, Canada) microscope camera. Analysis and quantification was carried out using Image J (Wayne Rasband, National Institute of Health, Bethesda, USA) by one observer who was blinded to the experimental groups.

2.3.5 MALDI Imaging Mass Spectrometry

Fresh frozen rat brains were sliced on a CM 1850 cryostat and 10 µm coronal sections were taken from the striatum (stroke injury site) for MALDI IMS analysis. Sections were thaw mounted onto a MALDI target plate and dried in a desiccator for 10 min. An artist's airbrush (Iwata HPBH, Japan) was used to apply 2 mL of 15 mg/mL 5-Chloro-3-mercaptopbenzothiazol (CMBT) (Sigma-Aldrich, Toronto, Canada) matrix dissolved in a 4:4:1 mixture of chloroform: ethanol:water solvent, allowing each layer to dry completely before spraying the next layer thus minimizing delocalization of molecules within the tissue. Once the matrix was uniformly applied to the plate surface and dried, the plate was inserted into a Sciex MALDI 4700 TOF/TOF mass spectrometer (Sciex, Foster City, CA,

USA). Prior to acquiring an image, the instrument was calibrated using five peptide standards (4700 Calibration Mixture, Sciex) at 50 ppm mass tolerance. Reflectron and negative ion modes were used for all image acquisitions. During the scanning process, a laser beam is directed across the selected tissue sections at 100 μm steps and a mass spectrum is collected for each x,y coordinate. The laser ablates the tissue and causes the desorbed molecules in the tissue to ionize. These ions travel down a flight tube where they separate based on their mass-to-charge (m/z) ratio to a detector which records this data and compiles it into both a mass spectrometry data plot and a molecular image. The instrument took approximately 2 hr for acquisition of each image. The region of interest (ROI) for this MALDI IMS study included both the core of the infarct and the periphery in order to assess general changes in ganglioside metabolism after stroke and $A\beta$ toxicity within the site of stroke injury. Representative MALDI IMS images were selected for the ET-1 group and $A\beta$ /ET-1 combined group for each species of ganglioside in order to better visualize the changes in expression. Representative IMS images from the $A\beta$ alone and control groups were not included as there were no significant alterations in ganglioside expression in any of these groups. The location of stroke injury within the striatum is highlighted with a green arrow in the MALDI IMS images. Three day (d) and 21 d time points were examined for each a-series ganglioside. The appropriate m/z ratio for each ganglioside species was confirmed using the Lipidmaps database (www.lipidmaps.org). Data was collected and analyzed as previously described (Fig 2.2).

2.3.6 *Data Analysis*

A single MALDI IMS image scan contains molecular information on the expression of each type of a-series ganglioside, the d18:1 and d20:1 species, as well as some unknown metabolic species. The molecular image can be used to locate a specific region of interest (ROI) such as the stroke region in the striatum where a mass spectrometry data plot is produced for that specific region for quantification. Multiple ROIs can be selected for comparison purposes. In this case, the injury site in one hemisphere was compared to the same location on the contralateral side of the brain. The peak height of each a-series ganglioside was quantified in both ROIs and, after baseline subtraction, a ratio was calculated for the differences in expression in the injured and non-injured tissue. The ratios

for multiple brain tissue scans in each group were compiled and a one way ANOVA was performed followed by a post-hoc Tukey's multiple comparisons test to determine if there were any differences in expression between the surgical groups and the controls at both time points. Error bars represent the standard error of the mean (SEM) for each group. A p-value of <0.05 was considered to be significant, $n = 4$ for each surgical group.

2.4 Results

2.4.1 *Increased GM3 expression within infarcted region of combined A β /ET-1 group persists at 21 d*

MALDI IMS results indicated a persistent perturbation in GM3 expression following stroke within the stroke region. Even though the MALDI MS instrument was capable of differentiating between the d18:1 and d20:1 species of GM3, signals from the d20:1 species fell below the threshold of detection and only signals from the d18:1 species were detected and quantified. At 3 d following surgery, MALDI IMS analysis demonstrated that GM3 expression did not change following ET-1 injection alone or A β injections alone, however did increase in the combined A β /ET-1 group (Fig 2.3 A and 2.3 B) within the stroke region. By 21 d after surgery, GM3 expression remained at control levels in the A β alone group while GM3 significantly increased in the ET-1 alone group and remained elevated in the combined A β /ET-1 group within the stroke region (Fig 2.3 A and 2.3 B). To complement the MALDI IMS data, GM3 was detected by IHC 3 and 21 d following surgery. There was no GM3 signal detected in control treated animals (data not shown), as expected due to the low abundance of this species in the healthy adult brain. By 3 d following surgery, GM3 signal was detected within the stroke region of both ET-1 alone and combined A β /ET-1 groups (Fig 2.3 C and 2.3 D). By 21 d following surgery, GM3 expression decreased within the infarct region of the ET-1 alone group compared to 3 d levels, whereas GM3 expression increased in the combined A β /ET-1 group over 3 d levels (Fig 2.3 C and 2.3 D). Similar to control and sham treated rats, there were no differences in GM3 expression (and all other gangliosides evaluated) within the right and left striatum of A β alone rats.

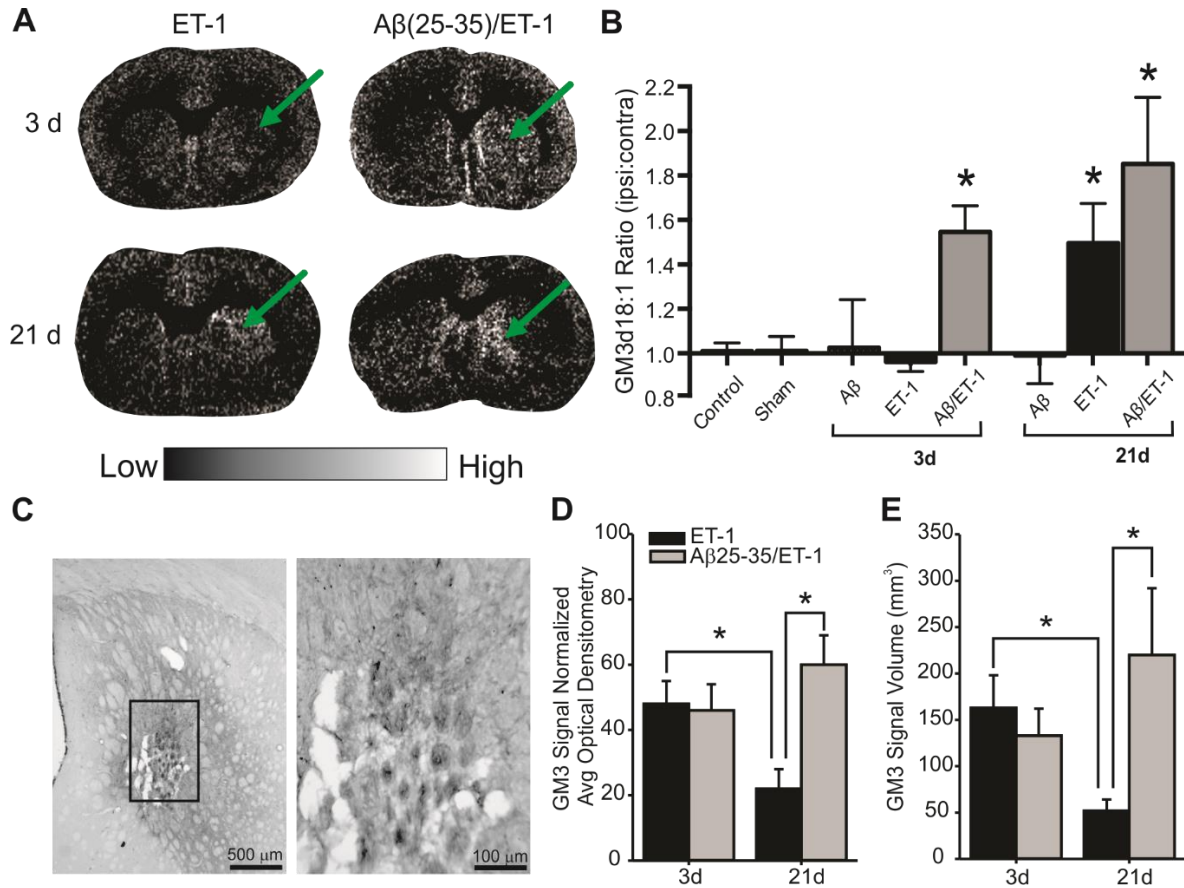


Figure 2.3: Increased GM3 expression within infarcted region of combined A β /ET-1 group persists at 21 d. (A) Representative MALDI IMS images of ganglioside GM3 d18:1 in stroke (ET-1 alone) and combined A β /ET-1 animals 3 and 21 d following surgery. Arrows indicate region of stroke induced infarct. Light regions in images represent areas of high expression while dark regions represent low levels of expression as indicated by intensity bar. (B) MALDI IMS quantification of ROIs from the striatum of control, sham surgery, A β alone, ET-1 alone, and combined A β /ET-1 animals at 3 d and A β alone, ET-1 alone, and combined A β /ET-1 animals at 21 d. Data are expressed as the ratio of ipsilateral to contralateral ROIs. * indicates statistical significance +/- SEM over control and sham surgical groups, one-way ANOVA, Tukey's post-hoc, $p < 0.05$ ($n = 4$ for each group). There was an increase in expression observed in both the ET-1 alone and combined A β /ET-1 groups from 3 to 21 d, however this was only statistically significant in the ET-1 alone group as the expression at 3 d was at control levels. (C,D) IHC detection and quantification of GM3 within the infarct region. Panel (C - right) is a higher magnification image of panel (C - left). * indicates statistical significance +/- SEM between groups, one-way ANOVA, Tukey's post-hoc, $p < 0.05$ ($n = 6$ for each group).

2.4.2 *GM3 accumulation is associated with increased neurodegeneration and decreased cell survival at 21 d at the site of injury*

To evaluate the consequence of elevated GM3 expression within the stroke region, levels of cellular degeneration and neuronal loss were assessed. FluoroJade B (FJB) staining, a non-specific marker of cell death, was used to assess cellular degeneration at both 3 and 21 d after surgery. Extensive FJB positive staining was observed within the borders of the infarct in both the ET-1 alone and combined A β /ET-1 groups (Fig 2.4 A). Quantification of FJB positive cells revealed no significant difference between the ET-1 alone and combined A β /ET-1 groups at 3 d following surgery (Fig 2.4 B). At 21 d post-surgery, the number of FJB-positive cells were lower in both ET-1 alone and combined A β /ET-1 groups compared to 3 d, however the combined group had significantly more degenerating cells (35% reduction from 3 d levels) within the ischemic region compared to the ET-1 alone group (65% reduction from 3 d levels). NeuN, a marker for mature neurons was used to assess the number of neurons that survived between 3 and 21 d within the infarcted striatum. At 3 d following stroke, there were equal numbers of NeuN positive neurons between ET-1 alone and combined A β /ET-1 groups. However, by 21 d, there were fewer NeuN positive neurons within the infarcted striatum in the combined group compared to the ET-1 alone group. Taken together with the FJB results, this suggests that the combined A β /ET-1 group experienced greater neuronal degeneration within the damaged striatum following stroke. To assess if GM3 expression was localized within neurons and if these neurons underwent degeneration, dual immunofluorescence labeling was performed (Fig 2.4 D). There was a high level of co-localization between NeuN and GM3 as well as between FJB and GM3, indicating that GM3 was expressed in degenerating neurons following stroke.

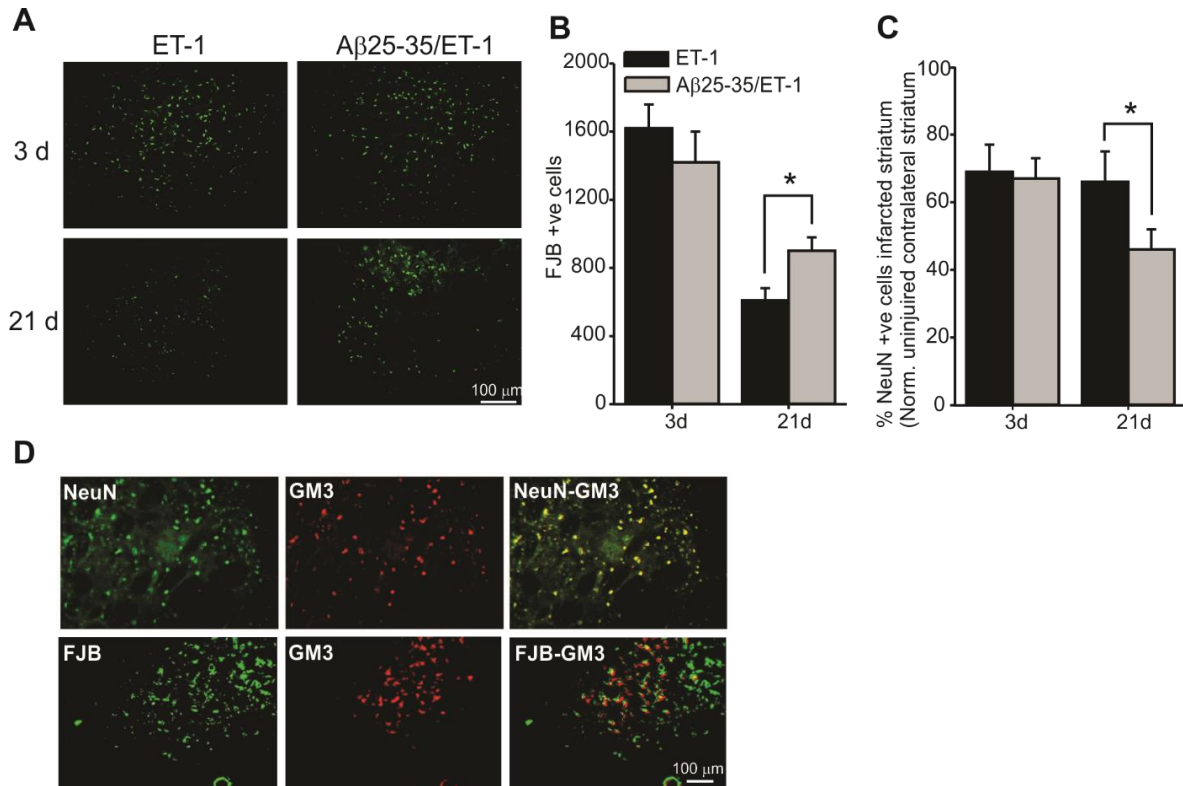


Figure 2.4: Effects of GM3 accumulation on neurodegeneration following stroke. (A) Photomicrographs of fluorojade-B immunofluorescence staining within the infarcted striatum of ET-1 and combined A β /ET-1 coronal rat brain sections. (B and C) Quantification of cell counts of FJB and NeuN cell counts. At 21 d following surgery, there was more FJB positive cells and less NeuN positive cells in the combined A β /ET-1 group compared to the ET-1 group according to one-way ANOVA and Tukey's post-hoc, $p < 0.05$ ($n = 6$ for each group). (D) Photomicrographs of immunofluorescence dual labelling showing co-localization between NeuN and GM3 (shown individually and overlaid) and FJB and GM3 (shown individually and overlaid) in the infarct region of a 21 d combined A β /ET-1 animal.

2.4.3 *Elevated GM2 at 3 d remains elevated at 21 d only in combined A β /ET-1 group*

Since GM3 levels were differently expressed between surgical groups, we next evaluated the levels of GM2. Interestingly, GM2 expression levels were slightly different than the observed changes in GM3. The expression patterns of both the d18:1 and d20:1 species were profiled and quantified by MALDI IMS (Fig 2.5). By 3 d following surgery, both GM2 d18:1 and GM2 d20:1 expression in the combined A β /stroke group was found to be significantly elevated compared to A β alone and control groups (grey bars in Fig 2.5 B and 2.5 D). Although GM2 expression in the ET-1 alone group also showed a very strong trend of increased expression in the GM2 d18:1 species, it was not found to be statistically significant (black bars in Fig 2.5 B). It was, however, found to be significantly elevated in the GM2 d20:1 species compared to A β alone and control groups (black bars in Fig 2.5 D). At 21 d post-surgery, GM2 expression returned to control levels in the ET-1 alone group for both the d18:1 and d20:1 species, but remained increased in the combined A β /ET-1 group compared to A β alone and control groups (grey bars in Fig 2.5 D), though this increased expression was only statistically significant in the d20:1 species.

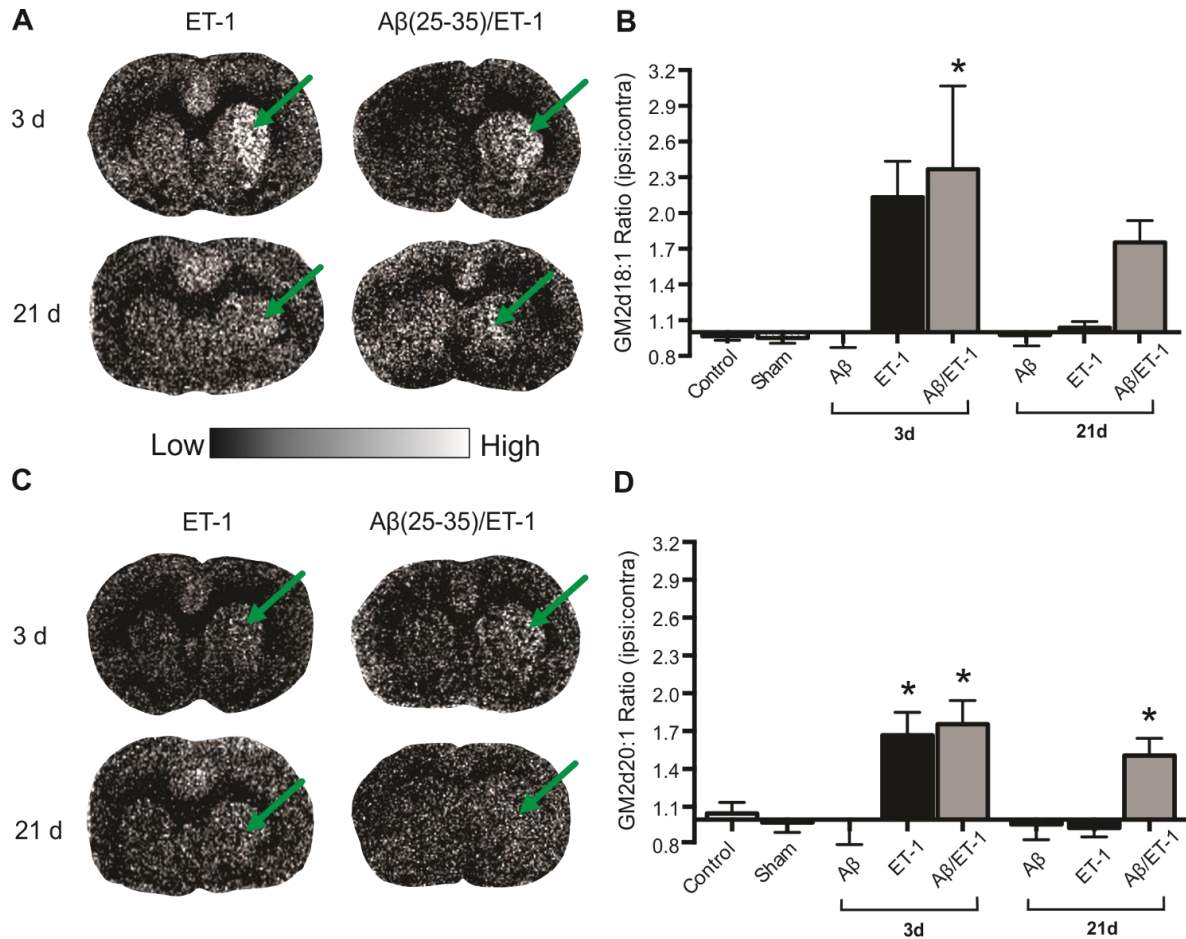


Figure 2.5: Elevated GM2 Expression at 3 d Remains Increased only in Combined A β /ET-1 Group. (A and C) Representative MALDI IMS images of GM2 d18:1 (A) and d20:1 (C) in stroke (ET-1 alone) and combined A β /ET-1 animals 3 and 21 d following surgery. Arrows indicate region of stroke induced infarct. (B and D) MALDI IMS quantification of ROI's from the striatum of control, sham surgery, A β alone, ET-1 alone, and combined A β /ET-1 animals at 3 d and A β alone, ET-1 alone, and combined A β /ET-1 animals at 21 d. Data are expressed as the ratio of ipsilateral to contralateral ROIs. Light regions in images represent areas of high expression while dark regions represent low levels of expression as indicated by intensity bar. There was no statistical increase in GM2 expression between 3 and 21 d in any group, however, GM2 expression in the ET-1 group decreased significantly from 3 to 21 d (back to control levels). * indicates statistical significance +/- SEM over control and sham surgical groups, one-way ANOVA, Tukey's post-hoc, $p < 0.05$ ($n = 4$ for each group).

2.4.4 *Elevated GM1 expression in combined A β /ET-1 group.*

Analysis of GM1 d18:1 expression was performed and data indicated no statistical difference between the ET-1 alone, A β alone, and control groups 3 d following surgery, however, GM1 expression in the combined A β /ET-1 group was significantly elevated compared to the other surgical and control groups (Fig 2.6 B). At 21 d, GM1 d18:1 expression showed the same expression profile between experimental groups with no statistical differences (Fig 2.6 B). Analysis of the d20:1 species of GM1 demonstrated significantly increased expression in the combined A β /ET-1 group compared to all surgical and control groups at both 3 and 21 d post-surgery (Fig 2.6 D).

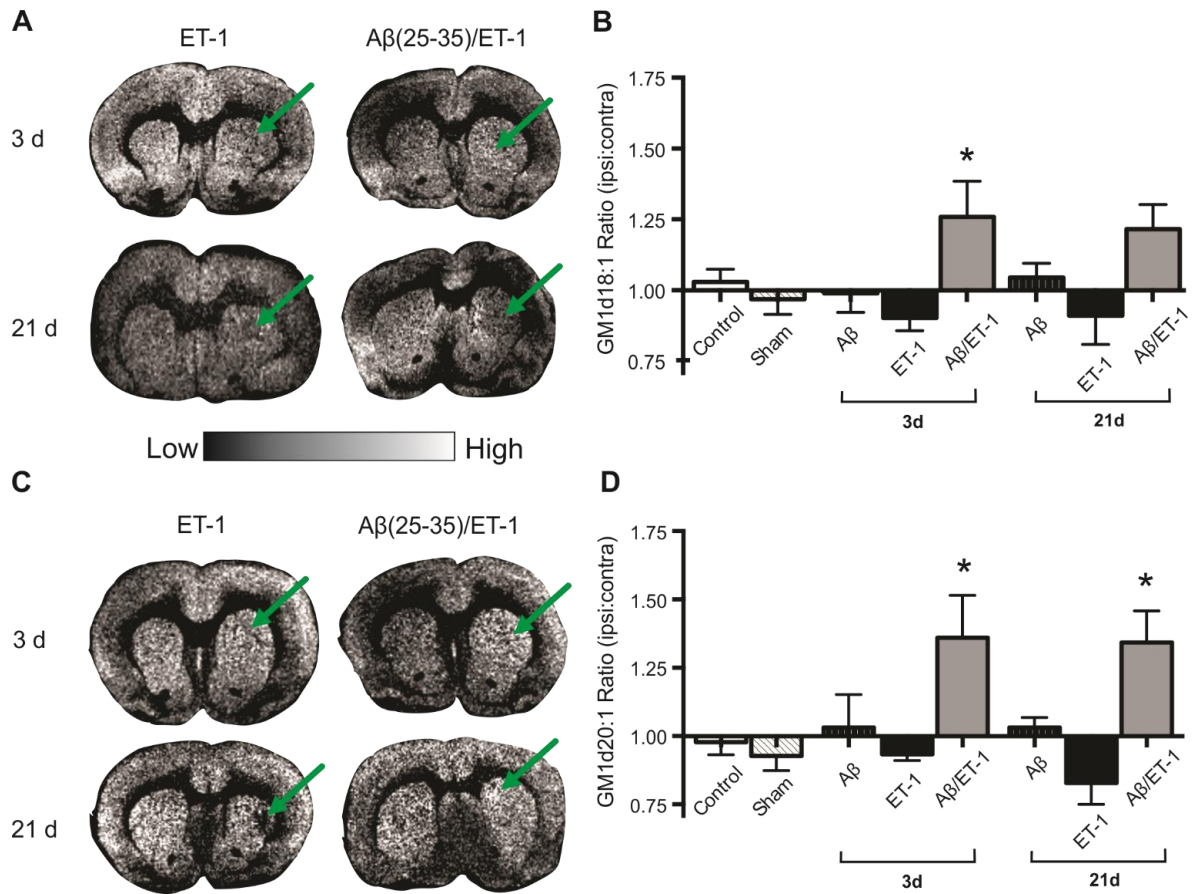


Figure 2.6: Elevated GM1 Expression in Combined A β /ET-1 Group. (A and C) Representative MALDI IMS images of GM1 d18:1 (A) and d20:1 (C) in stroke (ET-1 alone) and combined A β /ET-1 animals 3 and 21 d following surgery. Arrows indicate region of stroke induced infarct. (B and D) MALDI IMS quantification of ROI's from the striatum of control, sham surgery, A β alone, ET-1 alone, and combined A β /ET-1 animals at 3 d and A β alone, ET-1 alone, and combined A β /ET-1 animals at 21 d. Data are expressed as the ratio of ipsilateral to contralateral ROIs. Light regions in images represent areas of high expression while dark regions represent low levels of expression as indicated by intensity bar. There were no statistically significant changes in GM1 expression between 3 and 21 d in any of the groups. * indicates statistical significance +/- SEM over control and sham surgical groups in panel (B) and statistical significance over control, sham and ET-1 alone surgical groups in panel (D), one-way ANOVA, Tukey's post-hoc, $p < 0.05$ ($n = 4$ for each group).

2.4.5 *Increased GD1a [Na⁺] expression at 3 d in combined A β /ET-1 group*

All MALDI IMS experiments presented in this work were performed using negative ion mode. The most intense signals observed for GM1, GM2, and GM3 were their singly charged anions, $[M - H^+]^{1-}$ (M minus H⁺ ions). Given that sialic acid is the most acidic site of these gangliosides, and each GM1, GM2, and GM3 has one sialic acid, the deprotonation site is likely the sialic acid. GD1a on the other hand is the only ganglioside studied in this work having two sialic acid groups. However, the doubly charged GD1a anion, $[M - 2H^+]^{2-}$, was not observed by MALDI MS. Instead, the sodium and potassium adducts were observed as two distinct peaks, $[M - 2H^+ + Na^+]^{1-}$ and $[M - 2H^+ + K^+]^{1-}$, likely due to its considerable presence in tissue. Interestingly, GD1a showed very different patterns of expression for the sodium and potassium adduct ions. (Figs 2.7 and 2.8). At 3 d post-surgery, GD1a [Na⁺] d18:1 showed significantly increased expression in the combined A β /ET-1 group compared to controls (Fig 2.7 B and 2.7 D).

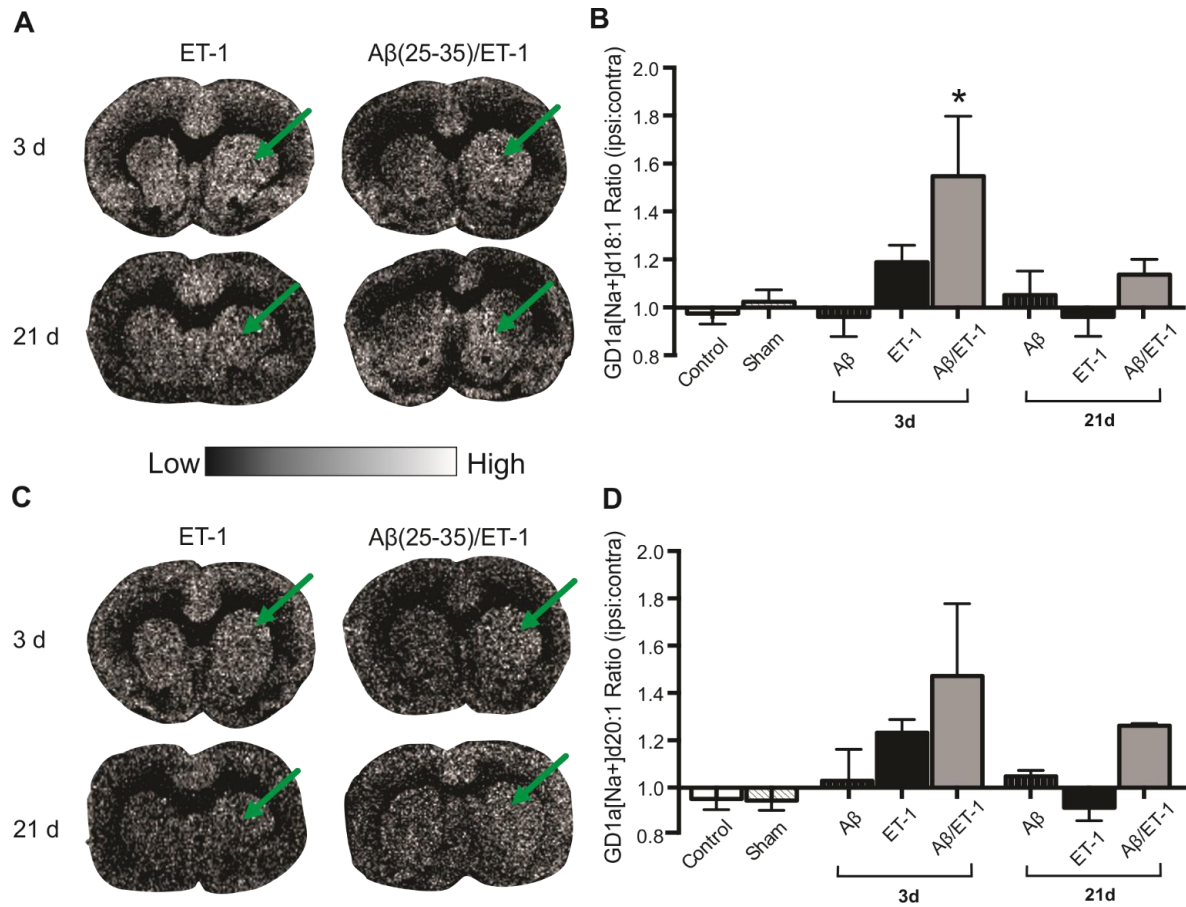


Figure 2.7: Increased GD1a [Na⁺] Expression at 3 d in Combined A β /ET-1 Group (A and C) Representative MALDI IMS images of GD1a [Na⁺] d18:1 (A) and d20:1 (C) in stroke (ET-1 alone) and combined A β /ET-1 animals 3 and 21 d following surgery. Arrows indicate regions of stroke induced infarct. (B and D) MALDI IMS quantification of ROI's from the striatum of control, sham surgery, A β alone, ET-1 alone, and combined A β /ET-1 animals at 3 d and A β alone, ET-1 alone, and combined A β /ET-1 animals at 21 d. Data are expressed as the ratio of ipsilateral to contralateral ROIs. Light regions in images represent areas of high expression while dark regions represent low levels of expression as indicated by intensity bar. GD1a [Na⁺] expression significantly decreased from 3 to 21 d in the d18:1 species. There were no other significant changes in expression between 3 and 21 d in any of the groups. * indicates statistical significance over control and sham surgical groups one-way ANOVA, Tukey's post-hoc, $p < 0.05$ ($n = 4$ for each group).

2.4.6 *Decreased expression of GD1a [K⁺] at 3 d in ET-1 alone group*

The d18:1 species expression in the combined A β /ET-1 group decreased at 21 d and was no longer different from the other groups. The potassium adduct of GD1a, (GD1a [K⁺]) (Fig 2.8) showed a completely different pattern of expression from the GD1a [Na⁺]. At 3 d post-surgery, the ET-1 alone group demonstrated a significantly decreased expression of GD1a [K⁺] compared to A β alone and control groups, but this returned to control levels by 21 d, whereas no statistical difference was observed at either time point in the combined A β /ET-1 group, although there was a trend of decreased expression as well (Fig 2.8 A and 2.8 B). A similar trend was observed for the GD1a [K⁺] 20:1 species (Fig 2.8 C and 2.8 D).

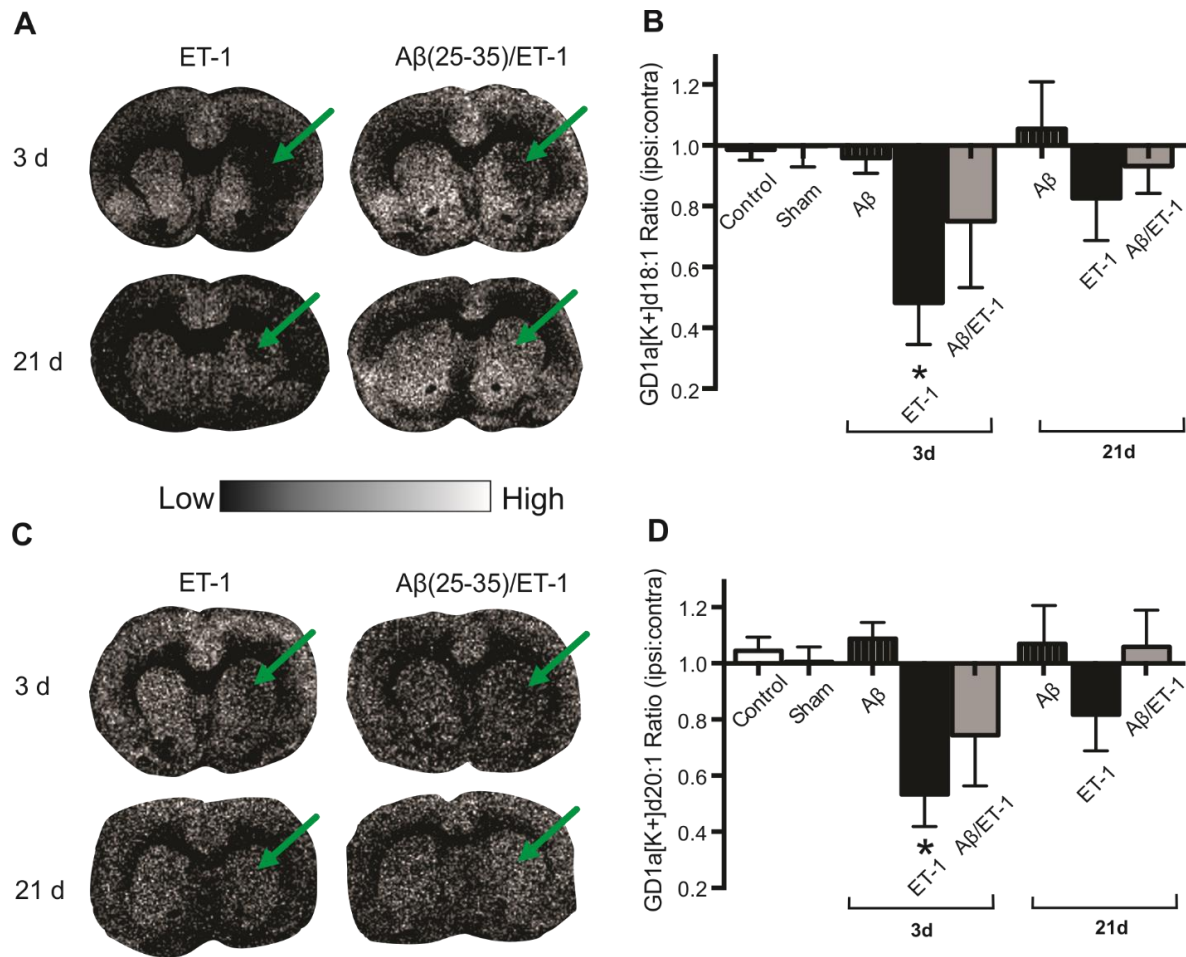


Figure 2.8: Decreased expression of GD1a [K⁺] at 3 d in ET-1 alone group. (A and C) Representative MALDI IMS images of GD1a [K⁺] d18:1 (A) and d20:1 (C) in stroke (ET-1 alone) and combined A β /ET-1 animals 3 and 21 d following surgery. Arrows indicate regions of stroke induced infarct. (B and D) MALDI IMS quantification of ROI's from the striatum of control, sham surgery, A β alone, ET-1 alone, and combined A β /ET-1 animals at 3 d and A β alone, ET-1 alone, and combined A β /ET-1 animals at 21 d. Data are expressed as the ratio of ipsilateral to contralateral ROIs. Light regions in images represent areas of high expression while dark regions represent low levels of expression as indicated by intensity bar. There were no statistically significant changes in expression between 3 and 21 d in any of the surgical groups. * indicates statistical significance over control groups, one-way ANOVA, Tukey's post-hoc, $p < 0.05$ ($n = 4$ for each group).

2.5 Discussion

Based on evidence from the literature (Chung et al., 2009; Nakatsuji & Miller, 2001; Prokazova et al., 2009; Sekigawa et al., 2011; Sohn et al., 2006; Woods et al., 2013; Yu, Suzuki & Yanagisawa, 2010; Yamamoto et al., 1996), the observed increase in simple ganglioside species GM2 and GM3 in the stroke region of the A β /ET-1 combined group at both 3 and 21 d after surgery is indicative of a more severe pathological response compared to ET-1 or A β alone. GM2 has been shown to be elevated immediately after TBI (Woods et al., 2013) and GM3 accumulation has been shown to increase toxicity and induce apoptosis in cells (Chung et al., 2009; Nakatsuji & Miller, 2001; Seyfired & Mukherjee, 2010; Sohn et al., 2006). The observed reduction of GM2 expression back to control levels following ET-1 alone at 21 d may imply that the brain has begun repair processes or the injury was less severe. GM2 expression levels within the combined A β /ET-1 rat brain remained elevated at 21 d which may indicate that the injury is persisting and thus more brain damage is occurring. This hypothesis supports previous pathological and behavioural findings using this combined animal model of A β /ET-1 in our lab (Amtul et al., 2014; Whitehead, Hachinski & Cechetto, 2005; Whitehead, Cheng, Hachinski, & Cechetto, 2005; Whitehead et al., 2007; Whitehead et al., 2011). It is possible that the observed accumulation of simple gangliosides is a result of the breakdown of the more complex a-series gangliosides via enzymatic degradation; however, the expression patterns of both GM1 and GD1a observed in this study suggest that the degradation pathways may be more complex. A slight decrease in GM1 ganglioside occurred in the ET-1 alone group while an increase in the simple species GM2 (at 3 d) and GM3 (at 21 d) was observed. This finding supports our initial A-series degradation hypothesis. Contrarily, in the combined A β /ET-1 group, in which previous studies have shown that stroke induced damage was more severe (Whitehead et al., 2005; whitehead et al., 2007; Amtul et al. 2014), a significant increase in GM1 expression was observed despite there also being a significant increase in both GM2 and GM3 at both 3 and 21 d. This finding does not rule out the A-series degradation hypothesis but suggests that the mechanism of simple ganglioside accumulation is more complex than degradation along the A-series pathway. Ganglioside synthesis from the common precursor GM3 can occur by adding sugar units to the oligosaccharide chain (i.e. along most of the A-series pathway) or by the addition of sialic acid residues (i.e. A to B-

series pathway). It is possible that in the combined A β /ET-1 group, where an increase in both simple and complex a-series gangliosides was observed, the accumulation was due to the degradation of the sialic acid residues of B- or C-series gangliosides thus resulting in an increase in the A-series species. Further study into the enzymatic activities that regulate ganglioside metabolism during and post-brain injury is warranted to address this question.

The accumulation of the simple ganglioside species GM3 is of particular interest due to evidence supporting its potential apoptotic properties (Chung et al., 2009; Nakatsuji & Miller, 2001; Seyfired & Mukherjee, 2010; Sohn et al., 2006). The immediate and significant increase along with the sustained expression of GM3 over time observed within in the combined A β /ET-1 rat brain may be reflective of the increased pathological response that was previously observed in this animal model (Amtul et al., 2014; Whitehead, Hachinski & Cechetto, 2005; Whitehead, Cheng, Hachinski, & Cechetto, 2005; Whitehead et al., 2007; Whitehead et al., 2011). Interestingly, GM3 did not show the same pattern of expression in the ET-1 alone brain, with a trend of increased expression only at 21 d post-surgery, suggesting that the interaction between A β and the stroke injury was responsible for the observed accumulation of GM3 in the combined group and may have played a mechanistic role in the synergism of these two pathologies. Unexpectedly, results from the GM3 IHC and MALDI IMS images from the ET-1 alone group (Fig 2.2) were not fully congruent. This may be explained by the difference in the techniques themselves as IHC and MALDI IMS do not necessarily measure the same thing, especially with respect to detection of lipids. IHC measures the ability of the ganglioside antibody to bind to, and label GM3 on cellular membranes while MALDI IMS measures the signal intensity of ions of a particular mass-to-charge ratio corresponding to GM3 molecules. The lack of specificity for ganglioside antibodies to bind and label tissues in IHC is a significant challenge in the glycosphingolipid field and thus is the principle reason MALDI IMS was chosen as the main technique in this study.

Previous work using a mouse model of stroke-reperfusion injury examined ganglioside expression in a number of key anatomical regions for ischemic risk, including the striatum, and found that there was an increase in complex ganglioside species GM1 and GD1a immediately after stroke which peaked at 3 d after injury then returned to basal

levels at later time points (Whitehead et al., 2011). This trend is similar to the results of the combined group in the current study. However, following stroke alone there was a decrease in GM1 and GD1a [K⁺] expression after injury. The differences in these results may be explained by the type and severity of injury the animals received. Whitehead et al. (2011) used a mouse model of middle cerebral artery occlusion (MCAO) that causes a severe, focal ischemic insult that damages a large region within the cerebral cortex, striatum, and hippocampus. This contrasts with the site specific striatal ET-1 ischemia model used in this study which was chosen as it best emulates the smaller, lacunar strokes seen in aging individuals who are at risk of developing dementia. The combination of A β -toxicity and stroke resulted in a more severe response than stroke alone, which may explain why the results of that surgical group better resemble the results of the severe MCAO stroke injury (Whitehead et al., 2011).

Since the d18:1 and d20:1 species are hypothesized to have unique functions within the cell (Sekigawa et al., 2011), where possible, both species were quantified and analyzed. Although the main patterns of expression were similar, significant changes in expression were observed in the d20:1 species that did not reach statistical significance in the d18:1 species. This leads to the possibility that a greater change in expression was occurring in the d20:1 species than its more prevalent d18:1 species within the site of ischemic injury; however, further investigations are needed to follow up on this finding. The significance of this finding lies in the potential for future therapeutics targeting gangliosides as the d20:1 form may prove to be a more efficient therapeutic target than the d18:1 species.

Although MALDI IMS has proven to be an invaluable and reliable tool for the investigation of ganglioside expression, this study is not without limitations. The most limiting factor to the use of MALDI IMS in clinically-relevant research is that it is generally considered to be only a semi-quantitative technique. According to Stoekli et al. (2007) and Lietz et al. (2013), MALDI IMS images differ from each other due to three main factors which vary from image to image: tissue heterogeneity, sample preparation, and ion suppression effects. These variations make it difficult to quantitatively compare between MALDI IMS images without producing a significant amount of error. However, this study was uniquely designed to circumvent all major sources of error that arise from

these factors. Firstly, MALDI IMS images from this study were not compared to each other but instead were compared to themselves. By comparing the stroke-injured hemisphere with the contralateral non-injured hemisphere, variability due to sample preparation and matrix application was negligible. Secondly, because the two quantified regions of interest were from the same tissue section on mirrored regions of each hemisphere of the brain, it can be assumed that any tissue heterogeneity would be equivalent in both regions and thus not a significant source of error. Finally, ionization suppression effects, which are mass spectrometry signals other than the signal of interest that suppress the overall signal obtained, can also be assumed to be equivalent based on this method of quantification. Quantification of MALDI IMS images remains a controversial and heavily researched area of study, and while our method of quantification does not eliminate all sources of error, variability, the largest source of error, was significantly minimized.

This study was able to show, for the first time, that ganglioside expression was not only altered in stroke injury but is also differentially altered in a comorbid rat model of A β toxicity and stroke. Translating these animal findings to a potential clinical environment, changes in ganglioside expression may be indicative of a new mechanism of synergy and possible site of intervention for those at risk or currently suffering from AD and stroke comorbidities.

2.6 References

- Abate, L. E., Mukherjee, P., & Seyfried, T. N. (2006). Gene-linked shift in ganglioside distribution influences growth and vascularity in a mouse astrocytoma. *Journal of Neurochemistry*, 98(6), 1973-1984.
- Sekigawa, A., Fujita, M., Sekiyama, K., Takamatsu, Y., Wei, J. & Hashimoto, M. (2011). Gangliosides as a double-edged sword in neurodegenerative disease.
- Amtul, Z., Nikolova, S., Gao, L., Keeley, R. J., Bechberger, J. F., Fisher, A. L., Cechetto, D. F. (2014). Comorbid a β toxicity and stroke: Hippocampal atrophy, pathology, and cognitive deficit. *Neurobiology of Aging*
- Ando, S., Chang, N. C., & Yu, R. K. (1978). High-performance thin-layer chromatography and densitometric determination of brain ganglioside compositions of several species. *Analytical Biochemistry*, 89(2), 437-450.

- Angel, P. M., Spraggins, J. M., Baldwin, H. S., & Caprioli, R. (2012). Enhanced sensitivity for high spatial resolution lipid analysis by negative ion mode matrix assisted laser desorption ionization imaging mass spectrometry. *Analytical Chemistry*, *84*(3), 1557-1564.
- Barrier, L., Ingrand, S., Damjanac, M., Rioux Bilan, A., Hugon, J., & Page, G. (2007). Genotype-related changes of ganglioside composition in brain regions of transgenic mouse models of alzheimer's disease. *Neurobiology of Aging*, *28*(12), 1863-1872.
- Bley, A. E., Giannikopoulos, O. A., Hayden, D., Kubilus, K., Tifft, C. J., & Eichler, F. S. (2011). Natural history of infantile GM2 gangliosidosis. *Pediatrics*, *128*(5), e1233-e1241.
- Cechetto, D. F., Hachinski, V., & Whitehead, S. N. (2008). Vascular risk factors and alzheimer's disease. *Expert Review of Neurotherapeutics*, *8*(5), 743-750.
- Chan, R. B., Oliveira, T. G., Cortes, E. P., Honig, L. S., Duff, K. E., Small, S. A., . . . Di Paolo, G. (2012). Comparative lipidomic analysis of mouse and human brain with alzheimer disease. *Journal of Biological Chemistry*, *287*(4), 2678-2688.
- Chung, T., Kim, S., Choi, H., Kim, K., Kim, M., Kim, S., . . . Kim, C. (2009). Ganglioside GM3 inhibits VEGF/VEGFR-2-mediated angiogenesis: Direct interaction of GM3 with VEGFR-2. *Glycobiology*, *19*(3), 229-239.
- Desplats, P. A., Denny, C. A., Kass, K. E., Gilmartin, T., Head, S. R., Sutcliffe, J. G., . . . Thomas, E. A. (2007). Glycolipid and ganglioside metabolism imbalances in huntington's disease. *Neurobiology of Disease*, *27*(3), 265-277.
- Jin, Y. P., Østbye, T., Feightner, J. W., Di Legge, S., & Hachinski, V. (2008). Joint effect of stroke and APOE 4 on dementia risk: The canadian study of health and aging. *Neurology*, *70*(1), 9-16.
- Jiwa, N. S., Garrard, P., & Hainsworth, A. H. (2010). Experimental models of vascular dementia and vascular cognitive impairment: A systematic review N. S. jiwa et al. vascular cognitive impairment: In vivo models. *Journal of Neurochemistry*, *115*(4), 814-828.
- Johnston, J. M., Nazar-Stewart, V., Kelsey, S. F., M, I. K., & Ganguli, M. (2000). Relationships between cerebrovascular events, APOE polymorphism and alzheimer's disease in a community sample. *Neuroepidemiology*, *9*(6), 320-326.
- Kotani, M., Kawashima, I., Ozawa, H., Ogura, K., Ishizuka, I., Terashima, T., & Tai, T. (1994). Immunohistochemical localization of minor gangliosides in the rat central nervous system. *Glycobiology*, *4*(6), 855-865.
- Kreutz, F., Frozza, R. L., Breier, A. C., de Oliveira, V. A., Horn, A. P., Pettenuzzo, L. F., . . . Trindade, V. M. T. (2011). Amyloid- β induced toxicity involves ganglioside

- expression and is sensitive to GM1 neuroprotective action. *Neurochemistry International*, 59(5), 648-655.
- Lietz, C., Gemperline, E., & Li, L. (2013). Qualitative and quantitative mass spectrometry imaging of drugs and metabolites. *Advanced Drug Delivery Reviews*, 65, 1074-1085.
- Lopez, P. H., & Schnaar, R. L. (2009). Gangliosides in cell recognition and membrane protein regulation. *Current Opinion in Structural Biology*, 19(5), 549-557.
- Martino, A., Safar, J., Callegaro, L., Salem, N., & Gibbs, C. (1993). Ganglioside composition changes in spongiform encephalopathies: Analyses of 263K scrapie-infected hamster brains. *Neurochemical Research*, 18(8), 907-913.
- Nakatsuji, Y., & Miller, R. H. (2001). Selective cell-cycle arrest and induction of apoptosis in proliferating neural cells by ganglioside GM3. *Experimental Neurology*, 168(2), 290-299.
- Prokazova, N. V., Samovilova, N. N., Gracheva, E. V., & Golovanova, N. K. (2009). Ganglioside GM3 and its biological functions. *Biochemistry (00062979)*, 74(3), 235-249.
- Richards, A. L., Lietz, C. B., Wager-Miller, J., Mackie, K., & Trimpin, S. (2012). Localization and imaging of gangliosides in mouse brain tissue sections by laserspray ionization inlet. *Journal of Lipid Research*, 53(7), 1390-1398.
- Schneider, J. S., Gollomp, S. M., Sendek, S., Colcher, A., Cambi, F., & Du, W. (2013). A randomized, controlled, delayed start trial of GM1 ganglioside in treated parkinson's disease patients. *Journal of the Neurological Sciences*, 324(1-2), 140-148.
- Seyfried, T. N., & Mukherjee, P. (2010). Ganglioside GM3 is antiangiogenic in malignant brain cancer. *Journal of Oncology*, 1-8.
- Snowdon DA, Greiner LH, Mortimer JA, Riley KP, Greiner PA,Markesbery WR. (1997). Brain infarction and the clinical expression of alzheimer disease: The nun study. *JAMA*, 277(10), 813-817.
- Sohn, H., Kim, Y., Kim, H., Kim, C., Cho, E., Kang, H., . . . Ko, J. H. (2006). Ganglioside GM3 is involved in neuronal cell death. *The FASEB Journal*, 20(8), 1248-1250.
- Stoeckli, M., Staab, D., Schweitzer, A., Gardiner, J., & Seebach, D. (2007). Imaging of a beta-peptide distribution in whole-body mice sections by MALDI mass spectrometry. *Journal of the American Society of Mass Spectrometry*, 18, 1921-1924.
- Svennerholm, L., & Gottfries, C. (1994). Membrane lipids, selectively diminished in alzheimer brains, suggest synapse loss as a primary event in early-onset form (type I) and demyelination in late-onset form (type II). *Journal of Neurochemistry*, 62(3), 1039-1047.

- Whitehead, S. N., Chan, K. H. N., Gangaraju, S., Slinn, J., Li, J., & Hou, S. T. (2011). Imaging mass spectrometry detection of gangliosides species in the mouse brain following transient focal cerebral ischemia and long-term recovery. *PLoS ONE*, *6*(6), e20808.
- Whitehead, S. N., Cheng, G., Hachinski, V. C., & Cechetto, D. F. (2007). Progressive increase in infarct size, neuroinflammation, and cognitive deficits in the presence of high levels of amyloid. *Stroke*, *38*(12), 3245-3250.
- Whitehead, S. N., Hachinski, V. C., & Cechetto, D. F. (2005). Interaction between a rat model of cerebral ischemia and β -amyloid toxicity: Inflammatory responses. *Stroke*, *36*(1), 107-112.
- Whitehead, S., Cheng, G., Hachinski, V., & Cechetto, D. F. (2005). Interaction between a rat model of cerebral ischemia and β -amyloid toxicity: II. effects of triflusal. *Stroke*, *36*(8), 1782-1789. doi:10.1161/01.STR.0000173405.02425.d6
- Woods, A. S., Colsch, B., Jackson, S. N., Post, J., Baldwin, K., Roux, A., Balaban, C. (2013). Gangliosides and ceramides change in a mouse model of blast induced traumatic brain injury. *ACS Chemical Neuroscience*, *4*(4), 594-600.
- Yamamoto, A., Haraguchi, M., Yamashiro, S., Fukumoto, S., Furukawa, K., Takamiya, K., Furukawa, K. (1996). Heterogeneity in the expression pattern of two ganglioside synthase genes during mouse brain development. *Journal of Neurochemistry*, *66*(1), 26-34.
- Yu, R. K., Nakatani, Y., & Yanagisawa, M. (2009). The role of glycosphingolipid metabolism in the developing brain. *Journal of Lipid Research*, *50*, S440-S445.
- Yu, R. K., Suzuki, Y., & Yanagisawa, M. (2010). Membrane glycolipids in stem cells. *FEBS Letters*, *584*(9), 1694-1699.

Chapter 3 : Age dependent and regional heterogeneity in the long-chain base of A-series gangliosides observed in the rat brain using MALDI Imaging

3

In Chapter 2, both d18:1 and d20:1 species of a-series gangliosides were altered in response to the various neurodegenerative injuries. Interestingly, the d20:1 species often showed a more a severe perturbation of their homeostatic distribution in response to the injuries, suggesting that these species may be particularly susceptible to dysregulation. Little is known of the functional implications of gangliosides with varying carbon lengths, particularly for the less abundant simple ganglioside species, however, complex gangliosides with longer carbon chains have been reported to accumulate in an age-dependent manner (Sugiura et al., 2008; Palestini et al., 1990; Sonnino et al., 2000). Limitations in the sensitivity and spatial resolution of MALDI IMS images of ganglioside observed in Chapter 2 meant that the d20:1 species of GM3 could not be detected. This led to establishment of refined sample preparation methodologies that, coupled with an upgraded instrument, led to dramatic improvements in ganglioside detection and spatial resolution (Appendix ii). Specifically, a modified sublimation protocol was developed which was tailored for the optimal detection of a-series gangliosides and published in the *Journal of Visualized Experiments* (Appendix iii). Therefore, armed with an improved MALDI IMS protocol, we sought to better understand the role of simple and complex ganglioside carbon chain length in the context of aging in Wt and Tg APP21 Fisher rats.

3.1 Abstract

Alterations in the long chain base of the sphingosine moiety of gangliosides have been shown to play a role in neurodevelopment and neurodegeneration. Indeed, the accumulation of d20:1 sphingosine has been referred to as a metabolic marker of aging in the brain, however, this remains to be shown in simple gangliosides GM2 and GM3. In this study, MALDI IMS was used to examine the neuroanatomical distribution of A-series

gangliosides with either 18 or 20 carbon sphingosine chains (d18:1 or d20:1) in Fisher 344 rats across the lifespan. The ratio of d20:1/d18:1 species was determined across 11 regions of interest in the brain. Interestingly, a decrease in the d20:1/d18:1 ratio for GM2 and GM3 was observed during early development with the exception of the peri-ventricular corpus callosum, where an age-dependent increase was observed for ganglioside GM3. An age-dependent increase in d20:1 species was confirmed for complex gangliosides GM1 and GD1 with the most significant increase during early development and a high degree of anatomical heterogeneity during aging. The unique neuroanatomically-specific responses of d20:1 ganglioside abundance may lead to a better understanding of regional vulnerability to damage in the aging brain.

3.2 Introduction

Gangliosides are a class of glycosphingolipids that are found throughout all cells of the body, with certain species enriched in the central nervous system (CNS). They are part of a large family of lipid species that form an important structural and functional component of lipid rafts, a functional domain of the cell membrane enriched in phospholipids, cholesterol, and gangliosides in which protein-lipid interactions occur leading to signal transduction (Sonnino, Mauri, Ciampa, & Prinetti, 2013; Yu, Tsai, & Ariga, 2012). Within the CNS, each ganglioside appears to have unique effects on signal transduction. For example, ganglioside GM1 has been shown to enhance neuroprotection through modulation of neurotrophin release (Rabin, Bachis, & Mocchetti, 2002) and ion transport (Wu & Ledeen, 1994), while accumulation of ganglioside GM3 has been shown to lead to apoptotic cell death in astrocytes (Nakatsuji & Miller, 2001) and neurons (Sohn et al., 2006). Moreover, perturbations in the homeostatic distribution of gangliosides has been observed in rodent models of brain injury such as middle cerebral arterial occlusion (MCAO) stroke (Whitehead et al., 2011), co-morbid stroke and amyloid beta toxicity (Caughlin et al., 2015), and traumatic brain injury (Woods et al., 2013), as well as in preclinical models and human patients with neurodegenerative diseases (Desplats et al., 2007; Di Pardo, Amico, & Maglione, 2016; Kaya et al., 2017; Oikawa et al., 2009; Yamamoto, Nostrand, & Yanagisawa, 2006). Thus, there has been increasing interest in the

maintenance/enhancement of ganglioside homeostasis as a treatment for neurodegenerative conditions.

Gangliosides are structurally composed of a hydrophilic domain, containing sialic acid residues attached to an oligosaccharide chain, along with a hydrophobic domain made up of a ceramide complex (Fig. 3.1 A). Ceramide is composed of a fatty acid attached to a sphingosine long-chain base (LCB). Gangliosides can be differentiated from each other based on the length of their oligosaccharide chain and the number of sialic acid residues in their hydrophilic domain, which determines the type of ganglioside as described by their designation (e.g. ganglio-monosialo 3 or GM3). Gangliosides can also be differentiated by the type of fatty acid and number of carbons present within their ceramide domain. The 18 carbon sphingosine, chemically denoted as d18:1, is the predominant species in brain gangliosides, with 20 carbon species (d20:1) being present in lower, but variable quantities (Rosenberg & Stern, 1966).

Alterations in the LCB have been linked to neurodevelopment and also implicated as a potential mechanism in the development of neurodegeneration (Caughlin et al., 2015; Tamai et al., 1979). Structurally, the additional carbons present on the ceramide moiety lead to an increase in volume of the hydrophobic portion of the molecule. This alters the organization of the membrane and its fluid properties (Masserini, Palestini, & Freire, 1989). Changes in the organization of the membrane has consequences for the ability of gangliosides in lipid-rich domains to interact with the external environment and carry out their function as modulators of cell signaling (Sonnino & Chigorno, 2000). Therefore, the presence of d18:1 or d20:1 species in the membrane may alter the effectiveness of signal transduction at the cell surface. The d20:1 species have also been referred to as a metabolic marker of aging (Palestini, Masserini, Sonnino, & Tettamanti, 1990) as these species have consistently been observed to increase with age in murine (Palestini et al., 1990; Palestini et al., 1993; Rosenberg & Stern, 1966; Sugiura et al., 2008; Valsecchi, Palestini, Chigorno, & Sonnino, 1996) and human brains (Mansson, Vanier, & Svennerholm, 1977). However, the literature on this topic has focused almost exclusively on major complex gangliosides GM1, GD1, GT1, and GQ1, with minimal neuroanatomically-specific information, and has not described how the LCB of minor, simple gangliosides shift during aging. This

information may be crucial as there is increasing evidence pointing to the potential role of simple ganglioside, such as GM3 and GM2, in the development and pathogenesis of neurodegenerative diseases and injuries (Caughlin et al., 2015; Whitehead et al., 2011; Woods et al., 2013), however, the role of the ceramide moiety remains unclear due to technical challenges in the detection of these low abundance species.

Previous investigations have used MALDI IMS to visualize d18:1 and d20:1 species of ganglioside GM1 (Caughlin et al., 2015; Sugiura et al., 2008; Weishaupt, Caughlin, Yeung, & Whitehead, 2015; Whitehead et al., 2011). This technique has the advantage of simultaneously detecting multiple species of gangliosides (and other molecules) within the same sample based on their abundance and neuroanatomical location. This tool is also a powerful technique to differentiate carbon numbers within ganglioside LCB, which cannot be done using antibody labelling. A study describing the expression of d18:1 and d20:1 species of all A-series gangliosides during the aging process has not yet been done. Therefore, the following study provides the first detailed examination of age-dependent changes in the LCB of both simple and complex A-series gangliosides across a large number brain regions in wildtype (Wt) and APP21 transgenic (Tg) Fisher 344 rats that contain the human mutations to the amyloid precursor protein (Agca et al., 2008; Weishaupt et al., 2015). We hypothesized that there would be significant regional differences in the ratio of d20:1 species relative to d18:1 across the brain throughout aging and that this would be enhanced in the Tg APP21 rat. To achieve this, we used MALDI IMS (Fig. 3.1 B+C), for accurate neuroanatomically-localized detection of d18:1 and d20:1 species across intact tissue sections.

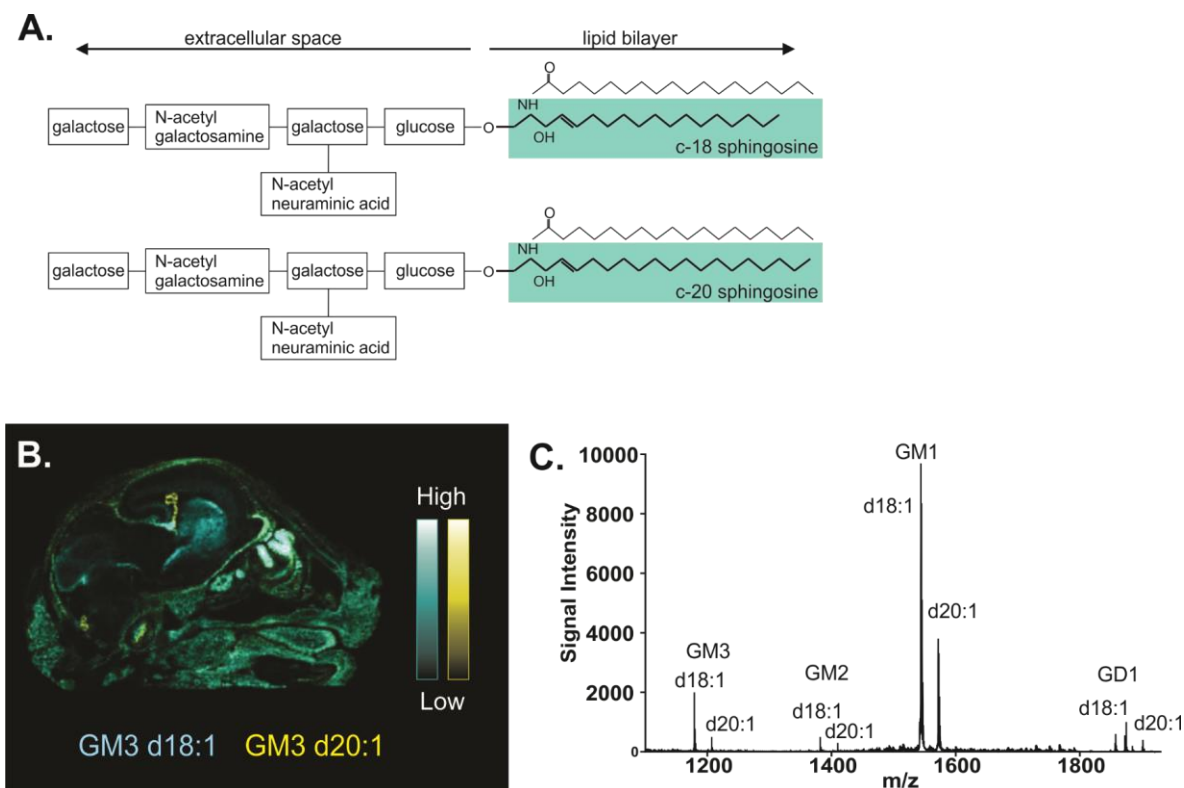


Figure 3.1: Ganglioside structure and detection using MALDI IMS. Chemical structure and MALDI IMS of d18:1 and d20:1 gangliosides. (A) Gangliosides are composed of both a hydrophilic domain which extends into the extracellular space, and hydrophobic ceramide anchor (highlighted) which is embedded in the cell membrane. The hydrophilic portion contains an oligosaccharide chain and sialic acid residues which determine the type of ganglioside (i.e. GM1, GM2, GM3). The hydrophobic portion of the molecule is made up of a fatty acid and a sphingosine LCB tail with varying numbers of carbons. (B) Representative MALDI IMS molecular image depicting anatomical distribution of d18:1 (blues), and d20:1 (yellow) GM3 species across a sagittal section of a P0 Fisher 344 rat head. (C) Representative mass spectrum using DAN matrix in negative reflection mode depicting the mass of a-series gangliosides (and corresponding m/z values) analyzed in the current study. From left to right: GM3 d18:1 (1179 Da), GM3 d20:1 (1207 Da), GM2 d18:1 (1382 Da), GM2 d20:1 (1409 Da), GM1 d18:1 (1543 Da), GM1 d20:1 (1572 Da), GD1a[K⁺] d18:1 (1872 Da) and GD1a[K⁺] d20:1 (1901 Da).

3.3 Materials and Methods

3.3.1 *Animal model*

All procedures involving live animals were in accordance with the guidelines of the Canadian Council on Animal Care and approved by the University of Western Ontario Animal Use Committee (Protocol 2014–2016). Wt and Tg APP21 Fisher 344 rats were kindly provided by Dr. Yukel Agca (University of Missouri) and bred in-house. Tg APP21 rats contained both human Swedish and Indiana mutations for the amyloid precursor protein gene. Because there were no significant transgene effects at each individual time point, the data for both Wt and Tg APP21 rats was pooled for all analysis for a final n value of 10 per group. Rats were aged to 4 different time points to be as representative as possible of the full lifespan, leading to a total of 40 rats included in the study. Rats were sacrificed via fresh-frozen extraction (described elsewhere) at either P0 (newborn), 3 months (m, young rats), 12 m (middle aged), or 20 m (old). Brains were stored at -80°C until processed for MALDI IMS.

3.3.2 *MALDI IMS*

Brain tissue (or whole heads for P0 rats) were sectioned on a cryostat (Thermo-Fisher Scientific CryoStar NX50) at a thickness of 10 μm and thaw mounted onto electrically conductive Indium-Tin-Oxide (ITO) slides (Hudson Surface Technology Inc., Old Tappan, NY, USA). The slides were then coated in a thin layer of 1,5-Diaminonaphthalene (DAN, Sigma-Aldrich, Oakville, ON, Canada) matrix via sublimation and incubated at -20°C overnight. After a 10 min desiccation period, a 5 peptide calibration standard was applied (Sciex, Farmingham, MA, USA) and allowed to dry. An image of the plate was scanned for reference in the instrument and the instrument calibrated using the spotted standards to a mass tolerance of 50 ppm. Images were acquired using a Sciex MALDI 5800 TOF/TOF instrument in negative ion reflectron mode. MS images were acquired at a 70 μm raster with 20 shots/spectrum. This protocol has been previously described in detail (Caughlin et al., 2017). Representative MALDI IMS images of each ganglioside species quantified in the current study are shown in Fig 3.2.

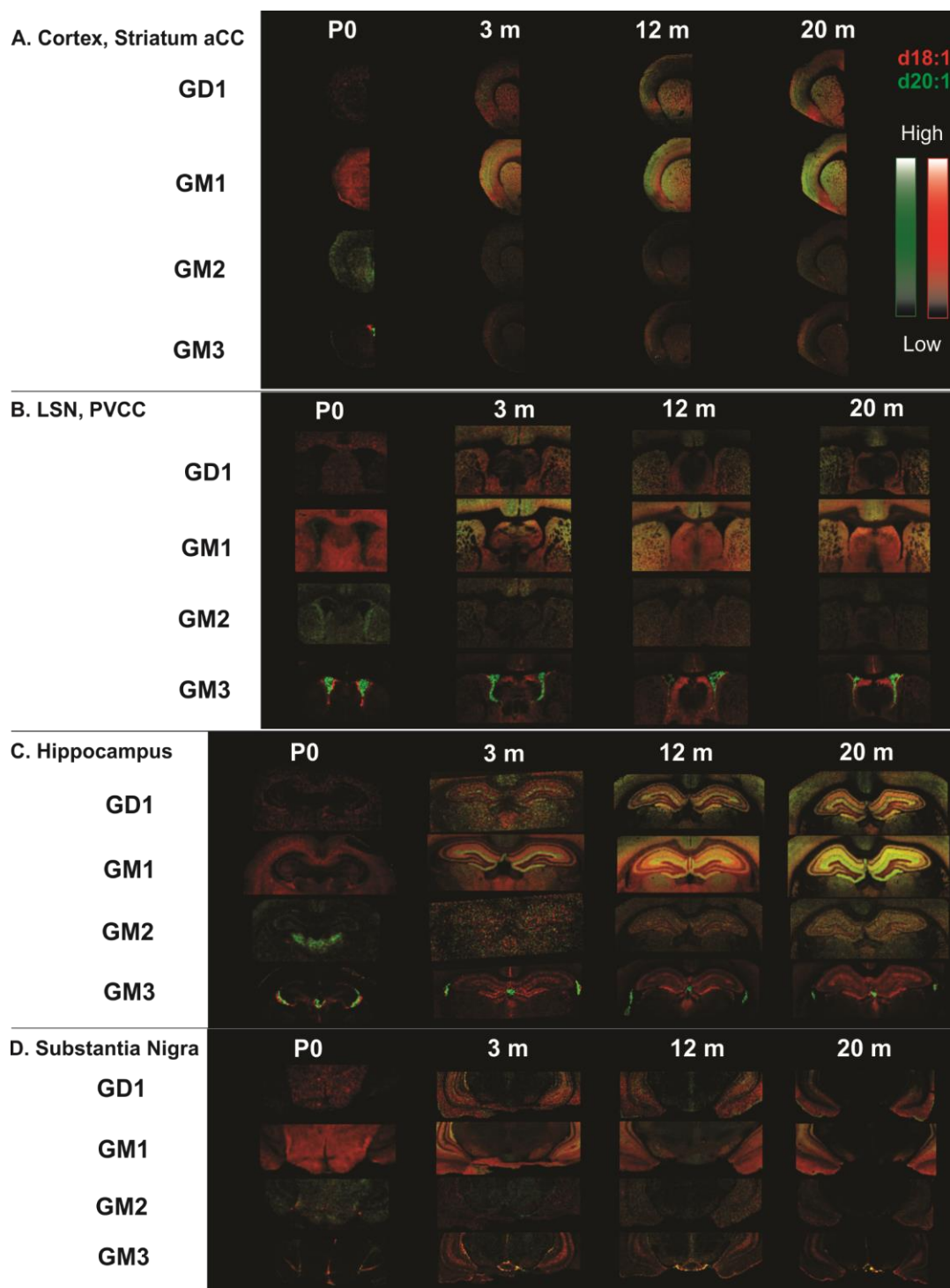


Figure 3.2: Representative MALDI IMS images of each a-series ganglioside in all 4 tissue sections. Representative images from the most anterior tissue section contained the ROIs for the cortical layers, striatum and aCC (A). The second tissue section contained the ROIs for the LSN and PVCC (B). The third section was at the level of the hippocampus and was used for all hippocampal ROIs (C). The most posterior section contained the ROI for the substantia nigra (D). Images are ordered from the earliest time point (P0 – left) to the latest time point (20 m – right) for each tissue section.

3.3.3 Data Analysis

The regions of interest (ROIs) were confirmed using the rat brain atlas by Paxinos & Watson (1998). A total of 11 ROIs were quantified across the brain and were grouped into discrete anatomical/functional regions for quantitation. These clustered groups include: sub-cortical structures (striatum, lateral septal nucleus, and substantia nigra), the cortex (superficial, intermediate, and deep layers of the cortex), the hippocampus (CA1, dentate gyrus molecular layer, dentate gyrus granular layer), and white matter (anterior corpus callosum and peri-ventricular corpus callosum). MALDI IMS images were analyzed using TissueView software (Version 2, Sciex). A total of 4 tissue sections per brain were used to isolate discrete anatomical regions in order to quantify the 11 regions of interest, for a total of 160 MALDI MS images (40 rats×4 sections) and 440 total datasets (40 rats×11 ROIs). Peaks corresponding to major a-series gangliosides were isolated and identified, as confirmed by previous studies (Chan et al., 2009; Dufresne et al., 2017; Sugiura et al., 2008; Woods et al., 2013) and the Lipidmaps database (www.lipidmaps.org). For quantification of MALDI-IMS data, the area under the curve (AUC) of the three largest isotopic peaks was determined and a ratio was obtained between the AUC of each species and total AUC. This corrected value was used to perform a ratio of the d20:1 species of each a-series ganglioside to the d18:1 species. This ratio value was used to make between group comparisons so as to reduce error produced by variability in sample preparation between images as previously published (Caughlin et al. 2015). For GD1, the more abundant K⁺ adduct peaks were used. Statistical analysis was performed using either a student's t-test or a two-way ANOVA, followed by a Tukey's post-hoc test.

3.4 Results

3.4.1 *Genotype differences in LCB restricted to GM3 within the peri-ventricular corpus callosum.*

No significant differences in regional abundance across age were observed between Wt and Tg APP21 rats with the exception of ganglioside GM3 in the peri-ventricular corpus callosum where the fold increase of d20:1/d18:1 between P0 and 20 m was found to be

significantly higher in Tg APP21 rats than their Wt counterparts (Fig. 3.3). Given the lack of genotype specific differences in d20:1/d18:1 ratios at each individual time point, all future analysis used pooled data from both Wt and Tg APP21 rats.

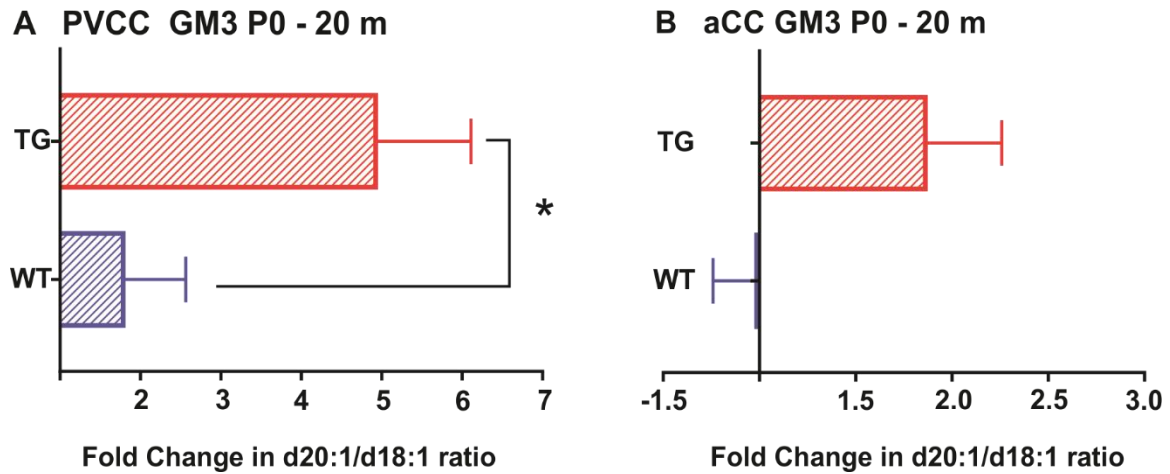


Figure 3.3: Increased d20:1/d18:1 GM3 ratio in PVCC between birth and old age in TgAPP21 rats. Quantification of MALDI IMS data showing the fold change in d20:1/d18:1 signal between birth (P0) and old age (20 m) in the PVCC (A) and corpus callosum (B). Tg APP21 rats showed a significant increase in the d20:1/d18:1 LCB ratio between birth and old age compared to their Wt counterparts in the PVCC. A similar pattern was observed in the aCC, however, the fold change was not statistically different in this region. This transgene difference explains the high degree of variability observed at each individual time point in white matter regions. Data represented as group Means \pm SEM, * indicates statistical significance, $p < 0.05$, via student's T test, $n=5$ for each time point.

3.4.2 *Significant anatomical heterogeneity throughout the rat life span within subcortical and basal ganglia structures for gangliosides GM1 and GM3*

Sub-cortical structures are susceptible to age related changes associated with Alzheimer's disease (basal forebrain) Parkinson's disease (substantia nigra) and Huntington's disease (striatum). We measured the ratio between d20:1 and d18:1 species of gangliosides within the lateral septal nucleus (LSN) of the basal forebrain, substantia nigra (SN), and striatum of rats from P0 to 20 m of age (Fig. 3.4 A). There were no regional differences in GM1 d20:1/d18:1 ratios in P0 rats. At 3 m, the d20:1/ d18:1 ratio was significantly lower in the SN (0.15) than the striatum (0.21), and remained the lowest of the three regions up to 20 m (Fig. 3.4 B). At 12 m, the ratio of GM1 d20:1/d18:1 species was significantly higher in the striatum (0.28) than the SN (0.20), with the LSN between the two (0.24), however, by 20 m, the regional differences shifted back to a similar pattern as that of 3 m, with both the striatum (0.25) and LSN (0.23) demonstrating significantly higher GM1 d20:1/d18:1 ratios than the SN (0.17). When measuring differences in d18:1/d20:1 ratios for GD1, no regional differences were observed at any time point in the basal ganglia (Fig. 3.4 C). The GD1 d20:1/d18:1 ratio increased from P0 to 12 m in all subcortical structures then dropped slightly by 20 m.

With respect to simple ganglioside GM3 during aging, the d20:1/d18:1 ratio increased slightly from P0 (0.43, 0.34) to 12 m (0.49, 0.39) within the LSN and striatum respectively. The d20:1/d18:1 GM3 ratio within the SN decreased significantly from 0.6 in P0 rats to 0.32 at 3 m, which then continued to decrease slightly up to 20 m (0.27) (Fig. 3.4 D). These divergent patterns for the GM3 LCB ratio during aging are indicative of significant regional differences within subcortical structures. Indeed, at P0, a regional difference was observed with significantly higher d20:1 content observed in the SN (0.6) over the striatum (0.35) and LSN (0.43). This pattern shifted at 12 m where the SN d20:1/d18:1 ratio decreased to 0.32 while the LSN ratio increased to 0.49, leading to a significant difference between these two brain regions. These regional differences disappeared at 20 m as the d20:1/ d18:1 ratio dropped in the LSN (0.38) (Fig. 3.4 D). There were no regional differences observed in the GM2 species (Fig. 3.4 E), however, all brain regions showed a significant decrease in the d20:1/d18:1 ratio between P0 and 3 m which then remained stable up to 20 m.

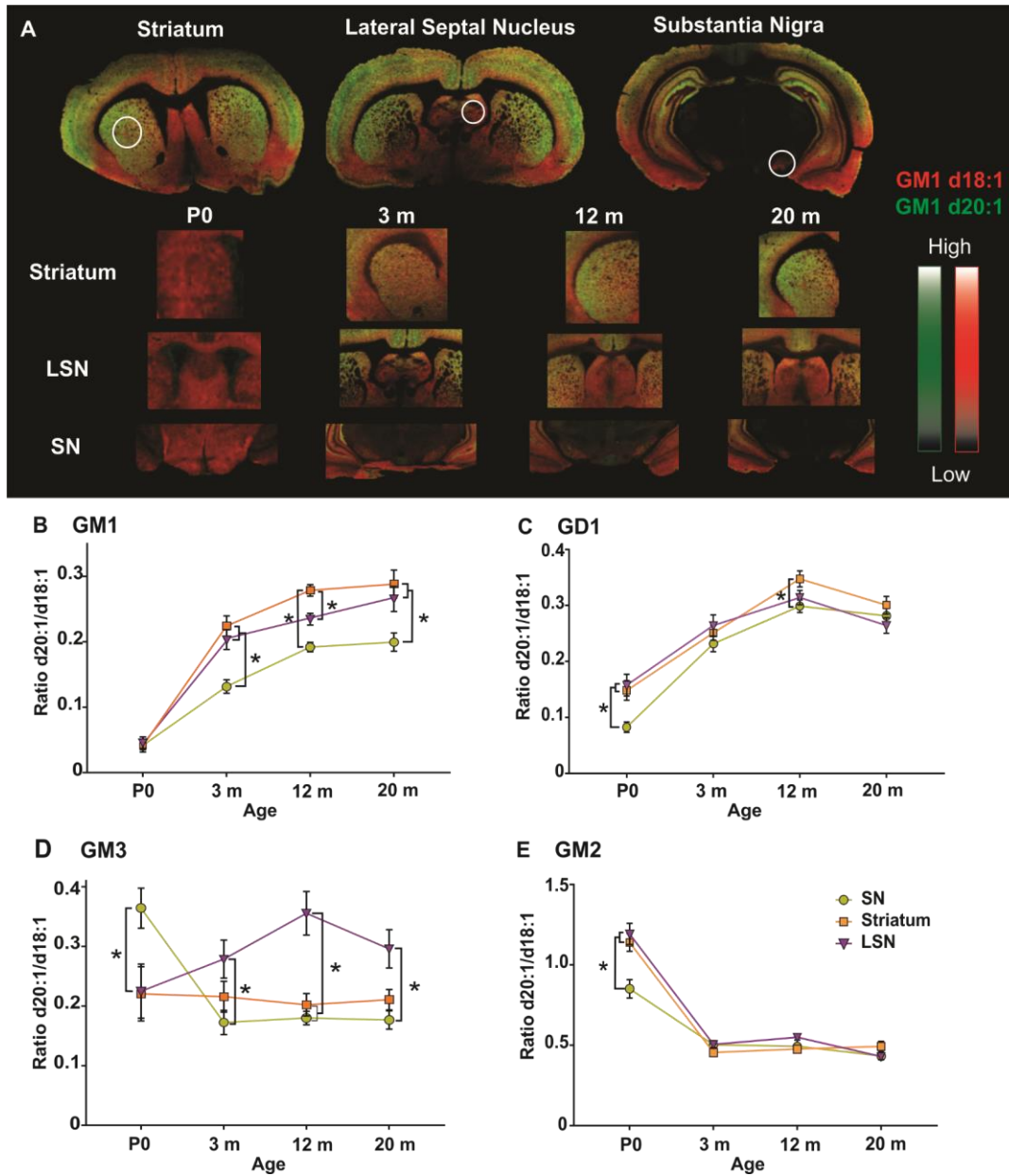


Figure 3.4: Significant regional heterogeneity in ganglioside LCB ratio among sub-cortical structures. Visualization of regional and age-dependent shifts in a-series gangliosides in sub-cortical rat brain structures. (A) Representative MALDI IMS overlay images showing the anatomical distribution of GM1 d18:1 (red) and d20:1 (green). (B–E) Quantification of the d20:1/d18:1 ratio at each time point for GM1 (B), GD1 (C), GM3 (D), and GM2 (E). The d20:1/d18:1 LCB ratio increased in an age-dependent manner for complex gangliosides GM1 and GD1 up to 12 m then plateaued up to 20 m (GM1) or decreased slightly (GD1). Significant anatomical heterogeneity in the LCB ratio was observed from simple ganglioside GM3 among sub-cortical structures, with a decrease during early development in the SN, and a stable ratio in the striatum and LSN throughout the lifespan. Data represented as group Means \pm SEM, *indicates statistical significance, $p < 0.05$, via two-way ANOVA, Tukey multiple comparisons test, $n = 10$ for each time point.

3.4.3 *Cortical layers show regional heterogeneity in ganglioside of LCB length*

Regional differences between the superficial, intermediate, and deep layers of the cerebral cortex have previously been reported (Weishaupt et al., 2015). The present study used similar cortical ROIs (Fig. 3.5 A) to evaluate alterations in the LCB length during aging in the rat. When measuring the LCB length of GM1, a similar d20:1/d18:1 ratio of 0.07–0.09 was observed in all three layers of the cortex of P0 rats (Fig. 3.5 B). All three layers demonstrated variable but increased d20:1/d18:1 GM1 during aging with a plateau observed at 12 m. Interestingly, the intermediate layer demonstrated the highest ratio of d20:1/d18:1 expression for GM1 which became apparent at 3 m (intermediate – 0.30, superior – 0.25, deep – 0.20) and continued to be significantly higher than the deep layers up to 20 m. A similar pattern was observed for LCB length of GD1 whereby P0 rats had similar ratios of d20:1/d18:1 throughout all layers of the cortex followed by an increase in the ratio of d20:1/d18:1 at 3 m and a plateau at 12 m (Fig. 3.5 C). Like GM1, GD1 in the intermediate layer of the cortex also demonstrated the greatest increase in the LCB ratio which was most apparent at 12 m (intermediate – 0.61, superficial – 0.39, deep – 0.45) and continued to be significantly higher than the other cortical layers up to 20 m. The aging abundance profile of simple gangliosides GM3 and GM2 LCBs was the opposite of their complex ganglioside counterparts whereby the d20:1/d18:1 ratio was highest at P0, and then decreased during early development, plateauing at 3 m (Fig. 3.5 D,E). The deep layers of the cortex showed a significantly higher d20:1/d18:1 ratio at 3 m (0.43) than the superficial layers (0.32) (Fig. 3.5 D). GM2 demonstrated regional differences only at 20 m (Fig. 3.5 E), with the intermediate layers of the cortex showing a significantly higher d20:1/d18:1 LCB ratio (0.78) than the superficial layers (0.66).

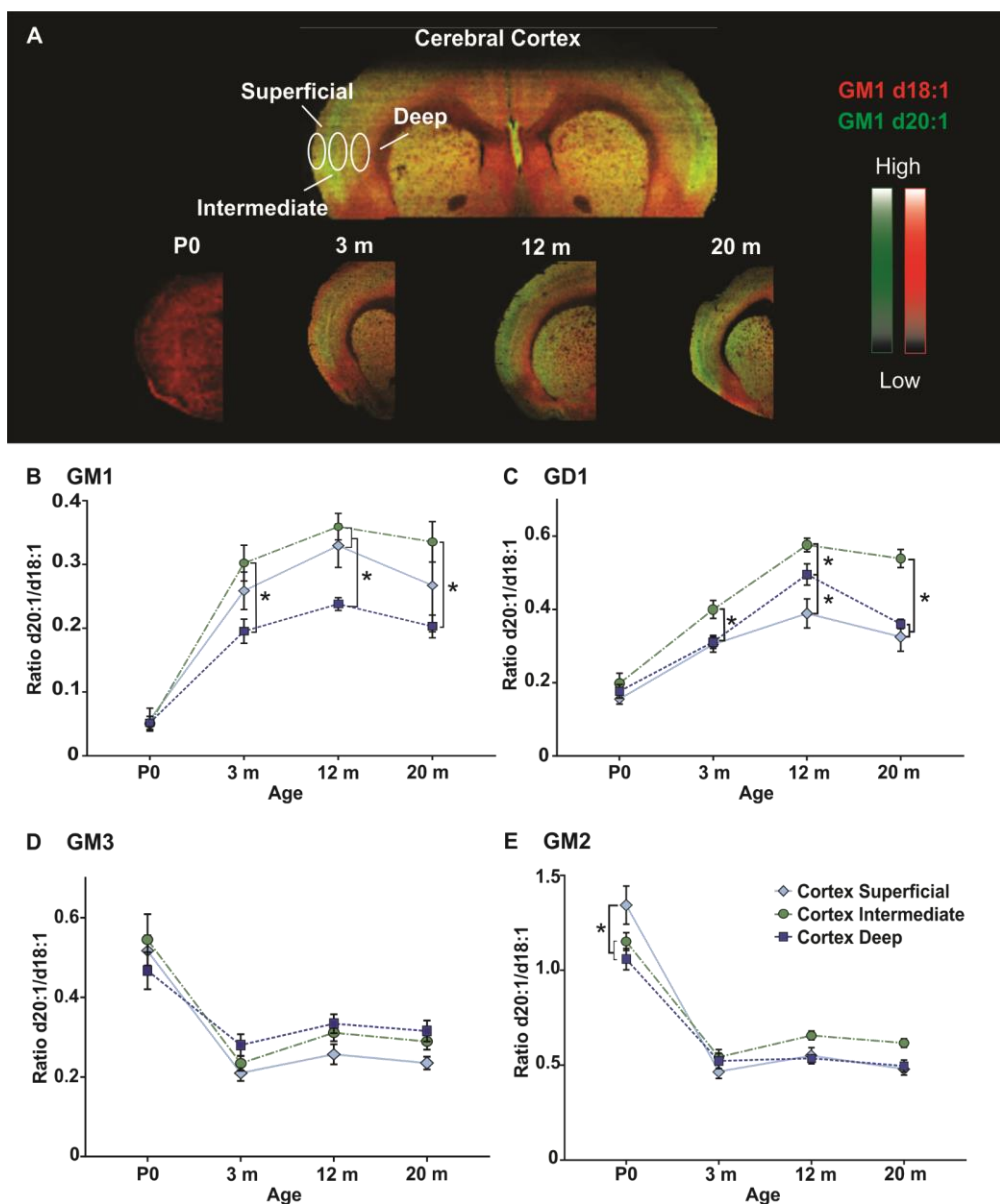


Figure 3.5: LCB ratio highest in superficial layers of the cortex and shows opposite pattern during early development among complex and simple gangliosides. Visualization of regional and age-dependent shifts in a-series gangliosides in the cerebral cortex of the rat. (A) Representative MALDI IMS overlay images showing the anatomical distribution of GM1 d18:1 (red) and d20:1 (green) across tissue along with the anatomical location of the ROIs in the superficial, intermediate, and deep layers of the cerebral cortex. (B–E) Quantification of the d20:1/d18:1 ratio at each time point for GM1 (B), GD1 (C), GM3 (D), and GM2 (E). The ratio of d20:1/d18:1 species increased in an age-dependent manner in complex gangliosides GM1 and GD1 up to 12 m of age, with the highest ratio observed in the intermediate layers of the cortex. The ratio then plateaued or decreased slightly at 20 m. The LCB ratio dropped between P0 and 3 m in simple gangliosides GM3 and GM2. Data represented as group Means \pm SEM, *indicates statistical significance, $p < 0.05$, via two-way ANOVA, Tukey multiple comparisons test, $n = 10$ for each time point.

3.4.4 *Hippocampus: Age-dependent accumulation in d20:1/d18:1 species in the dentate gyrus molecular layer observed in complex gangliosides only.*

Three regions of the hippocampus (Fig. 3.6 A) were selected for analysis based on previous reports of regional differences in the ratio of d20:1/d18:1 for GM1 (Sugiura et al., 2008; Weishaupt et al., 2015). The d20:1/d18:1 ratio of GM1 increased in an age-dependent manner within the CA1 and dentate gyrus (DG) molecular layer (mol) of the hippocampus, however, the ratio remained stable in the granular layer (gr) of the DG throughout the rat lifespan (Fig. 3.6 B). There were no regional differences within the hippocampus at P0, however, pronounced regional differences were observed between all three layers post-natally. The ratio of d20:1/d18:1 GM1 was highest in the DG mol where it increased from 0.14 at P0 to 0.44 at 3 m and continued to increase up to 20 m (0.51). A similar pattern was observed within the CA1 (P0–0.18, 3 m – 0.27, 20 m 0.33). The DG gr showed the lowest d20:1/d18:1 ratio of GM1 within the hippocampus remaining relatively unchanged from P0 (0.18) to 20 m (0.17). As noted in the previous brain regions, the d20:1/d18:1 ratio of GD1 was higher at P0 than for GM1. However, unlike GM1, not all layers of the hippocampus showed age-dependent increases in the ratio of d20:1/d18:1 species. This trend was only observed in the DG mol where the d20:1/d18:1 ratio increased from 0.26 at P0 to 0.4 at 3 m, and continued to increase to 0.52 at 12 m, where it plateaued up to 20 m (Fig. 3.6 C). The DG gr demonstrated an unexpected decrease in the ratio of GD1 d20:1/d18:1 between P0 (0.37) and 3 m (0.25) which then increased at 12 m (0.34) only to drop back down at 20 m (0.24). Equally interestingly, the CA1 region showed no change in the LCB ratio between P0 and 3 m, but increased between 3 m (0.26) and 12 m (0.37), then dropped slightly at 20 m (0.3).

As was observed in the cortex, the ratio of d20:1/d18:1 for simple gangliosides GM2 and GM3 was highest at P0 followed by a large decrease at 3 m where it remained at this level or decreased slightly at 20 m (Fig. 3.6 D,E). There were no regional differences in the GM3 LCB ratio within the hippocampus, however, the d20:1/d18:1 ratio did decrease between P0 and 20 m (CA1 0.61–0.26, DG mol 0.55–0.22, DG gr 0.48–0.22), with the most significant drop occurring in early development. There were modest but statistically significant differences in the GM2 d20:1/d18:1 ratio at P0 (Fig. 3.6 D; CA1 – 1.17, DG gr – 1.31) and 12 m (DG mol – 0.86, DG gr – 0.72) within the hippocampus.

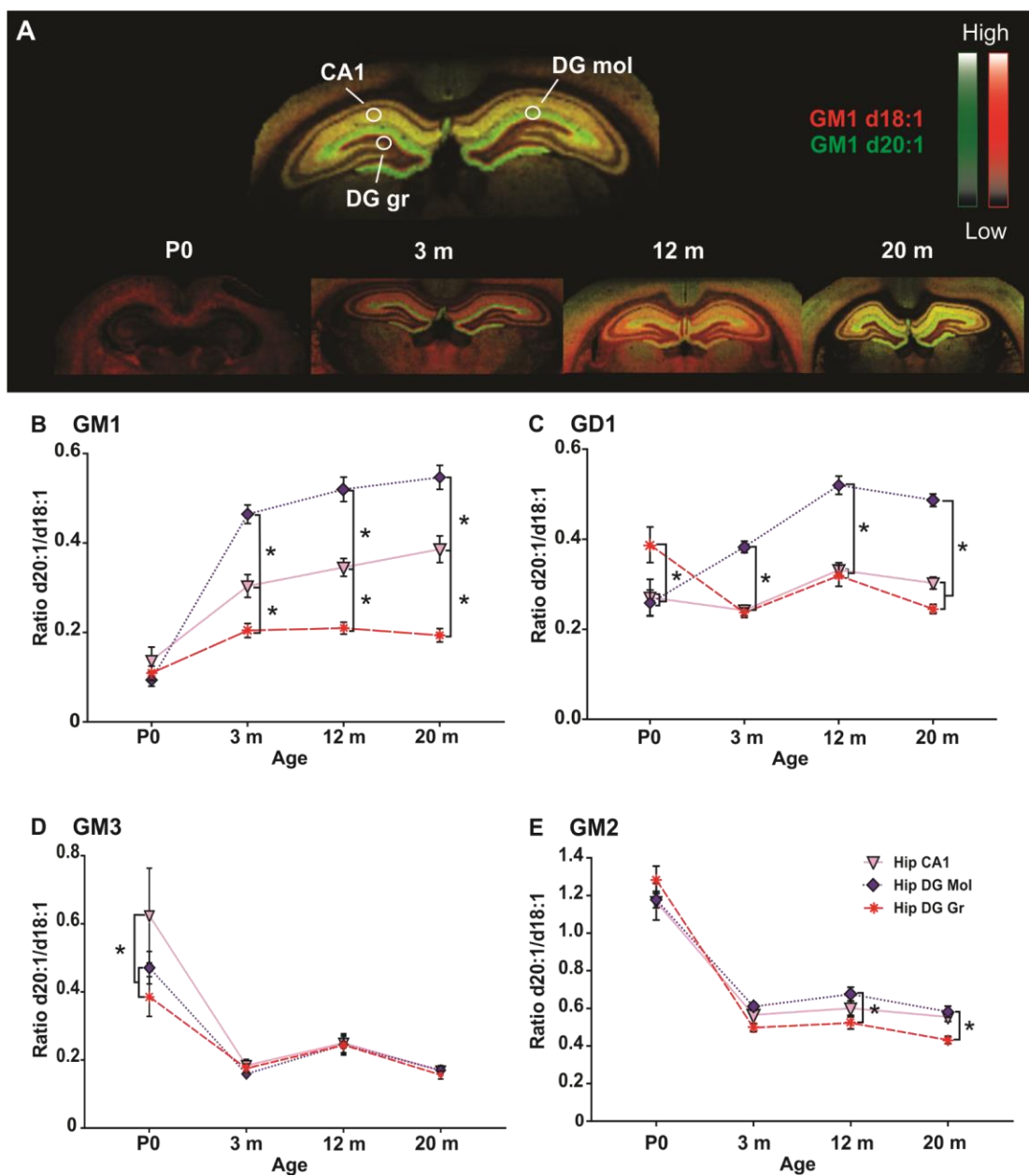


Figure 3.6: Significant regional heterogeneity in d20:1/d18:1 ratio during aging among hippocampal layers. Visualization of regional and age-dependent shifts in A-series gangliosides in the hippocampus of the rat. (A) Representative MALDI IMS overlay images showing the anatomical distribution of GM1 d18:1 (red) and d20:1 (green). (B–E) Quantification of the d20:1/d18:1 ratio at each time point showing the significant regional differences across the lifespan for each A-series ganglioside, GM1 (B), GD1 (C), GM3 (D), and GM2 (E). Significant anatomical heterogeneity in the age-dependent accumulation of d20:1 species was observed in the various sub-regions of the hippocampus for complex gangliosides GM1 and GD1 while the LCB ratio dropped during early development in simple gangliosides GM3 and GM2. Data represented as group Means \pm SEM, * indicates statistical significance, $p < 0.05$, via two-way ANOVA, Tukey multiple comparisons test, $n = 10$ for each time point.

3.4.5 *Age-dependent increase in LCB ratio observed in the white matter for both complex gangliosides and simple ganglioside GM3.*

Changes in white matter have been linked to several aging related neurodegenerative diseases. We investigated two distinct regions within the corpus callosum that clinically demonstrate differing vulnerability to structural changes in AD patients (Gao et al., 2014) (Fig. 3.7 A). The two regions used in our analysis were the anterior corpus callosum (aCC) adjacent to the striatum, and a more caudal sampling from the white matter adjacent to the ventricles, peri-ventricular corpus callosum (PVCC). Interestingly, the PVCC expressed higher ratios of d20:1/d18:1 ganglioside species than the more rostral aCC. Both GM1 and GD1 gangliosides showed an increase in d20:1 species up to 12 m which then plateaued to 20 m (Fig. 3.7 B,C). For GM1 (Fig. 3.7 B), the d20:1/d18:1 ratio increased significantly from P0 (aCC -0.07, PVCC - 0.08) to 3 m (aCC - 0.13, PVCC - 0.14), and continued to increase at 12 m (aCC - 0.18, PVCC - 0.21). A more pronounced age-dependent increase in d20:1 species was observed for ganglioside GD1 in the PVCC. The d20:1/d18:1 ratio increased between each time point (Fig. 3.7 C; P0 - 0.22, 3 m - 0.48, 12 m - 0.7, 20 m - 0.75). For the aCC, a similar pattern was observed to that of the PVCC, however, the d20:1/d18:1 ratio dropped between 12 m (0.5) and 20 m (0.4). Interestingly, regional differences were observed between the two white matter regions for the GD1 LCB ratio which became apparent at 3 m (PVCC - 0.48, aCC - 0.3) and continued at 12 m (PVCC - 0.7, aCC - 0.5) and 20 m (PVCC - 0.75, aCC - 0.4).

The aging shifts of LCBs were completely different between simple gangliosides GM2 and GM3 (Fig. 3.7 D,E). The ratio of d20:1/d18:1 for GM3 increased steadily in the PVCC throughout aging, similar to what was observed for GM1 and GD1 (Fig. 3.7 D; P0 - 0.58, 3 m - 0.67, 12 m - 0.82, 20 m - 0.96) whereas the aCC remained relatively constant (P0 - 0.5, 3 m - 0.54, 12 m - 0.59, 20 m - 0.55) resulting in significant differences between the aCC and PVCC ratios at 12 and 20 m of age. This was the only brain region to show an increase in the GM3 d20:1/d18:1 ratio during aging. Simple ganglioside GM2 (Fig. 3.7 E) showed a similar pattern to that of the other brain regions, with a significant decrease in the d20:1/d18:1 ratio from P0 (aCC -1.06, PVCC -1.14) to 3 m (aCC -0.74,

PVCC – 0.74) where the ratio remained unchanged up to 20 m in the PVCC (0.75) and dropped slightly in the aCC (0.65).

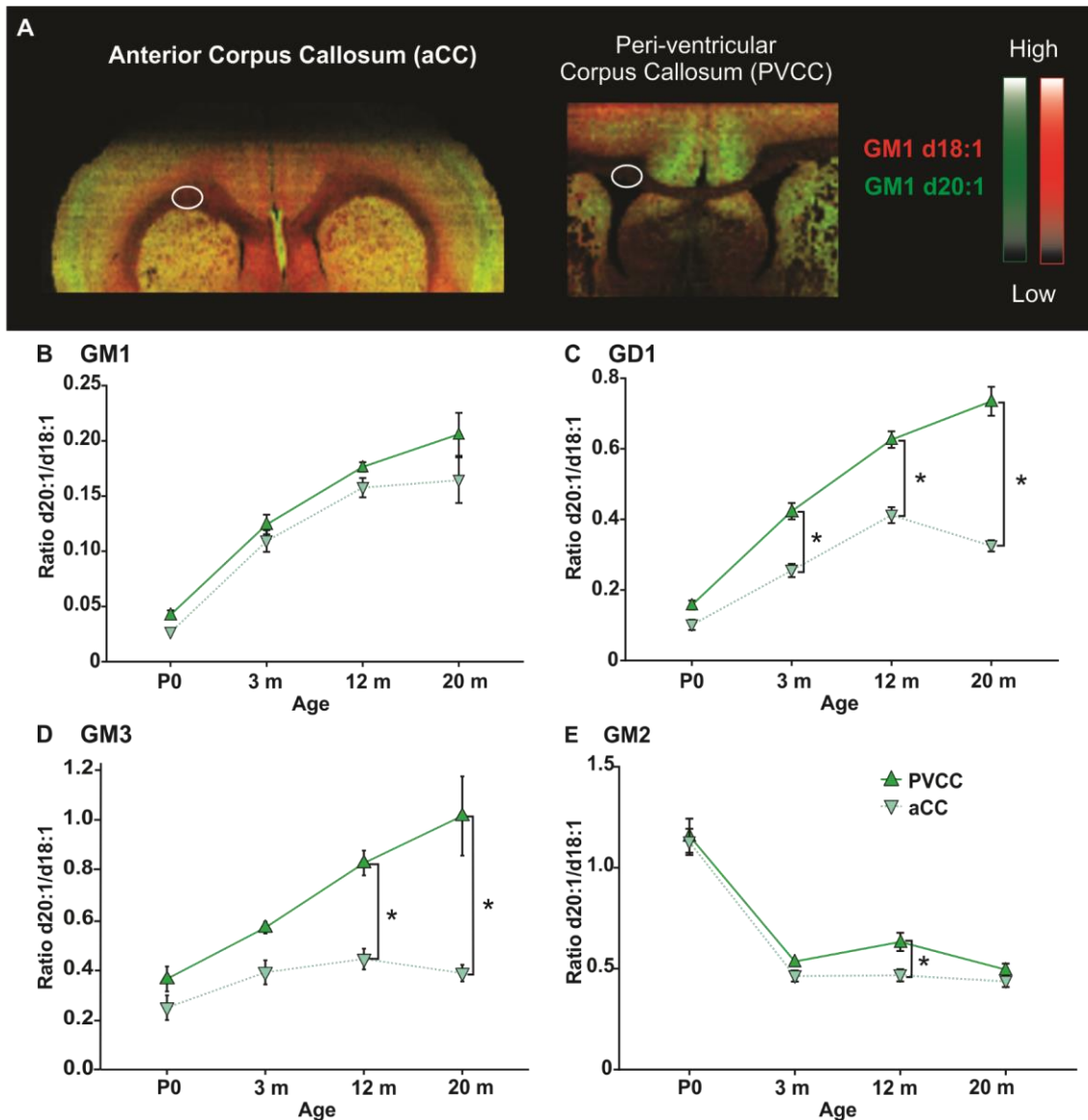


Figure 3.7: Unique pattern of d20:1 LCB accumulation in the white matter for simple ganglioside GM3 as well as significant differences among white matter regions during aging. Visualization of regional and age-dependent shifts in a-series gangliosides in the white matter of the rat. (A) Representative MALDI IMS overlay images showing the anatomical distribution of GM1 d18:1 (red) and d20:1 (green) (B–E) Quantification of the d20:1/d18:1 ratio at each time point showing the significant regional differences across the lifespan for each a-series ganglioside, GM1 (B), GD1 (C), GM3 (D), and GM2 (E). An age-dependent increase in the d20:1/d18:1 ratio was observed in the PVCC for gangliosides GM1, GD1, and also simple ganglioside GM3. Data represented as group Means \pm SEM, *indicates statistical significance, $p < 0.05$, via two-way ANOVA, Tukey multiple comparisons test, $n = 10$ for each time point.

3.4.6 Overall age effects

In order to make global anatomical and age-dependent comparisons between all 11 regions of interest in d20:1/d18:1 content, the fold change was calculated between P0 and 3 m old rats (Fig. 3.8 A–D). This time period corresponds to the early post-natal stages of neurodevelopment and also served as the time period of the greatest observed changes in LCB length in the current study. We also calculated the fold change between 3 m and 20 m, a time period corresponding adolescence and old age in Fisher rats (Fig. 3.8 E–H).

There was a 1.5–4 fold increase in the ratio of d20:1/d18:1 species between P0 and 3 m for ganglioside GM1 in most brain regions examined, with the exception of the DG gr layer of the hippocampus, which remained unchanged. The largest fold increases occurred in the cerebral cortex, striatum, and the DG mol (Fig. 3.8 A). There was a 1.5–3 fold increase in the d20:1/d18:1 ratio for ganglioside GD1 between birth and 3 m, with the exception of the CA1 and DG gr of the hippocampus, in which the former remained unchanged, and the latter decreased 1.5 fold (Fig. 3.8 B). The largest fold increase in GD1 d20:1/d18:1 content during early development occurred in the cerebral cortex and white matter regions. GM3 d20:1/d18:1 content decreased 1.5 to 3 fold across the brain with the exception of the two white matter regions, the LSN, and the striatum which remained unchanged (Fig. 3.8 C). GM2 d20:1/d18:1 content decreased roughly 2 fold across all brain regions examined, with the largest drop occurring in the superficial layer of the cortex and DG gr of the hippocampus (Fig. 3.8 D).

During adulthood, the PVCC showed the largest fold increase for gangliosides GM1, GD1, and GM3 (Fig. 3.8 E–G). The PVCC was the only brain region which the d20:1/d18:1 ratio was significantly altered between 3 and 20 m of age. For ganglioside GD1, the PVCC along with the intermediate layers of the cerebral cortex and DG mol layer of the hippocampus had significantly elevated d20:1/d18:1 ratios, all other regions remained either unchanged or increased less than 50% during adulthood (Fig. 3.8 F). The PVCC was the only region where the LCB of GM3 was significantly increased between 3 and 20 m, however, the DG gr layer of the hippocampus showed a significant decrease within the same period, while all other brain regions remained statistically unchanged (Fig.

3.8 G). There were no significant alterations in the d20:1/d18:1 ratio of GM2 between 3 m and 20 m of age (Fig. 3.8 H).

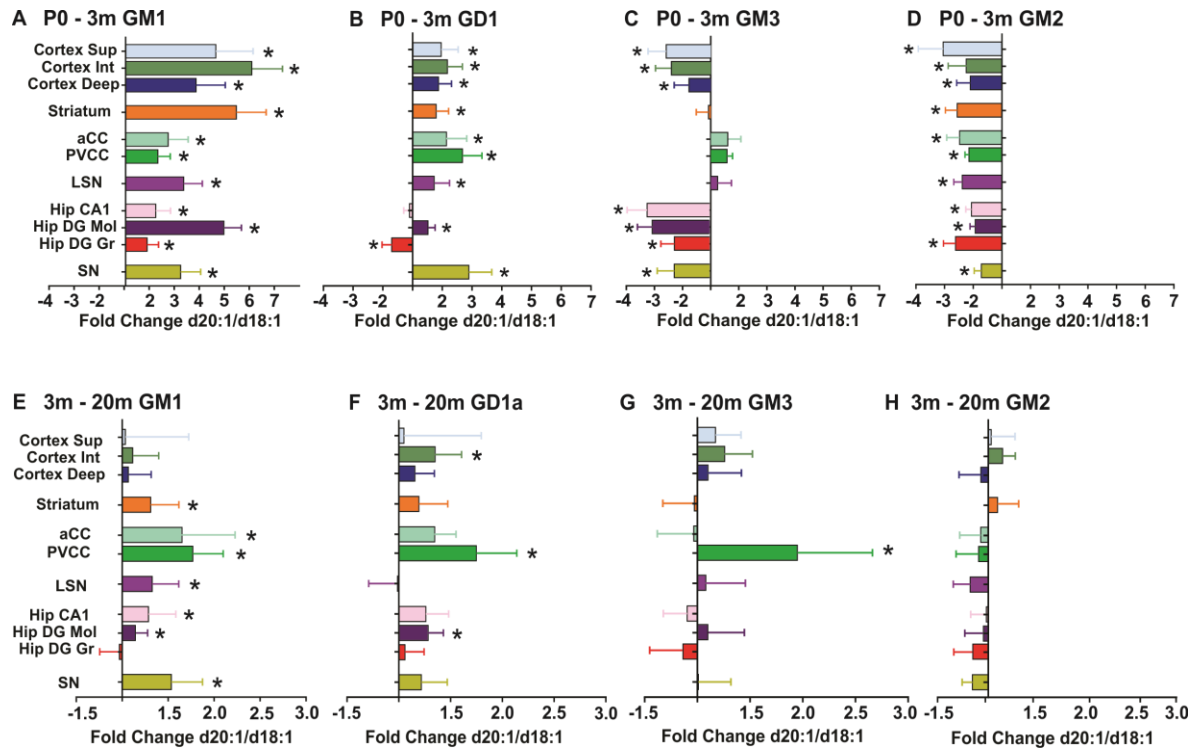


Figure 3.8: Differential alterations in LCB during early brain development and adulthood in Fisher rats. Overall age effects of d20:1/d18:1 ratio during post-natal rat brain development and adulthood. Quantification of the fold-change in the d20:1/d18:1 ratio between P0 - 3 m (A–D) and 3 m–20 m (E–H). Ganglioside GM1 shows a significant fold increase between P0 and 3 m (A) which only continued to increase in the PVCC during adulthood (E). Ganglioside GD1 increased in all brain regions except the CA1 and DG gr layers of the hippocampus in early development (B) with a few regions continuing to increase into old age (F). Ganglioside GM3 showed either a decreased or stable LCB ratio in early development (C) which remained unchanged throughout adulthood except for the PVCC, which increased, and the DG gr, which decreased (G). Ganglioside GM2 LCB ratio decreased significantly in early development across the brain (D) and remained stable throughout adulthood (H). In order to calculate the global changes in early development and adulthood, an average value for the d20:1/d18:1 ratio was calculated (either P0 or 3 m) and used for comparison to each animal in the later time point (3 m or 20 m). Data represented as group Means \pm SEM, *indicates statistical significance, $p < 0.05$, via two-way ANOVA, Tukey multiple comparisons test, $n = 10$ for each time point.

3.5 Discussion

Work in this study describes the age-dependent changes in the d20:1/d18:1 ratio of gangliosides across multiple cortical, subcortical, and white matter regions of the brain using MALDI IMS. It is the first to examine age-related alterations in the LCB of minor ganglioside components GM2 and GM3 which are currently gaining interest as potential mediators of neurodegeneration in a number of neurodegenerative diseases and injuries (Caughlin et al., 2015; Dufresne et al., 2017; Kaya et al., 2017; Whitehead et al., 2011; Woods et al., 2013). This work builds upon previous studies by Weishaupt et al. 2015, which described regional differences in the d18:1/d20:1 ratio of ganglioside GM1 in 3 m old Fisher rats, as well as the work of Sugiura et al. 2008, which was the first to use MALDI IMS to describe age-dependent changes within hippocampus of mice. The current study confirmed many of the findings from the aforementioned studies pertaining to complex gangliosides GM1 and GD1. For example, Weishaupt et al. 2015 used similar regions of interest in the cortex and found, like the current study, that the lowest d20:1/d18:1 ratio occurred in the deep layers of the cortex, with significantly higher ratios in the intermediate and superficial layers. Anatomically, the intermediate and superficial layers of the cortex have a particularly high density of neurons which receive inputs from cholinergic neurons in the basal forebrain (Garofalo, Ribeiro-da-Silva, & Cuello, 1993) while the deep layers of the cortex have high connectivity to thalamic nuclei (Zarrinpar & Callaway, 2006). A heterogeneous expression of A-series gangliosides have also been reported in various layers of brain cortices of normal and injured mice. Specifically, Kwak et al. 2005 found that ganglioside GM3 was upregulated in deep layers of the cortex (layers 4-6) after an MCAO stroke injury while GM1 was upregulated in more superficial layers (2-3) as well as the deep layers. The regional differences in the d20:1/d18:1 ratio observed in the current study may also reflect important functional differences in connectivity within the cortex that play a role in normal brain aging as well as the brain's response to injury, however, this connection remains unclear and would be an interesting avenue of further investigation.

We also observed significant regional differences within the various layers of the rat hippocampus from 3 m of age through to 20 m. The DG mol showed the highest ratio of

d20:1/d18:1 gangliosides followed by the CA1 and DG gr. Sugiura et al. 2008 reported an age-dependent accumulation of d20:1 species of ganglioside GD1 compared to d18:1 species in the DG molecular layer of the mouse hippocampus. While this age-dependent accumulation was also observed in the current study, the CA1 region was only observed to increase between P0 and 12 m of age, while the DG gr showed a decrease in d20:1/d18:1 between P0 and 20 m. This data suggests that not all layers of the hippocampus show an increase in GD1 d20:1/d18:1 ratio between birth and old age, which may be related to the various functions of different anatomical domains within the hippocampus. For example, the DG mol is known to be a critical area of connectivity in the perforant pathway, which receives input from the entorhinal cortex and sends connections to the CA3 (Witter & Amaral, 1991). It has been previously suggested that the high proportion of d20:1 species observed in the DG mol could be linked to the particular vulnerability of this perforant pathway to neurodegeneration during the development of Alzheimer's disease (Hirano-Sakamaki et al., 2015). Similarly, the sub-cortical structures examined in the current study are particularly vulnerable to the development of neurodegenerative diseases and perturbations in ganglioside homeostasis, as previously mentioned. Treatments focused on restoring depleted complex ganglioside GM1 have been therapeutically promising both in pre-clinical models of neurodegenerative diseases and clinically (Kreutz et al., 2011; Maglione et al., 2010; Schneider et al., 2013), pointing to the importance of understanding these ganglioside perturbations during aging. Interestingly, very different patterns of d20:1/d18:1 LCB ratios were observed for simple ganglioside GM3 among these sub-cortical structures throughout the lifespan of the Fisher rats. The LCB ratio dropped during early development only in the SN (similar to the hippocampus and cortex) while levels remained unchanged in the striatum and LSN. This regional and age-dependent heterogeneity in GM3 LCB suggests that the d20:1 species of GM3 is differentially regulated within these subcortical structures and may be an indicator of regional vulnerability to damage and/or disease during aging.

While information on general alterations in the LCB length of simple gangliosides is scarce, our findings do not match with what has been hypothesized to occur based on previous studies conducted on complex gangliosides. Specifically, the age dependent accumulation of d20:1 species in the brain has been suggested to be a hallmark of the aging

process (Palestini et al., 1993), however this assertion was based on the analysis of complex gangliosides only. The results of the current study demonstrated that, relative to the d18:1 species, d20:1 content generally decreased between P0 and 3 m of age for gangliosides GM2 and GM3 and this ratio remains fairly constant throughout adult life. One potential reason for the observed decrease in the d20:1/d18:1 ratio in the early life of the rat may be related to the role of these gangliosides during neurodevelopment. It is possible that the observed decrease in d20:1 content in simple gangliosides may be due to an increase in d18:1 content during the first 3 months, however, this remains unclear in the current study and is thus an important caveat. Future studies which examine and compare alterations in individual ganglioside species may address this pitfall.

Overall, data from this study showed that the greatest changes in LCB composition occurred between P0 and 3 m of age in the rat. This finding is in accordance with previous literature, using alternative techniques, focused on the very early stages of development (Palestini et al., 1990; Valsecchi et al., 1996). We demonstrated that the alterations in LCB length between P0 and 3 m of age was highly variable depending not only on the ganglioside species, whether it be simple or complex, but more importantly on the brain region as well. In addition to examining the changes in LCB length in the early stages of rat brain development, we included a detailed report of the LCB length changes in the mature brain in order to determine if there are distinct regions and/or gangliosides that are particularly connected to the process of aging in the rat brain. Interestingly, the PVCC showed the largest fold increase in the d20:1/d18:1 ratio during adulthood for complex gangliosides GM1 and GD1, as well as the pro-apoptotic simple ganglioside GM3. This accumulation of d20:1 species in the PVCC suggests that this region of the brain may be particularly susceptible to the effects of aging and neurodegeneration in rats. Indeed, alterations in gangliosides abundance has been shown to produce abnormalities in white matter (Sheikh et al., 1999) and more recently, Di Pardo, Amico, and Maglione 2016 found decreased levels of complex gangliosides in the corpus callosum of a mouse model of Huntington's disease. Moreover, the PVCC was the only region that showed an age-dependent increase in the proportion of simple ganglioside GM3 d20:1. This finding in particular supports the notion of susceptibility to neurodegeneration due to the toxic nature of GM3 accumulation reported in the literature (Chung et al., 2009; Nakatsuji & Miller,

2001; Prokazova, Samovilova, Gracheva, & Golovanova, 2009; Sohn et al., 2006), the reported accumulation of GM3 in senescence-accelerated mice (Ohsawa & Shumiya, 1991), as well as increased simple ganglioside content in the brains of both animal models and clinical patients with AD (Kaya et al., 2017; Oikawa et al., 2009; Yamamoto et al., 2006). Regional differences between the two sub-regions of white matter observed in the current study may also have clinical relevance. In a study using magnetic resonance imaging to evaluate white matter hyperintensities in human patients with cerebrovascular diseases, the authors found that PVWM hyperintensities, but not deep white matter hyperintensities, were associated with aging and the incidence of dementia (Gao et al., 2014). Future studies should focus on evaluating the mechanism for ganglioside LCB alterations during aging in order to determine whether there are links to white matter-specific pathological changes associated with brain aging and disease.

Although the mechanisms involved in the age-dependent accumulation of d20:1 gangliosides are not fully understood, there are several theories as to what may contribute to this finding. Firstly, it has been suggested that different types of enzymes, or enzyme modulators capable of distinguishing between LCB, may be present and are differentially active throughout neurodevelopment and aging (Palestini et al., 1990; Sonnino & Chigorno, 2000). Alternatively, Palestini et al. 1990 suggested that d20:1 intermediates may be preferentially used during biosynthesis and recycling of ganglioside degradation products with aging. Rosenberg and Stern 1966 were one of the first to report an age-dependent increase in d20:1 sphingosine in the murine brain. In that study, using whole brain extracts, they also found that there was an age-dependent decrease of stearic acid content in ganglioside fractions. Overall, these studies along with the current study suggest that understanding the role of LCB length in mediating in neurodevelopment and brain aging are worthy pursuits for continued investigation.

MALDI IMS is currently the only technique capable of simultaneously providing accurate detection, ionic abundance, and anatomical distribution data of gangliosides based on both their oligosaccharide and ceramide moieties, making it a powerful analytical tool for the study of gangliosides in the brain. The evolution of MALDI instrumentation along with refined sample preparation protocols allows for very high resolution imaging for the

visualization and analysis of discrete anatomical structures within intact tissue sections. This technique, however, is not without drawbacks. It is considered a semi-quantitative technique due to variability in sample preparation and instrumentation between runs. Additionally, detection of multisialylated ganglioside species such as GD1 are susceptible to in-source fragmentation and ionize attached to salt adducts [Na⁺] and [K⁺] (Richards et al., 2012). These factors dampen the signal obtained for this species and complicate the interpretation of GM1 data as well. However, because the current study quantified the ratio of one species to another within the same spectrum (d20:1/d18:1), direct comparisons between images and individual species abundance was avoided, thus reducing the effects of dampened signal and error produced by between-scan variability. In the end, the numerous benefits of MALDI IMS outweigh the pitfalls and it continues to be the most valuable tool for the investigation of membrane lipids in the brain.

Overall, data from our study, for the first time, provide insight into the changing composition of simple ganglioside LCB throughout the brain during aging and provide a more in depth examination of LCB alterations in complex gangliosides. This study contains the most detailed examination of the anatomical distribution of d18:1 and d20:1 ganglioside species to date in order to better understand the role of these membrane lipids during aging. Detailed analyses of ganglioside anatomical distribution patterns and abundance during healthy and pathological aging may provide valuable insight for the creation of effective lipid-derived therapeutics for neurodegenerative diseases and injuries.

3.6 References

- Agca, C., Fritz, J. J., Walker, L. C., Levey, A. I., Chan, A. W., Lah, J. J., & Agca, Y. (2008). Development of transgenic rats producing human beta-amyloid precursor protein as a model for Alzheimer's disease: Transgene and endogenous APP genes are regulated tissue-specifically. *BMC Neuroscience*, *9*(1), 28.
- Caughlin, S., Hepburn, J. D., Park, D. H., Jurcic, K., Yeung, K. K. C., Cechetto, D. F., & Whitehead, S. N. (2015). Increased expression of simple ganglioside species GM2 and GM3 detected by MALDI Imaging Mass Spectrometry in a combined rat model of A β toxicity and stroke. *PLoS ONE*, *10*(6), 1–17.

- Caughlin, S., Park, D. H., Yeung, K. K.-C., Cechetto, D. F., & Whitehead, S. N. (2017). Sublimation of DAN Matrix for the Detection and Visualization of Gangliosides in Rat Brain Tissue for MALDI Imaging Mass Spectrometry. *Journal of Visualized Experiments*, (121).
- Chan, K., Lanthier, P., Liu, X., Sandhu, J. K., Stanimirovic, D., & Li, J. (2009). MALDI mass spectrometry imaging of gangliosides in mouse brain using ionic liquid matrix. *Analytica Chimica Acta*, 639(1–2), 57–61.
- Chung, T. W., Kim, S. J., Choi, H. J., Kim, K. J., Kim, M. J., Kim, S. H., ... Kim, C. H. (2009). Ganglioside GM3 inhibits VEGF/VEGFR-2-mediated angiogenesis: Direct interaction of GM3 with VEGFR-2. *Glycobiology*, 19(3), 229–239.
- Desplats, P. A., Denny, C. A., Kass, K. E., Gilmartin, T., Head, S. R., Sutcliffe, J. G., ... Thomas, E. A. (2007). Glycolipid and ganglioside metabolism imbalances in Huntington's disease. *Neurobiology of Disease*, 27(3), 265–277.
- Di Pardo, A., Amico, E., & Maglione, V. (2016). Impaired levels of gangliosides in the corpus callosum of Huntington disease animal models. *Frontiers in Neuroscience*, 10, 1–8.
- Dufresne, M., Guneyasu, D., Patterson, N. H., Marcinkiewicz, M. M., Regina, A., Demeule, M., & Chaurand, P. (2017). Multimodal detection of GM2 and GM3 lipid species in the brain of mucopolysaccharidosis type II mouse by serial imaging mass spectrometry and immunohistochemistry. *Analytical and Bioanalytical Chemistry*, 409, 1425–1433.
- Gao, Z., Wang, W., Wang, Z., Zhao, X., Shang, Y., Guo, Y., ... Wu, W. (2014). Cerebral microbleeds are associated with deep white matter hyperintensities, but only in hypertensive patients. *PLoS ONE*, 9(3), 1–8.
- Garofalo, L., Ribeiro-da-Silva, A., & Cuello, A. C. (1993). Potentiation of nerve growth factor-induced alterations in cholinergic fibre length and presynaptic terminal size in cortex of lesioned rats by the monosialoganglioside GM1. *Neuroscience*, 57(1), 21–40.
- Hirano-Sakamaki, W., Sugiyama, E., Hayasaka, T., Ravid, R., Setou, M., & Taki, T. (2015). Alzheimer's disease is associated with disordered localization of ganglioside GM1 molecular species in the human dentate gyrus. *FEBS Letters*, 589(23), 3611–3616.
- Kaya, I., Brinet, D., Michno, W., Syvanen, S., Sehlin, D., Zetterberg, H., ... Hanrieder, J. (2017). Delineating Amyloid Plaque Associated Neuronal Sphingolipids in Transgenic Alzheimer's Disease Mice (tgArcSwe) Using MALDI Imaging Mass Spectrometry. *ACS Chemical Neuroscience*, 8, 347–355.
- Kreutz, F., Frozza, R. L., Breier, A. C., de Oliveira, V. a, Horn, A. P., Pettenuzzo, L. F., ... Trindade, V. M. T. (2011). Amyloid- β induced toxicity involves ganglioside expression and is sensitive to GM1 neuroprotective action. *Neurochemistry International*, 59(5), 648–55.
- Kwak, D. H., Kim, S. M., Lee, D. H., Kim, J. S., Kim, S. M., Lee, S. U., ... Choo, Y. K. (2005). Differential expression patterns of gangliosides in the ischemic cerebral cortex

- produced by middle cerebral artery occlusion. *Molecules and Cells*, 20(3), 354–360.
- Maglione, V., Marchi, P., Di Pardo, A., Lingrell, S., Horkey, M., Tidmarsh, E., & Sipione, S. (2010). Impaired ganglioside metabolism in Huntington's disease and neuroprotective role of GM1. *The Journal of Neuroscience: The Official Journal of the Society for Neuroscience*, 30(11), 4072–4080.
- Mansson, J. E., Vanier, M. T., & Svennerholm, L. (1977). Changes in the fatty acid and sphingosine composition of the major gangliosides of human brain with age. *Short Communications*, (July), 159–161.
- Masserini, M., Palestini, P., & Freire, E. (1989). Influence of glycolipid oligosaccharide and long-chain base composition on the thermotropic properties of dipalmitoylphosphatidylcholine large unilamellar vesicles containing gangliosides. *Biochemistry*, 28(12), 5029–5034.
- Nakatsuji, Y., & Miller, R. H. (2001). Selective cell-cycle arrest and induction of apoptosis in proliferating neural cells by ganglioside GM3. *Experimental Neurology*, 168(2), 290–9.
- Ohsawa, T., & Shumiya, S. (1991). Age-related alteration of brain gangliosides in senescence-accelerated mouse (SAM)-P/8. *Mechanisms of Ageing and Development*, 59, 263–274.
- Oikawa, N., Yamaguchi, H., Ogino, K., Taki, T., Yuyama, K., Yamamoto, N., ... Yanagisawa, K. (2009). Gangliosides determine the amyloid pathology of Alzheimer's disease. *Neuroreport*, 20(12), 1043–1046.
- Palestini, P., Masserini, M., Fiorilli, A., Calappi, E., & Tettamanti, G. (1993). Age-Related Changes in the Ceramide Composition of the Major Gangliosides Present in Rat Brain Subcellular Fractions Enriched in Plasma Membranes of Neuronal and Myelin Origin. *Journal of Neurochemistry*, 61(3), 955–960. x
- Palestini, P., Masserini, M., Sonnino, S., & Tettamanti, G. (1990). Changes in the ceramide composition of rat forebrain gangliosides with age. *Journal of Neurochemistry*, 54(1), 230–235.
- Prokazova, N. V., Samovilova, N. N., Gracheva, E. V., & Golovanova, N. K. (2009). Ganglioside GM3 and its biological functions. *Biochemistry. Biokhimiia*, 74(3), 235–249.
- Rabin, S. J., Bachis, A., & Mocchetti, I. (2002). Gangliosides activate Trk receptors by inducing the release of neurotrophins. *Journal of Biological Chemistry*, 277(51), 49466–49472.
- Richards, A. L., Lietz, C. B., Wager-miller, J., Mackie, K., & Trimpin, S. (2012). Localization and imaging of gangliosides in mouse brain tissue sections by laserspray ionization inlet. *Journal Of Lipid Research*, 53, 1390–1398.
- Rosenberg, a, & Stern, N. (1966). Changes in sphingosine and fatty acid components of the gangliosides in developing rat and human brain. *Journal of Lipid Research*, 7(1), 122–131.

- Schneider, J. S., Gollomp, S. M., Sendek, S., Colcher, A., Cambi, F., & Du, W. (2013). A randomized, controlled, delayed start trial of GM1 ganglioside in treated Parkinson's disease patients. *Journal of the Neurological Sciences*, 324(1–2), 140–148.
- Sheikh, K. a, Sun, J., Liu, Y., Kawai, H., Crawford, T. O., Proia, R. L., ... Schnaar, R. L. (1999). Mice lacking complex gangliosides develop Wallerian degeneration and myelination defects. *Proceedings of the National Academy of Sciences of the United States of America*, 96(13), 7532–7.
- Sohn, H., Kim, Y. S., Kim, H. T., Kim, C. H., Cho, E. W., Kang, H. Y., ... Ko, J. H. (2006). Ganglioside GM3 is involved in neuronal cell death. *The FASEB Journal : Official Publication of the Federation of American Societies for Experimental Biology*, 20(8), 1248–1250.
- Sonnino, S., & Chigorno, V. (2000). Ganglioside molecular species containing C18- and C20-sphingosine in mammalian nervous tissues and neuronal cell cultures. *Biochimica et Biophysica Acta*, 1469(2), 63–77.
- Sonnino, S., Mauri, L., Ciampa, M. G., & Prinetti, A. (2013). Gangliosides as regulators of cell signaling: Ganglioside-protein interactions or ganglioside-driven membrane organization? *Journal of Neurochemistry*, 124(4), 432–435.
- Sugiura, Y., Shimma, S., Konishi, Y., Yamada, M. K., & Setou, M. (2008). Imaging mass spectrometry technology and application on ganglioside study; visualization of age-dependent accumulation of C20-ganglioside molecular species in the mouse hippocampus. *PloS One*, 3(9), e3232.
- Tamai, Y., Ohtani, Y., Miura, S., Narita, Y., Iwata, T., Kaiya, H., & Namba, M. (1979). Creutzfeldt-Jakob disease--alteration in ganglioside sphingosine in the brain of a patient. *Neuroscience Letters*, 11(1), 81–86.
- Valsecchi, M., Palestini, P., Chigorno, V., & Sonnino, S. (1996). Age-related changes of the ganglioside long-chain base composition in rat cerebellum. *Neurochemistry International*, 28(2), 183–187.
- Weishaupt, N., Caughlin, S., Yeung, K. K.-C., & Whitehead, S. N. (2015). Differential Anatomical Expression of Ganglioside GM1 Species Containing d18:1 or d20:1 Sphingosine Detected by MALDI Imaging Mass Spectrometry in Mature Rat Brain. *Frontiers in Neuroanatomy*, 9(DEC), 155.
- Whitehead, S. N., Chan, K. H. N., Gangaraju, S., Slinn, J., Li, J., & Hou, S. T. (2011). Imaging mass spectrometry detection of gangliosides species in the mouse brain following transient focal cerebral ischemia and long-term recovery. *PloS One*, 6(6), e20808.
- Witter, M., & Amaral, D. (1991). Entorhinal cortex of the monkey: V. Projections to the dentate gyrus, hippocampus, and subicular complex. *Journal of Comparative Neurology (1911)*, 307(3), 437–459.
- Woods, A. S., Colsch, B., Jackson, S. N., Post, J., Baldwin, K., Roux, A., ... Balaban, C. (2013). Gangliosides and ceramides change in a mouse model of blast induced

- traumatic brain injury. *ACS Chemical Neuroscience*, 4(4), 594–600.
- Wu, G., & Ledeen, R. W. (1994). Gangliosides as modulators of neuronal calcium. *Progress in Brain Research*, 101, 101–112.
- Yamamoto, N., Nostrand, W. E. Van, & Yanagisawa, K. (2006). Further evidence of local ganglioside-dependent amyloid b -protein assembly in brain. *Neuroreport*, 17(16), 16–18.
- Yu, R. K., Tsai, Y. T., & Ariga, T. (2012). Functional roles of gangliosides in Neurodevelopment: An overview of recent advances. *Neurochemical Research*, 37(6), 1230–1244.
- Zarrinpar, A., & Callaway, E. M. (2006). Local Connections to Specific Types of Layer 6 Neurons in the Rat Visual Cortex Local Connections to Specific Types of Layer 6 Neurons in the Rat Visual Cortex. *J Neurophysiol*, 95, 1751–1761.

Chapter 4 : Membrane lipid homeostasis in a prodromal rat model of AD: Characteristic profiles in ganglioside distributions during aging detected using MALDI imaging mass spectrometry

In the previous chapter, accumulation of d20:1 ganglioside species in the aging brain was found to be more complex than previously thought. Firstly, simple gangliosides GM3 and GM2 generally showed a stable or decreased ratio of d20:1/d18:1 species during aging, countering the hypothesis that the accumulation of d20:1 species is a hallmark of the aging process (Palestini et al., 1990). Secondly, the pattern of the d20:1/d18:1 ratio during aging was highly heterogeneous across the brain, particularly for simple ganglioside GM3. To build upon the findings of the previous chapter, we next examined the abundance of each ganglioside species separately for a more detailed examination and comparison of simple and complex ganglioside patterns during aging in wild-type (Wt) and transgenic (Tg) APP21 Fisher rats. Additionally, a MALDI tandem MS (MS/MS) experiment was performed in order to identify some of the major ganglioside species examined in this work. The results has been provided as an appendix (**Appendix iv**).

4.1 Abstract

Accumulation of simple gangliosides GM2 and GM3 and gangliosides with longer long-chain bases (d20:1) have been linked to toxicity in the brain and the pathogenesis of Alzheimer's disease (AD). Conversely, complex gangliosides, such as GM1, have been shown to be neuroprotective. Recent evidence using matrix-assisted laser desorption ionization (MALDI) imaging mass spectrometry (IMS) has demonstrated that a-series gangliosides are differentially altered during normal aging, yet it remains unclear how simple species are shifting relative to complex gangliosides in the prodromal stages of AD. Ganglioside profiles in Wt and Tg APP21 Fischer rats were detected and quantified using MALDI-IMS at P0 (birth), 3, 12, and 20 months (m) of age and each species quantified to allow for individual species comparisons. Tg APP21 rats were found to have a decreased level of complex gangliosides in a number of brain regions as compared to Wt rats and showed higher levels of ganglioside GM3. A unique pattern of expression was observed in

the white matter as compared to gray matter regions, with an age-dependent decrease in GD1 d18:1 species that was more pronounced in Tg APP21 rats coupled with significantly elevated levels of GM3 only in Tg APP21 rats. These results are indicative of a pathological shift in ganglioside homeostasis during aging that is worsened in Tg APP21 rats.

4.2 Introduction

Mounting evidence points to the complex interaction of risk factors that can lead to the development of neurodegenerative diseases in the aging brain. As such, there is increased interest in identifying early indicators of brain vulnerability. These early changes could hold the key to a better understanding of disease progression and help identify mechanisms for preventative intervention. The cell membrane is the first line of defense against changes in the external environment. It can dictate how cells respond to adverse stimuli and ultimately determine the fate of the cell. Gangliosides are sialic acid-containing glycosphingolipids (GSLs) enriched within brain which form an important component of lipid rafts in cell membranes. Lipid rafts are a major site of cell signal transduction and serve as a platform for protein-protein and protein-lipid interactions (Sonnino et al., 2013; Yu et al., 2012). The healthy brain maintains a homeostatic distribution of gangliosides in order to regulate signal transduction, however, perturbations in this distribution have been observed in both pre-clinical models and clinical cases of neurodegenerative diseases such as Alzheimer's disease (AD) (Oikawa et al., 2009), Huntington's disease (Maglione et al., 2010), Parkinson's disease (Schneider et al., 2013), as well as prion diseases (Ohtani et al., 1996; Tamai et al., 1979). Ganglioside distribution has also been found to be perturbed in response to neurodegenerative injuries such as stroke (Caughlin et al., 2015; Whitehead et al., 2011) and traumatic brain injury (Woods et al., 2013).

Glycosphingolipids are made up of two main domains, an oligosaccharide moiety exposed to the extracellular environment, and a ceramide moiety embedded within the lipid bilayer. The oligosaccharide moiety acts as a coding unit which can dictate the types of interactions that take place within a specific microdomain (Ledeen & Wu, 2015). The

ceramide moiety contains a sphingosine tail with varying numbers of carbons which can alter the fluidic properties of the membrane and has regulatory effects on the oligosaccharide moiety (Masserini et al., 1989). A-series gangliosides contain structurally simpler precursor species GM3 and GM2 and complex species GM1 and GD1. Complex gangliosides are the predominant form of gangliosides expressed within the healthy adult brain while simple gangliosides are only expressed in small quantities.

The quantity of simple and complex gangliosides shifts during early development and is dictated by the expression and activity of metabolic enzymes such as sialyltransferases and glycosyltransferases. After birth, synthesis of complex gangliosides is upregulated while synthesis of simple gangliosides is downregulated (Rosenberg & Stern, 1966). This shift in expression during early development is related to the function of each ganglioside. For example, simple ganglioside GM3 has been shown to upregulate apoptotic and inhibit angiogenic vascular endothelial growth factor (VEGF) signalling pathways *in vitro* (Chung et al., 2009; Nakatsuji & Miller, 2001; Sohn et al., 2006), an important function in early brain development to regulate plasticity, but potentially problematic if upregulated in the adult brain. Moreover, accumulations of simple gangliosides in the brain have been linked in a number of neurodegenerative diseases (Dufresne et al., 2017) and injuries (Caughlin et al., 2015; Whitehead et al., 2011; Woods et al., 2013).

Ganglioside GM1 is highly expressed throughout the mammalian brain but is particularly abundant in cerebral white matter (Ledeen & Wu, 2015; Rubovitch et al., 2017). In rats, increases in GM1 during development are thought to be linked to myelin thickening (Aydin et al., 2000). GD1 is highly expressed in the dendrites and synapses of rat brains and is thought to play an important role in cell differentiation as well as cell contact and interaction during development (Aydin et al., 2000; Palestini et al., 1990). Total ganglioside content has been observed to increase 8 fold in adult mouse brains compared to embryonic mouse brains. In humans, complex gangliosides GM1 and GD1 increase 12 – 15 fold between gestation and infancy (Yu et al., 2009). This increase in complex gangliosides is thought to be vital to the proper maintenance of brain networks during adulthood.

Altered ganglioside homeostasis has been observed in the brains of patients with AD such that there is a depletion of protective complex gangliosides GD1 and GM1 along with an increase in simple gangliosides GM2 and GM3. In early onset AD, complex gangliosides have been observed to decrease 58-70% in gray matter regions and 81% in frontal white matter (Svennerholm & Gottfries, 1994). An accumulation of simple ganglioside GM3 has been observed both clinically in patients with AD and in transgenic mouse models of AD, which show regional accumulations of GM3 in the entorhinal cortex, forebrain, and surrounding cerebral blood vessels (Chan et al., 2012; Knight et al., 2014; Yamamoto et al., 2006). Previous evidence has shown that there are significant regional differences in the vulnerability to altered lipid metabolism in the human AD brain (Cutler et al., 2004; Hirano-Sakamaki et al., 2015). The balance between complex and simple gangliosides may play an important role in the development and progression of AD. Indeed, Oikawa et al. showed that transgenic mice overexpressing mutant amyloid precursor protein (APP) coupled with a defective GM2 synthase gene demonstrated increased GM3, decreased GM1 and a concomitant deposition of beta-amyloid within their brain (Oikawa et al., 2009). Additionally, alterations in the ceramide moiety of gangliosides may also play an important role in the development of neurodegenerative diseases. The accumulation of long chain ceramides during normal aging has been observed in the mouse brain (Cutler et al., 2004; Sugiura et al., 2008). Moreover, post-mortem brains of patients with AD have shown that the accumulation of long chain ceramides was exacerbated in regions which were susceptible to neurodegeneration and was correlated with disease severity (Cutler et al., 2004). Oikawa et al. 2009, found an increased ratio of d20:1 to d18:1 species of GD1b in the cerebral cortex of brains of patients with AD compared to controls and suggested that this increased ratio may be a major cause of enhance A β assembly in the brain. An altered d20:1/d18:1 species ratio was also observed in the molecular layer of the hippocampus in human AD brains suggesting a role for variable sphingosine base length in mediating neurodegeneration along the perforant pathway (Hirano-Sakamaki et al., 2015). These studies highlight the importance of examining both the ceramide and oligosaccharide domains of gangliosides within the context of patients with AD.

To date, there is very little understanding from a neuroanatomical perspective on how gangliosides change their composition profile during aging, partly due to a lack of technology capable of performing such analysis. MALDI IMS can overcome this challenge by performing mass spectrometry directly on intact brain tissue to provide neuroanatomical spatial information with respect to the gangliosides. The following study uses MALDI IMS to detect and quantify gangliosides in multiple brain regions during aging in the rat. We can further test the hypothesis of ganglioside perturbation as an early indicator of AD using a Tg rat (APP21). These Tg rats were created on a Fischer 344 background and express the human amyloid precursor protein (APP) gene with both the Swedish and Indiana mutations (Agca et al., 2008). As reported previously, these rats do not develop histological hallmarks of AD spontaneously when aged up to 30 months (Rosen et al., 2012). They do, however, develop histopathological signs of AD when challenged with brain extract from AD patients injected intracerebrally (Rosen et al., 2012), or when experimental hydrocephalus is induced (Silverberg et al., 2015). More importantly, these rats show age related cognitive impairment related to white matter damage, making them a strong pre-clinical model to investigate the prodromal phase of AD (Levit et al., 2017).

4.3 Materials and Methods

4.3.1 Animal Model

All procedures involving live animals were in accordance with the guidelines of the Canadian Council on Animal Care and approved by the University of Western Ontario Animal Use Committee (Protocol 2014–2016). Wild-type (WT) Fischer and transgenic (Tg) APP21 rats (Agca et al., 2008) were kindly provided by Dr. Yuksel Agca (University of Missouri) and bred in-house. Tg APP21 rats are homozygous for both human Swedish and Indiana mutations for the APP gene. Rats were euthanized at either P0 (newborn), 3 months (m, young rats), 12 m (middle aged), or 20 m (old), with an N of 5 rats (either Wt or Tg APP21) per group. Intact fresh frozen brains were stored at -80° C until processed for MALDI IMS.

4.3.2 MALDI IMS

Brain tissues (or whole heads for P0 rats) were sectioned on a cryostat (Thermo-Fisher Scientific CryoStar NX50, Toronto, Canada) at a thickness of 10 μm and thaw mounted onto electrically conductive Indium-Tin-Oxide (ITO) slides (Hudson Surface Technology Inc., Old Tappan, NY, USA). Slides were then coated with a thin layer of 1,5-Diaminonaphthalene (DAN, Sigma-Aldrich, Oakville, ON, Canada) matrix via sublimation and incubated at -20°C overnight. After a 10 min desiccation period, calibration standards were applied (Sciex, Farmingham, MA, USA) and allowed to dry before an image of the plate was scanned for reference in the instrument. Images were acquired using a Sciex MALDI 5800 TOF/TOF instrument in negative ion reflectron mode. The instrument is equipped with a 349 nm Nd:YLF “OptiBeam On-Axis” laser. The laser pulse rate used was 1000 Hz. Data acquisition and processing of profiling data were respectively done using a TOF-TOF Series Explorer and Data Explorer (SCIEX). ITO-coated glass slides with tissue sample sections were mounted onto a MALDI plate adapter and loaded into the mass spectrometer. Mass calibration was conducted at a 50 ppm mass tolerance and MS images were acquired at a 70 μm raster with 20 shots/spectrum. This protocol has been previously described in detail elsewhere (Caughlin et al., 2017).

4.3.3 Data Analysis

The regions of interest (ROIs) were confirmed using the rat brain atlas by Paxinos & Watson (1998). A total of 11 ROIs (**Fig. 4.1**) were quantified across the brain and were grouped into discrete anatomical/functional regions for quantitation. These clustered groups include: sub-cortical structures (striatum, lateral septal nucleus - LSN, and substantia nigra - SN), cortical layers (superficial, intermediate, and deep), the hippocampus (CA1, dentate gyrus - DG molecular layer, DG granular layer), and white matter (anterior corpus callosum – aCC, and peri-ventricular corpus callosum - PVCC). MALDI IMS was analyzed using TissueView software (Version 2, Sciex). A total of 4 tissue sections per brain were used to isolate discrete anatomical regions in order to quantify the 11 regions of interest in the current study. Peaks corresponding to major α -series gangliosides were isolated, as confirmed through the Lipidmaps database (www.lipidmaps.org). In order to quantify changes in individual ganglioside species, the

total signal for each ROI in each image was summed by calculating the area under the curve (AUC) of the mass spectrum (between m/z 1100-1930) using Graphpad Prism (Version 7). The AUC of the 3 largest isotopic peaks for each individual ganglioside was summed and a ratio of the AUC of the individual ganglioside species relative to the total spectrum AUC of the ROI was determined. For GD1, both Na^+ and K^+ adduct peaks were detected and showed similar patterns, therefore, the more abundant K^+ adduct was used to represent GD1 data. For data analysis pertaining to Figure 2, the AUC of simple gangliosides (GM3 and GM2 d18:1 and d20:1) were summed and compared to the total AUC of all A-series gangliosides at each time point for both Wt and Tg APP21 rats. Statistical analysis was performed using a two-way ANOVA, followed by a Sidak's post-hoc test \pm SEM.

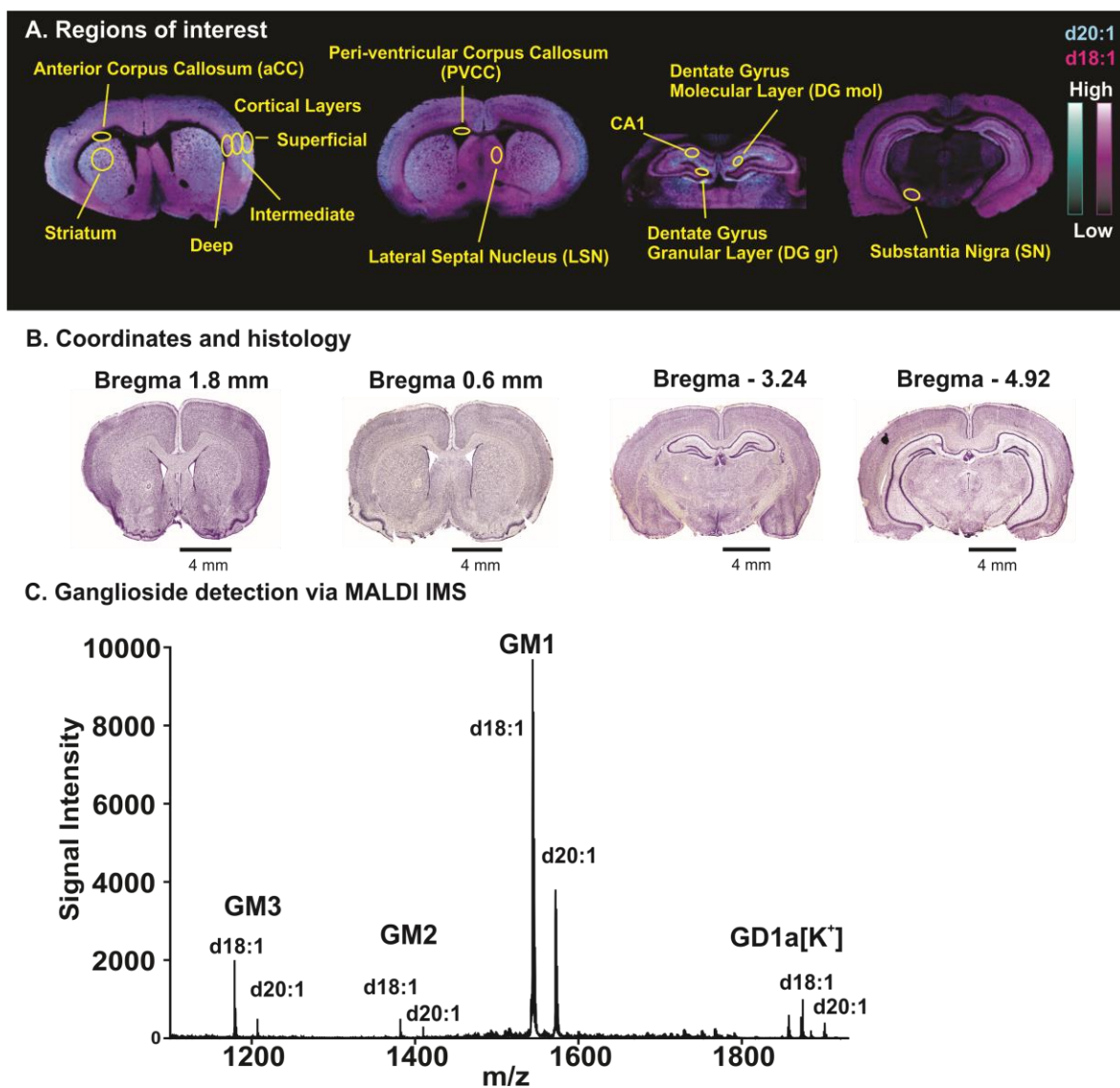


Figure 4.1: MALDI IMS Detection and visualization of A-series gangliosides across rat brain tissue. A-series gangliosides contain species GM3, GM2, GM1, and GD1 and can be detected using DAN matrix in negative ion mode as d18:1 species (the predominant form) or d20:1 species via MALDI IMS. (A) Representative MALDI IMS overlaid images of four tissue sections containing the 11 regions of interest examined in the current study. Each region of interest is circled in yellow and labelled for reference. (B) Representative H&E histology sections indicating the coordinates of each section according to the rat brain atlas by Paxinos & Watson (C) MALDI IMS data plot showing peaks corresponding to d18:1 and d20:1 a-series gangliosides along a 1100 – 1950 mass range.

4.4 Results

4.4.1 Increased proportion of simple gangliosides at 12 m in Tg APP21 rats across the brain

An accumulation of simple gangliosides has been observed clinically in AD brains, however it remains unclear whether this accumulation occurs in the prodromal stages of AD and whether alterations in levels of simple gangliosides can be observed in normal aging. We predicted that Tg APP21 rats would show a higher proportion of simple gangliosides than Wt rats and that this difference due to the effect of transgene would appear at the latest time point (20 m). Although Tg APP21 rats did show a higher proportion of simple gangliosides, this transgene effect was not observed in 20 m rats. It was instead observed at 12 m (**Fig. 4.2 C**) which then disappeared at 20 m (**Fig. 4.2 D**). The transgene effect was statistically significant in several brain regions including white matter regions (PVCC and aCC), intermediate and deep cortical layers, DG gr layer of the hippocampus, and the striatum (**Fig. 4.2 C**).

As expected, the highest percentage of simple gangliosides was observed at P0 (**Fig. 4.2 A**), which then dropped by 3 m and remained relatively stable up to 20 m (**Fig. 4.2 B,D**). This finding fits with the reported downregulation of simple ganglioside synthetic enzymes and upregulation of complex ganglioside synthesis during early development in rats (Rosenberg & Stern, 1966). Although no significant transgene differences were observed at P0, regional differences were apparent. The DG gr layer of the hippocampus showed the highest percentage of simple gangliosides along with the DG mol and CA1 hippocampal layers and the LSN (**Fig. 4.2 A**), while the deep layers of the cortex and the aCC showed the lowest percentage of simple gangliosides. Interestingly, regional differences in the quantity of simple gangliosides were less pronounced after birth and shifted at 3 m such that the PVCC showed the highest proportion of simple gangliosides in the brain, along with the DG gr layer of the hippocampus and SN (**Fig. 4.2 B**). At 12 m, regional differences became more pronounced as the proportion of simple gangliosides increased in certain brain regions, particularly in Tg APP21 rats, such as the white matter, DG gr layer of the hippocampus, as well as intermediate and deep cortical layers (**Fig. 4.2 C**). The regional distribution of simple gangliosides at 20 m was similar to that of 3 m, but

the highest proportion of simple gangliosides was observed in the DG gr layer of the hippocampus (**Fig. 4.2 D**). These results suggest that the quantity and regional distribution of simple gangliosides in the aging brain varies and that a potentially detrimental shift in ganglioside homeostasis occurs as early as 12 m in Tg APP21 rats.

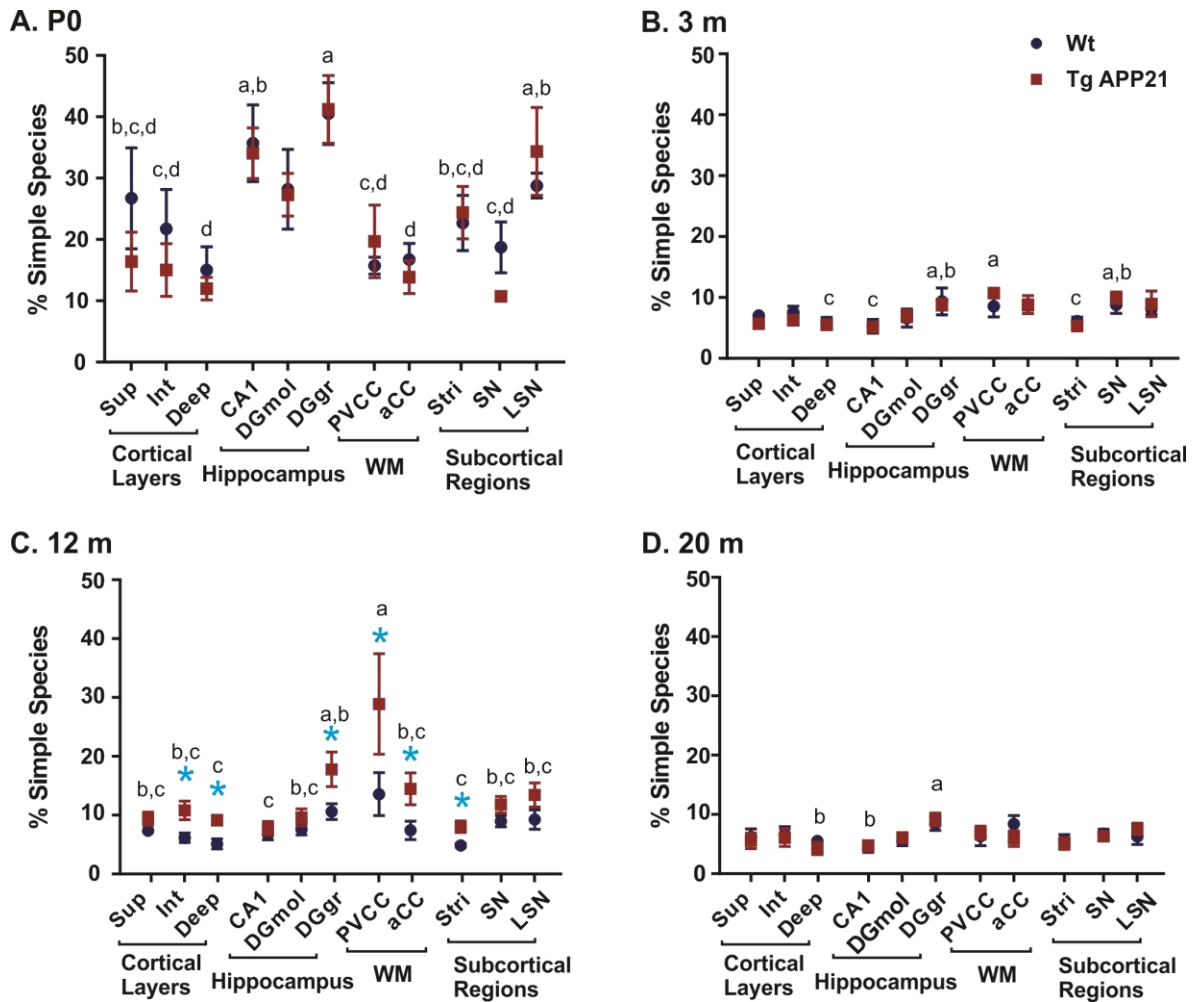


Figure 4.2: The percentage distribution of simple gangliosides in various brain regions of Tg APP21 rats. MALDI IMS area under curve (AUC) data was pooled for each A-series gangliosides to show the percentage of simple gangliosides at each time point as compared to total A-series ganglioside AUC for both Wt and Tg APP21 rats. (A) Highest percentage of simple gangliosides observed in P0 rats. (B) Simple ganglioside content decreased at 3 m and showed an alteration in regional abundance, with fewer regional differences. (C) Transgene differences were observed at 12 m (as indicated by blue *) with the increase in simple gangliosides being more pronounced in Tg APP21 rats. (D) Simple ganglioside content dropped again at 20 m and regional differences decreased. Significant regional differences are indicated with letters a-d. Brain regions with different letters were found to be statistically different from each other (Wt and Tg APP21 data pooled for regional analysis) while regions with no letters indicate no significant difference from any other brain region. *indicates statistical significance, $p < 0.05$ via multiple T-tests; letter indicates statistical significance, $p < 0.05$ via two-way ANOVA, Tukey multiple comparisons post-hoc test.

4.4.2 *GD1 d18:1 species decreased in the gray matter of Tg APP21 rats with maintenance or increases in d20:1 species*

A-series gangliosides were analyzed individually (**Fig 4.3**) relative to P0 in order to better understand age-dependent shifts in complex and simple gangliosides, and to determine the source of the increased proportion of simple gangliosides in Tg APP21 rats observed at 12 m in Figure 4.2. The d18:1 and d20:1 species of each a-series ganglioside were analyzed and presented separately, as the ratio between the d20:1/d18:1 species of complex gangliosides has been reported to increase in an age-dependent manner during normal aging in mice (Sugiura et al., 2008) and has shown unique alterations in the hippocampus of AD patients compared to controls (Hirano-Sakamaki et al., 2015). However, it remains unclear if the altered ratio is caused by an increase in d20:1 species or a decrease in the d18:1 species. In general, GD1 d18:1 levels dropped at 12 m in both Wt and Tg APP21 rats but either dropped more significantly or continued to drop up to 20 m in Tg APP21 rats whereas levels generally increased at 20 m in Wt rats. In the cortex, the abundance of GD1 d18:1 species increased between P0 and 3m in both Wt and Tg APP21 rats, with the exception of the deep layers of the cortex where levels remained statistically unchanged in Tg APP21 rats. Levels then dropped between 3 and 12 m and remained stable until 20 m in the Int and Deep layers. In the Superficial layers, GD1 d18:1 species remained stable between 3 and 20 m in Wt rats while levels dropped at 12 m in Tg APP21 rats such that they were no longer significantly different from P0 levels. However, levels then increased again at 20 m in Tg APP21 rats (**Fig. 4.3 B**).

Similar to the cortex, GD1 d18:1 levels increased between P0 and 3 m throughout the hippocampus. Levels then steadily dropped between 3 m and 20 m in Tg APP21 rats but increased at 20 m in Wt rats. This led to the Wt, but not Tg APP21 rats showing significantly elevated levels of GD1 d18:1 species compared to P0 at 20 m in the CA1 and DG mol layers of the hippocampus (**Fig. 4.3 C**). Among the subcortical structures, GD1 d18:1 species increased between P0 and 3 m in the striatum and LSN, but only increased significantly in Wt rats in the SN (**Fig. 4.3 D**). Levels remained statistically elevated from P0 in both Wt and Tg APP21 rats up to 20 m in the striatum despite a slight drop at 12 m (**Fig 4.3 D** – left panel). Wt and Tg APP21 rats showed opposite patterns at 20 m within the LSN and SN regions with GD1d18:1 increasing significantly from P0 levels only in Tg

APP21 rats in the LSN (**Fig 4.3 D** – center panel) and only in Wt rats in the SN (**Fig 4.3 D** – right panel).

Age-dependent increases in the ratio of d20:1/d18:1 species of GD1 have been reported in the mouse hippocampus during normal aging (Sugiura et al., 2008) While GD1 d18:1 showed between a 2 – 5 fold increase from P0 throughout the brain, d20:1 species of GD1 increased between 3 – 8 fold, with the largest increase observed in the DG mol layer of the hippocampus and striatum. This supports the hypothesis that d20:1 species are indeed increasing in the brain compared to d18:1 species. However, the increase in d20:1 species was not observed to be age-dependent in most brain regions. In the SN, striatum, hippocampus, DG mol, intermediate and deep layers of the cortex, GD1 d20:1 species increased between P0 and 3 m then remained significantly elevated but stable up to 20 m in both Wt and Tg APP21 rats (**Fig 4.3 E-G**). A similar pattern occurred in the superficial layers of the cortex but was only significantly elevated from P0 in Wt rats (**Fig 4.3 E** – left panel). In the hippocampus, Wt and Tg APP21 rats showed divergent patterns at 20 m with GD1 d20:1 species decreasing in Tg APP21 rats and increasing in Wt rats, leading to statistical differences relative to P0 levels (**Fig 4.3 F**). The only transgene difference observed for GD1 d20:1 species was in the LSN where levels dropped in Wt rats at 20 m and increased in Tg APP21 rats, contrary to what was observed in the hippocampus, leading to a statistical difference between the two groups (**Fig. 4.3 G** – center panel). Overall, results of MALDI IMS analysis of GD1 suggests that the increased ratio of d20:1/d18:1 species previously reported is due to both an increase/stable abundance of d20:1 species and a decreased in d18:1 species during aging.

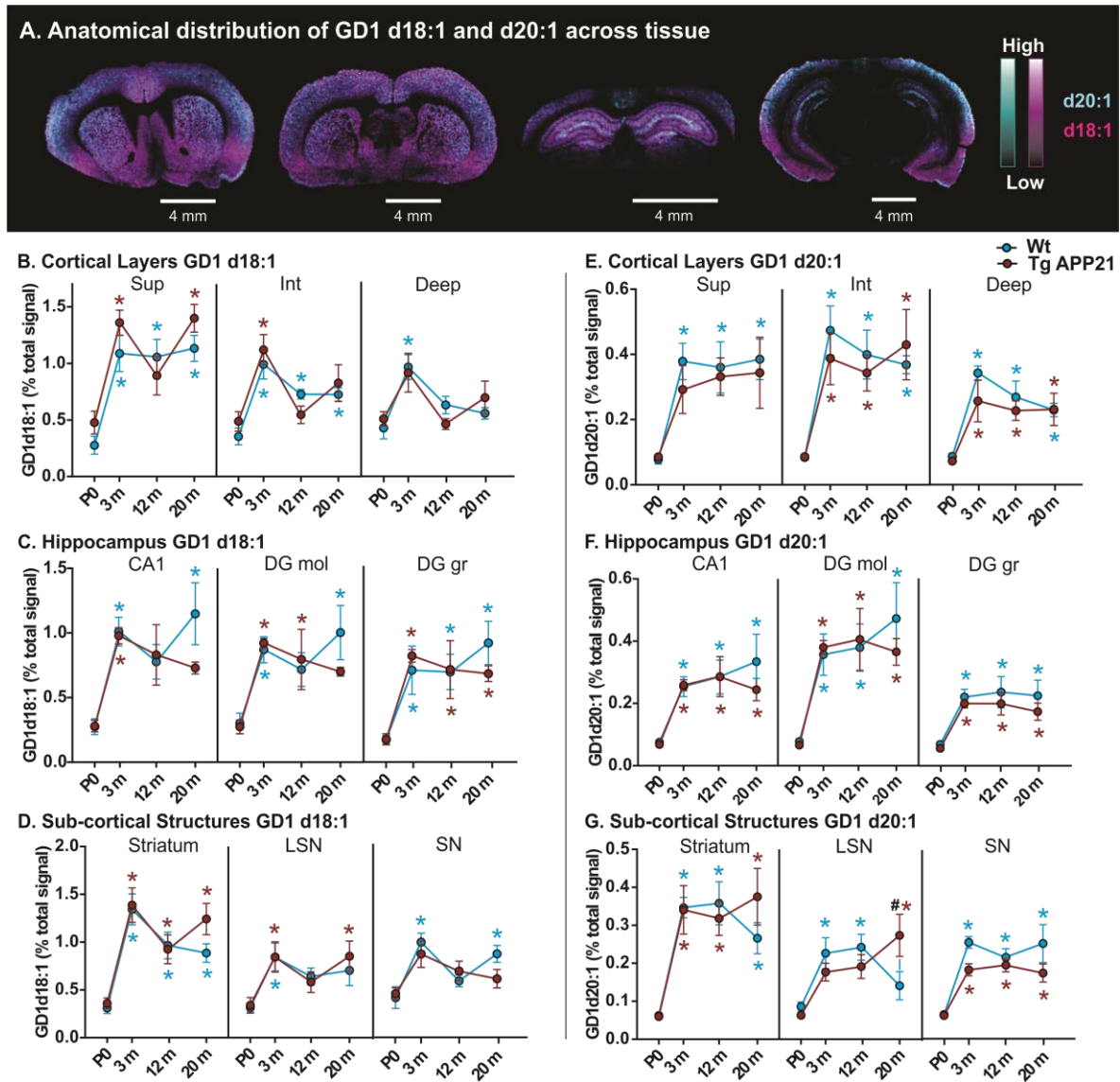


Figure 4.3: Distribution of the GD1 d18:1 and d20:1 species during aging. (A) Representative MALDI IMS overlaid images showing the anatomical distribution of the d18:1 (magenta) and d20:1 species (cyan) of GD1. (B-G) Quantification of MALDI IMS data showing the percent of GD1 d18:1 (B-D) and d20:1 (E-G) species compared to the total signal at each time point. GD1 d18:1 dropped at 12m in both Wt and Tg APP21 rats which either continued to drop at 20 m or increased slightly. Statistical differences were observed in relative to P0 throughout aging (B-D). GD1 d20:1 species increased significantly between P0 and 3 m which then remained stable or increased slightly at 20 m (E-G). A transgene difference was observed at 20 m in the LSN in which Tg APP21 rats showed elevated levels of d20:1 species of GD1 whereas levels dropped in Wt rats (G – center panel). * indicates statistical significance, $p < 0.05$ via two-way ANOVA, Tukey post-hoc test.

4.4.3 *Significant increase in GM1 observed during aging with characteristic drop in d18:1 species at 12 m*

The largest increase in complex gangliosides GD1 and GM1 occurred between P0 and 3 m due to alterations in synthetic enzyme regulation during early post-natal development (Yu et al., 2009) and was more pronounced for d20:1 species than d18:1 species. The increase between P0 and 3 m was greater for GM1 d20:1 species (5 – 17 fold) than for GD1 d20:1 species (3 – 4 fold), with a greater degree of anatomical heterogeneity. Unlike GD1, GM1 reached its highest abundance at 20 m in all brain regions, suggesting an age-dependent accumulation. However, this accumulation was not linear and after the initial increase after birth, remained either stable or decreased slightly between 3 m and 12 m. GM1 levels then increased between 12 m and 20 m for both the d18:1 and d20:1 species (**Fig. 4.4**).

GM1d18:1 species increased from around 5% of the total signal at P0 to 20% at 3 m. The LSN and SN showed the lowest levels of GM1 d18:1 of all gray matter brain regions at 3 m. The pattern of GM1 d18:1 species abundance was very similar between Wt and Tg APP21 rats throughout aging, with no transgene differences observed; however, statistical differences were observed relative to P0 throughout aging which varied depending on transgene (**Fig. 4.4 B-D**). Wt rats showed slightly higher levels of GM1 d18:1 in the LSN and SN at 12 and 20 m respectively (**Fig 4.4 D** – center and right panels), while Tg APP21 rats showed higher levels of GM1 d18:1 species in the intermediate layers of the cortex at 3 m (**Fig 4.4 B** – center panel). Additionally, GM1 d18:1 species decreased at 12 m in Tg APP21 rats across the brain while levels remained stable in a number of brain regions examined in Wt rats.

GM1 d20:1 species increased from below 1% of the total signal at P0 to around 4% at 3 m in cortical and sub cortical brain regions as well as the DG gr layer of the hippocampus (**Fig 4.4 E-F**). The CA1 and DG mol layers showed the most significant increase in GM1 d20:1 species, increasing to 6 and 8% of the total signal by 3 m and continued to increase to 10% by 20 m in the DG mol. (**Fig. 4.4 F** – left and center panels). Overall, GM1 showed an age-dependent increase with only minor variations between Wt and Tg APP21 rats.

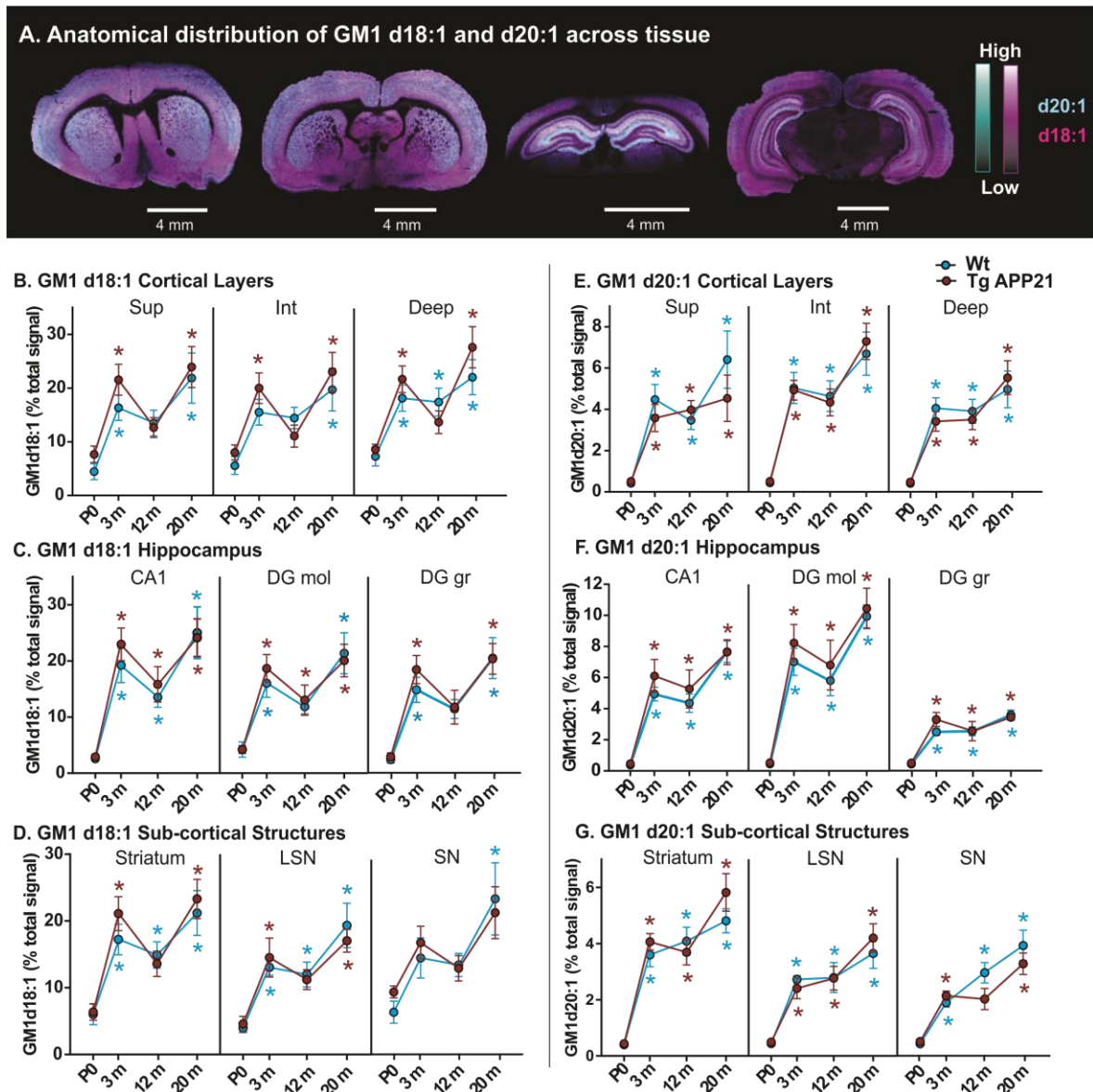


Figure 4.4: Increased levels of GM1 during aging with characteristic drop at 12 m in Fischer rats. (A) Representative MALDI IMS overlaid images showing the anatomical distribution of GM1 d18:1 (magenta) and d20:1 (cyan) species across intact tissue sections containing all regions of interest. (B-G) Quantification of MALDI IMS data showing the percent signal of GM1 d18:1 (B-D) and d20:1 (E-G) species relative to total signal. GM1d18:1 increased between P0 and 3 m which then decreased at 12 m in both Wt and Tg APP21 rats and increased again by 20 m (B-D). GM1 d20:1 species increased in an age-dependent manner throughout the brain with the highest levels observed in the CA1 and DG mol layers of the hippocampus (E-F). * indicates statistical significance, $p < 0.05$ via two-way ANOVA, Tukey post-hoc test.

4.4.4 Decreased GM2 d20:1 species in early life with elevated levels of GM2 d18:1 species in Tg APP21 rats.

Little is known on how simple gangliosides are altered during normal aging. However, based on their reported upregulation in a number of neurodegenerative injuries and diseases, including AD, as well as the observed increase in the proportion of simple gangliosides at 12 m in the current study, we analyzed the anatomical distribution and abundance of the d18:1 and d20:1 species of simple ganglioside GM3 and GM2 in order to compare their alterations in abundance to complex gangliosides in Wt and Tg APP21 rats.

GM2 d18:1 species remained statistically unchanged throughout the lifespan of both Wt and Tg APP21 rats, however, Tg APP21 rats showed a strong trend of increased abundance over Wt rats (**Fig. 4.5 B-D**). This was particularly evident at 12 m as Wt rats showed either stable or decreased levels of GM2d18:1 relative to 3 m whereas levels increased in Tg APP21 rats. This divergence in d18:1 species patterns led to a statistical transgene difference in the striatum, with significantly more GM2 d18:1 species observed in Tg APP21 rats. One exception to this trend was observed in the DG mol layer of the hippocampus where GM2 d18:1 levels dropped significantly from P0 levels at 20 m. Interestingly, GM2 d20:1 species showed more robust changes with aging. GM2 d20:1 species dropped significantly in all gray matter regions between P0 and 3 m in both Wt and Tg APP21 rats and remained stable up to 20 m (**Fig. 4.5 E,F**). Tg APP21 rats showed a slight increase in GM2 d20:1 species at 12 m while levels in Wt rats remained stable, with the exception of the LSN and SN. These results demonstrate that the d20:1 species of GM2, and not the d18:1 species, were decreased during early development and remained stable during adulthood and that Tg APP21 rats have slightly elevated levels of GM2 over their Wt counterparts.

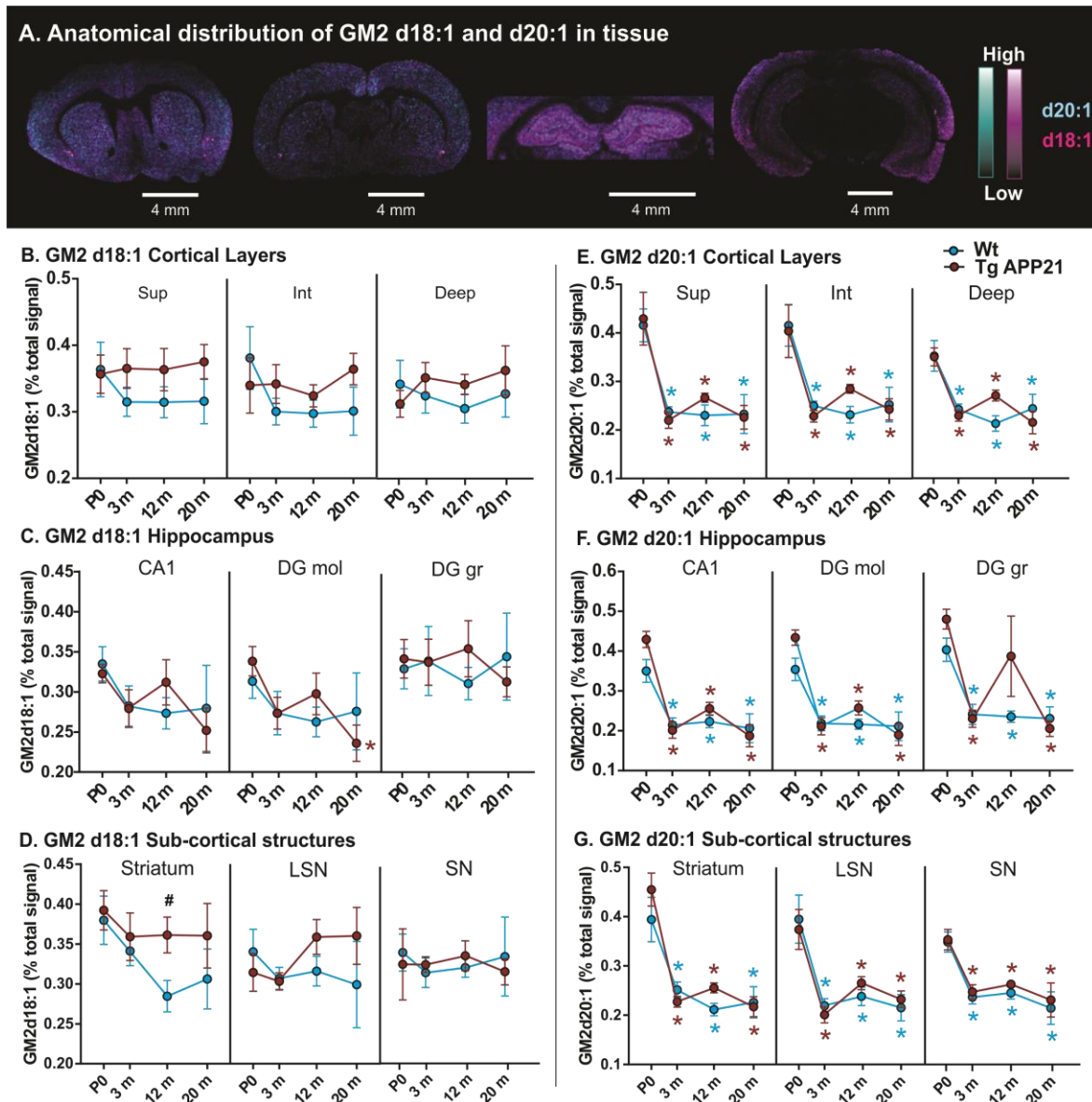


Figure 4.5: Tg APP21 rats have elevated levels of GM2 with a significant drop in GM2 d20:1 species in early life for both groups. (A) Representative MALDI IMS overlaid images showing the anatomical distribution of GM2 d18:1 (magenta) and d20:1 (cyan) species across intact tissue sections containing all regions of interest. (B-G) AUC Quantification of MALDI IMS data showing the signal corresponding to d18:1 (B-D) and d20:1 (E-G) species of GM2 as a percentage of total signal. (B-D) GM2 d18:1 species often showed diverging patterns of abundance between Wt and Tg APP21 rats throughout the lifespan, with a trend of increased GM2 d18:1 species in Tg APP21 rats, however, this was not statistically significant. (E-G) GM2 d20:1 species dropped significantly from P0 levels at 3 m in all brain regions and remained stable up to 20 m with a trend of increased GM2 d20:1 species at 12 m in Tg APP21 rats. * indicates statistical significance, $p < 0.05$ via two-way ANOVA, Tukey post-hoc test.

4.4.5 *Early increases in GM3 in Tg APP21 rats with transgene differences at 12 m.*

Simple ganglioside GM3 has been widely studied in the field of oncology due to its ability to induce apoptosis, decrease angiogenesis, and prevent cell proliferation when accumulated in vitro (Chung et al., 2009; Nakatsuji & Miller, 2001; Prokazova et al., 2009; Sohn et al., 2006). In the brain, GM3 has been associated with the propagation of neurodegeneration after stroke (Caughlin et al., 2015; Whitehead et al., 2011) and the seeding of toxic A β fibrils in mouse models of AD (Kreutz et al., 2011; Oikawa et al., 2009). GM3 d18:1 was observed to be anatomically located in medial structures of the brain and lining ventricular regions (**Fig. 4.6 A**).

Unlike GM2, no consistent trend in the overall GM3 d18:1 species abundance was observed during aging, rather, Tg APP21 rats and levels varied based on anatomical brain region. For instance, Tg APP21 rats were born with significantly higher levels of GM3 d18:1 species in the striatum, LSN, and DG gr layer of the hippocampus, with a similar trend in the DG mol layer (**Fig. 4.6 B-D**). A significant transgene difference was observed at 3 m in the CA1 and DG mol layers of the hippocampus, with elevated levels of GM3 in Tg APP21 rats over Wt rats (**Fig. 4.6 C**). Finally, a similar transgene difference in GM3 d18:1 species was observed at 12 m in the intermediate layers of the cortex (**Fig. 4.6 B**). Wt rats showed a consistent pattern of decreased or stable GM3 d18:1 species at 12 m whereas this species generally increased in Tg APP21 rats at the same point. GM3 d18:1 species were most abundant in the striatum, LSN, and DG gr layer of the hippocampus at birth whereas the cortical layers and SN showed the lowest abundance. Because GM3 d18:1 species showed a trend of accumulating in an age-dependent manner in the DG gr of Tg APP21 rats, it consistently showed the highest levels throughout aging, reaching 1.6% of the total signal by 20 m of age (**Fig 4.6 C – right panel**). Tg APP21 rats also displayed a more severe fluctuation of GM3 d18:1 species relative to P0 than Wt rats, generally showing elevated levels from birth, with the exception of the striatum, LSN, and CA1, which decreased or remained stable after P0. Overall, Tg APP21 rats at some point during aging had increased levels of GM3 d18:1 species over Wt rats in all brain regions examined.

More consistent trends were observed for GM3 d20:1 species across the brain with similar patterns observed among discrete brain regions. As was observed with simple ganglioside GM2, a divergence in ganglioside patterns occurred at 12 m between Wt and Tg APP21 rats. While GM3 d20:1 species either remained stable or decreased between 3 and 12 m in Wt rats, Tg APP21 rats showed elevated levels at this time point. This led to significant transgene differences in the intermediate and deep layers of the cortex, with a similar trend in all other selected brain regions, with the exception of the SN. GM3 d20:1 species remained statistically unchanged between P0 and 20 m among all layers of the cortex (**Fig. 4.6 E**). Hippocampal layers showed a different pattern, with a drop in GM3 d20:1 species observed between P0 and 3 m which then remained stable up to 20 m (**Fig. 4.6 F**). This drop was most significant in the CA1 layer with statistical differences from P0 levels observed for both Wt and Tg APP21 rats. The striatum showed a similar pattern to that of the hippocampal layers with a drop in GM3 d20:1 species between P0 and 3 m. Levels then continued to drop and became statistically lower than P0 at 12 m only in Wt rats, whereas levels increased slightly in Tg APP21 rats (**Fig. 4.6 G – left panel**). The LSN showed a similar pattern to that of the cortical layers, remaining statistically unchanged between P0 and 20 m (**Fig. 4.6 G – center panel**). While GM3 d20:1 species also remained statistically unchanged during aging in the SN, Wt and Tg APP21 rats showed opposite patterns during early life, with a slight drop observed in Wt rats between P0 and 3 m which then gradually increased up to 20 m and a slight increase between P0 and 3 m in Tg APP21 rats which then gradually dropped until 20 m (**Fig. 4.6 G – right panel**). Overall, these results indicate that there is an increased abundance of GM3 gangliosides in Tg APP21 rats in early and mid-life and unique patterns of abundance during aging among Wt and Tg APP21 rats.

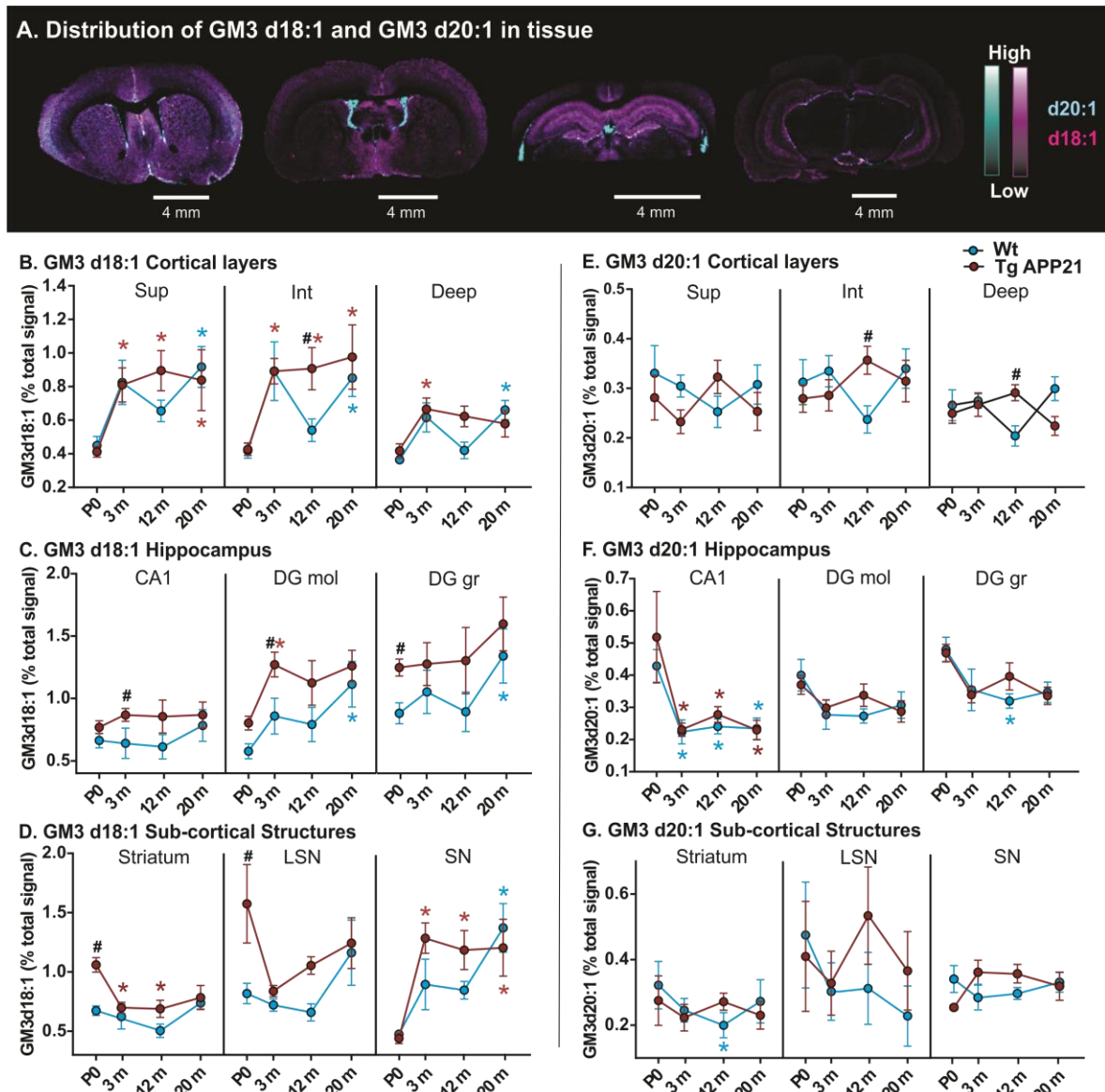


Figure 4.6: Increased GM3 in Tg APP21 rats. (A) Representative MALDI IMS overlaid images showing the anatomical distribution of GM3 d18:1 (magenta) and d20:1 (cyan) species across intact tissue sections containing all regions of interest. (B-G) Quantification of MALDI IMS data showing the signal corresponding to d18:1 (B-D) and d20:1 species (E-G) of GM3 relative to total signal. (B-D) Significant transgene differences were observed at P0, 3 m and 12 m across the various brain regions, with Tg APP21 rats displaying elevated levels of GM3 d18:1 species over their Wt counterparts. GM3 d20:1 species remained statistically unchanged from P0 in the cortical layers, however, Tg APP21 rats showed significantly elevated levels over Wt rats at 12 m in the Int and Deep layers (E). GM3 species dropped between P0 and 3 m in the hippocampus, particularly in the CA1 region, then remained stable up to 20 m (F). Each sub-cortical layer had a slightly different GM3 d20:1 species pattern during aging, with the striatum showing a similar pattern to that of hippocampal regions, the LSN having a similar pattern to that of the cortical layers, and the SN showing opposite patterns between Wt and Tg APP21 rats (G). * indicates statistical significance, $p < 0.05$ via two-way ANOVA, Tukey post-hoc test.

4.4.6 Age-dependent decrease in GD1 d18:1 species in white matter regions with increases in simple gangliosides only in Tg APP21 rats.

A unique ganglioside pattern was observed in the white matter as compared to gray matter regions during aging, thus these regions are presented separately. Interestingly, an age-dependent decrease in GD1 d18:1 species in the PVCC was observed, with a similar drop occurring between 3 and 12 m in the aCC (**Fig 4.7 A**). This pattern is unlike the gray matter regions, which all showed either a stable or increased abundance of GD1 d18:1 species during early development. GD1 d20:1 species increased significantly between P0 and 12 m only in the Wt rats where it then dropped significantly by 20 m. In Tg APP21 rats, GD1 d20:1 species showed a trend of increasing in an age-dependent manner up to 20 (**Fig 4.7 B - left**). In the aCC, GD1 d20:1 species increased significantly between P0 and 3 m in both Wt and Tg APP21 rats where it then gradually decreased up to 20 m (**Fig. 4.7 B – right**). Overall, GD1 levels appear to decrease in the white matter during the later stages of the rat lifespan.

Complex ganglioside GM1 showed similar patterns of abundance in white matter to what was observed in gray matter regions, with an increase in GM1 d18:1 species between P0 and 20 m, along with a drop at 12 m (**Fig 4.7 C – left panel**). However, this drop only occurred in Tg APP21 rats in the aCC while it remained stable in the Wt rats (**Fig 4.7 C – right panel**), suggesting that GM1 levels may be more severely depleted in Tg APP21 rats at this time point. GM1 d20:1 species increased significantly between P0 and 3 m, and again between 12 m and 20 m while remaining stable between 3 m and 12 m in the PVCC. Overall, GM1 species accumulate during both early development and during the later stages of aging in the rat.

Simple gangliosides GM2 and GM3 also showed unique alterations in abundance in the white matter as compared to gray matter regions with a number of transgene differences. For example, GM2 d18:1 species increased between P0 and 3 m in both the PVCC and aCC where it decreased slightly but remained stable up to 20 m in the Wt rats. However, GM2 d18:1 species continued to increase or remained stable up to 12 m in Tg APP21 rats, becoming significantly elevated from P0 levels in the PVCC and remaining elevated up to 20 m (**Fig 4.7 E**). The d20:1 species of GM2 decreased slightly between P0

and 3 m in the white matter where it remained stable in the PVCC of Wt rats and continued to drop up to 12 m in the aCC, decreasing significantly from P0 levels. Tg APP21 rats instead showed a slight increase in GM2 d20:1 species at 12 m which then decreased by 20 m (**Fig 4.7 F**). Overall, Tg APP21 rats showed higher levels of GM2 at 12 m over their Wt counterparts.

Similar to what was observed in the striatum, LSN, and DG gr regions for GM3 d18:1 species, Tg APP21 rats showed elevated levels of GM3 d18:1 species at birth over their Wt counterparts, however, this difference was not statistically significant. GM3 d18:1 species remained fairly stable between birth and old age in Wt rats, whereas levels remained elevated in Tg APP21 rats such that there was a significant transgene difference observed at 12 m in both the PVCC and aCC before levels dropped at 20 m (**Fig 4.7 G**). An age-dependent increase in GM3 d20:1 species was observed only in Tg APP21 rats up to 12 m of age where it became significantly increased from P0 levels in the PVCC and remained significantly elevated at 20 m. This increase in GM3 d20:1 species up to 12 m led to a statistical difference between Wt and Tg APP21 rats at 12 m in the aCC (**Fig 4.7 H**). Taken together, these results suggest a more severe pathological shift in white matter ganglioside content during aging that is enhanced in Tg APP21 rats.

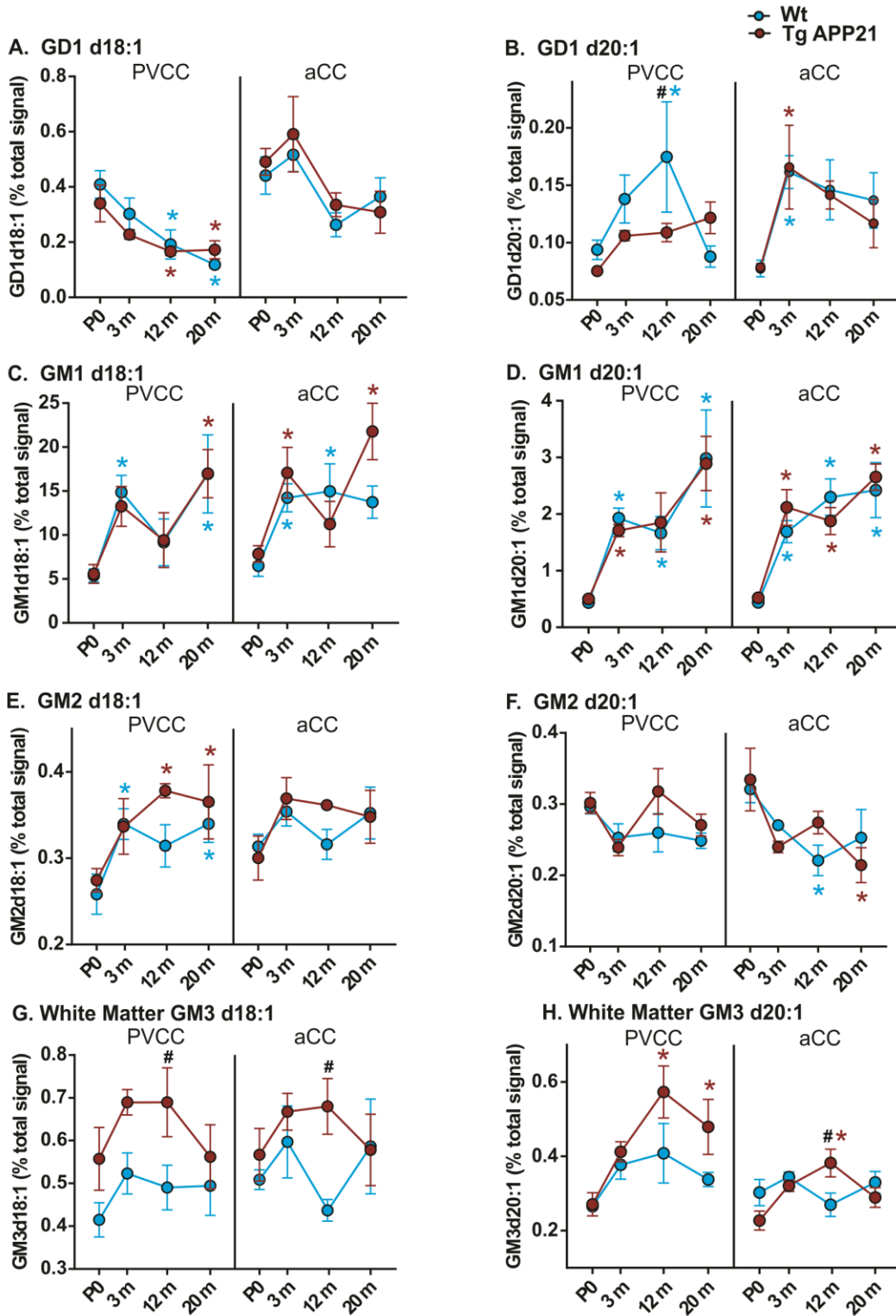


Figure 4.7: Unique ganglioside alterations in white matter regions of the brain during aging. AUC Quantification of MALDI IMS data in the white matter showing the signal corresponding to each a-series ganglioside as a percentage of the total signal, with the d18:1 species on the left and d20:1 species on the right. (A) GD1 d18:1 species decreased in an age-dependent manner up to 20 m in the PVCC (left). A similar trend was observed in the aCC, however, the Wt rats only showed a significant decrease after 3 m. (B) GD1 d20:1 species increased in an age-dependent manner in the PVCC up to 12 m in Wt rats and 20 m in Tg APP21 rats, whereas a significant increase in GD1 d20:1 species was only observed between P0 and 3 m in the aCC before dropping until 20 m. (C+D) GM1 d18:1 species increased between P0 and 20 m, however, the characteristic drop in GM1 content observed at 12 m was more pronounced in Tg APP21 rats in the aCC. (E) GM2 d18:1 species increased significantly between P0 and 12 m only in Tg APP21 rats and remained elevated at 20 m in the PVCC. (F) GM2 d20:1 species dropped significantly from P0 levels at 12 m in the aCC of Wt rats but did not drop until 20 m in Tg APP21 rats. GM3 d18:1 species showed a trend of increased abundance at 12 m in the aCC of Tg APP21 rats (G+H) Tg APP21 rats showed significantly elevated levels of GM3 at 12 m over their Wt counterparts as well as a significant increase in GM3 d20:1 species from P0 levels at 12 and 20 m in the PVCC. * indicates statistical significance from P0, # indicates statistical significance between Wt and Tg APP 21 rats, $p < 0.05$ via two-way ANOVA, Tukey post-hoc test.

4.5 Discussion

This is the first study to examine age and neuroanatomic-specific alterations in the expression profile of a-series gangliosides in both Wt and Tg APP21 rats using MALDI IMS. Gangliosides have been observed to shift in a characteristic manner during AD such that there is a depletion of complex gangliosides, such as GM1, and an accumulation of simple ganglioside GM3 (Chan et al., 2012; Knight et al., 2014; Svennerholm & Gottfries, 1994; Yamamoto et al., 2006). The reason for this shift in ganglioside homeostasis is poorly understood but has been suggested to play an important mechanistic role in the development of AD (Oikawa et al., 2009). MALDI IMS is the only technique capable of accurately detecting gangliosides based on both their oligosaccharide and ceramide moieties while simultaneously providing high resolution imaging of the ionic distribution across intact tissue sections, making it the ideal tool for the study of membrane lipids in the aging brain. However, it is important to note that this technique is not without limitations. For example, due to run-to-run variation in sample preparation and instrument variables, MALDI IMS data is considered to be semi-quantitative. While there is currently no single approach to quantifying MALDI-IMS data, the goal remains to reduce run-to-run variability as much as possible in order to obtain the most accurate and meaningful results. In the current study, we compared the area under the curve corresponding to each individual ganglioside species to the total signal of the spectrum within a mass range of 1100-1950 in order to minimize sources of variability. While gangliosides account for the largest peaks in this mass range, as can be seen in Figure 4.1 C, smaller, unidentified peaks are also present which may fluctuate during aging, thus affecting total signal. Therefore, while MALDI IMS remains an incredibly powerful tool for the analysis of gangliosides, limitations surrounding the semi-quantitative nature of the technique should be considered when interpreting the data.

An examination of the percentage of simple gangliosides GM3 and GM2 compared to total a-series gangliosides at each time point revealed a high degree of anatomical heterogeneity in the proportion of simple gangliosides throughout the brain at P0 which may be related to the function of these brain regions during development and adulthood. For example, The DG gr layer of the hippocampus showed the highest percentage of simple

gangliosides at P0 of all the 11 regions of interest across the brain. This layer is composed largely of the cell bodies of granule cells which project dendrites and processes into the DG mol layers of the hippocampus. This is a region where neurogenesis is thought to occur, not only during development, but throughout adulthood as well (Amaral, Scharfman, & Lavenex, 2007). Neurogenesis in the DG gr layer is said to be in a steady-state as opposed to an accretion over time, this implies tight regulation of neurogenesis in this region (Amaral et al., 2007). It is possible that the increased abundance of simple gangliosides in this region may thus be related to the regulation of neurogenesis in the DG gr layer of the hippocampus. Indeed, the DG gr layer had one of the highest proportions of simple gangliosides at every time point, further supporting this hypothesis.

The percentage of simple gangliosides dropped at 3 m, again, matching what has been reported to occur with ganglioside synthetic enzymes during this period (Rosenberg & Stern, 1966). Indeed, the most significant increase in complex gangliosides occurred between P0 and 3 m, which would account for the decreased relative abundance of simple gangliosides at this time point. One of the most intriguing findings, however, was the increased percentage of simple gangliosides at 12 m in many brain regions which was enhanced in Tg APP21 rats such that a number of transgene differences were observed across the brain. This increase in simple gangliosides was accompanied by a concurrent drop in complex gangliosides at 12 m, which would account for the significant increase in the proportion of simple gangliosides at this time point. These findings suggests that a pathological shift in the homeostasis of gangliosides may be occurring as early as 12 m of age and is enhanced in Tg APP21. This evidence supports the hypothesis that lipid alterations may occur in the prodromal stages of AD.

Age-dependent changes in complex gangliosides have been previously examined using liquid chromatography-based techniques. In a study published in 2000, Aydin et al. found that ganglioside GM1 increased slightly between 3 and 24 months of age, while GD1 increased up to 12 m then dropped by 20 % by 24 m. A similar pattern was observed in the current study. Aydin et al. also found an age-dependent increase in GM1 fractions compared to other complex gangliosides, however, the authors ascribed this finding to a decrease in GD1 and GT1 components rather than an increase in GM1, which was found to

remain relatively stable at later time points (Aydin et al., 2000). GM1 d20:1 species in particular showed a higher fold increase in abundance from P0 than GM1 d18:1 species and increased up to 20 m in most brain regions. This finding confirms the presence of an age-dependent accumulation of long chain ceramide species in the brain, as has been previously reported (Hirano-Sakamaki et al., 2015; Palestini et al., 1993; Sugiura et al., 2008).

While GM1 was found to be consistently increased during adulthood in both Wt and Tg APP21 rats, a less pronounced effect was observed for ganglioside GD1. The d20:1 species showed, in most cases, an age-dependent increase up to 12 m which then plateaued or decreased at 20 m. Wt rats also showed higher levels of GD1 than Tg APP21 rats in a number of brain regions, particularly at 20 m in the hippocampus. Although the senescence-related drop in GD1 and GT1 described by Aydin et al., 2000 is not fully understood, the authors suggest that it may be related to degenerative processes in dendrites and synapses in which these species are highly expressed. Alternatively, the breakdown of GD1 may be related to maintenance of GM1 (Aydin et al., 2000). In a study which measured GM1, GD1, and GT1 levels in the CSF of “probable AD” patients versus age-matched controls, an increase in GM1 levels was observed, particularly in younger “probable AD” patients while GD1 and GT1 levels were decreased, suggesting that this breakdown may be further enhanced in during AD development and progression (Blennow et al., 1992). The neuroprotective properties of GM1 have been well documented and are ascribed to its ability to modulate neurotrophin release and regulate ion transport (Ledeen & Wu, 2015; Wu & Ledeen, 1994). In fact, of all the a-series gangliosides, GM1 has been found to have a high degree of functional importance in the maintenance of cells. This is further supported by the finding of GM1’s resistance to breakdown by sialidase as compared to other complex gangliosides (Palestini et al., 1993). Multi-sialylated species, such as GD1 and GT1, are highly susceptible to sialidase (Palestini et al., 1993), leading some to suggest that it may serve as a reserve pool for the maintenance of GM1 levels in the brain (Ledeen & Wu, 2015). The transgene difference observed in the current study with respect to the drop in GD1 levels may therefore be the result of an increased need to breakdown GD1 in order to maintain GM1 levels in Tg APP21 rats. Future studies should address the changes in both ganglioside synthetic and catabolic enzymes during aging.

A previous study in our lab reported a decrease the d20:1/d18:1 species ratio of GM2 between P0 and 3 m which remained stable up to 20 m (Caughlin et al., 2017b). The current study confirms that this decreased ratio was due to a significant drop in d20:1 species of GM2 and not an increase in d18:1 species, which remained statistically unchanged throughout the rat lifespan. Tg APP21 rats also showed a trend of increased GM2 at 12 m across a number of brain regions and led to a significant transgene difference in striatum. Interestingly, the accumulation of GM2 has been reported in human brains of patients with AD and frontotemporal dementia (Pernber et al., 2012), thus, the increased abundance of GM2 in our Tg APP21 rats may be indicative of a pathological shift in ganglioside homeostasis.

GM3 has been shown to upregulate pro-apoptotic signaling pathways as well inhibit VEGF receptor activity leading to toxicity when accumulated in neural cells (Chung et al., 2009; Nakatsuji & Miller, 2001) and is thought to play an important mechanistic role in the development of AD (Oikawa et al., 2009). Several transgene differences were observed in which Tg APP21 rats had significantly elevated levels of GM3 over Wt rats. Interestingly, Tg APP21 rats were born with higher levels of GM3 d18:1 species than Wt rats which remained elevated throughout aging. The observed increase in GM3 coupled with elevated levels of GM2 in Tg APP21 rats suggests that the brains of these rats may be entering a state of vulnerability earlier than previous thought and supports the hypothesis of a pathological shift in ganglioside homeostasis in Tg APP21 rats.

Ganglioside-based alterations in the white matter of the aging brain have been observed to be different than those of the gray matter (Caughlin et al., 2017b). Ganglioside GD1 d18:1 showed a very unique age-dependent decrease in abundance in white matter that has not been previously reported. This drop in d18:1 species was accompanied by the maintenance or increase in d20:1 species. Previous work in our lab examining the ratio of d20:1 species relative to d18:1 found a significant age-dependent increase in the GD1 d20:1/d18:1 ratio in the PVCC, with a similar trend occurring in the aCC (Caughlin et al., accepted). It was assumed that this increased ratio was caused by the age-dependent accumulation of d20:1 species, as had been reported in gray matter regions. However, the current study demonstrates that the increased ratio was instead due to a significant drop in

the d18:1 species, highlighting the importance of analyzing gangliosides individually. Another unique alteration in white matter was observed for ganglioside GM3 in that levels of d20:1 species were significantly elevated only in Tg APP21 rats. The white matter of the brain has demonstrated a particular vulnerability during aging (Gao et al., 2014). While GD1 was not observed to be a major component of white matter in the current study, it has been identified as an important binding site for myelin-associated protein (MAG), which plays a major role in the formation and maintenance of myelin in the central nervous system (Al-bashir, Mellado, & Filbin, 2016). The age-dependent depletion of GD1 along with the increased abundance of simple ganglioside GM3 in Tg APP21 rats may be indicative of a mechanism of neurodegeneration in this region during AD.

The brains of aging Tg APP21 rats are thought to be in a vulnerable state due to the accumulation of APP. It is possible that the vulnerable state of the Tg APP21 rat brain may have deleterious effects on the proper functioning of cell membranes and that, in an attempt to restore/maintain homeostatic GM1 levels, GD1 is degraded to GM1. An examination of the activities of sialidase and sialyl-transferase enzymes is a future goal and would provide valuable insight into this hypothesis. A greater understanding of the role of altered lipid profiles in the aging and injured brain could lead to the development of lipid-based biomarkers for individuals at risk of developing neurodegenerative diseases as well as more effective lipid-targeted therapeutics for the early stages of AD.

4.6 References

- Agca, C., Fritz, J. J., Walker, L. C., Levey, A. I., Chan, A. W., Lah, J. J., & Agca, Y. (2008). Development of transgenic rats producing human beta-amyloid precursor protein as a model for Alzheimer's disease: Transgene and endogenous APP genes are regulated tissue-specifically. *BMC Neuroscience*, *9*(1), 28.
- Al-bashir, N., Mellado, W., & Filbin, M. T. (2016). Sialic Acid Is Required for Neuronal Inhibition by Soluble MAG but not for Membrane Bound MAG. *Frontiers in Molecular Neuroscience*, *9*(April), 1–7.
- Amaral, D., Scharfman, H., & Lavenex, P. (2007). The Dentate Gyrus: fundamental neuroanatomical organization. *Progress in Brain Research*, (163), 3–22.
- Aydin, M., Cengiz, S., Ag, B., & Han, E. (2000). Age-related Changes in GM1 , GD1a , GT1b Components of Gangliosides in Wistar Albino Rats. *Cell Biochemistry and*

Function, 45(March 1999), 41–45.

- Blennow, K., Davidsson, P., Wallin, A., Fredman, P., Gottfries, C. G., Manesson, J. E., & Svennerholm, L. (1992). Differences in cerebrospinal fluid gangliosides between “probable Alzheimer’s disease” and normal aging. *Aging (Milano)*, 4(0394–9532), 301–306.
- Caughlin, S., Hepburn, J. D., Park, D. H., Jurcic, K., Yeung, K. K. C., Cechetto, D. F., & Whitehead, S. N. (2015). Increased expression of simple ganglioside species GM2 and GM3 detected by MALDI Imaging Mass Spectrometry in a combined rat model of A β toxicity and stroke. *PLoS ONE*, 10(6), 1–17.
- Caughlin, S., Park, D. H., Yeung, K. K.-C., Cechetto, D. F., & Whitehead, S. N. (2017). Sublimation of DAN Matrix for the Detection and Visualization of Gangliosides in Rat Brain Tissue for MALDI Imaging Mass Spectrometry. *Journal of Visualized Experiments*, (121).
- Chan, R. B., Oliveira, T. G., Cortes, E. P., Honig, L. S., Duff, K. E., Small, S. a, Di Paolo, G. (2012). Comparative lipidomic analysis of mouse and human brain with Alzheimer disease. *The Journal of Biological Chemistry*, 287(4), 2678–88.
- Chung, T. W., Kim, S. J., Choi, H. J., Kim, K. J., Kim, M. J., Kim, S. H., Kim, C. H. (2009). Ganglioside GM3 inhibits VEGF/VEGFR-2-mediated angiogenesis: Direct interaction of GM3 with VEGFR-2. *Glycobiology*, 19(3), 229–239.
- Cutler, R. G., Kelly, J., Storie, K., Pedersen, W. A., Tammarra, A., Hatanpaa, K., Mattson, M. P. (2004). Involvement of oxidative stress-induced abnormalities in ceramide and cholesterol metabolism in brain aging and Alzheimer’s disease. *Proc.Natl.Acad.Sci.U.S.A*, 101(7), 2070–2075.
- Dufresne, M., Guneyusu, D., Patterson, N. H., Marcinkiewicz, M. M., Regina, A., Demeule, M., & Chaurand, P. (2017). Multimodal detection of GM2 and GM3 lipid species in the brain of mucopolysaccharidosis type II mouse by serial imaging mass spectrometry and immunohistochemistry. *Analytical and Bioanalytical Chemistry*, 409, 1425–1433.
- Gao, Z., Wang, W., Wang, Z., Zhao, X., Shang, Y., Guo, Y., Wu, W. (2014). Cerebral microbleeds are associated with deep white matter hyperintensities, but only in hypertensive patients. *PLoS ONE*, 9(3), 1–8.
- Hirano-Sakamaki, W., Sugiyama, E., Hayasaka, T., Ravid, R., Setou, M., & Taki, T. (2015). Alzheimer’s disease is associated with disordered localization of ganglioside GM1 molecular species in the human dentate gyrus. *FEBS Letters*, 589(23), 3611–3616.
- Knight, E. M., Williams, H. N., Stevens, A. C., Kim, S. H., Kottwitz, J. C., Morant, A. D., Boyd, R. E. (2014). Evidence that small molecule enhancement of β -hexosaminidase activity corrects the behavioral phenotype in Dutch APP E693Q mice through reduction of ganglioside-bound A β , 20(1), 109–117.
- Kreutz, F., Frozza, R. L., Breier, A. C., de Oliveira, V. a, Horn, A. P., Pettenuzzo, L. F.,

- Trindade, V. M. T. (2011). Amyloid- β induced toxicity involves ganglioside expression and is sensitive to GM1 neuroprotective action. *Neurochemistry International*, 59(5), 648–55.
- Ledeen, R. W., & Wu, G. (2015). The multi-tasked life of GM1 ganglioside, a true factotum of nature. *Trends in Biochemical Sciences*, 40(7), 407–418.
- Levit, A., Regis, A. M., Garabon, J. R., Oh, S., Desai, S. J., Rajakumar, N., Whitehead, S.N. & Allman, B. L. (2017). Behavioural inflexibility in a comorbid rat model of striatal ischemic injury and mutant hAPP overexpression. *Behavioural Brain Research*, 333(March), 267–275.
- Maglione, V., Marchi, P., Di Pardo, A., Lingrell, S., Horkey, M., Tidmarsh, E., & Sipione, S. (2010). Impaired ganglioside metabolism in Huntington's disease and neuroprotective role of GM1. *The Journal of Neuroscience : The Official Journal of the Society for Neuroscience*, 30(11), 4072–4080.
- Masserini, M., Palestini, P., & Freire, E. (1989). Influence of glycolipid oligosaccharide and long-chain base composition on the thermotropic properties of dipalmitoylphosphatidylcholine large unilamellar vesicles containing gangliosides. *Biochemistry*, 28(12), 5029–5034.
- Nakatsuji, Y., & Miller, R. H. (2001). Selective cell-cycle arrest and induction of apoptosis in proliferating neural cells by ganglioside GM3. *Experimental Neurology*, 168(2), 290–9.
- Ohtani, Y., Tamai, Y., Ohnuki, Y., & Miura, S. (1996). Ganglioside alterations in the central and peripheral nervous systems of patients with Creutzfeldt-Jakob disease. *Neurodegeneration*, 5(4), 331–338.
- Oikawa, N., Yamaguchi, H., Ogino, K., Taki, T., Yuyama, K., Yamamoto, N., Yanagisawa, K. (2009). Gangliosides determine the amyloid pathology of Alzheimer's disease. *Neuroreport*, 20(12), 1043–1046.
- Palestini, P., Masserini, M., Fiorilli, A., Calappi, E., & Tettamanti, G. (1993). Age-Related Changes in the Ceramide Composition of the Major Gangliosides Present in Rat Brain Subcellular Fractions Enriched in Plasma Membranes of Neuronal and Myelin Origin. *Journal of Neurochemistry*, 61(3), 955–960.
- Palestini, P., Masserini, M., Sonnino, S., & Tettamanti, G. (1990). Changes in the ceramide composition of rat forebrain gangliosides with age. *Journal of Neurochemistry*, 54(1), 230–235.
- Prokazova, N. V, Samovilova, N. N., Gracheva, E. V, & Golovanova, N. K. (2009). Ganglioside GM3 and its biological functions. *Biochemistry. Biokhimiia*, 74(3), 235–249.
- Rosenberg, a, & Stern, N. (1966). Changes in sphingosine and fatty acid components of the gangliosides in developing rat and human brain. *Journal of Lipid Research*, 7(1), 122–131.
- Schneider, J. S., Gollomp, S. M., Sendek, S., Colcher, A., Cambi, F., & Du, W. (2013). A

- randomized, controlled, delayed start trial of GM1 ganglioside in treated Parkinson's disease patients. *Journal of the Neurological Sciences*, 324(1–2), 140–148.
- Sohn, H., Kim, Y. S., Kim, H. T., Kim, C. H., Cho, E. W., Kang, H. Y., ... Ko, J. H. (2006). Ganglioside GM3 is involved in neuronal cell death. *The FASEB Journal : Official Publication of the Federation of American Societies for Experimental Biology*, 20(8), 1248–1250.
- Sonnino, S., Mauri, L., Ciampa, M. G., & Prinetti, A. (2013). Gangliosides as regulators of cell signaling: Ganglioside-protein interactions or ganglioside-driven membrane organization? *Journal of Neurochemistry*, 124(4), 432–435.
- Sugiura, Y., Shimma, S., Konishi, Y., Yamada, M. K., & Setou, M. (2008). Imaging mass spectrometry technology and application on ganglioside study; visualization of age-dependent accumulation of C20-ganglioside molecular species in the mouse hippocampus. *PloS One*, 3(9), e3232.
- Svennerholm, I., & Gottfries, C. (1994). Membrane Lipids , Selectively Diminished in Alzheimer Brains , Suggest Synapse Loss as a Primary Event in Early-Onset Form (Type I) and Demyelination in Late-Onset Form (Type 11). *Journal of Mass Spectrometry : JMS*, 62, 1039–1047.
- Tamai, Y., Ohtani, Y., Miura, S., Narita, Y., Iwata, T., Kaiya, H., & Namba, M. (1979). Creutzfeldt-Jakob disease--alteration in ganglioside sphingosine in the brain of a patient. *Neuroscience Letters*, 11(1), 81–86.
- Whitehead, S. N., Chan, K. H. N., Gangaraju, S., Slinn, J., Li, J., & Hou, S. T. (2011). Imaging mass spectrometry detection of gangliosides species in the mouse brain following transient focal cerebral ischemia and long-term recovery. *PloS One*, 6(6), e20808.
- Woods, A. S., Colsch, B., Jackson, S. N., Post, J., Baldwin, K., Roux, A., Balaban, C. (2013). Gangliosides and ceramides change in a mouse model of blast induced traumatic brain injury. *ACS Chemical Neuroscience*, 4(4), 594–600.
- Wu, G., & Ledeen, R. W. (1994). Gangliosides as modulators of neuronal calcium. *Progress in Brain Research*, 101, 101–112.
- Yamamoto, N., Nostrand, W. E. Van, & Yanagisawa, K. (2006). Further evidence of local ganglioside-dependent amyloid b -protein assembly in brain. *Neuroreport*, 17(16), 16–18.
- Yu, R. K., Nakatani, Y., & Yanagisawa, M. (2009). The role of glycosphingolipid metabolism in the developing brain. *Journal of Lipid Research*, 50 Suppl, S440–S445.
- Yu, R. K., Tsai, Y. T., & Ariga, T. (2012). Functional roles of gangliosides in Neurodevelopment: An overview of recent advances. *Neurochemical Research*, 37(6), 1230–1244.

Chapter 5 : Restoring ganglioside homeostasis after stroke using chloroquine is associated with pathological and functional improvements in Wistar rats

In Chapter 4, a pattern of ganglioside dysregulation was observed in the Tg APP21 rats whereby the d20:1 species of both GM3 and GD1 were increased in a number of brain regions susceptible to injury in the aging brain such as the white matter and the DG mol layer of the hippocampus. Tg APP21 rats also displayed a lower abundance of both d18:1 and d20:1 species of GM1 at the later time points over Wt rats, indicating that the overall levels of GM1 were lower in the Tg APP21 rats. GM1 is known to exert a number of neuroprotective functions in the brain and may thus be a mechanism that leaves the brain vulnerable to injury in the Tg APP21 rats. In the current chapter, we explore the potential therapeutic benefits of preventing the catabolism of GM1 and the subsequent accumulation of toxic simple gangliosides after stroke using the lysosomotropic agent Chloroquine.

5.1 Abstract

Perturbations of ganglioside homeostasis have been observed following stroke whereby simple gangliosides GM2 and GM3 accumulate while protective complex species GM1 and GD1 are reduced, leading to the hypothesis that complex species are being degraded to simple species. Thus, there is a need for therapeutic interventions which can prevent ganglioside dysregulation after stroke. A pharmacological intervention using chloroquine (CQ) was selected for its transient lysosomotropic properties which disrupt the activity of catabolic ganglioside enzymes. CQ was administered both *in vitro*, to primary cortical neurons exposed to GM3 toxicity, and *in vivo*, to 3 month old male Wistar rats that underwent a severe stroke, induced through the co-administration of a striatal endothelin-1 (ET-1) injection and intracerebral-ventricular injections of A β (25-35). CQ was administered (45mg/kg i.p.) for 7 consecutive days beginning 3 days prior to surgery and gangliosides were examined using MALDI imaging mass spectrometry at 3 and 21 days after the injury. The ladder motor task was used to examine the functional effects of CQ treatment on day 20. CQ treatment prevented ganglioside dysregulation 3 d post-stroke and

partially prevented complex ganglioside depletion 21 d post-stroke. Exogenous GM3 was found to be toxic to primary cortical neurons which was protected by CQ treatment. Motor deficits were prevented in the forelimbs of rats with CQ treatment and were associated with decreased inflammation, neurodegeneration, and an increase in cell survival at the site of injury. CQ prevents ganglioside dysregulation acutely, protects against GM3 toxicity in neurons, and is associated with long-term functional and pathological improvements after stroke in the rat.

5.2 Introduction

Strokes are the most frequent cause of permanent disability in individuals aged 60 years and older with the global burden of stroke care expected to increase in line with the aging population (Chamorro, Dirnagl, Urra, & Planas, 2016; Feigin et al., 2014). However, there is currently no clinically effective approach to prevent the damage caused by stroke with the exception of tissue plasminogen activator, which has a very narrow therapeutic window of effectiveness (Zhang et al., 2015). Therefore, the development of new preventative approaches and therapeutic interventions which can improve recovery after stroke injuries is imperative. Membrane lipid dysregulation is observed after neurodegenerative injuries in the brain and is thought to play a key mechanistic role in the propagation of neurodegeneration (Caughlin et al., 2015), thus, preventing this dysregulation may provide a novel avenue of intervention for stroke injuries.

Gangliosides are a major component of lipid rafts and play an important role in protein-lipid interactions on the cell surface leading various signal transduction events. Structurally, simple minor gangliosides GM2 and GM3, while crucial during neurodevelopment, have been linked to neurodegeneration in the adult brain. GM3 in particular has been shown to upregulate pro-apoptotic signaling pathways (Nakatsuji & Miller, 2001), inhibit angiogenesis (Chung et al., 2009; Seyfried & Mukherjee, 2010) as well as cell proliferation (Choi et al., 2006), leading to toxicity when accumulated in neural cells (Prokazova et al., 2009; Sohn et al., 2006). Perturbations in ganglioside homeostasis resulting in the depletion of the more abundant protective complex species, GM1 and GD1,

along with the accumulation of toxic simple species have been observed in response to neurodegenerative insults such as stroke and traumatic brain injuries (TBI) (Caughlin et al., 2015; Whitehead et al., 2011; Woods et al., 2013). Additionally, previous work from our lab has demonstrated that the degree of ganglioside dysregulation is correlated with the severity of the neurodegenerative insult, with more severe stroke insults resulting in an earlier and prolonged accumulation of toxic simple ganglioside species (Caughlin et al., 2015). Altogether, this suggests that ganglioside dysregulation may be playing an important role in the propagation of neurodegeneration following stroke.

Therapies targeting the restoration of depleted GM1 in the brain through exogenous administration have demonstrated a strong protective effect in preclinical models of stroke (Carolei et al., 1991; Karpiak, Li, & Mahadik, 1987; Kharlamov et al., 1994; Li, Tian, Long, Chen, & Lu, 2016; Zhang et al., 2015) and was found to prevent behavioural deficits in mice following TBI (Rubovitch et al., 2017). GM1 is thought to exert its protective effects through modulation of neurotrophin release and the maintenance of ion balance (Ledeen & Wu, 2015; Lim, Esfahani, Avdoshina, & Mocchetti, 2011; Rabin et al., 2002; Zhang et al., 2015). However, clinically, GM1 administration alone has produced mixed results and has often failed to confer adequate protection following stroke (Argentino et al., 1989; Candelise, 2002; Hoffbrand et al., 1988). One potential explanation for this finding may be that the restoration of complex gangliosides alone does not prevent those species from being enzymatically degraded to simple gangliosides during the ischemic cascade, thus the resulting toxicity is not prevented. Therefore, there is a need for targeted therapies which can prevent the catabolism of complex gangliosides as well as the resulting accumulation of toxic simple species in order to better protect cells from the damage associated with ganglioside dysregulation after a neurodegenerative injury.

Chloroquine is best known as an anti-malarial drug but has also been used as an anti-rheumatic agent due to its anti-inflammatory properties (Lehmeyer, 1978). It has been shown to reduce the accumulation of reactive oxygen species after glutamate-induced toxicity in hippocampal HT22 cells (Hirata et al., 2011) and block the activity of Toll-like receptor 3-mediated inflammatory pathway following stroke in rats (Cui et al., 2013). In addition to its widely acknowledged role in the inhibition of autophagy, low doses of CQ

have also been shown to have beneficial effects on the vascular system through vessel normalization (Maes et al., 2014) and protection of the blood brain barrier (Hirata et al., 2011). CQ freely diffuses across lipid bilayers as it is uncharged at neutral pH, but is a weak base and becomes protonated upon entering acidic compartments such as lysosomes, causing it to accumulate in acidic organelles and raise their pH above their acidic optimum (Ohkuma & Poole, 1978). This disrupts the normal function of acidic lysosomal enzymes such as β -galactosidase and β -hexosaminidase, the enzymes responsible for the catabolism of complex ganglioside GM1 to simple species GM2 and GM3 (Riboni et al., 1991). CQ has been used to inhibit the catabolism of gangliosides *in vitro* (Riboni et al., 1995; Riboni et al., 1991; Shacka, Klocke, & Roth, 2006), making it a promising candidate for the prevention ganglioside dysregulation after stroke.

In the current study, we used several experimental approaches to examine the effects of CQ treatment in the brain stroke in the rat. Our previous work in this area demonstrated that co-administration of endothelin-1 (ET-1) into the striatum to produce focal ischemia, alongside with bilateral intracerebral-ventricular injections of toxic A β (25-35) in Wistar rats, produces a more severe neurodegenerative response as well as increased ganglioside dysregulation than either ET-1 stroke or A β toxicity alone (Caughlin et al., 2015; Whitehead et al., 2005). Therefore, this particular model was chosen for the present study as it is the ideal platform to assess the effects of CQ treatment on ganglioside homeostasis as well as pathological and functional recovery after a severe stroke. In order to visualize and quantify the abundance of gangliosides in the rat brain, MALDI IMS was performed at 3 and 21 days post-stroke. For the first time, we further demonstrate the toxicity of GM3 accumulation on primary cortical neurons and show the neuroprotective effect of CQ treatment in neurons. Finally, we show the restoration of behavioural deficits following CQ treatment in rats post-stroke (**Fig. 5.1**).

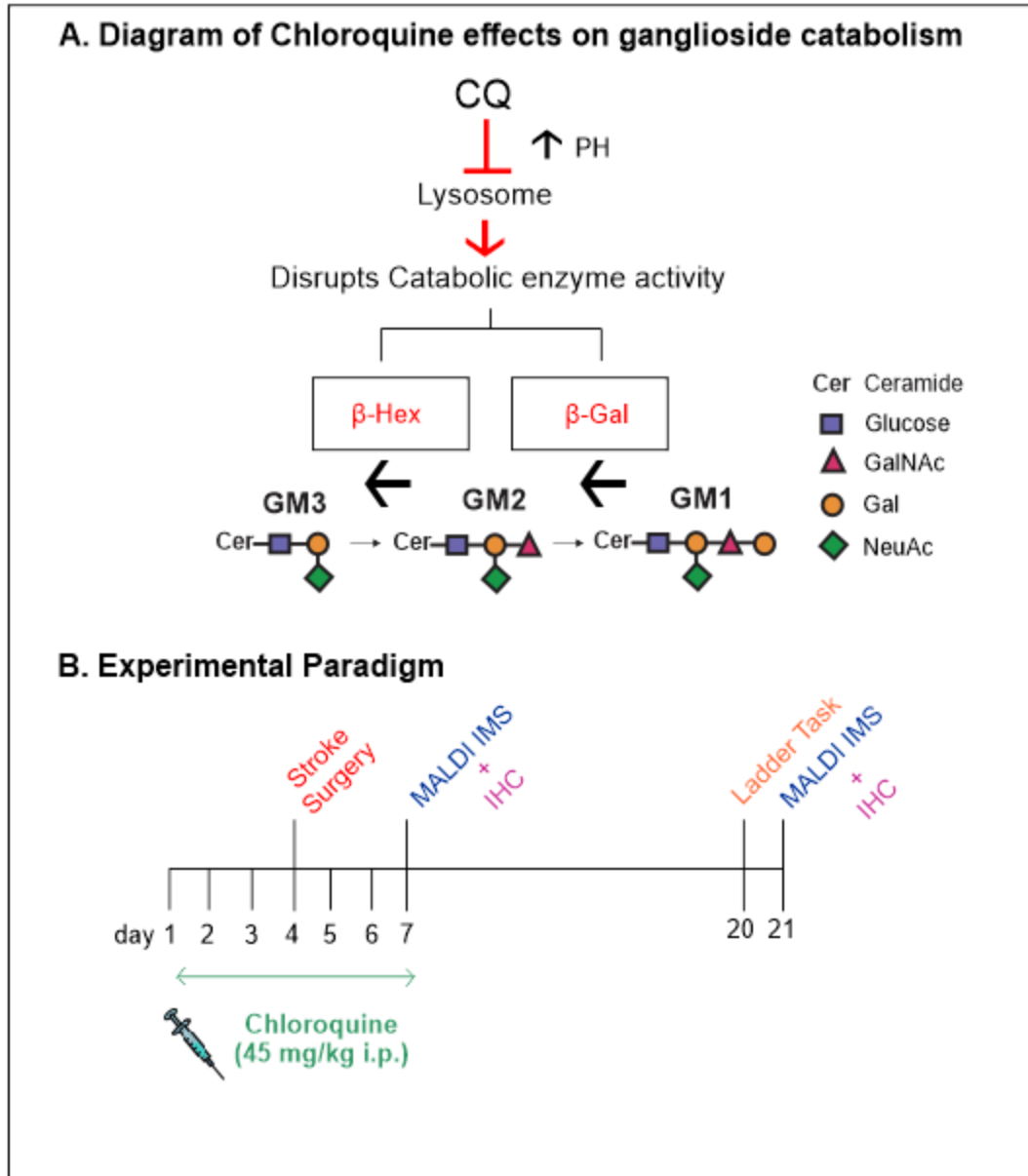


Figure 5.1: Chloroquine and ganglioside catabolism. (A) Schematic diagram of the Chloroquine-mediated disruption of gangliosides catabolism. Chloroquine accumulates in acidic compartments such as lysosomes which raises the pH above its acidic optimum and disrupts the activity of ganglioside catabolic enzymes β -galactosidase, which cleaves a galactose (Gal) subunit from the GM1 oligosaccharide chain to form GM2, and β -hexosaminidase, which cleaves an N-acetylgalactosamine (GalNAc) sugar subunit to form GM3. With the catabolic enzymes disrupted, CQ can transiently block the degradation of complex gangliosides in response to a stroke. (B) Experimental paradigm. Rats in the treatment group were administered a daily intraperitoneal injection of CQ (45 mg/kg) beginning 3 days prior to stroke surgery and ending 3 days post-stroke. MALDI and IHC took place 3 d post stroke (day 7) and 21 d post-stroke. On day 20 post-stroke, rats underwent behavioural testing.

5.3 Materials and Methods

5.3.1 *Stroke Model*

All animal handling and surgical procedures were in accordance with guidelines of the Canadian Council on Animal Care and approved by the University of Western Ontario Animal Use Subcommittee. Three month-old male Wistar rats weighing 300–400 g (Charles River Laboratories, Quebec, Canada) were housed in pairs under standard conditions (12:12 light/dark cycle) and provided food and water ad libitum. Rats were randomly assigned to experimental groups and were housed individually following surgery. To induce the severe stroke injury, rats received both a bilateral intra-cerebral ventricular injection of the toxic amyloid beta (A β) fragment (25-35) followed by a unilateral striatal injection of ET-1, a potent vasoconstrictor as previously described (Caughlin et al., 2015). This enhanced stroke model has previously been shown to exacerbate the pathological response (inflammation, neurodegeneration and infarct size) (Whitehead et al., 2007, 2005) and more severely perturb ganglioside homeostasis than either injury alone (Caughlin et al., 2015), providing the ideal platform to test a therapeutic agent aimed at restoring ganglioside homeostasis. Control surgery rats underwent identical surgical procedures with injections being replaced with saline. A total of 80 rats were used for the current study with 5 rats per group used for MALDI IMS analysis at 3 and 21 d, 6 rats per group for IHC, and 8 rats per group used for behavioural analysis.

5.3.2 *Chloroquine Administration*

Chloroquine (CQ, Sigma-Aldrich, St. Louis, USA) was prepared daily at a concentration of 45 mg/mL in 0.9 % saline. Animals were weighed immediately prior to injection and were administered 45 mg/kg of CQ by intraperitoneal (i.p.) injection for seven consecutive days beginning 3 days prior surgery and ending 3 days after surgery (**Fig 5.1 B**).

5.3.3 *Immunohistochemistry and Fluoro Jade B*

Immunohistochemistry, standard histochemistry, and Fluoro Jade B staining were performed as previously described (Caughlin et al., 2015).

5.3.4 *Primary cortical neuron cultures*

Primary cortical neurons were extracted from Wistar rat embryos and plated on coverslips in 24-well plates as previously described (Park et al., 2016). Half of the media was exchanged with fresh neurobasal media (NBM) every 2 days until 14 days *in vitro* (DIV). Each coverslip represented a single biological replicate with 8 biological replicates in each experimental group. Experiments were repeated on 3 separate cultures. On DIV 13, each well in the 24-well plates were assigned as either control cells, CQ control cells (0.1 μM of chloroquine dissolved in NBM), 1 μM of GM3, 100 μM of GM3, 1 μM GM3 with CQ, or 100 μM GM3 with CQ. Cells were then fixed with 4 % paraformaldehyde for 15 min then washed 3x with 10 mM PBS either 1, 6, 24, or 48 h after administration of CQ and/or GM3. Propidium Iodide (PI) was administered (1 mg/mL) 45 min before cell fixation in order to assess cell viability via fluoresce microscopy. Cells were also fluorescently stained with TUNEL using a cell death apoptosis kit (Sigma, St. Louis, MO, U.S.A.) after fixation to assess apoptotic cell death and mounted onto microscope glass slides with Fluoroshield (Sigma, Toronto, Canada) containing DAPI (Sigma, Toronto, Canada).

5.3.5 *Fluorescence Microscopy*

Neurons were imaged with DAPI (blue), TUNEL (green), and PI (red) and quantified using a Nikon Eclipse Ni (Nikon Instruments Inc., Melville, NY, U.S.A.) microscope and Nikon Analysis software. Microscope settings for each fluorescent filter were kept consistent for all analysis. Nikon analysis software allows for cell counting based on staining intensity and cell shape. This feature was used to perform all quantification of DAPI, TUNEL, and PI positive cell staining. Positive TUNEL and PI staining was presented as a ratio to total DAPI positive cells.

5.3.6 *MALDI IMS*

Rats from each experimental group (n = 5) were sacrificed at either 3 or 21 d post-surgery for MALDI IMS analysis. Rat brains were removed via fresh frozen extraction and prepared for MALDI IMS following the protocol published in Caughlin et al., 2017 (Caughlin et al., 2017). Briefly, frozen rat brains were sectioned coronally at a thickness of 10 μm . Sections were obtained from the site of stroke injury (bregma +1.92 mm) then

mounted onto indium-tin-oxide (ITO) slides. 1,5-Diaminonaphthalene (DAN) matrix was then applied via sublimation followed by overnight incubation at - 20° C. Images were acquired in negative mode with a 70 uM laser step size. Data was exported to Tissue View (Sciex, Toronto, Canada) to visualize ganglioside distribution. Representative MALDI Images were exported from Tissue View to be pseudo-coloured and overlaid in Image J (Wayne Rasband, National Institutes of Health, Bethesda, MD, U.S.A.). MALDI data was acquired in Tissue View by isolating a region of interest (ROI) of equal size at the site of stroke within the striatum and in the corresponding contralateral uninjured striatum (comparable ROIs were used in control animals when no stroke was present). The numerical data from each A-series ganglioside species was then imported into Prism statistical software to determine the area under the curve (AUC) corresponding to the 3 largest isotopic peaks of each species. This AUC measurement was then divided by the total signal as a means of normalizing the data for between scan comparisons. The AUC of the individual species relative to total signal was then compared between the ipsilateral hemisphere and contralateral hemisphere to the stroke.

5.3.7 *Ladder task – Motor assessment.*

The ladder test was used to assess motor function and determine if CQ treatment could rescue any motor impairments induced by the stroke. The ladder task consists of two long pieces of plexi-glass 20 cm apart with metal pegs placed at irregular intervals along the bottom. The ladder is raised 30 cm above the ground and connects an empty cage to the rat's home cage. The rat is placed at one end of the ladder (with the empty cage) and must cross the ladder to reach its home cage on the opposite side. The home cage and empty cage are switched sides after 3 successful runs of the ladder in one direction. A total of 6 runs (3 from each direction) were used to calculate the average number of correct paw placements, errors in paw placement, and peg misses with each limb. Metz et al., described correct paw placement and total misses along with 5 different types of errors in paw placement that can occur in the ladder test (Metz & Whishaw, 2002). For the purpose of the current study, the four variations of errors described by Metz et al., were grouped together and simply referred to as "errors".

5.3.8 *Novel Object Recognition – Short Term Memory Task*

The novel object recognition task (NOR) can be used to assess both short and long term memory depending of the experimental paradigm (Antunes et al., 2012). In the current study, rats were first habituated to an empty box for 10 min at which time they were returned to their home cage for a delay period of 45 min before being placed back into the box. The box contained two identical objects, either two robot toys or two dinosaur toys. A video camera was placed above the box to record the movements of the rats while they familiarized themselves with the objects for 4 min. The rats were then removed from the box and placed back in their home cage for a 1 hr delay period. After the 1 hr delay, rats were placed back in the box for a third time but with one of the objects having been replaced with a novel objects (one robot, one dinosaur). The rats were then allowed to explore both objects again for 4 min before being placed back in their home cage. The objects were rotated for each trial and carefully wiped down with 70% ethanol and allowed to dry between each session, along with the inside of the box to avoid familiarity based on scent. The location of the novel object was also rotated to be either on the right of the left side of the box for each trial. Sham surgery control rats showed no preference for either the robot or dinosaur objects, despite the variability in colour and shape, and were thus judged to be suitable objects for this task. The video recording and a stopwatch were used to add up the total amount of time rats spent interacting with each object during the familiarization and novel object trials. "Interaction" was defined as sniffing, touching, standing, or rearing on the objects. There was no statistical difference between the amount of time rats spent with the two identical objects during the familiarization trial (data not shown). Data is represented for the NOR trial as the percent of time rats spent with either the familiar or novel objects out of the total amount of time spent exploring both objects. A two-way ANOVA and tukey multiple comparisons test was performed to establish statistical differences between groups ($p < 0.05$).

5.3.9 *Data Analysis*

Data are represented as mean +/- the standard error of the mean. Statistical analysis was performed using a two-way ANOVA with a Tukey's post-hoc test. N values are described in each figure legend.

5.4 Results

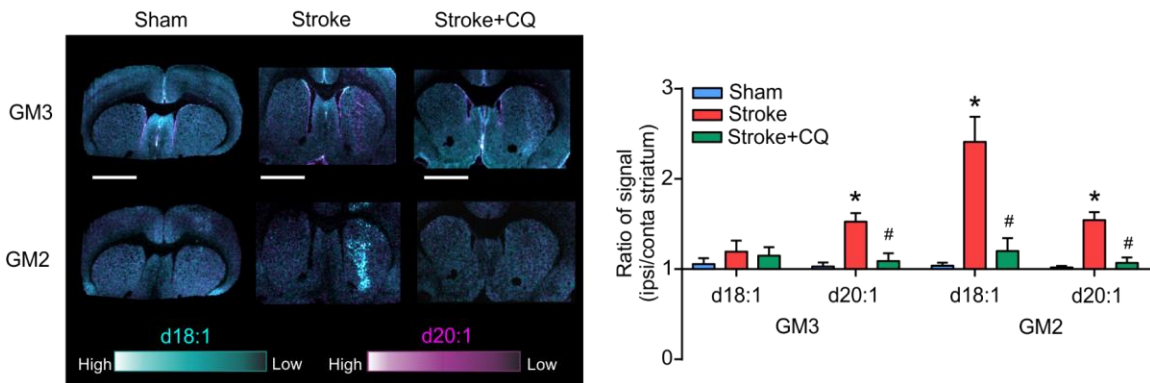
5.4.1 *Pathological shift in ganglioside homeostasis prevented with CQ treatment at 3 d*

Ganglioside homeostasis has been shown to be severely perturbed in the early stages of recovery after a stroke such that an accumulation of simple ganglioside species and a depletion of complex species is observed at the site of injury and is correlated to the severity of the neurodegenerative insult (Caughlin et al., 2015). This finding would suggest that complex gangliosides, which are protective to cells, may be undergoing degradation in response to the injury, leading to the accumulation of toxic simple species, further perpetuating neurodegenerative damage. Using MALDI IMS, we examined the ability of CQ (45 mg/kg i.p.) to prevent the dysregulation of ganglioside homeostasis after a severe stroke injury. Sham surgery rats were used as controls and displayed no significant differences in ganglioside abundance between the ipsilateral and contralateral sides of the brain in response to the surgical procedures (**Fig 5.2 A+B**). Confirming previous findings from our lab, the stroke-injured rats showed a significant increase in simple gangliosides 3 day after injury. The d18:1 and d20:1 species of GM2 showed the most significant increase in abundance in response to the injury, while only the d20:1 species of GM3 was significantly increased at the site of injury (**Fig 5.2 A**). CQ treatment resulted in a significant reduction in the abundance of simple ganglioside species at the site of injury compared to the untreated stroke group, showing no significant differences from sham-surgery controls (**Fig 5.2 A**). Therefore, CQ treatment successfully prevented the accumulation of simple ganglioside species 3 days after a severe stroke insult.

In addition to examining the ability of CQ to prevent the accumulation of simple gangliosides, we examined the abundance of protective complex gangliosides GM1 and GD1 to determine if CQ treatment can prevent their depletion at the site of the stroke. Ganglioside GD1 attaches to salt adducts $[K^+]$ and $[Na^+]$ when analyzed via MALDI IMS. These two adducts of GD1 have previous been observed to have unique responses following stroke (Caughlin et al., 2015), therefore we included both adducts in all of the following analyses. As predicted, both the d18:1 and d20:1 species of ganglioside GM1 were significantly lower at the site of injury compared to controls 3 days post-surgery (**Fig**

5.2 B). Similar to what was previously reported for the $[K^+]$ and $[Na^+]$ adducts of GD1, they indeed showed unique responses following stroke such that the $[K^+]$ adduct of GD1 was significantly depleted at the site of injury, while the $[Na^+]$ adduct remained unchanged. Treatment with CQ prevented the depletion of both the d18:1 and d20:1 species of ganglioside GM1 and the $[K^+]$ adduct of GD1 while significantly increasing the abundance of d18:1 GD1 $[Na^+]$ at the site of injury compared to untreated injured rats. Overall, these results suggest that CQ treatment is effective at restoring ganglioside homeostasis 3 days after a severe stroke injury.

A. MALDI IMS of simple gangliosides 3 d post-stroke



B. MALDI IMS of complex gangliosides 3 d post-stroke

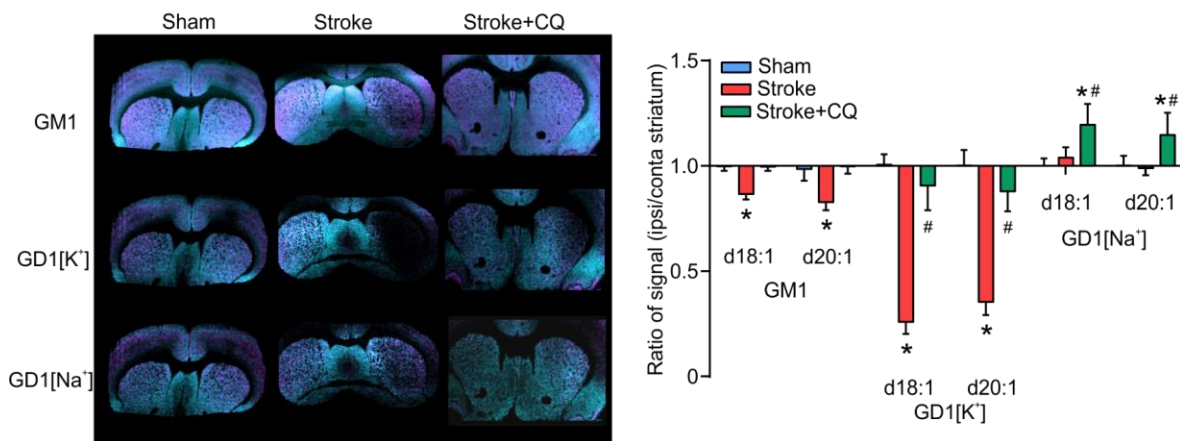


Figure 5.2: Ganglioside homeostasis restored at 3 d in comorbid injured rats treated with CQ. (A) MALDI IMS overlaid images (left) and data (right) showing the AUC ratio of simple gangliosides GM3 and GM2 in the ipsilateral versus contralateral hemisphere to the site of injury in sham surgery, stroke, and CQ treated stroke rats 3 d after surgery. Gangliosides GM3 d20:1, GM2 d18:1, and GM2 d20:1 were all significantly elevated in response to the stroke injury which was prevented with CQ treatment. (B) MALDI IMS overlaid images (left) and quantified data (right) showing the ratio of abundance of complex gangliosides GM1, GD1[K⁺], and GD1[Na⁺] in the ipsilateral versus contralateral hemisphere to the site of injury at 3 d. Both GM1 and GD1[K⁺] were significantly depleted in response to the stroke insult whereas GD1[Na⁺] remained unchanged. CQ treatment prevented the depletion of GM1 and GD1[K⁺] while increasing the abundance of GD1[Na⁺] at the site of injury. Data presented as the ratio between the ipsilateral and contralateral hemispheres to the stroke injury \pm SEM, $n = 5$ per group. Scale bar is equal to 4 mm. * Indicates significant difference from control group, # indicates significant difference between stroke and CQ-treated groups, $p < 0.05$ via two-way ANOVA, Tukey post-hoc test.

5.4.2 *Ganglioside homeostasis partially restored by CQ 21 d after comorbid stroke injury*

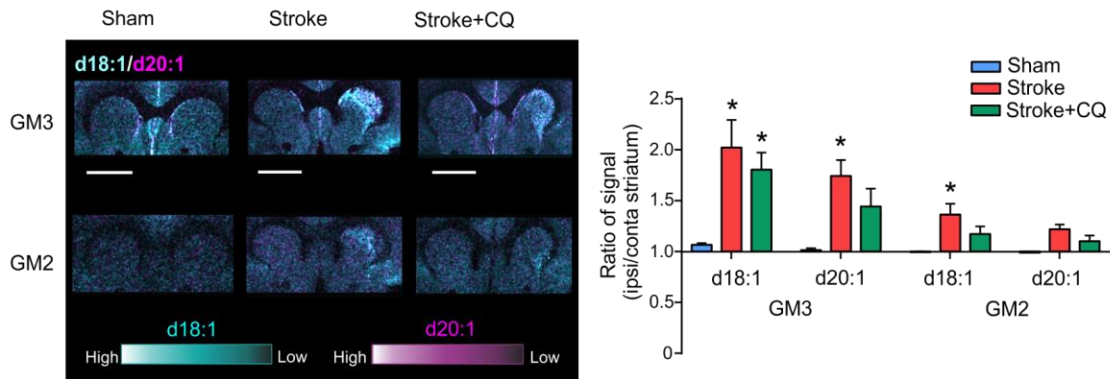
Previous work from our lab has demonstrated that the comorbid stroke injury used in the current study results in increased inflammation, larger stroke size, and poorer cognitive outcomes at the later stages of recovery than when just stroke or A β toxicity are present alone (Whitehead et al., 2007, 2005). This increased neurodegenerative response at later time points was also associated with an increased abundance of simple ganglioside species within the site of injury (Caughlin et al., 2015), further supporting the proposed role of simple ganglioside accumulation in the perpetuation of neurodegeneration after stroke. We examined the distribution of A-series gangliosides 21 days after stroke, as previously described, in order to examine the effect of CQ treatment on ganglioside homeostasis during the later stages of recovery.

Simple ganglioside GM3 showed a significant increase in abundance for both the d18:1 and d20:1 species 21 days following stroke (**Fig 5.3 A**). While GM2 levels decreased from their initial upregulation in the early stages of recovery, d18:1 species of GM2 remained significantly higher than controls even at 21 d (**Fig 5.3 A**). This response to the stroke is consistent with what has been previously reported by our group (Caughlin et al., 2015). CQ treatment was not able to significantly reduce the increased abundance of either GM3 or GM2 at the site of injury 21 d post-stroke, although d20:1 species of GM3 and both GM2 species were not significantly different from controls either. This suggests that the accumulation of certain simple ganglioside species were, at least, partially reduced during the later stages of recovery with CQ treatment.

Complex gangliosides, on the other hand, were still subject to the protective action of CQ 21 d post-stroke. Injured rats continued to show a significant depletion of complex gangliosides GM1 and GD1 at the site of injury, indicating that these species may have continued to undergo degradation 21 d after the stroke. CQ treatment prevented this significant drop in GM1 and significantly increased the abundance of GD1 species at the site of injury, although GD1 [K⁺] levels in the CQ treated injured rats were still significantly lower than controls (**Fig 5.3 B**). While the degree of protection conferred by CQ in the maintenance of ganglioside homeostasis following stroke was reduced at the

later stages of recovery, CQ effectively reduced the degree of ganglioside perturbation, particularly for complex ganglioside species.

A. MALDI IMS of simple gangliosides 21 d post-stroke



B. MALDI IMS of complex gangliosides 21 d post-stroke

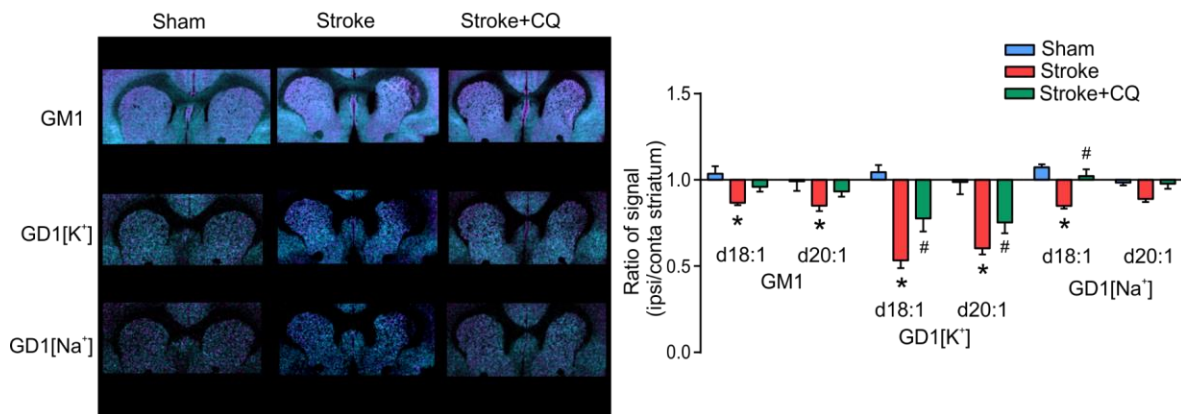


Figure 5.3: Partial restoration of complex ganglioside homeostasis observed at 21 d via MALDI IMS. (A) MALDI IMS overlaid images (left) and data (right) showing the AUC ratio of simple gangliosides GM3 and GM2 in the ipsilateral versus contralateral hemisphere to the site of injury in sham surgery, stroke, and CQ treated stroke rats 21 d after surgery. GM3 d18:1, GM3 d20:1, and GM2 d18:1 were all significantly elevated over controls at the site of injury at 21 d after surgery. This increase in simple gangliosides was not significantly reduced through CQ treatment, however, GM3 d20:1 and GM2 d18:1 were not significantly elevated over controls either. (B) MALDI IMS overlaid images (left) and quantified data (right) showing the ratio of abundance of complex gangliosides GM1, GD1[K⁺], and GD1[Na⁺] in the ipsilateral versus contralateral hemisphere to the site of injury at 21 d post-surgery. All complex gangliosides examined, with the exception of GD1[Na⁺] d20:1 were significantly reduced at the site of injury 21 d after surgery. GM1 and GD1[Na⁺] levels were not significantly different from controls in CQ treated rats and GD1[K⁺] abundance was significantly increased compared to untreated injured rats. Data presented as the ratio between the ipsilateral and contralateral hemispheres to the stroke injury \pm SEM, $n = 5$ per group. Scale bar is equal to 4 mm. * Indicates significant difference from controls, # indicates significant difference between stroke and CQ-treated groups, $p < 0.05$ via two-way ANOVA, Tukey post-hoc test.

5.4.3 *Exogenous GM3 results in toxicity in primary cortical neurons which is protected by CQ treatment*

Toxicity associated with the accumulation of GM3 has been established in a number of neural (Nakatsuji & Miller, 2001; Sohn et al., 2006) and non-neural cell lines (Choi et al., 2006; Chung et al., 2009; Seyfried & Mukherjee, 2010) but has yet to be demonstrated in a rat primary neuron cell line. Given our previously published and current findings that GM3 is increased post stroke, and that CQ can acutely reduce this increase in GM3, we sought to determine if GM3 could directly cause neurodegeneration. GM3 was administered to primary cortical neurons cultured from embryonic Wistar rats after 14 days in vitro (d.i.v.) at either a low dose (1 μ M) or a high dose (100 μ M) and cell viability was assessed through TUNEL and Propidium Iodide (PI) staining 1, 6, 24, and 48 hrs after administration.

The exogenous administration of gangliosides has been shown to lead to their incorporation into the plasma membrane of mammalian cells (Choi et al., 2006; Riboni et al., 1991; Nakatsuji & Miller, 2001). A separate experimental group was co-administered a low dose of CQ (1 μ M) along with either the low or high dose of GM3 in order to determine if CQ can prevent changes in cell viability induced by the exogenous administration of GM3. CQ administration alone did not significantly alter TUNEL or PI positive staining from control levels (data not shown). A low dose of GM3 (1 μ M) was found to significantly increase TUNEL and PI positive staining 48 hrs after administration compared to controls (**Fig 5.4 A**). While CQ treatment prevented the increase in PI positive staining at this time point, it did not significantly reduced TUNEL positive staining. In the high dose (100 μ M) GM3 groups, an increase in TUNEL and PI positive staining was observed at 24 and 48 hrs after administration relative to controls which was significantly reduced through treatment with CQ (**Fig 5.4 B**). Overall, our results show that exogenous administration of both low and high doses of GM3 resulted in a significant increase in apoptosis and a decrease in cell viability which can be prevented by co-administration with CQ.

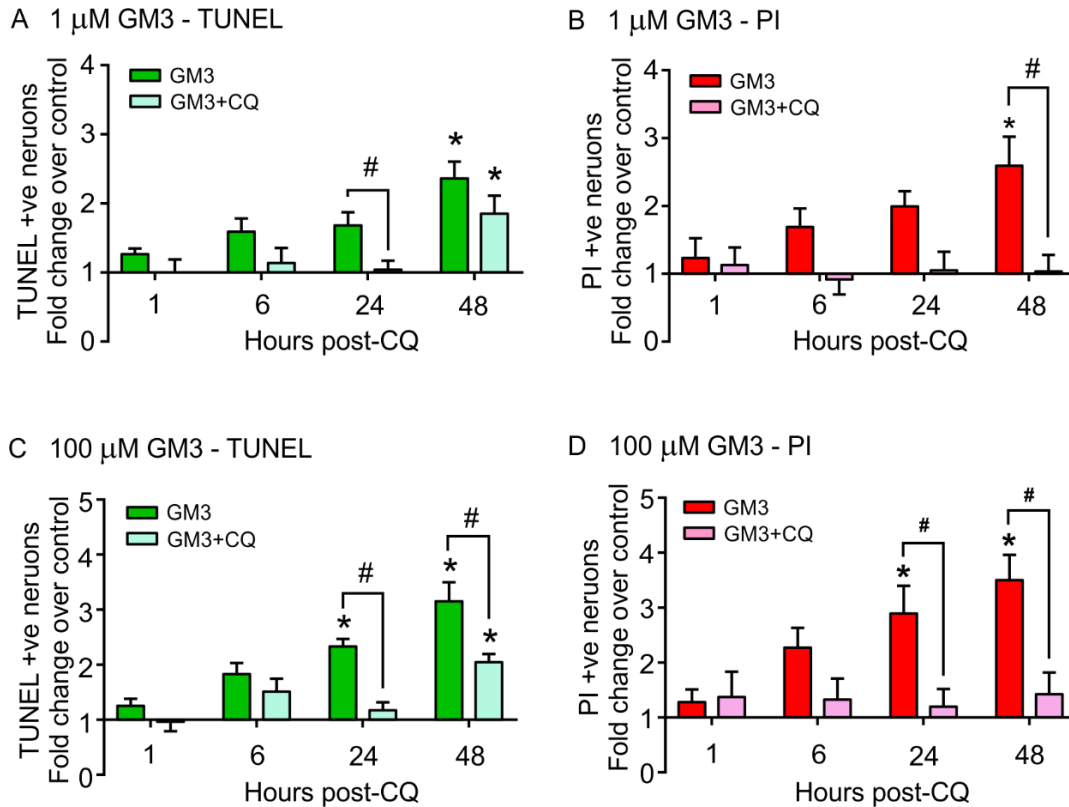


Figure 5.4: CQ increases cell viability and decreases apoptosis in response to toxic low and high dose GM3 administration. (A) Quantification of TUNEL and PI positive staining relative to control primary cortical neurons administered a low dose (1 μ M) GM3 or co-administered CQ (1 μ M) with low dose GM3. Low dose GM3 significantly increase TUNEL and PI positive staining relative to controls at 48 hrs after GM3 administration. PI positive staining, but not TUNEL positive staining was significantly reduced by co-administration of low dose GM3 with CQ. (B) Quantification of TUNEL and PI positive staining relative to control primary cortical neurons administered a high dose (100 μ M) GM3 or co-administered CQ (1 μ M) with high dose GM3. High dose GM3 resulted in a significant increase in both TUNEL and PI positive staining at 24 and 48 hrs. CQ treatment significantly reduced TUNEL and PI positive staining at 24 and 48 hrs compared to high dose GM3 alone. However, a significant increase in TUNEL positive staining was observed at 48 hrs in the CQ treated cells. Data presented as a fold change relative to control cells \pm SEM, $n = 6$ per group * $p < 0.05$ via two-way ANOVA, Tukey post-hoc test.

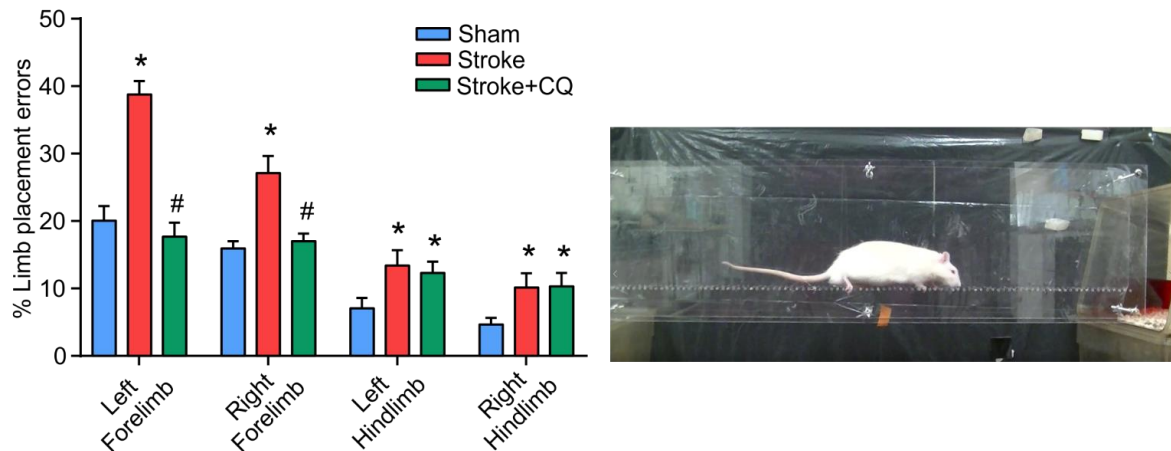
5.4.4 *Stroke-induced motor and cognitive impairments prevented by CQ treatment.*

Impairments in motor function and gait are a common complication of sub-cortical stroke in the rat, generally affecting both fore- and hind-limbs on the contralateral side of the body to a greater extent than the ipsilateral side. In order to assess motor function in our rats, we used the ladder task which examines the rat's ability to cross a horizontal ladder with unevenly spaced metal pegs. This task requires the rat to correctly place their paws on each rung of the ladder in order to reach the other side. We assessed the total number of limb placement errors (described by Metz et al., 2002) in both the fore-limbs and hind-limbs of the rat in each of the experimental groups to determine if CQ treatment can protect against stroke-induced impairments of motor function. As expected, stroke-injured rats displayed significantly more errors in limb placement during the ladder task than the sham surgery control group for all four limbs (**Fig 5.5 A**). Interestingly, the fore-limbs of the injured rats showed a higher number of limb placement errors than the hind-limbs. As expected, the contralateral fore-limb, displayed the highest number of limb placement errors. CQ-treated rats showed a significant reduction in fore-limb placement errors compared to the untreated stroke group, with no significant differences in performance from the control group (**Fig 5.5 A**). However, this protective effect of CQ treatment was not observed in the hind-limbs of the CQ treated rats, which showed a significant increase in limb placement errors compared to controls, similar to the stroke group. Overall, CQ treatment was effective at preventing fore-limb, but not hind-limb motor impairments after stroke injury.

CQ has previously been shown to prevent stroke-induced deficits of short-term memory in Sprague-Dawley rats using an electroshock Y-maze task (Cui et al., 2013). We therefore assessed the short-term memory of sham surgery, stroke-injured, and CQ-treated stroke rats 20 days after surgery using a Novel Object Recognition task (NOR). In this task, rats are first introduced to two identical objects and are given 4 minutes to explore and interact with the objects. After 1 hr, rats are returned to the box with one of the objects having been replaced with a novel object and are allowed to again explore and interact with the objects for an additional 4 min. As expected, Sham-surgery rats spent significantly more time interacting with the novel object than the familiar object (**Fig 5.5 B**). This occurs due to the rat's preference for interacting with novel objects. Stroke-injured rats, on the

other hand, spent the same amount of time exploring both the novel and familiar objects (**Fig 5.5 B**). The lack of preference for the novel object is indicative of an impairment in short-term memory in the stroke injured rats (Antunes & Biala, 2012). Interestingly, CQ-treated stroke injured rats spent significantly more time with the novel object than the familiar object. Although the degree of preference for the novel object was not identical to that of the sham-surgery control group, these results suggest that short-term memory deficits induced by the stroke injury can be prevented with CQ treatment.

A. Ladder Test - Motor assessment



B. Novel Object Recognition Task - Short term memory assessment

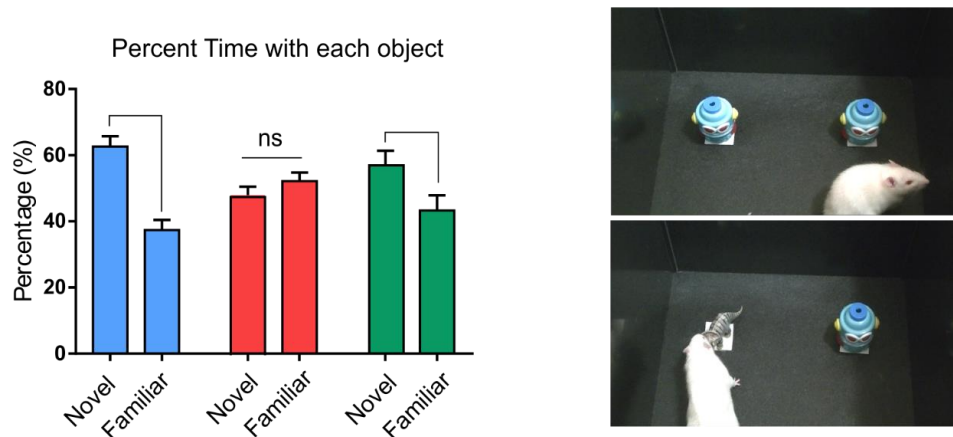


Figure 5.5: Reduced forelimb Motor and cognitive impairments in stroke injured rats treated with CQ. (A) Quantification of limb placement errors on the Ladder motor assessment task (top) with representative image of ladder task (right). Stroke injured rats showed a significant increase in limb placement errors compared to controls in all four limbs. The number of limb placement errors was significantly reduced in the forelimbs of rats treated with CQ. CQ treatment did not significantly reduced the number of limb placement errors in the hind-limbs of stroke injured rats. (B) Quantification of time spent with novel and familiar objects on Novel Object Recognition task (NOR – bottom) with representative image of NOR task. Sham surgery control rats spent significantly more time with the novel object than familiar object while stroke injured rats spent the same amount of time with both objects, indicating a deficit of short-term memory, CQ treated rats, like control rats, spent significantly more time with the novel object than the familiar object, suggesting that memory deficits were prevented by CQ treatment. * Indicates sig difference from control group, # indicates sig difference between stroke and CQ-treated group, $p < 0.05$ via two-way ANOVA, Tukey post-hoc test.

5.4.5 *Reduced brain pathology at 21 d in CQ-treated stroke injured rats*

The stroke model used in the current study has previously been shown to produce an increase in infarct size as well as an exacerbated inflammatory response (Whitehead et al., 2007, 2005). We used immunohistochemistry to examine cell survival, neurodegeneration, and inflammation at the site of injury within each experimental group at 3 and 21 d post-stroke in order to assess the effects of CQ treatment on pathology at the site of injury. NeuN, a neuronal nuclear antigen, was used to assess cell survival. Stroke injured rats treated with CQ had significantly more NeuN positive staining at the site of injury compared to untreated stroke injured rats at both 3 and 21 d post-stroke (**Fig 5.6 A**). Fluoro Jade B was used as a marker of neurodegeneration and was significantly reduced in CQ treated rats at 21 d compared untreated stroke injured rats (**Fig 5.6 B**). Inflammation was assessed using the microglia marker OX-6. Stroke injury led to a significant increase in OX-6 positive staining at the site of injury at 21 d (**Fig 5.6 C**). CQ treatment in stroke injured rats prevented the significant increase in OX-6 positive staining observed in untreated stroke rats at 21 d post-stroke, indicating that inflammation was significantly reduced in CQ-treated rats. Overall, the results demonstrate a neuroprotective effect (increase in NeuN, decrease in FJB) with a concomitant decrease in neuroinflammation post-stroke with CQ administration.

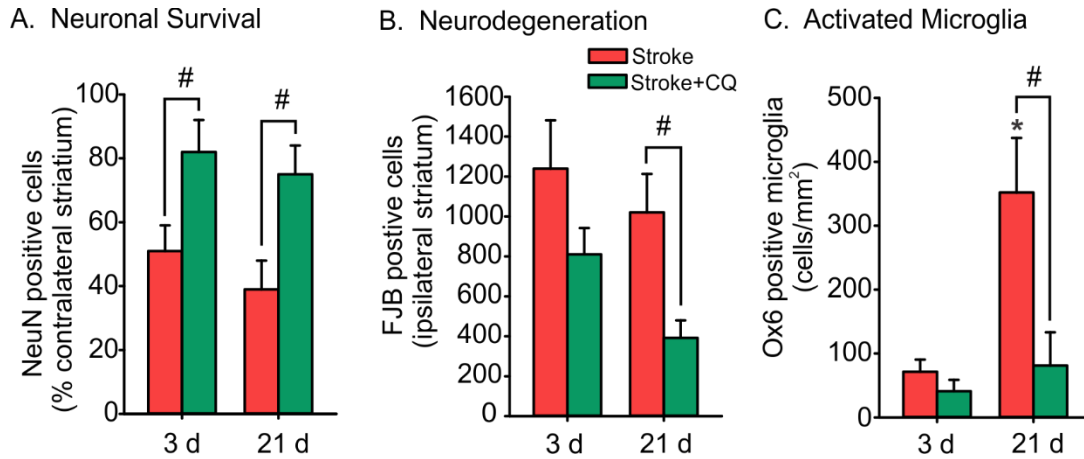


Figure 5.6: CQ treatment reduces brain pathology after stroke. IHC Quantification of NeuN (A), Fluoro jade B (B), and OX-6 (C) staining at the site of injury at 3 and 21 d post stroke. CQ treatment significantly increased positive NeuN staining at the site of injury at both 3 and 21 days post stroke compared to the untreated stroke group (A). FJB staining was significantly reduced at the site of stroke injury at 21 d in CQ treated rats (B). CQ treatment prevented the significant increase in OX-6 staining observed in the stroke group at 21 d (C). * Indicates sig difference from stroke 3 d group, # indicates sig difference between stroke and CQ-treated groups, $p < 0.05$ via two-way ANOVA, tukey multiple comparisons.

5.5 Discussion

In the current study, we used MALDI IMS, IHC, primary cortical neurons, and a behavioural task to examine the effect of CQ treatment on neurodegeneration. The combination of these techniques allows for the most in-depth examination of ganglioside dysregulation after stroke to date and provides novel insight into the benefits of pharmacological interventions targeting ganglioside metabolism for neurodegeneration.

CQ treatment successfully prevented ganglioside dysregulation of both complex and simple species 3 d post-stroke. These findings support our hypothesis that CQ can be used to prevent the degradation of complex gangliosides and accumulation of simple gangliosides acutely after stroke. Ganglioside dysregulation was partially prevented 21 d post-stroke by CQ treatment and was more effective at preventing complex ganglioside degradation than simple ganglioside accumulation. Several additional species of GM3 with a varied number of carbons in their ceramide moieties were also detected and showed a similar pattern in response to stroke injury and CQ treatment as the d18:1 and d20:1 species at both time points (**appendix v**). Treatment at this time point was also associated with a significant decrease in inflammation, neurodegeneration, and cell death at the site of injury, and significantly reduced motor impairments in the forelimbs of stroke-injured rats. It is possible that preventing ganglioside dysregulation in the early stages of recovery was sufficient to confer long-term protection during recovery from stroke. Indeed, in the case of ischemic reperfusion injuries, neuroprotection strategies in the acute stage are crucial in mediating damage to penumbral regions and ultimately the severity of long term impairments (Chamorro et al., 2016; Ginsberg, 2016). Alternatively, it is possible that the pre-treatment phase of the CQ paradigm was able to confer protection to neurons prior to the stroke, leading to increased membrane lipid integrity and a less severe acute injury response. In this way, the results of the current study point to a potential preventative intervention that may be neuroprotective to individuals at high risk of developing stroke injuries or recurring strokes. The timing of CQ administration may also be an important factor when considering its therapeutic window (Maes et al., 2014), thus it is possible that altering the timing of the treatments would provide a more effective long term therapeutic response.

Additionally, we showed, for the first time, that the exogenous administration of GM3 to primary cortical neurons at both a low and high doses was toxic to primary cortical neurons, supporting the hypothesis that the accumulation of this simple ganglioside at the site of injury after a stroke may be playing a mechanistic role in the propagation of neurodegeneration. CQ administration effectively reduced apoptosis and increased cell viability in primary cortical neurons exposed to exogenous GM3. Although the mechanisms in which CQ was able to protect primary cortical neurons from GM3 toxicity remain unclear, it is possible that CQ was able to block GM3 from binding and/or incorporating into cells to effect cell signaling and alter membrane composition. Further investigation into the interaction of CQ with GM3 in neural cells are needed to address this question. Regardless, this finding points to the possibility that CQ may not only be preventing the breakdown of complex gangliosides in response to the stroke through its lysosomotropic properties, but may also confer protection against external sources of GM3 present in the extracellular environment during the ischemic cascade.

Rubovitch et al., suggest that the restoration of GM1 shortly after the injury may be preventing the cascade of events that lead to neurodegeneration after stroke (Rubovitch et al., 2017). Mechanisms such as excitatory amino acids (EAs), nitric oxide, inflammatory mediators, reactive oxygen species, immune modulation, withdrawal of trophic factors, and apoptosis are all thought to be involved in the development of the ischemic cascade (Zhang et al., 2015). Interestingly, GM1, like CQ, has been found to inhibit autophagy after a stroke injury (Li et al., 2016) and can upregulate brain-derived neurotrophic factor (Lim et al., 2011), promoting cell survival. GM1 has also been associated with the attenuation of secondary neuronal damage when administered in the acute stages of stroke by blocking of EAs-related neurotoxicity (Lipartiti et al., 1990). One of the protective effects of CQ administration observed in the current study was the restoration of depleted GM1 at the site of injury. It is, therefore, possible that the decreased pathological response and motor impairments observed in the treated rats at the later time point were associated with both the attenuation of simple ganglioside accumulation in the acute stages of recovery along with the maintenance of GM1 levels throughout.

Overall, chloroquine treatment can be used to restore ganglioside homeostasis after a severe ischemic stroke injury and is associated with long-term pathological and functional improvements in rats. Interventions targeting membrane lipid dysregulation may be a crucial component of effective multifactorial approaches to stroke prevention and treatment and are worthy of further investigation.

5.6 References

- Antunes, M., & Biala, G. (2012). The novel object recognition memory: neurobiology, test procedure, and its modifications. *Cogn Process, 13*, 93-110.
- Argentino, C., Sacchetti, M., Toni, D., Savoini, G., D'Arcangelo, E., Erminio, F., Fieschi, C. (1989). GM1 Ganglioside Therapy in Acute Ischemic Stroke. *Stroke, 20*(9), 1143–1149.
- Candelise, L. (2002). Gangliosides for Acute Ischemic Stroke. *Stroke, 33*(9), 2336–2336.
- Carolei, A., Fieschi, C., & Bruno, R. (1991). Monosialoganglioside GM1 in cerebral ischemia. *Cerebrovascular and Brain Metabolism Reviews, 3*(2), 134–157.
- Caughlin, S., Hepburn, J. D., Park, D. H., Jurcic, K., Yeung, K. K. C., Cechetto, D. F., & Whitehead, S. N. (2015). Increased expression of simple ganglioside species GM2 and GM3 detected by MALDI Imaging Mass Spectrometry in a combined rat model of A β toxicity and stroke. *PLoS ONE, 10*(6), 1–17.
- Caughlin, S., Park, D. H., Yeung, K. K.-C., Cechetto, D. F., & Whitehead, S. N. (2017). Sublimation of DAN Matrix for the Detection and Visualization of Gangliosides in Rat Brain Tissue for MALDI Imaging Mass Spectrometry. *Journal of Visualized Experiments*, (121).
- Chamorro, Á., Dirnagl, U., Urra, X., & Planas, A. M. (2016). Neuroprotection in acute stroke : targeting excitotoxicity , oxidative and nitrosative stress , and inflammation. *Lancet Neurol, 15*, 869–81.
- Choi, H., Chung, T., Kang, S., Lee, Y., Ko, J., Kim, J., & Kim, C. (2006). Ganglioside GM3 modulates tumor suppressor PTEN-mediated cell cycle progression — transcriptional induction of p21 WAF1 and p27 kip1 by inhibition of PI-3K / AKT pathway. *Glycobiology, 16*(7), 573–583.
- Chung, T. W., Kim, S. J., Choi, H. J., Kim, K. J., Kim, M. J., Kim, S. H., ... Kim, C. H. (2009). Ganglioside GM3 inhibits VEGF/VEGFR-2-mediated angiogenesis: Direct interaction of GM3 with VEGFR-2. *Glycobiology, 19*(3), 229–239.
- Cui, G., Ye, X., Zuo, T., Zhao, H., Zhao, Q., Chen, W., & Hua, F. (2013). Chloroquine pretreatment inhibits toll-like receptor 3 signaling after stroke. *Neuroscience Letters*,

548, 101–104.

- Feigin, V. L., Forouzanfar, M. H., Krishnamurthi, R., Mensah, G. A., Bennett, D. A., Moran, A. E., ... Ezzati, M. (2014). from the Global Burden of Disease Study 2010. *Lancet*, 383(9913), 245–254.
- Ginsberg, M. D. (2016). Progress in Neurobiology Expanding the concept of neuroprotection for acute ischemic stroke : The pivotal roles of reperfusion and the collateral circulation. *Progress in Neurobiology*, 145–146, 46–77.
- Hirata, Y., Yamamoto, H., Shukry Moursy Atta, M., Mahmoud, S., Oh-hashii, K., & Kiuchi, K. (2011). Chloroquine inhibits glutamate-induced death of a neuronal cell line by reducing reactive oxygen species through sigma-1 receptor. *Journal of Neurochemistry*, 119, 839–847.
- Hoffbrand, B., Bungley, P., Oppenheimer, S., & Sheldon, C. (1988). Short report Trial of ganglioside GM 1 in acute stroke. *Journal of Neurology, Neurosurgery, and Psychiatry*, 51, 1213–1214.
- Karpiak, S., Li, Y., & Mahadik, S. (1987). Gangliosides (GM1 and AGF2) reduce mortality due to ischemia: Protection of membrane function. *Stroke*, 184–187.
- Kharlamov, a, Zivkovic, I., Polo, a, Armstrong, D. M., Costa, E., & Guidotti, A. (1994). LIGA20, a lyso derivative of ganglioside GM1, given orally after cortical thrombosis reduces infarct size and associated cognition deficit. *Proceedings of the National Academy of Sciences of the United States of America*, 91(14), 6303–7.
- Ledeen, R. W., & Wu, G. (2015). The multi-tasked life of GM1 ganglioside, a true factotum of nature. *Trends in Biochemical Sciences*, 40(7), 407–418.
- Lehmeyer, J. E. (1978). Effect of anti-inflammatory drugs and agents that elevate intracellular cyclic AMP on the release of toxic oxygen metabolites by phagocytes: studies in a model of tissue. *Clinical Immunology and Immunopathology*.
- Li, L., Tian, J., Long, M. K., Chen, Y., & Lu, J. (2016). Protection against Experimental Stroke by Ganglioside GM1 Is Associated with the Inhibition of Autophagy. *PLoS One*, 11(1), 1–13.
- Lim, S. T., Esfahani, K., Avdoshina, V., & Mocchetti, I. (2011). Neuropharmacology Exogenous gangliosides increase the release of brain-derived neurotrophic factor. *Neuropharmacology*, 60(7–8), 1160–1167.
- Lipartiti, M., Seren, M. S., Lazzaro, A., Koga, T., Mazzari, S., Facci, L., & Leon, A. (1990). Monosialo ganglioside effects following cerebral ischemia: Relationship with anti-neuronotoxic and pro-neuronotrophic effects. *Acta Neurobiol. Exp.* 2
- Maes, H., Kuchnio, A., Peric, A., Moens, S., Nys, K., Bock, K. De, ... Agostinis, P. (2014). Article Tumor Vessel Normalization by Chloroquine Independent of Autophagy. *Cancer Cell*, 26, 190–206. <https://doi.org/10.1016/j.ccr.2014.06.025>
- Metz, G. A., & Whishaw, I. Q. (2002). Cortical and subcortical lesions impair skilled walking in the ladder rung walking test : a new task to evaluate fore- and hindlimb

- stepping , placing , and co-ordination. *Journal of Neuroscience Methods*, 115, 169–179.
- Nakatsuji, Y., & Miller, R. H. (2001). Selective cell-cycle arrest and induction of apoptosis in proliferating neural cells by ganglioside GM3. *Experimental Neurology*, 168(2), 290–9.
- Ohkuma, S., & Poole, B. (1978). Fluorescence probe measurement of the intralysosomal pH in living cells and the perturbation of pH by various agents. *Proceedings of the National Academy of Sciences of the United States of America*, 75(7), 3327–3331.
- Park, D. H., Wang, L., Pittock, P., Lajoie, G., & Whitehead, S. N. (2016). Increased Expression of GM1 Detected by Electrospray Mass Spectrometry in Rat Primary Embryonic Cortical Neurons Exposed to Glutamate Toxicity. *Analytical Chemistry*, 88, 7844–7852.
- Prokazova, N. V, Samovilova, N. N., Gracheva, E. V, & Golovanova, N. K. (2009). Ganglioside GM3 and its biological functions. *Biochemistry. Biokhimiia*, 74(3), 235–249.
- Rabin, S. J., Bachis, A., & Mochetti, I. (2002). Gangliosides activate Trk receptors by inducing the release of neurotrophins. *Journal of Biological Chemistry*, 277(51), 49466–49472.
- Riboni, L., Caminiti, A., Bassi, R., & Tettamanti, G. (1995). The degradative pathway of gangliosides GM1 and GM2 in Neuro2a cells by sialidase. *Journal of Neurochemistry*, 64(1), 451–454.
- Riboni, L., Prinetti, A., Bassi, R., & Tettamanti, G. (1991). Cerebellar granule cells in culture exhibit a ganglioside-sialidase presumably linked to the plasma membrane. *FEBS*, 287(1,2), 42–46.
- Rubovitch, V., Zilbe, Y., Chapman, J., Schreiber, S., & Pick, C. G. (2017). Restoring GM1 ganglioside expression ameliorates axonal outgrowth inhibition and cognitive impairments induced by blast traumatic brain injury. *Scientific Reports*, (December 2016), 1–12.
- Seyfried, T. N., & Mukherjee, P. (2010). Ganglioside GM3 Is Antiangiogenic in Malignant Brain Cancer. *Journal of Oncology*, 2010.
- Shacka, J. J., Klocke, B. J., & Roth, K. A. (2006). Autophagy, bafilomycin and cell death: the “a-B-cs” of plecomacrolide-induced neuroprotection. *TL - 2. Autophagy*, 2 *VN-readcube.com*(3), 228–230.
- Sohn, H., Kim, Y. S., Kim, H. T., Kim, C. H., Cho, E. W., Kang, H. Y., ... Ko, J. H. (2006). Ganglioside GM3 is involved in neuronal cell death. *The FASEB Journal : Official Publication of the Federation of American Societies for Experimental Biology*, 20(8), 1248–1250.
- Whitehead, S. N., Chan, K. H. N., Gangaraju, S., Slinn, J., Li, J., & Hou, S. T. (2011). Imaging mass spectrometry detection of gangliosides species in the mouse brain following transient focal cerebral ischemia and long-term recovery. *PloS One*, 6(6),

e20808.

- Whitehead, S. N., Cheng, G., Hachinski, V. C., & Cechetto, D. F. (2007). Progressive increase in infarct size, neuroinflammation, and cognitive deficits in the presence of high levels of amyloid. *Stroke; a Journal of Cerebral Circulation*, *38*(12), 3245–50.
- Whitehead, S. N., Hachinski, V. C., & Cechetto, D. F. (2005). Interaction between a rat model of cerebral ischemia and beta-amyloid toxicity: inflammatory responses. *Stroke; a Journal of Cerebral Circulation*, *36*(1), 107–12.
- Woods, A. S., Colsch, B., Jackson, S. N., Post, J., Baldwin, K., Roux, A., ... Balaban, C. (2013). Gangliosides and ceramides change in a mouse model of blast induced traumatic brain injury. *ACS Chemical Neuroscience*, *4*(4), 594–600.
- Zhang, J., Fang, X., Zhou, Y., Deng, X., Lu, Y., Li, J., ... Xu, R. (2015). The Possible Damaged Mechanism and the Preventive Effect of Monosialotetrahexosylganglioside in a Rat Model of Cerebral Ischemia-Reperfusion Injury. *Journal of Stroke and Cerebrovascular Disease*, *24*(7), 1471–1478.

Chapter 6 : Discussion

6.1 Summary

The purpose of the studies presented in this work was to better understand the role of ganglioside dysregulation in neurodegeneration and aging. To accomplish this, we first used animal models of stroke and A β toxicity to examine the interaction between simple ganglioside accumulation and the severity of neurodegenerative injury. We then considered the role of simple and complex gangliosides with either 18 or 20 carbons present in their ceramide moiety in Wt and Tg APP21 Fischer rats to determine if the LCB ratio shifted in a characteristic manner among all a-series gangliosides. Next, we further examined the abundance of each individual ganglioside species in the aging brain of Wt and Tg APP21 Fischer rats to better understand the unique patterns of alterations that occur in simple and complex gangliosides during aging. Finally, a pharmacological agent (CQ) was used to assess protection from ganglioside dysregulation after a severe stroke in Wistar rats.

6.2 Gangliosides and pathological inflammation

The brain's major immune/inflammatory cells, astrocytes and microglia, are thought to play an important role in the accumulation of simple ganglioside species in response to injury and disease. GM3 has been reported to be an important component of astrocytes. Indeed, it has been reported to be the major ganglioside in rat and chick primary cultured astrocytes according to HPTLC and IHC analysis, along with simple species GD3, while complex species GM1 was not detected (Asou, Hirano, & Uyemura, 1989; Murakami et al., 1999; Sbaschnig-Agler, Dreyfus, & Norton, 1988). The composition of gangliosides in astrocytes is thought to be fluid, changing depending on their activation state (Raff et al., 1983). Kawai et al., found that GD3 was elevated in reactive astrocytes but not normal astrocytes which the authors hypothesized may be related to astrocyte's role in lesion repair as GD3 was increased in glial scars (Kawai et al., 1994). These studies support the hypothesis that GM3 accumulation is linked to the neuroinflammatory process and provides an interesting rationale for further investigations of the role of GM3 and GD3 in astrocytes.

While little is known of the ganglioside composition of microglia, a similar increase in simple gangliosides has been reported in microglia in response to environmental stressors. A study by Simon et al., showed that microglia release simple ganglioside GD3 in response to inflammatory cytokines and lipopolysaccharide (LPS) and that an increase in GD3 is toxic to oligodendrocytes, leading to apoptosis (Simon et al., 2002). Oligodendrocytes are particularly vulnerable to inflammatory cytokines, with TNF- α and interferon- γ thought to play a major role in their degeneration (D'souza, Alinauskas, & Antel, 1996; Vartanian, Li, Zhao, & Stefansson, 1995). The authors confirmed the toxicity of elevated GD3 on oligodendrocytes by exogenous administration of several gangliosides to *in vitro* cultures of oligodendrocytes and saw that only exogenous GD3 lead to an increase in cell death markers and condensation/fragmentation of the nucleus of oligodendrocytes (Simon et al., 2002). Indeed, unpublished work from our lab has shown that cultured microglia also release GM3 in response to LPS, further supporting the hypothesis that brain inflammatory cells may be contributing to the accumulation of simple gangliosides under toxic/stressful conditions.

6.3 Ganglioside dysregulation

This work provides detailed evidence of the degree and location of ganglioside dysregulation during neurodegeneration and aging in the brain of rats, however, much remains to be explored. To better understand the accumulation of simple gangliosides, there is a need for a thorough examination of the enzymes that govern their metabolism. Chapter 5 provided compelling evidence that the depletion of complex gangliosides is tied to the accumulation of simple species as the disruption of catabolic enzymes by CQ restored the homeostatic distribution of all a-series gangliosides acutely after a stroke injury. A detailed examination of mRNA and protein expression of all catabolic enzymes using polymerase chain reaction (PCR) and western blotting could reveal if certain enzymes are more affected than others in response to neurodegeneration, thus providing a more specific target for ganglioside dysregulation treatments.

Additionally, while the work presented here focuses exclusively on the distribution of a-series gangliosides, b-series gangliosides have also been implicated in the pathogenesis of neurodegenerative diseases such as HD (Di Pardo, Amico, & Maglione, 2016), with

simple ganglioside GD3 being linked to toxicity, similar to GM3 (Desplats et al., 2007; Scorrano, Petronilli, Lisa, & Bernardi, 1999). An interesting avenue of further study would be to examine how the ratio of a to b series gangliosides are altered during aging and if the Tg APP21 rats or rats who have undergone stroke would show a different distribution of these species. Additionally, although gangliosides have important regulatory functions in the cell and are thus of particular interest in the context of injury and disease, their behaviour only scratches the surface of the total burden of lipid dysregulation in the brain. Other membrane associated lipids such as phospholipids and cholesterol are also altered in response to changes in the external environment. Techniques such as MALDI IMS can, and are, being used to better understand the global impact of lipid dysregulation in the brain.

6.4 Role of the ceramide moiety in aging and neurodegeneration

Prior to this work, the accumulation of d20:1 species in the brain was thought to be a metabolic marker of aging in the brain (Palestini, Masserini, Sonnino, & Tettamanti, 1990; Sugiura et al., 2008). Chapters 3 and 4 demonstrated that the accumulation of d20:1 species in the brain is far more complex than previously hypothesized, with a high degree of anatomical heterogeneity. We showed, for the first time, that the d20:1 species of simple gangliosides do not increase in an age-dependent manner, with the exception of GM3 in the white matter. We also showed that an increase in the proportion of d20:1 species relative to d18:1 does not necessarily mean that the d20:1 species are accumulating, but rather could be indicative of a depletion of d18:1 species, as was observed for complex ganglioside GD1 in the white matter.

While the functional consequences of alterations in the ceramide moiety are thought to be related to membrane fluidity and cell signaling properties on the membrane, much remains unknown (Masserini, Palestini, & Freire, 1989; Sonnino & Chigorno, 2000). However, this work provides new, detailed information regarding their anatomical distribution during aging, which may help elucidate the role of the ceramide moiety. For example, Hirano-Sakamaki et al., found that 18 carbon species of GM1 and GD1 are highly expressed in the hilum and inner molecular layers of the hippocampus. These regions contain mossy fiber axons and dendrites from granule cells and play a critical role in memory and learning, which suggests that the 18 carbon species of complex gangliosides

may be critical to these processes. The increased abundance of complex d20:1 species in the molecular layer suggest that these species are highly localized on axons and perforant pathway fibers from entorhinal cortex neurons, a pathway highly susceptible to neurodegeneration in AD (Hirano-Sakamaki et al., 2015). This study suggests the regional distribution of ganglioside species with various carbon chain length may be crucial to the functions of that brain region.

Furthermore, Cutler et al., described a correlation between the location of long chain ceramide accumulation and brain regions which were susceptible to pathology in AD patients (Cutler et al., 2004). Therefore, it is possible that the brain regions which showed the highest ratio of d20:1 to d18:1 species in Chapter 3 are most vulnerable to the development of pathology in our rats. The regions with the highest overall d20:1/d18:1 ratios included the DG Mol layer of the hippocampus, intermediate layer of the cortex, and the white matter PVCC for complex gangliosides, and the PVCC, and to a lesser extent the aCC, striatum, and LSN for simple ganglioside GM3 (GM2 showed a fairly stable ratio in all brain regions). Indeed, Chapter 4 revealed several differences with regards to the ceramide moiety in Tg APP21 and Wt rats which support this hypothesis. Firstly, Tg APP21 rats had elevated d20:1 species of GD1 at 20 m in the PVCC over Wt rats, while the aCC showed a more severe depletion of d18:1 species at 20 m. Secondly, Tg APP21 rats accumulated d20:1 species of GD1 earlier than their Wt counterparts in the DG Mol layer of the hippocampus and did not show an increase in d18:1 species at 20 m that was observed in Wt rats. Thirdly, the intermediate layer of the cortex showed the largest discrepancy between d18:1 and d20:1 species of GM1 and GD1 for both Wt and Tg APP21 rats, with relatively stable levels of d18:1 during aging accompanied by a significant increase in d20:1 species. However, Wt rats had significantly more d18:1 species of GD1 at 12 m, with a similar pattern observed for GM1. Altogether, Tg APP21 rats had either higher levels of d20:1 species or lower levels of d18:1 species in all three of the aforementioned brain regions. In terms of simple ganglioside GM3, Tg APP21 rats showed significantly more d20:1 species in all cortical, subcortical, and white matter brain regions at 12 m than Wt rats. However, this significant increase only persisted at 20 m in the PVCC. Thus, while the d20:1 species of GM3 did not necessarily accumulate in an age dependent manner across the brain, Tg APP21 rats still showed higher levels of these

species than their Wt counterparts, suggesting that an increase in d20:1 species may be a mechanism which makes the brain more susceptible to damage in Tg APP21 rats.

6.5 CQ and ganglioside metabolism – limitations/benefits

In chapter 5, CQ treatment prevented the dysregulation of gangliosides 3 d after a severe stroke injury. However, the effect of this treatment was not as pronounced at 21 d and a toxic pattern of ganglioside distribution began to emerge. It has been suggested that CQ may be more effective in treating damage caused by ischemic reperfusion injuries in the early stages of recovery than later stages (Fang, Liu, Dahmen, & Dirsch, 2013). Further studies examining the effects of CQ on ganglioside metabolism after stroke are needed to establish the optimal timing for effective treatment.

The inhibition of ganglioside catabolic enzymes by CQ leads to the accumulation of GM1 through a number of different mechanisms. Other than preventing direct GM1 catabolism, CQ can increase GM1 indirectly through GD1a. Riboni et al., demonstrated that GD1a and b can be broken down by sialidase at the level of the plasma membrane, independent of the lysosome, while the degradation of GM1 to GM2 and GM3 were lysosome-dependent (Riboni, Prinetti, Bassi, & Tettamanti, 1991). This suggests that CQ's ability to increase GM1 likely stems not only from the disruption of catabolic enzymes which degrade GM1, but also from the normal degradation of GD1 to GM1 by membrane-bound sialidase which then accumulates as GM1. For this reason, targeting the catabolic enzymes β Gal and β Hex may be a particularly effective approach for both preventing the accumulation of simple gangliosides and increasing/maintaining GM1 levels.

One limitation of using CQ to modulate the catabolism of gangliosides *in vivo* is that this compound has a number of biological effects both within and outside of the lysosome, therefore, the beneficial effects of CQ treatment after stroke demonstrated in chapter 5 cannot be strictly ascribed to the restoration of ganglioside homeostasis. CQ is a known inhibitor of autophagy and has been used in pre-clinical models and clinically as an anti-inflammatory agent (Ferraz et al., 1994; Popert, Meijers, Sharp, & Bier, 1961; Suarez-Almazor et al., 2000; Yang et al., 2013), both functions which have also been shown to be beneficial in treating stroke injuries (Cui et al., 2013; Hirata et al., 2011; Li et al., 2016;

Zheng et al., 2014). Therefore, it is possible that these mechanisms may also be playing a role in reducing stroke pathology and preventing behavioural deficits in the rats. However, chapter 5 also demonstrates, for the first time, that CQ is able to reduce toxicity caused by the exogenous administration of GM3 in primary cortical neurons. These results directly link the therapeutic effects of CQ with a ganglioside-derived mechanism of toxicity. Importantly, these results were recapitulated in the *in vivo* rat model 3 d post-stroke, in which the increase in toxic simple gangliosides was prevented by CQ treatment. While the findings of chapter 2 demonstrated that ganglioside dysregulation was tied to the severity of neurodegeneration, chapter 5 showed that the restoration of ganglioside homeostasis by CQ was tied to pathological and functional recovery from a severe neurodegenerative stroke.

In the end, Chapter 5 serves as a valuable proof of principle that ganglioside dysregulation can be treated using the anti-malarial drug CQ and that the restoration of ganglioside homeostasis is associated with pathological and functional recovery. While CQ itself is known to produce a variety of symptoms in humans, such as severe stomach pains, psychosis, delirium, vomiting, and blurred vision, synthetic analogues of CQ have been created which have the same properties but produce milder symptoms. In a clinical setting, a pharmacological agent, such as CQ, could be administered alone or in conjunction with other therapies as part of a multi-factorial approach to treatment in patients who have either suffered a stroke or are at high risk of suffering from recurring strokes. However, further studies are needed to demonstrate the specific role of β Gal and β Hex inhibition in neurodegeneration.

6.6 Alternative approaches for modulation of ganglioside metabolism

In order to better understand the specific effects associated with the restoration of ganglioside homeostasis during neurodegeneration, catabolic enzymes β Gal and β Hex would have to be selectively targeted and transiently blocked. Although there is currently no pharmacological agent which can accomplish this, genetic approaches may hold the key to answering this question.

KO animal models have been developed which lack the synthetic enzymes necessary for the formation of certain types of gangliosides, leading to a depletion of downstream gangliosides. These models have been useful in understanding the role of the depleted species during development and in the adult brain (Chiavegatto, Sun, Nelson, & Schnaar, 2000; Harlalka et al., 2013; Takamiya et al., 1996). KO models targeting the catabolic enzymes have also been developed that lead to an accumulation of the upstream species. For example, the β Gal KO mouse model leads to an accumulation of GM1. These models are generally used to simulate gangliosidoses (Hauser, Kasperzyk, D'Azzo, & Seyfried, 2004; Tessitore et al., 2004). A permanent KO of any gene associated with ganglioside metabolism or catabolism would disrupt the normal homeostatic balance needed at various stages of development. Thus, while KO models can be quite specific in their genetic target, they do not offer the required transient properties to be a useful therapeutic approach to treating ganglioside dysregulation and would not be transferable to a clinical setting. Rather a genetic knock-down approach would be more suitable.

Small interfering ribonucleic acid, or siRNA, is a technique used for sequence specific knock down of a desired gene, for example, β Gal. The sequence is synthetically created then injected into the cell (*in vitro*) or desired region (*in vivo*). The effects are transient as the siRNA eventually gets degraded or diluted below a therapeutic threshold (Whitehead, Langer, & Anderson, 2009). siRNA has been shown to last between 3-7 d in rapidly dividing cells, and several weeks in non-dividing cells (Bartlett & Davis, 2006). Future studies using siRNA to target β Gal and β Hex both in *in vitro* models of toxicity and *in vivo* models of stroke may reveal specific neuroprotective mechanisms involved in preventing ganglioside dysregulation.

6.7 Gangliosides and white matter

One of the most interesting findings from chapter 3 and 4 was the unique changes in ganglioside composition that occurred in the white matter of both Wt and Tg APP21 rats during aging. The age-dependent increase in the d20:1/d18:1 LCB ratio of GD1 in the white matter observed in chapter 3 was revealed to be the result of an age-dependent depletion of d18:1 species with only a minor increase in the d20:1 species, an effect that was exacerbated in the Tg APP21 rats. This GD1 pattern was unique to the white matter,

with an increased or stable abundance of d18:1 species during aging throughout the rest of the brain. As previously mentioned, GD1 is a major receptor for MAG binding and plays an important role in the long term stability of axons. Thus, a depletion of these species in the white matter of the aging brain may represent a mechanism of vulnerability to axonal damage in the corpus callosum. Indeed, depletion of GD1 and GM1 has been observed in the corpus callosum of a pre-clinical model of HD and may, according to the authors, represent a critical molecular change influencing the pathogenesis of neurodegenerative diseases (Di Pardo et al., 2016).

Chapter 3 also showed that GM3 had a unique pattern of abundance in the white matter during aging, with an age-dependent increase in the d20:1/d18:1 LCB ratio. This ratio either decreased or remained unchanged between birth and old age in every other brain region. Chapter 4 expanded upon these findings and revealed that both the d18:1 and d20:1 species of GM3 were significantly higher at 12 m in Tg APP21 rats in brain regions such as the substantia nigra and cortex, an effect that was masked in chapter 3 due to the focus on the d20:1/d18:1 ratio. These results suggest that GM3 accumulation during aging may play a much larger role than anticipated in the brains of Tg APP21 rats. Importantly, the increased GM3 LCB ratio observed in the PVCC in chapter 3 was found to be the result of an increase in d20:1 species in Tg APP21 rats at both 12 and 20 m, and not a decrease in the d18:1 species. The accumulation of GM3 in the white matter of Tg APP21 rats is of particular interest due to its hypothesized role in the development of vascular dementia. GM3 was reported to be a major component of vascular smooth vessel walls in the brain and is thought to be critical driver of A β aggregation in blood vessel walls of Tg APP mice with the Dutch mutation (Yamamoto, Hirabayashi, Amari, & Yamaguchi, 2005). Indeed, our Fischer Tg APP21 rats are vulnerable to the development of micro-infarcts in the corpus callosum as they age, a pathology reminiscent of leukaoriosis in human patients with vascular dementia. Thus, the data presented in this work supports the hypothesis of GM3 accumulation as a driver of early pathology in AD and an important target for preventative interventions.

6.8 MALDI IMS – limitations and future directions

Advancements in the MALDI IMS technique have increased exponentially in the last decade, not only in terms of technology, but also in sample preparation methodology. The deposition of dry matrix by sublimation has enabled increased sensitivity and spatial resolution of lipid imaging that has made the findings reported in this work possible. However, there remain a number of limitations to the technique that we, and others in the MALDI IMS field, are working on improving moving forwards.

One of the largest pitfalls of MALDI IMS is the semi-quantitative nature of the data it produces. Finding new statistical approaches to analyzing the data and reducing error produced by between scan variability is one the biggest challenges currently facing the field. In chapter 2, the average peak height corresponding to the three largest isotopic peaks was used to perform a ratio between the stroke-injured, ipsilateral hemisphere in the rat brain compared to the undamaged tissue of the contralateral hemisphere. The three largest isotopic peaks of each species were used to ensure the data was as representative as possible of abundance of each ion. Although it is often the case, the first isotopic peak is not always the largest, and thus, measuring only one isotopic peak can be misleading. By comparing the ratio of each species within two regions of interest of the same image, error produced by between scan variability was greatly reduced. In chapters 3, 4, and 5, the peak height analysis was replaced by an area under the curve (AUC) measurement, which has become a common method of quantifying MALDI IMS data in similar published studies (Sugiura et al., 2008; Weishaupt, Caughlin, Yeung, & Whitehead, 2015). In chapter 3, this AUC measurement was used to calculate the ratio between the d20:1 and d18:1 species of each ganglioside, which, similar to chapter 2, prevented the need for direct image comparisons. Data from chapters 4 and 5 were further normalized by a total ion current ratio, comparing the AUC of each species to the total AUC of the mass spectrum, allowing for between species comparisons. Chapter 5 combined the analytical approaches of chapters 2 and 4 by both normalizing the data to the total ion current and comparing the injured ipsilateral hemisphere with the undamaged contralateral hemisphere. Although the approach to data analysis had evolved throughout this work, the field of IMS is always pushing for newer, more quantitative approaches to analyzing MALDI IMS data.

Standards of specific ions of interest can be used for tandem MS (MS/MS) to identify ions that have a low abundance in tissue samples (Chan et al., 2009; Dufresne et al., 2017). However, pure standards of each ganglioside species do not currently exist, limiting the applications of this method for large scale ganglioside identification and analysis. Using mathematical algorithms to cluster trends in MALDI MS data peak distribution, called principle component analysis (PCA), has been used to describe differences between experimental groups or identify patterns in MALDI IMS data (Hong et al., 2016). These alternative approaches to quantifying and analyzing MALDI IMS data may increase the robustness of findings.

Advancements in technology are also a key factor in addressing some of the limitations of MALDI IMS. For example, with the Sciex 5800 MALDI instrument used in chapters 3 through 5, acquisition of a full rat brain coronal section took upwards of 2 hrs and 30 min at a spatial resolution of 70 μ M. This long acquisition time makes running an experiment with a large sample size very costly and time consuming. Additionally, certain dry matrices begin sublimating while under the vacuum of the instrument, further limiting the types of matrices that can be used to acquire these full images. New MALDI MS instruments have been developed to address these issues including the recent launch of the Bruker Rapiflex MALDI MS, which can acquire images several times faster than any previous model (Prentice & Caprioli, 2016). This opens the door to a new realm of application opportunities and greatly increases the number of dry matrices that can be used to acquire large images (Potocnik et al., 2015). Increasing acquisition time makes the application of full body imaging more practical, which would allow for a more detailed examination of lipid distribution across the entire body of healthy and diseased/injured mice or rats, or tracking a peripherally administered drug to its target location. Full body imaging and Rapiflex technology would offer an interesting expansion to the work presented here.

6.9 Significance of the research

Our brains are largely composed of lipids, yet their role in aging and disease remains poorly understood. This work provides a unique interdisciplinary approach to examining the role of gangliosides during aging and neurodegeneration. Novel insight into the age-

dependent accumulation of long chain gangliosides was provided, showing, for the first time, that it is not a hallmark of the aging process but rather is largely dependent on ganglioside structure and anatomical location. The white matter was identified as a region that is particularly susceptible to ganglioside dysregulation in Tg APP21 rats and showed unique age-dependent alterations in ganglioside composition compared to grey matter regions. Further, a link between the severity of neurodegeneration and the degree of ganglioside dysregulation was shown and identified the depletion of complex species GM1 and GD1, along with the accumulation of GM3 and GM2 as major pathological events at the site of stroke injury. It also demonstrates that ganglioside dysregulation can be prevented with CQ and provides a foundation upon which refined, specific inhibitors of ganglioside catabolism can be examined as potential preventative/therapeutic approaches to ganglioside dysregulation. Overall, ganglioside dysregulation was highlighted as a crucial component of a highly complex set of pathological events which can play a mechanistic role in the propagation of neurodegeneration after stroke and increase susceptibility to the development of neurodegenerative diseases, making it a worthy target of future investigation. However, in the end, this work underlines the vast gap in knowledge that exists with regards to the role of membrane lipids in the brain and the need for innovative interdisciplinary approaches to better understand their role in health, disease, and injury.

6.10 References

- Asou, H., Hirano, S., & Uyemura, K. (1989). Ganglioside Composition of Astrocytes. *Cell Structure and Function*, *14*, 561–568.
- Bartlett, D. W., & Davis, M. E. (2006). Insights into the kinetics of siRNA-mediated gene silencing from live-cell and live-animal bioluminescent imaging. *Nucleic Acids Research*, *34*(1), 322–333.
- Chan, K., Lanthier, P., Liu, X., Sandhu, J. K., Stanimirovic, D., & Li, J. (2009). MALDI mass spectrometry imaging of gangliosides in mouse brain using ionic liquid matrix. *Analytica Chimica Acta*, *639*(1–2), 57–61. 1

- Chiavegatto, S., Sun, J., Nelson, R. J., & Schnaar, R. L. (2000). A functional role for complex gangliosides: motor deficits in GM2/GD2 synthase knockout mice. *Experimental Neurology*, *166*(2), 227–34.
- Cui, G., Ye, X., Zuo, T., Zhao, H., Zhao, Q., Chen, W., & Hua, F. (2013). Chloroquine pretreatment inhibits toll-like receptor 3 signaling after stroke. *Neuroscience Letters*, *548*, 101–104.
- Cutler, R. G., Kelly, J., Storie, K., Pedersen, W. A., Tammara, A., Hatanpaa, K., ... Mattson, M. P. (2004). Involvement of oxidative stress-induced abnormalities in ceramide and cholesterol metabolism in brain aging and Alzheimer's disease. *Proc.Natl.Acad.Sci.U.S.A*, *101*(7), 2070–2075.
- D'souza, S. D., Alinauskas, K. A., & Antel, J. (1996). Ciliary neurotrophic factor selectively protects human oligodendrocytes from tumor necrosis factor-mediated injury. *Journal of Neuroscience Research*, *43*(3), 289–298.
- Desplats, P. A., Denny, C. A., Kass, K. E., Gilmartin, T., Head, S. R., Sutcliffe, J. G., ... Thomas, E. A. (2007). Glycolipid and ganglioside metabolism imbalances in Huntington's disease. *Neurobiology of Disease*, *27*(3), 265–277.
- Di Pardo, A., Amico, E., & Maglione, V. (2016). Impaired levels of gangliosides in the corpus callosum of Huntington disease animal models. *Frontiers in Neuroscience*, *10*, 1–8.
- Dufresne, M., Guneyasu, D., Patterson, N. H., Marcinkiewicz, M. M., Regina, A., Demeule, M., & Chaurand, P. (2017). Multimodal detection of GM2 and GM3 lipid species in the brain of mucopolysaccharidosis type II mouse by serial imaging mass spectrometry and immunohistochemistry. *Analytical and Bioanalytical Chemistry*, *409*, 1425–1433.
- Fang, H., Liu, A., Dahmen, U., & Dirsch, O. (2013). Dual role of chloroquine in liver ischemia reperfusion injury : reduction of liver damage in early phase , but aggravation in late phase. *Cell Death and Disease*, *4*(6), e694-9.

- Ferraz, M. B., Pinheiro, G. R. C., Helfenstein, M., Albequerque, E., Rezende, C., & Roimicher, L. (1994). Combination therapy with methotrexate and chloroquine in rheumatoid arthritis: A multicenter randomized placebo-controlled trial. *Scandinavian Journal of Rheumatology*, *23*(5), 231–236.
- Harlalka, G. V., Lehman, A., Chioza, B., Baple, E. L., Maroofian, R., Cross, H., ... Crosby, A. H. (2013). Mutations in B4GALNT1 (GM2 synthase) underlie a new disorder of ganglioside biosynthesis. *Brain*, 1–7.
- Hauser, E. C., Kasperzyk, J. L., D’Azzo, A., & Seyfried, T. N. (2004). Inheritance of lysosomal acid β -galactosidase activity and gangliosides in crosses of DBA/2J and knockout mice. *Biochemical Genetics*, *42*(7–8), 241–257.
- Hirano-Sakamaki, W., Sugiyama, E., Hayasaka, T., Ravid, R., Setou, M., & Taki, T. (2015). Alzheimer’s disease is associated with disordered localization of ganglioside GM1 molecular species in the human dentate gyrus. *FEBS Letters*, *589*(23), 3611–3616.
- Hirata, Y., Yamamoto, H., Shukry Moursy Atta, M., Mahmoud, S., Oh-hashii, K., & Kiuchi, K. (2011). Chloroquine inhibits glutamate-induced death of a neuronal cell line by reducing reactive oxygen species through sigma-1 receptor. *Journal of Neurochemistry*, *119*, 839–847.
- Hong, J. H., Kang, J. W., Kim, D. K., Baik, S. H., Kim, K. H., Shanta, S. R., ... Kim, K. P. (2016). Global changes of phospholipids identified by MALDI imaging mass spectrometry in a mouse model of Alzheimer’s disease. *Journal Of Lipid Research*, *57*, 36–45.
- Kawai, K., Kuroda, S., Watarai, S., Takahashi, H., & Ikuta, F. (1994). Occurrence of GD3 ganglioside in reactive astrocytes—an immunocytochemical study in the rat brain. *Neuroscience Letters*, *174*(2), 225–227.
- Li, L., Tian, J., Long, M. K., Chen, Y., & Lu, J. (2016). Protection against Experimental Stroke by Ganglioside GM1 Is Associated with the Inhibition of Autophagy. *PloS*

One, 11(1), 1–13.

- Masserini, M., Palestini, P., & Freire, E. (1989). Influence of glycolipid oligosaccharide and long-chain base composition on the thermotropic properties of dipalmitoylphosphatidylcholine large unilamellar vesicles containing gangliosides. *Biochemistry*, 28(12), 5029–5034.
- Murakami, K., Asou, H., Adachi, T., Takagi, T., Kunimoto, M., Saito, H., & Uyemura, K. (1999). Neutral glycolipid and ganglioside composition of type-1 and type-2 astrocytes from rat cerebral hemisphere. *Journal of Neuroscience Research*, 55(3), 382–393.
- Palestini, P., Masserini, M., Sonnino, S., & Tettamanti, G. (1990). Changes in the ceramide composition of rat forebrain gangliosides with age. *Journal of Neurochemistry*, 54(1), 230–235.
- Popert, A. J., Meijers, K. A. E., Sharp, J., & Bier, F. (1961). Chloroquine diphosphate in rheumatoid arthritis. A controlled trial. *Ann Rheum Dis*, 20, 18–35.
- Potocnik, N., Porta, T., Becker, M., Heeren, R. M. A., & Ellis, S. R. (2015). Use of advantageous , volatile matrices enabled by next-generation high-speed matrix-assisted laser desorption / ionization time-of- flight imaging employing a scanning laser beam. *Rapid Commun Mass Spectrom*, 29, 2195–2203.
- Prentice, B., & Caprioli, R. (2016). The need for speed in matrix-assisted laser desorption/ionization imaging mass spectrometry. *Postdoc J*, 4(3), 3–13.
- Raff, M., Abney, E., Cohen, J., Lindsay, R., & Noble, M. (1983). Two types of astrocytes in cultures of developing rat white matter: Differences in morphology, surface gangliosides, and growth characteristics. *The Journal of Neuroscience*, 3(6), 1289–1300.
- Riboni, L., Prinetti, A., Bassi, R., & Tettamanti, G. (1991). Cerebellar granule cells in culture exhibit a ganglioside-sialidase presumably linked to the plasma membrane. *FEBS*, 287(1,2), 42–46.

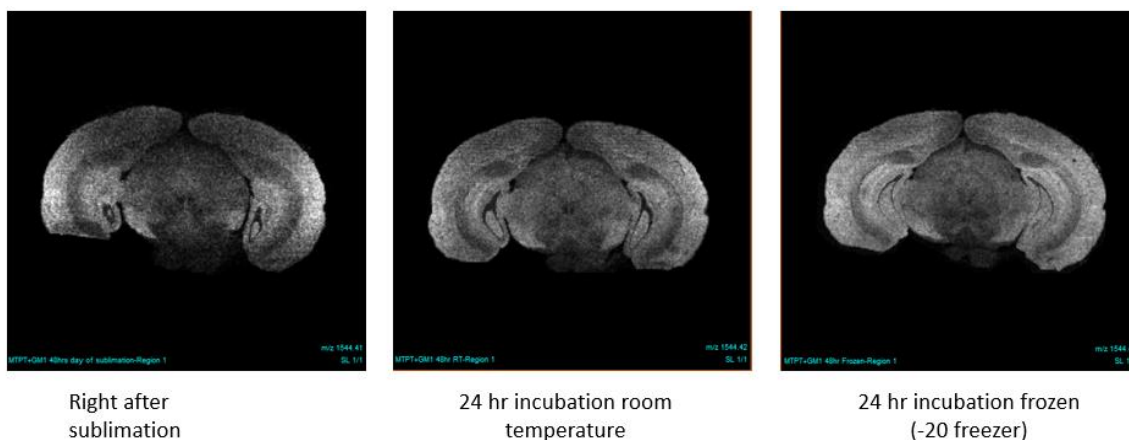
- Sbaschnig-Agler, M., Dreyfus, H., & Norton, W. T. (1988). Gangliosides of cultured astroglia. *Brain Research*, *461*(1), 98–106.
- Scorrano, L., Petronilli, V., Lisa, F. Di, & Bernardi, P. (1999). Commitment to Apoptosis by GD3 Ganglioside Depends on Opening of the Mitochondrial Permeability Transition Pore. *The Journal of Biological Chemistry*, *274*(32), 22581–22585.
- Simon, B. M., Malisan, F., Testi, R., Nicotera, P., & Leist, M. (2002). Disialoganglioside GD3 is released by microglia and induces oligodendrocyte apoptosis. *Cell Death and Differentiation*, *9*, 758–767.
- Sonnino, S., & Chigorno, V. (2000). Ganglioside molecular species containing C18- and C20-sphingosine in mammalian nervous tissues and neuronal cell cultures. *Biochimica et Biophysica Acta - Reviews on Biomembranes*, *1469*(2), 63–77.
- Suarez-Almazor, M. E., Belseck, E., Shea, B., Homik, J., Wells, G., & Tugwell, P. (2000). Antimalarials for treating rheumatoid arthritis. *The Cochrane Review*.
- Sugiura, Y., Shimma, S., Konishi, Y., Yamada, M. K., & Setou, M. (2008). Imaging mass spectrometry technology and application on ganglioside study; visualization of age-dependent accumulation of C20-ganglioside molecular species in the mouse hippocampus. *PloS One*, *3*(9), e3232.
- Takamiya, K., Yamamoto, a, Furukawa, K., Yamashiro, S., Shin, M., Okada, M., ... Aizawa, S. (1996). Mice with disrupted GM2/GD2 synthase gene lack complex gangliosides but exhibit only subtle defects in their nervous system. *Proceedings of the National Academy of Sciences of the United States of America*, *93*(20), 10662–7.
- Tessitore, A., Martin, M. P., Sano, R., Ma, Y., Mann, L., Ingrassia, A., ... Azzo, A. (2004). G M1 -Ganglioside-Mediated Activation of the Unfolded Protein Response Causes Neuronal Death in a Neurodegenerative Gangliosidosis. *Molecular Cell*, *15*, 753–766.
- Vartanian, T., Li, Y., Zhao, M., & Stefansson, K. (1995). Interferon- γ -Induced Oligodendrocyte Cell Death : Implications for the Pathogenesis of Multiple Sclerosis. *Molecular Medicine*, *1*(7), 732–743.

- Weishaupt, N., Caughlin, S., Yeung, K. K.-C., & Whitehead, S. N. (2015). Differential Anatomical Expression of Ganglioside GM1 Species Containing d18:1 or d20:1 Sphingosine Detected by MALDI Imaging Mass Spectrometry in Mature Rat Brain. *Frontiers in Neuroanatomy*, 9(DEC), 155.
- Whitehead, K. A., Langer, R., & Anderson, D. G. (2009). Knocking down barriers: advances in siRNA delivery. *Nature Reviews Drug Discovery*, 8, 129–138.
- Yamamoto, N., Hirabayashi, Y., Amari, M., & Yamaguchi, H. (2005). Assembly of hereditary amyloid b -protein variants in the presence of favorable gangliosides. *FEBS Letters*, 579, 2185–2190.
- Yang, R., Wang, Q., Min, L., Sui, R., Li, J., & Liu, X. (2013). Monosialoanglioside improves memory deficits and relieves oxidative stress in the hippocampus of rat model of Alzheimer's disease. *Neurological Sciences*, 34(8), 1447–1451.
- Zheng, Y., Hou, J., Liu, J., Yao, M., Li, L., Zhang, B., ... Wang, Z. (2014). Inhibition of Autophagy Contributes to Melatonin-Mediated Neuroprotection Against Transient Focal Cerebral Ischemia in Rats. *Journal of Pharmacological Sciences*, 124, 354–364.

Appendices

Appendix i: Incubation time and spatial resolution

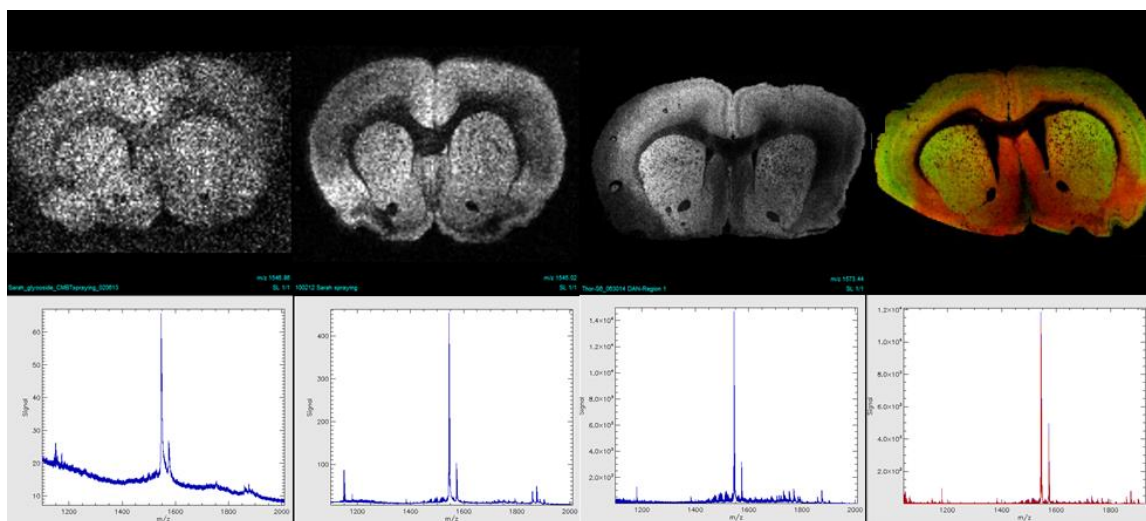
A number of troubleshooting experiments were performed in order to establish a working protocol that enhanced both the detection of gangliosides as well as spatial resolution. One experiment which demonstrated superior imaging resolution was the addition of an incubation period between sublimation and image acquisition. This effect was enhanced when the tissue was stored at -20°C as opposed to room temperature. This is thought to occur due to increased interaction time between the matrix and the tissue, as well as a rehydration effect when the tissue is removed from the freezer and placed in the desiccator.



Appendix i: Effect of incubation time and freezing on spatial resolution of ganglioside GM1 in MALDI imaging of mouse brain tissue. All tissue samples were sectioned and sublimated at the same time to avoid day-to-day variation in sample prep parameters. The left panel shows the spatial resolution of GM1 on a mouse brain tissue section when the image was acquired as soon as sublimation was completed. The image appears to have an uneven signal intensity across the tissue and has a “grainy” appearance as compared to the other images. The middle panel shows a separate tissue imaged after a 24 hr incubation period at room temperature. The image appears to be much more even and less pixelated. The final panel on the right show the spatial resolution of a third tissue section after a 24 hr incubation period in a -20°C freezer. Signal intensity of GM1 appears to have been increased evenly across the tissue as compared to the other panels and spatial resolution also increased, making it possible to observe discrete anatomical features of the tissue.

Appendix ii: Evolution of MALDI IMS sample prep protocols

The development of an optimized sample prep protocol is imperative for the detection and visualization of gangliosides across brain tissue sections. Significant improvements in sample prep and instrumentation between chapters 2 and 5 of this work occurred which allowed for improvements in accurate detection and visualization of A-series gangliosides across the rat brain.



Appendix ii: The evolution of the MALDI IMS protocol and improvements in signal intensity and spatial resolution over time. The first panel shows a representative image from one of the first MALDI IMS experiments at the beginning of this work performed using a Sciex 4700 MALDI instrument and CMBT matrix dissolved in a solvent and sprayed using a pneumatic sprayer. Refinements in the CMBT protocol led to improved spatial resolution and increased the signal to noise (S/N) ratio (shown in panel 2). With the purchase of an updated Sciex 5800 MALDI instrument and the use of a sublimation protocol with DAN matrix, sensitivity and spatial resolution exponentially increased (panel 3). Finally, further refinements in sample prep methodologies and image processing using Image J software to pseudocolour and overlay species allowed for the simultaneous visualization of different species (panel 4).

Appendix iii: Sublimation protocol

A specialized MALDI IMS sample prep protocol was developed upon completion of chapter 2 in order to improve MS signal and imaging resolution of gangliosides. This protocol was created to address limitations in sensitivity observed in chapter 2. For example, the d20:1 species of GM3 fell below the threshold of detection, thus, valuable information on the abundance of a toxic ganglioside species in the context of neurodegeneration was missing. This protocol, in conjunction with an updated MALDI MS instrument allowed for a more detailed analysis of ganglioside dysregulation in the rat brain and was published in the *Journal of Visualized Experiments* in February 2017. This manuscript was accompanied by a visual demonstration of the protocol to allow other researchers to replicate the technique used in this work.

Sublimation of DAN Matrix for the Detection and Visualization of Gangliosides in Rat Brain Tissue for MALDI Imaging Mass Spectrometry

Abstract

Sample preparation is key for optimal detection and visualization of analytes in MALDI IMS experiments. Determining the appropriate protocol to follow throughout the sample preparation process can be difficult as each step must be optimized to comply with the unique characteristics of the analytes of interest. This process involves not only finding a compatible matrix that can desorb and ionize the molecules of interest efficiently, but also selecting the appropriate matrix deposition technique. For example, a wet matrix deposition technique, which entails dissolving a matrix in solvent, is superior for desorption of most proteins and peptides, whereas dry matrix deposition techniques are particularly effective for ionization of lipids. Sublimation has been reported as a highly efficient method of dry matrix deposition for the detection of lipids in tissue by MALDI IMS due to the homogeneity of matrix crystal deposition and minimal analyte delocalization as compared to many wet deposition methods (Hankin, Barkley & Murphy, 2007; Thomas, Charbonneau, Fournaise & Chaurand, 2012). Broadly, it involves placing a sample and powdered matrix in a vacuum-sealed chamber with the samples pressed against a cold surface. The apparatus is then lowered into a heated bath (sand or oil), resulting in

sublimation of the powdered matrix onto the cooled tissue sample surface. Here we describe a sublimation protocol using 1,5-diaminonaphthalene (DAN) matrix for the detection and visualization of gangliosides in the rat brain using MALDI IMS.

Introduction

Matrix-assisted Laser Desorption/Ionization (MALDI) Imaging Mass Spectrometry (IMS) is becoming a highly sought after technique for visualization of the spatial distribution of lipids, peptides and proteins across intact sample surfaces. MALDI IMS was previously known as an analytical technique for pre-purified analytes, but in recent years, it has been drawing attention in many other disciplines because of the ability to combine the accuracy of mass spectrometry with high resolution visual/anatomical reference points without the need for any external labelling.

As the scientific pool of researchers utilizing this technique continues to grow, there is increased need for standardized, easy-to-follow protocols to assist in the development and optimization of IMS experiments. Gangliosides, a group of membrane lipids highly abundant in the central nervous system, are ideal for MALDI IMS experiments as their location, embedded within the membrane, makes certain species impossible to detect using conventional Immuno-labelling. Additionally, we have shown, using MALDI IMS, that these lipids, which function as modulators of cell signaling, among other things, have unique anatomical distribution patterns in the healthy rodent brain that are altered after brain injury (Caughlin et al., 2015; Weishaupt, Caughlin, Yeung & Whitehead, 2015; Whitehead et al., 2011). Gangliosides are located at a higher mass range compared to most lipid species, and are thus most suited to the MALDI imaging platform.

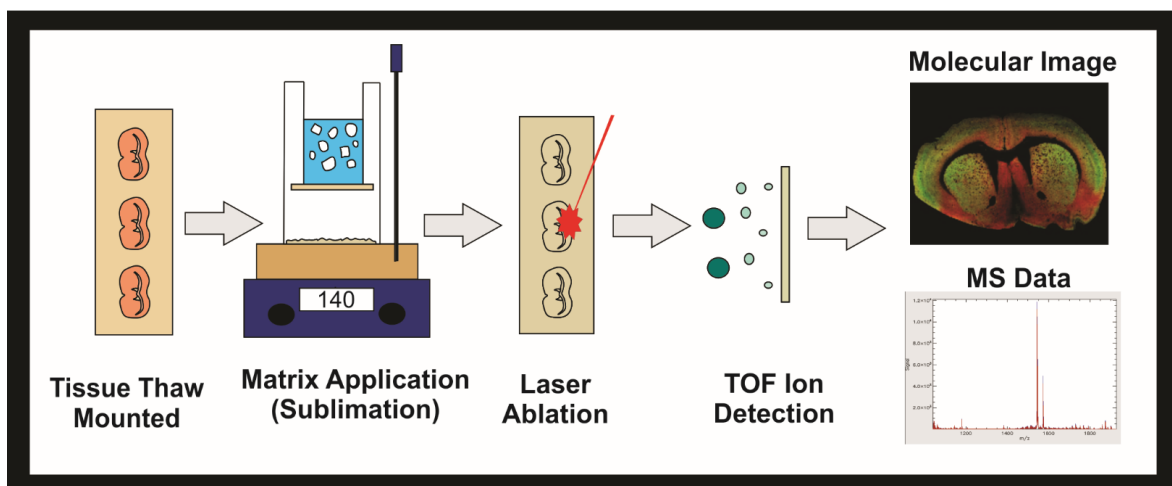


Figure 1. Workflow of MALDI IMS Experiment.

Diagram of the general workflow of a MALDI IMS experiment using sublimation. Tissue frozen at $-80\text{ }^{\circ}\text{C}$ is sectioned in a cryostat and $10\text{ }\mu\text{m}$ sections are thaw mounted onto conductive ITO slides. The slide is then placed in a desiccator until sublimation. Slides are inserted into the sublimation apparatus and an even layer of matrix is applied to the tissue sample surface. Samples are frozen overnight in a $-20\text{ }^{\circ}\text{C}$ freezer then placed in a desiccator for 10 min. Once standards have been applied, the samples are inserted into the MALDI instrument where a laser is directed across the tissue causing desorbed molecules in the matrix to ionize. The ions travel down a flight tube and separate based on their mass (time-of-flight/TOF) until they reach the detector. The information on the ionic abundance of analytes within a predetermined mass-to-charge (m/z) range is displayed as both a molecular image and mass spectrum. This data can be used to both visualize and quantify the ionic abundance of the analyte of interest within the imaged tissue.

Sample preparation for MALDI IMS is highly variable as each step of the process must be customized to the analytes of interest. The defining feature of MALDI-based experiments is the use of a matrix coating deposited onto the sample surface prior to analysis. In addition to the role of absorbing and transferring radiation energy from the laser during the ablation process, the matrix also serves to isolate various analytes from the sample, thereby facilitating the analysis of compounds of interest (Fuchs et al., 2010; Barcelo-Coblijn & Fernandez, 2015). Homogenous application of the matrix to the sample surface is the most crucial step in the sample preparation process. Improper matrix deposition can lead to large heterogeneous matrix crystal formations and the development of artifacts, low ion-signal, and poor reproducibility (Barcelo-Coblijn & Fernandez, 2015)(**Figure 1**).

Due to the affinity of certain matrices to isolate specific analytes, the type of matrix selected for an experiment can significantly alter the outcome. The matrices used for imaging of proteins and peptides often differ from those used for imaging lipids and the process is further complicated by the need for additional procedures such as washing and rehydration steps in order to successfully detect signals from tissue. Although washing steps exist for the enhancement of lipid signals (Angel, Spraggins, Baldwin & Caprioli, 2012), they are not a prerequisite for the detection of most lipid species. When selecting a matrix for a lipid imaging experiment, it is important to consider the polarity of the lipid of interest as this will narrow the range of suitable matrices. For example, gangliosides contain sialic acid residues which give them an overall negative polarity. There are a number of matrices that can effectively desorb and ionize gangliosides from tissue; however, factors such as matrix-derived peaks in the spectrum and stability of the matrix under vacuum must be taken under consideration. 1,5-diaminonaphthalene (DAN) matrix is sufficiently stable under instrument vacuum conditions for the majority of imaging applications and has demonstrated a high degree of sensitivity for lipid desorption and can be used for the analysis of lipids in both positive and negative ion modes (Thomas, Charbonneau, Fournaise & Chaurand, 2012). DAN matrix, when compared to other negative lipid affinity matrices such as dihydroxybenzoic acid (DHB), 9-aminoacridine (9-AA), and 5-chloro-2-mercaptobenzothiazole (CMBT), was able to most efficiently desorb gangliosides from rat brain tissue in negative ion mode (manuscript in preparation).

Selecting the appropriate method of matrix deposition is of equal importance to selecting the matrix itself. Wet matrix deposition methods wherein the solid matrix is dissolved in an organic solvent, and deposited by pneumatic or automated sprayers or spotters, are particularly effective for the desorption of proteins and peptides as the liquid permeates the sample to allow for extraction of compounds and co-crystallization with the matrix. Although these techniques can also be used for lipid applications, analyte delocalization and uneven matrix crystal formations are common occurrences due to the high abundance and solubility of lipids in solvents, particularly in tissue (Thomas, Charbonneau, Fournaise & Chaurand, 2012; Murphy et al., 2011). Because lipids are readily ionized from tissue, dry matrix deposition techniques, such as sublimation, offer a simple, cost effective alternative to sprayers while circumventing many of the drawback of these techniques. The success of sublimation in MALDI IMS experiments is attributed to features such as microcrystalline matrix morphology which increases the surface area for matrix-analyte binding, increased matrix purity, and homogenous matrix deposition leading to increased reproducibility compared to wet matrix techniques (Hankin, Barkley & Murphy, 2007; Jaskolla, Karas, Roth & Steinert, 2009).

Sublimation involves heating a powdered matrix under vacuum immediately below a cooled sample surface resulting in solid to gas-phase transition of the powdered matrix followed by deposition onto the tissue sample surface. During sublimation, matrix deposition can be controlled by varying factors such as time, temperature and pressure to provide highly reproducible results. A single sublimation experiment can take anywhere from 5 to 20 min depending on the type of matrix selected, which can be re-used several times before disposal. The apparatus can be purchased commercially at a fraction of the price of automated sprayers and is easily taken apart for cleaning and maintenance. The low cost and relative simplicity of this matrix deposition technique make it ideal for researchers beginning or expanding upon lipid imaging applications in MALDI IMS. Although information detailing protocols for sublimation of tissues for IMS have been reported (Rourke et al., 2015), few standardized protocols exist which focus on the basic workflow involved with carrying out a sublimation experiment for imaging high mass lipids in negative ion mode, making it difficult to establish the technique without extensive trial and error. The following is an experimental protocol aiming to fill that gap for the

sublimation of DAN matrix onto rat brain sections for high resolution imaging and detection of gangliosides (**Figure 2**).

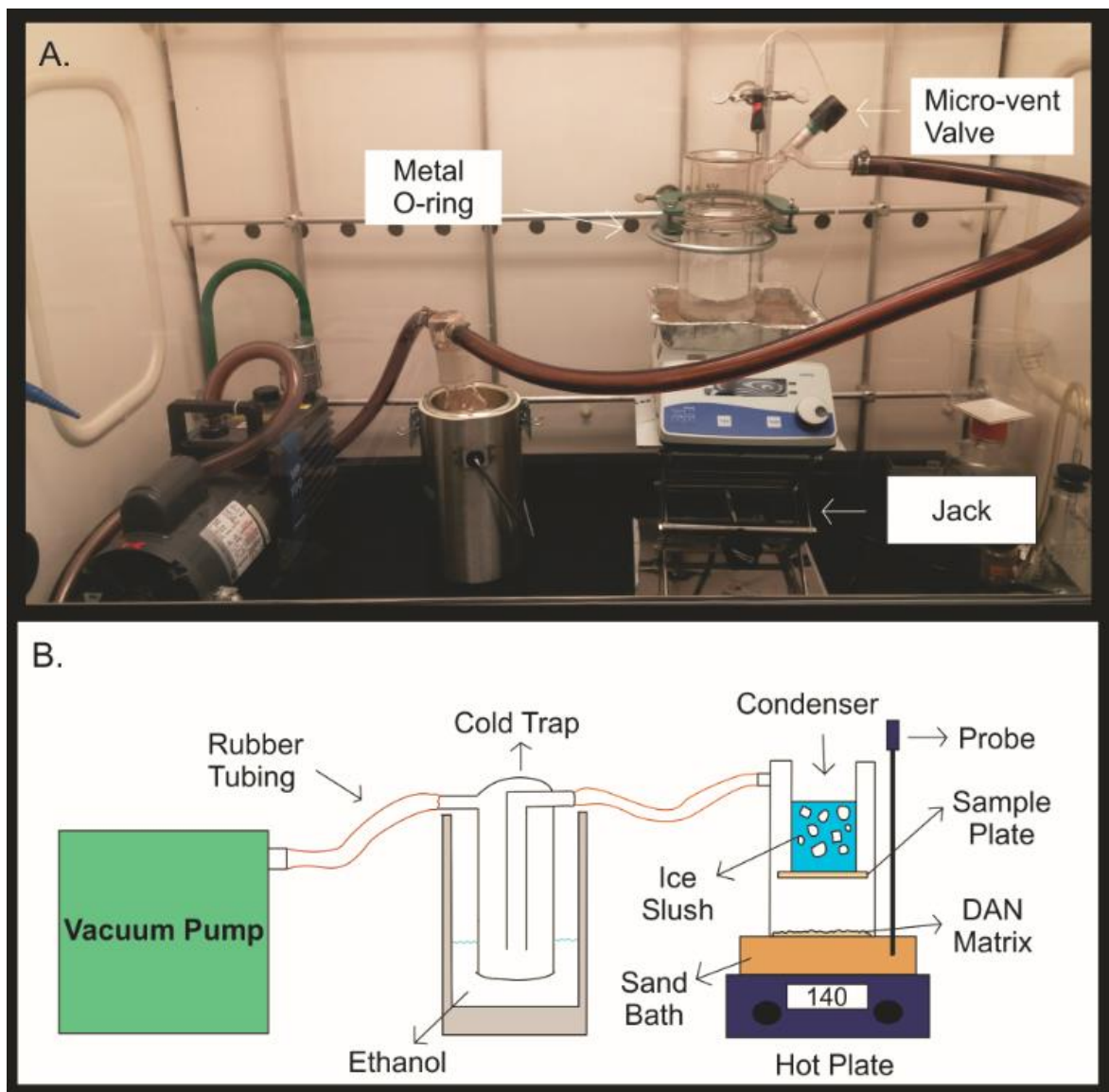


Figure 2. Sublimation Apparatus.

Photograph (A) and schematic diagram (B) of the sublimation apparatus. The vacuum pump is connected by rubber tubing to a cold trap filled with 300 mL of ethanol. The cold trap is then connected by rubber tubing to the sublimation apparatus. The apparatus is made up of two separate pieces of glassware that are sealed together with a metal U-joint. The top half of the sublimator contains the condenser which is filled with ice slush. The sample plate is taped onto the bottom of the condenser, inside the sealed glass apparatus. The bottom half of the sublimation apparatus contains the DAN matrix, spread out evenly facing the sample plate. During sublimation, the glass apparatus is placed on a sand bath heated to 140 °C by a hot plate directly below it. The temperature probe helps maintain a stable temperature throughout the sublimation experiment through feedback of the sand bath temperature compared to the preset temperature for the experiment.

Protocol

All animal handling procedures described below adhere to the University of Western Ontario's animal care committee (2016-014).

1. Tissue Preparation and Sectioning

1.1. Extract brain tissue from the rat through a process known as "Fresh Frozen Extraction" (FFE).

- a. Euthanize the rat with an overdose of pentobarbital sodium and monitor reflexes in the limbs. Once all reflexes have ceased, sever the head of the rat using a guillotine.
- b. Carefully separate the muscles and other tissues from the skull using a scalpel. Use bone-cutting forceps to break the skull to expose the brain, starting from the base of the skull (foramen magnum) to the anterior portion.
- c. Once the brain is exposed, carefully scoop it out with a surgical spatula and immediately place on crushed dry ice for flash freezing.

NOTE: The brain will be very malleable. Therefore, take extreme care when placing the brain on dry ice. If the brain is crushed or pressed against a surface, it will alter its shape and freeze in that position.

1.2. Remove fresh frozen tissue (not perfused with formaldehyde or embedded in OCT) from - 80° C freezer and place on dry ice.

1.3. Place several drops of water on a cryostat holder and place on either dry ice or cryostat freeze bar. Press tissue lightly onto cryostat holder as it begins to freeze and hold until water freezes around the base of the tissue and anchors it in place. Add additional water to further secure the tissue on the holder if necessary.

NOTE: Water is used instead of OCT media for mounting tissue in order to avoid contamination of the tissue with compounds which can affect the detection of the desired signal.

1.4. Position tissue in cryostat. Section tissue up to the desired anatomical location. Ensure that the cutting thickness is between 8 - 12 μm .

NOTE: When sectioning tissue in communal cryostat devices, it is imperative that separate materials such as blades, brushes, anti-roll bars, and holders be used in order to avoid contamination with embedding compounds. The inside of the cryostat should also be cleaned thoroughly with ethanol before use.

1.5. Using the cryostat anti-roll bar, slowly section flattened tissue sections. Holes or markings on the tissue can occur if the roll bar placement is incorrect or blade is dull. Move the tissue to the center of slicing platform using clean paintbrushes.

1.6. Mounting

a. Freeze conductive slides or metal plates by placing them in the cryostat while slicing. When the slide is completely frozen, carefully move the sectioned tissue onto the conductive surface of the slide using clean paintbrushes. Once all tissue sections are positioned correctly on the slide, place a finger under the slide, opposite the tissue, and press until the section thaws.

NOTE: Sections may fold or curl during the thawing process when using this mounting method. This can be reduced by keeping the slide in the cryostat when thawing the tissue. If these issues become problematic, an alternative, warm-mount method is listed below.

b. Alternatively, take a room temperature Indium-tin Oxide (ITO) slide (or metal plate) and lightly press down on frozen tissue section on the slicing platform surface, conductive side down. This will lead to the tissue section thawing evenly onto the surface of the slide with little curling or folding of the tissue.

NOTE: Condensation may appear below the section when mounting using this method which may lead to loss of certain proteins and lipids.

1.7. Place slides with tissue in a desiccator for 5 - 10 min.

2. Sublimator Apparatus Set-up

NOTE: Perform these steps in a fume hood.

2.1. Place a sand bath in an aluminum container onto a hot plate, with the hot plate on a metal scissor lift of appropriate surface area (*i.e.* larger than the hot plate). Turn on the hot plate and set the temperature to 140 °C.

NOTE: The melting point for DAN matrix is between 187 - 190 °C. Do not exceed this temperature on the hotplate.

- a. If the hot plate is equipped with a temperature feedback probe, use it to monitor sand temperature throughout the experiment and ensure temperature consistency. This feature can assist with experiment reproducibility across various sublimation experiments.

NOTE: The sand bath should be contained within an aluminum container as a glass container may shatter at high temperatures.

2.2. Place 300 mg of DAN matrix onto the bottom surface of sublimation apparatus. Place the matrix in the center of the apparatus and spread out in an even layer in the approximate width and length of the slide being sublimated.

CAUTION: DAN matrix is toxic. Therefore, it is important wear gloves, masks, and safety goggles at all times when handling the powdered matrix. DAN should be stored in the dark as it is light sensitive.

2.3. Tape a metal plate onto the inner surface of the apparatus with the plate making direct contact with the bottom of the condenser in order to ensure even distribution of temperature cooling across the entire surface of the slide during sublimation. Alternatively, sand the bottom of the condenser to ensure a flat surface.

a. Place the tape along the outer edges of the plate and adhere to the sides of the inner glassware. If the tape is placed under the plate and adheres to the bottom of the inner glass surface, the temperature distribution may not be even and could result in uneven matrix distribution across the surface of the slide.

b. Tape a blank (test) slide diagonally across the surface of the metal plate with the tape again placed on the outer edges of the slide.

2.4. Connect the top and bottom portions of the apparatus, with a rubber O-ring in the middle to ensure a complete seal.

2.5. Place a metal U-joint around the center of the apparatus and tighten vices until the top and bottom half of the apparatus are sealed tightly together. Place in the metal O-ring above the sand bath.

2.6. Take a handful of crushed ice and place it in the condenser. Fill condenser $\frac{1}{4}$ to $\frac{1}{2}$ full with cold water to create ice slush. The ice slush will cool the metal plate on the inside of the apparatus and subsequently the slide adhered to it. Wait at least 5 min for the temperature to reach a steady state.

2.7. Pour 300 mL of ethanol in the cold trap container and place the glassware into the container. Drop 2 - 3 small pieces of dry ice into the ethanol in the bottom of the cold trap container. The cold trap input has a glass tube running to the bottom of the cylinder, while the output does not.

2.8. Connect the vacuum pump to the cold trap output using rubber tubing. Use another piece of rubber tubing to connect the cold trap input to the sublimation apparatus. Ensure that the tubing is tightly secured using metal clamps if available.

2.9. Use the vacuum pump to deliver a vacuum of 30 - 50 mT. Allow the pump to run for at least 5 min for pressure equilibration. Vices on U-ring of sublimation apparatus may have to be tightened again once the vacuum pump is turned on because of decreased pressure in the apparatus.

NOTE: It is highly recommended that a vacuum gauge be attached to the pump to monitor the pressure of vacuum during the experiment and to test for leaks in pressure in order to achieve the highest possible reproducibility between experiments. However, most pumps are designed to maintain a constant pressure, therefore the gauge may not be essential for experienced users. Additionally, vacuum seal grease can be used to help maintain vacuum pressure.

3. Sublimation

3.1. Ensure that the sand bath temperature has stabilized at 140 °C and that the apparatus is secured in the metal O-ring above the sand bath with all tubing connected and the vacuum turned on.

3.2. Set timer for 7 min but do not start timer. Slowly raise the scissor lift and sand bath up to the sublimation apparatus until the U-joint of the sublimator is well above the metal O-ring. This extra space allows for adjustment of the apparatus on the sand.

a. Quickly press the sublimator gently on the sand surface to ensure that the apparatus is sitting evenly on the sand, and then immediately start the timer.

3.3. When the timer sounds, turn off the vacuum pump and carefully lower the scissor lift until the sublimator is no longer touching the sand bath and is sitting securely in the metal O-ring.

a. Slowly loosen the micro-vent valve to release pressure in the apparatus. Loosen the metal clamp around the rubber tubing of the sublimation apparatus and slowly begin to loosen the tube. Once the rubber tube has been loosened slightly, bend the tube to one side to allow residual pressure to escape.

b. When ambient pressure returns, carefully remove the rubber tubing from the sublimation apparatus.

3.4. Loosen the vices on the U-joint of the apparatus and remove. Carefully separate the two halves of the sublimation apparatus and pull off the slide from the top of the inner glassware. Examine slide to confirm even matrix distribution.

NOTE: If matrix is uneven, the powdered matrix in the bottom of the sublimator can be repositioned or the sublimator apparatus can be repositioned in the sand for the next slide. The sublimation process can be repeated several times using the same matrix, however, the matrix will eventually become darker from repeated heat exposure and the quantity of powder will decrease such that the sublimation time will have to be adjusted slightly to compensate. For this reason, it is important to monitor the amount of matrix being sublimated after each experiment to ensure consistency in matrix deposition between slides

3.5. If the distribution and amount of matrix sublimated is sufficient, tape a new slide with tissue onto the inside of the sublimator and repeat Section 3.

NOTE: For quality control (QC) purposes, the amount of matrix sublimated can be measured after each experiment by weighing the slide before and after sublimation and dividing the weight of sublimated matrix with the surface area of the slide 2, it should be noted that due to the lack of precision of most scales beyond 4 decimal points and variability between scales, these measurements should be only be used a guide for optimal matrix deposition as opposed to a fully quantifiable means of QC unless a high precision balance is used (see **Figure 3**).

4. Tissue Storage/Rehydration

4.1. After sublimation, store slides in a sealed container or small cassette in sealed plastic bag.

4.2. Incubate slides in -20 °C freezer for 2 h or overnight.

NOTE: The goal of the freezing process is to act as a rehydration step for the desorption of tissue materials into the matrix. The freezing process has also been shown to prevent degradation of lipid signals for up to 1 week when stored at -80 °C (Patterson, Thomas & Chaurand, 2014). For this reason, the amount of time the samples are stored in the freezer can be varied to a certain degree to suit the needs of the experimenter without significantly altering signal detection (as observed in our lab). However, we have noticed some discoloration of matrix when samples are frozen for longer than 24 h at -20 °C. Thus, we

recommend imaging the sublimated tissue before that time or storing tissue at -80 °C for longer incubation periods.

4.3. Remove slides from freezer (and container) and place in a desiccator for 5 - 10 min.

5. Imaging and Analysis

5.1. Remove slides from desiccator and apply instrument standards to ensure mass accuracy of MALDI instrument during imaging. The type of standards will vary depending on instrumentation. Standards are generally applied evenly across entire slide, surrounding tissue to be imaged (**Figure 3 D**).

5.2. Insert slide into MALDI instrument and follow manufacturer's instructions for imaging experiments (instrument methods should be optimized for a 1,000 - 2,000 mass range). Representative result (**Figure 4**) was acquired in reflectron negative mode with a 70 μm raster and 20 shots/spectrum (acquisition time \sim 2 h).

Representative Results

Upon completion of the sublimation experiment, the two halves of the glass apparatus are separated in the fume hood and the slide, taped to the condenser, can be removed (**Figure 3 A**). At this point, the slide should be examined for uneven matrix distribution and the time, temperature, or placement of the apparatus in the sand bath may have to be adjusted for the next slide. A successful DAN sublimation experiment will result in an even coating of grey/brown matrix along the surface of the slide where the anatomical features of the tissue can be clearly visualized and the amount of matrix on the glass slide is similar to the amount on the tissue (**Figure 3 B**). For example, if too much matrix has been sublimated on the tissue, the thickness of the matrix will cover the features of the tissue and only the general shape will be discernable. However, if too little matrix is sublimated, the tissue will have a darker appearance than the rest of the slide (**Figure 3 C**). Both too much and too little matrix will result in poor signal in the MALDI instrument. For quality control purposes, Thomas *et al.* weighed the amount of matrix deposited on the slide and divided the weight by the surface area of the slide. They reported an optimal amount of matrix deposition for several matrices including DAN ($110 \mu\text{g}/\text{cm}^2$)². Although most balances

lack the precision needed to replicate such results, we have attempted this method of QC; however, due to a high degree of variability, we can only advise a suitable range of matrix deposition found to be associated successful versus unsuccessful sublimation experiments with DAN matrix as determined through signal detection in the instrument. A matrix measurement of below 100 $\mu\text{g}/\text{cm}^2$ was associated with "too little" matrix conditions while a measurement of above 140 $\mu\text{g}/\text{cm}^2$ was associated with "too much". Matrix deposition between 100 and 140 $\mu\text{g}/\text{cm}^2$ was found to be an optimal quantity for imaging with DAN matrix. Calibrating standards should be applied on the glass slide around the tissue samples to ensure the mass accuracy of the detected IMS signals (**Figure 3 D**)

In a MALDI IMS experiment, the molecular image allows for the visualization of the spatial distribution of the analyte of interest along with any unknown species that may be present in a given mass range. The molecular images of gangliosides in this experiment were overlaid using ImageJ software to show the anatomical distribution of several ganglioside species across the cortical and subcortical regions of the rat brain (**Figure 4 A**). The most abundant gangliosides in the brain are the A-series species GD1a and GM1 but also contain gangliosides GM2 and GM3 which can all be found between the 1,000-2,000 m/z mass range, a higher mass range than most common brain lipids, making these gangliosides easy to identify along the spectrum (**Figure 4 B**). The ionic abundance of each ganglioside species can be used to semi-quantify differences or changes in ganglioside species within the same image. Because a certain amount of variability in sample prep cannot be avoided in IMS, between scan comparisons are considered to be semi-quantitative.

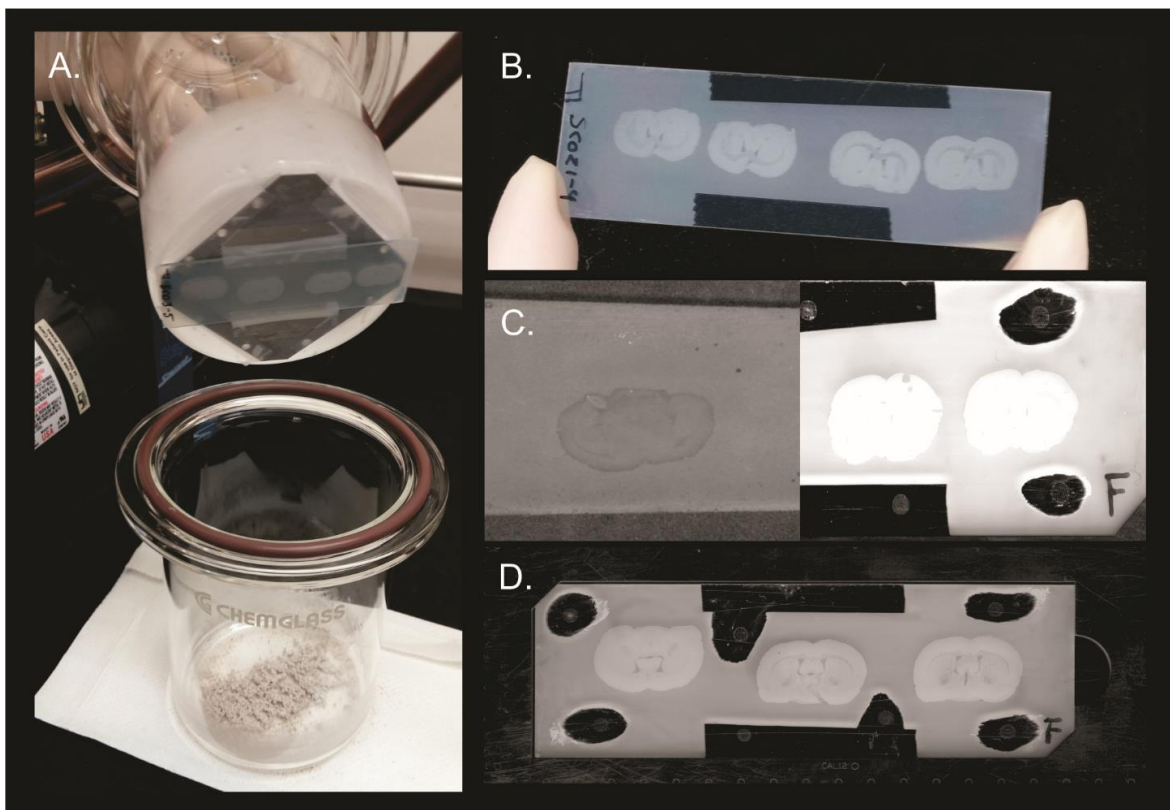


Figure 3: DAN Sublimation.

Representative results of sublimation of DAN matrix on rat brain tissue. **(A)** Upon completion of sublimation, the two halves of the apparatus are separated and the slide is removed from the condenser. **(B)** DAN matrix spreads evenly across multiple rat brain tissue sections on the surface of the slide to allow for highly reproducible results (between 100 - 150 $\mu\text{g}/\text{cm}^2$). **(C)** Examples of failed sublimation experiments where too little matrix (left - $<90 \mu\text{g}/\text{cm}^2$) or too much matrix (right - $>150 \mu\text{g}/\text{cm}^2$) was deposited. Too little matrix will result in insufficient desorption of analytes, while too much matrix will not allow the laser to penetrate to the tissue during acquisition, resulting in low ion detection. **(D)** Slide containing rat brain tissue sections sublimated with DAN matrix and calibration standards applied is ready for insertion into MALDI instrument for imaging.

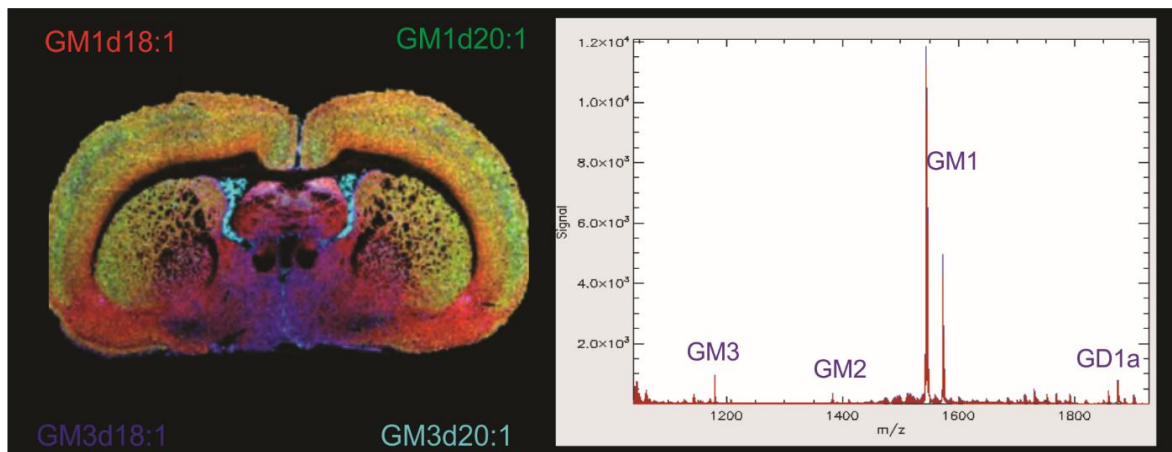


Figure 4: MALDI IMS of Gangliosides in the Rat Brain.

Representative MALDI IMS molecular image and mass spectrum of gangliosides in the rat brain after sublimation with DAN matrix. The molecular image is a composite of multiple ganglioside species in the spectrum overlaid and pseudocolored using Image J software to show the unique anatomical distribution of ganglioside species throughout the brain. Species GM1d18:1 (red, mass ~1,547 Da), GM1d20:1 (green, mass ~1,573 Da), GM3d18:1 (blue, mass ~1,178 Da), and GM3d20:1 (teal, mass ~1,207 Da) are represented. The mass spectrum displays ionic abundance of analytes within a 1,000 - 2,000 mass range. The major A-series gangliosides are labelled along the spectrum.

Discussion

This work details a standardized protocol of matrix sublimation on tissue for the detection of negatively charged lipids, such as gangliosides, in MALDI IMS experiments. Sample preparation for MALDI IMS is highly variable and must be customized to suit the unique properties of the analyte of interest. The application of matrix onto the tissue sample surface is a crucial aspect of the sample preparation process with regards to the quality of results in IMS. Particular care should be taken when selecting matrices, ensuring that the matrix is compatible with the analyte of interest and is free of matrix-derived artifacts in the spectrum. Sublimation is a dry matrix deposition technique which provides a high degree of matrix crystal homogeneity with little delocalization of lipids on tissue. DAN matrix in particular shows a high degree of sensitivity for the desorption of a group of negatively charged membrane lipids called gangliosides, as demonstrated in rat brain sections, and is stable under vacuum for extended periods of time, allowing for compatibility with the majority of imaging applications. DAN matrix has the additional benefit of also having a high affinity for positively charged lipid species, thus increasing the versatility of this matrix for MALDI IMS applications (Thomas, Charbonneau, Fournaise & Chaurand, 2012). It should also be noted that multiple lipid species, including phospholipids, can be detected simultaneously when using this IMS protocol.

A thorough examination of the properties of DAN matrix as compared to 9 other commonly used matrices has been previously published (Thomas, Charbonneau, Fournaise & Chaurand, 2012). In this article, the authors highlight the increased sensitivity of DAN matrix in negative ion mode as compared to the other matrices examined as well as the capability for high resolution imaging using DAN. DAN matrix was found to have the highest overall performance for negative polarity ions. Interestingly, it performed equally well for positive polarity ions. Other common matrices which have demonstrated high affinity for negative polarity ions include DHA, DHB, and 9-AA. The efficiency of DHA as a matrix is limited by its low stability under vacuum which makes it impractical for most imaging applications (Thomas, Charbonneau, Fournaise & Chaurand, 2012). 9-AA has the benefit of producing low background noise and demonstrated enrichment of sulfatide signals in the 750 - 950 mass range in negative mode compared to DHB matrix (Cheng et

al., 2010). Although DHB has been shown to be very effective in positive mode, it yields lower negative polarity ion signal as compared to DAN matrix (Thomas, Charbonneau, Fournaise & Chaurand, 2012). DAN matrix also demonstrated increased sensitivity in negative ion mode in the lower mass range (650 - 950) compared to DHB (Thomas, Charbonneau, Fournaise & Chaurand, 2012). Additionally, it has been reported that DHB can form significant matrix clusters in negative ion mode up to 750 Da 2.

Another method of dry matrix deposition has been described by Puolitaival *et al.*, in which ground matrix is passed through a fine sieve and deposited onto the sample surface. The authors compared this dry method of matrix deposition to a wet matrix manual spray technique and found that they gave comparable signal for phospholipids in the 450 - 1,200 mass range (Puolitaival, Burnam, Cornett & Caprioli, 2008). One study used both sublimation and dry-coating with a sieve to examine phospholipid expression, however, the authors did not comment on how the two techniques compared in terms of image resolution or ion signal yield (Chaurand, Cornett, Angel & Caprioli, 2011).

In order to ensure the widest possible range of applicability, the protocol presented was a basic workflow that will allow both new and more specialized users of MALDI IMS to achieve highly reproducible results for a wide variety of lipid imaging applications. However, sublimation protocols can be modified to meet the unique circumstances of the experiment. For example, the fine matrix crystal deposition provided by sublimation allows for the option to reverse the order of sample preparation by pre-coating slides/plates with matrix prior to mounting the tissue. The matrix can be sublimated onto the conductive surface in advance and stored in a dark environment for later use thus reducing sample preparation time post-sectioning while still maintaining high sensitivity for lipid detection (Grove, Frappier & Caprioli, 2011; Yang & Caprioli, 2011). Another modification that can be made to this protocol to enhance signal for the detection of lipids is a 2 min wash with ammonium formate (Angel, Spraggins, Baldwin & Caprioli, 2012).

Although sublimation can circumvent many of the drawbacks of most wet deposition techniques, such as smaller, more homogenous matrix crystal deposition (Hankin, Barkley & Murphy, 2007), decreased delocalization of analytes, and low cost as

compared to automated sprayers, some variability in the sample preparation process is unavoidable. In the case of sublimation, there are several factors which may cause minute differences from one experiment to another and can include the following which have been observed in our lab. There can be differences in the position of the sublimation apparatus on the sand. When running several sublimation experiments back-to-back, the sand in the sand bath may begin to shift its position which can affect the dispersion of heat throughout the sand bath. Flattening the sand before each round of sublimation can also change the dispersion of heat as sand that has been displaced may take time to return to a uniform temperature. Sublimation time may have to be adjusted slightly between each round to compensate for shifting sand in the sand bath. Alternatively, use of an oil bath may lead to more homogenous heat dispersion.

Secondly, the amount of matrix at the bottom of the sublimator can vary. DAN matrix has a clumpy grey appearance and has a tendency to form large clusters. These clusters can be manually broken up and arranged in the bottom of the sublimator but cannot be completely eliminated. Large clusters of matrix will take longer to heat and sublime than smaller pieces which can affect the end product of the sublimation.

The vacuum output on the sublimation apparatus is another critical factor. Most sublimators are made with a single vacuum output onto which tubing is attached to connect it to the vacuum pump during sublimation. Because the pressure is being regulated on that side of the apparatus, there may be a slight unevenness of the matrix deposition, with more being deposited on the side with the vacuum output. This can be somewhat compensated for by shifting either the position of the apparatus in the sand, the position of the matrix in the bottom of the sublimator, or by changing the position of the slide/plate on the condenser. These factors are the main drawbacks of the sublimation technique and for this reason it is crucial to run a test slide through the sublimation process before running experimental sample so that time can be adjusted to compensate for these variables.

Another reported drawback of sublimation is that the detection of higher mass analytes is limited by insufficient analyte extraction and/or mixing with matrix. A rehydration step after sublimation can help pull out these higher mass analytes to

circumvent this issue. This is typically achieved using a humidity chamber (Gemperline, Rawson & Li, 2014). However, in this protocol, a freezing step is added after sublimation which achieves the same purpose. The freezing and subsequent thawing (in a desiccator) of the samples before insertion in the MALDI instrument causes condensation to form on the surface of the sample which temporarily rehydrates the sample to allow for the extraction of higher mass lipids while preserving the tissue for analysis (Patterson, Thomas & Chaurand, 2014; Yang & Caprioli, 2013).

Overall, sublimation is a highly sensitive and cost effective method of matrix application for the detection of lipids in MALDI IMS experiments. Indeed, our group has noticed significant improvements to IMS results when we shifted from using an air-spray method 3 to a sublimation method 4 for matrix deposition. The present protocol is appropriate for a number of lipid imaging applications but can be modified to suit the needs of the experimenter.

References

Angel, P. M., Spraggins, J. M., Baldwin, H. S., & Caprioli, R. Enhanced sensitivity for high spatial resolution lipid analysis by negative ion mode matrix assisted laser desorption ionization imaging mass spectrometry. *Anal. Chem.* **84**, 1557-1564 (2012).

Barceló-Coblijn, G., & Fernández, J. A. Mass spectrometry coupled to imaging techniques: the better the view the greater the challenge. *Front Physiol.* **6** (3), 1-5 (2015).

Caughlin, S. *et al.* Increased Expression of Simple Ganglioside Species GM2 and GM3 Detected by MALDI Imaging Mass Spectrometry in a Combined Rat Model of A β Toxicity and Stroke. *PLoS ONE.* **10**, e0130364 (2015).

Chaurand, P., Cornett, D., Angel, P., & Caprioli, R. From Whole-body Sections Down to Cellular Level, Multiscale Imaging of Phospholipids by MALDI Mass Spectrometry. *Mol Cell Proteomics.* **10**, O110.004259 (2011).

Cheng, H., Sun, G., Yang, K., Gross, R. W., & Han, X. Selective desorption/ionization of sulfatides by MALDI-MS facilitated using 9-aminoacridine as matrix. *J. Lipid Res.* **51**, 1599-609 (2010).

Fuchs, B., Süß, R., & Schiller, J. An update of MALDI-TOF mass spectrometry in lipid research. *Progress in Lipid Research.* **49**, 450-475 (2010).

Gemperline, E., Rawson, S., & Li, L. Optimization and comparison of multiple MALDI matrix application methods for small molecule mass spectrometric imaging. *Anal. Chem.* **86**, 10030-10035 (2014).

Grove, K.J., Frappier, S.L., & Caprioli, R.M. Matrix pre-coated MALDI MS targets for small molecule imaging in tissues. *J. Am. Soc. Mass Spectrom.* **22**, 192-195 (2011).

Hankin, J. A., Barkley, R. M., & Murphy, R. C. Sublimation as a method of matrix application for mass spectrometric imaging. *J. Am. Soc. Mass Spectrom.* **18**, 1646-1652 (2007).

Jaskolla, T.W., Karas, M., Roth, U., & Steinert, K. Comparison between vacuum sublimed matrices and conventional dried droplet preparation in MALDI-TOF mass spectrometry. *J. Am. Soc. Mass Spectrom.* **20**, 1104-1115 (2009).

Murphy, R. C., Hankin, J. A., Barkley, R. M., & Zemski Berry, K. A. MALDI imaging of lipids after matrix sublimation/deposition. *Biochim. Biophys. Acta.* **1811**, 970-5 (2011).

Patterson, N. H., Thomas, A., & Chaurand, P. Monitoring time-dependent degradation of phospholipids in sectioned tissues by MALDI imaging mass spectrometry. *J Mass Spectrom.* **49**, 622-7 (2014).

Puolitaival, S. M., Burnum, K. E., Cornett, D. S., & Caprioli, R. M. Solvent-free matrix dry-coating for MALDI imaging of phospholipids. *J. Am. Soc. Mass Spectrom.* **19**, 882-6 (2008).

Rourke, M. B., Raymond, B. B., Djordjevic, S. P., & Padula, M. P. A versatile cost-effective method for the analysis of fresh frozen tissue sections via matrix-assisted laser desorption/ionisation imaging mass spectrometry. *Rapid Commun. Mass Spectrom.* **29**, 637-44 (2015).

Thomas, A., Charbonneau, J. L., Fournaise, E., & Chaurand, P. Sublimation of new matrix candidates for high spatial resolution imaging mass spectrometry of lipids: enhanced information in both positive and negative polarities after 1,5-diaminonaphthalene deposition. *Anal. Chem.* **84**, 2048-2054 (2012).

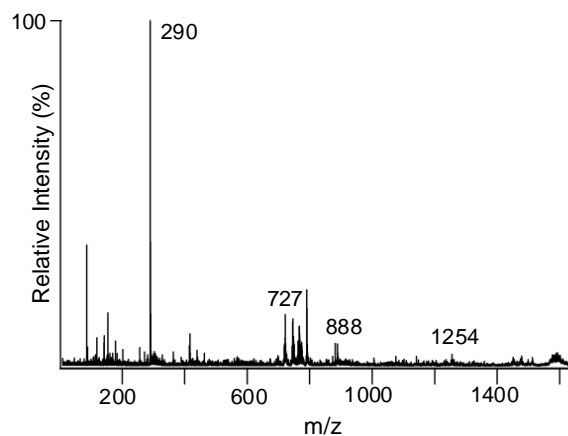
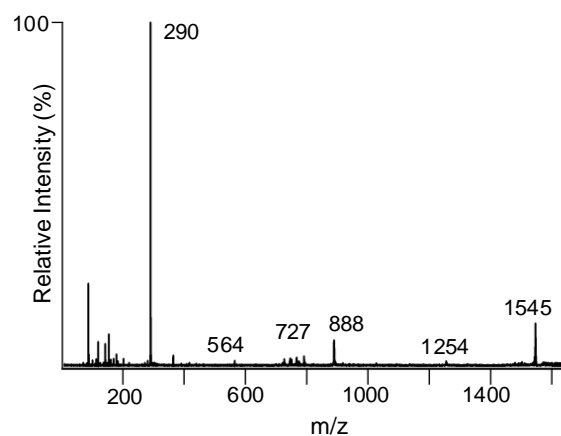
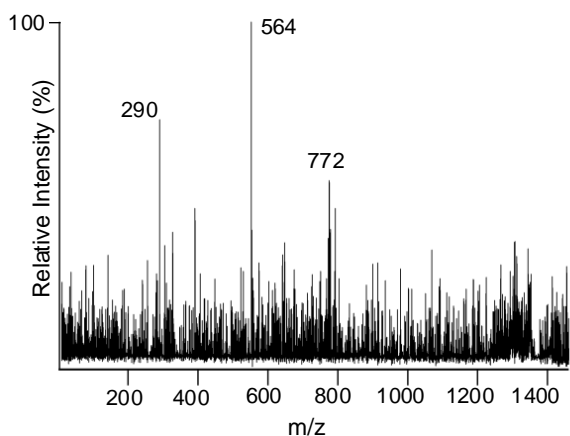
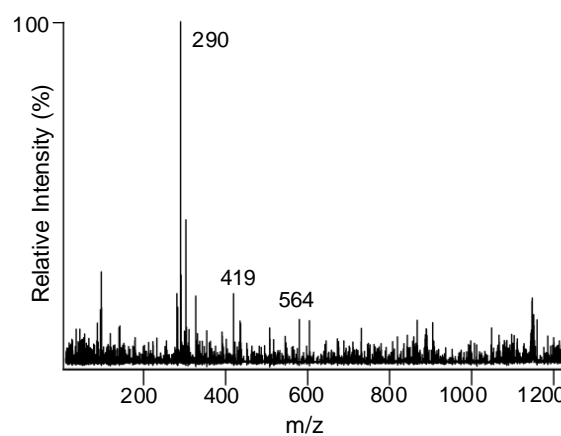
Weishaupt, N., Caughlin, S., Yeung, K., & Whitehead, S. Differential Anatomical Expression of Ganglioside GM1 Species Containing d18:1 or d20:1 Sphingosine Detected by MALDI Imaging Mass Spectrometry in Mature Rat Brain. *Front Neuroanatomy.* **9** (155) (2015).

Whitehead, S. *et al.* Imaging Mass Spectrometry Detection of Gangliosides Species in the Mouse Brain following Transient Focal Cerebral Ischemia and Long-Term Recovery. *PLoS ONE.* **6** (6), e20808 (2011).

Yang, J., & Caprioli, R.M. Matrix precoated targets for direct lipid analysis and imaging of tissue. *Anal. Chem.* **85**, 2907-2912 (2013).

Appendix iv: MS/MS identification of gangliosides

Tandem mass spectrometry (MS/MS) is often performed in MALDI-based experiments in order to identify molecules of interest within a mass spectrum based on their fragmentation patterns. Although there are a number of challenges associated with on-tissue MS/MS fragmentation of ions in negative mode, mostly related to diminished signal as compared to positive mode, MS/MS was performed, where possible, in order to confirm the identity of some of the major A-series gangliosides examined in this work.

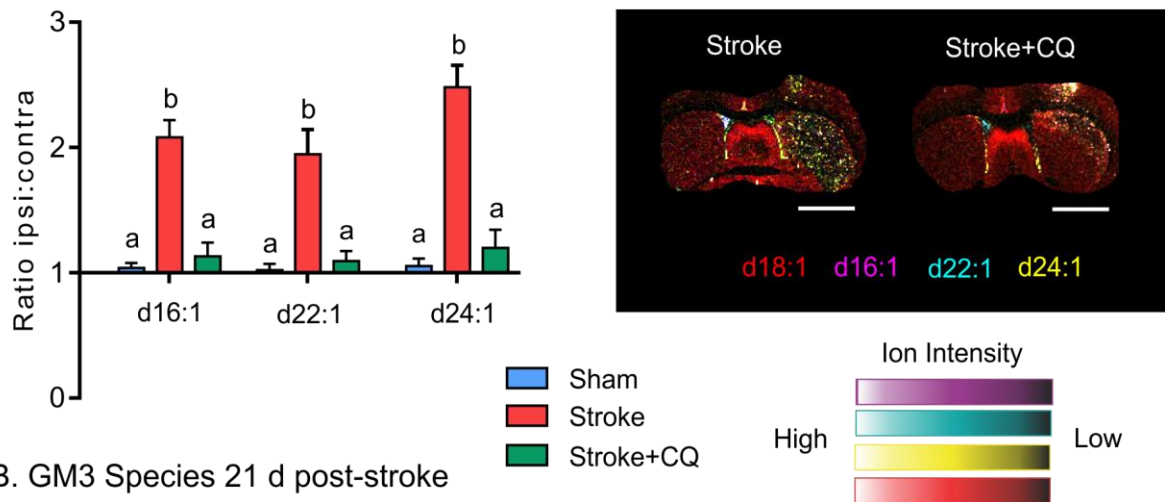
A. GM1 d18:1**B. GM1 d20:1****C. GM2 d18:1****D. GM3 d18:1**

Appendix iii. On-tissue negative mode MS/MS identification of the major ganglioside species. A. GM1 d18:1 (m/z 1547); B. GM1 d20:1 (m/z 1572); C. GM2 d18:1 (m/z 1384); D. GM3 d18:1 (m/z 1181). MS/MS spectra produced the diagnostic fragmentation ions which corresponded to the data reported by Dufresne et al., 2016 (PMID: 27873002). Generally, fragmentation confirmed that sialic acid produced an intense peak at m/z 290 with additional characteristic fragmentation of various sugar units (m/z 564, 727, and/or 888). Characterization of gangliosides was performed on-tissue using a SCIEX 5800 MALDI TOF-TOF mass spectrometer. DAN matrix was applied onto tissue sections by sublimation and negative ion MS/MS spectra were acquired. The detector multiplier voltage was maximized at 2.25 kV and a total of 900 shots per spectrum was acquired in a continuous stage motion. Following the external calibration at ± 50 ppm mass tolerance, the precursor ion was isolated within an m/z window of 40 FWHM (full width at half maximum) resolution and fragmented in a posts-source decay mechanism. MS/MS mode experiments were conducted using 10 to 20% higher laser energy compared to the MS mode, in order to promote fragmentation of the analytes of interest for structural identification.

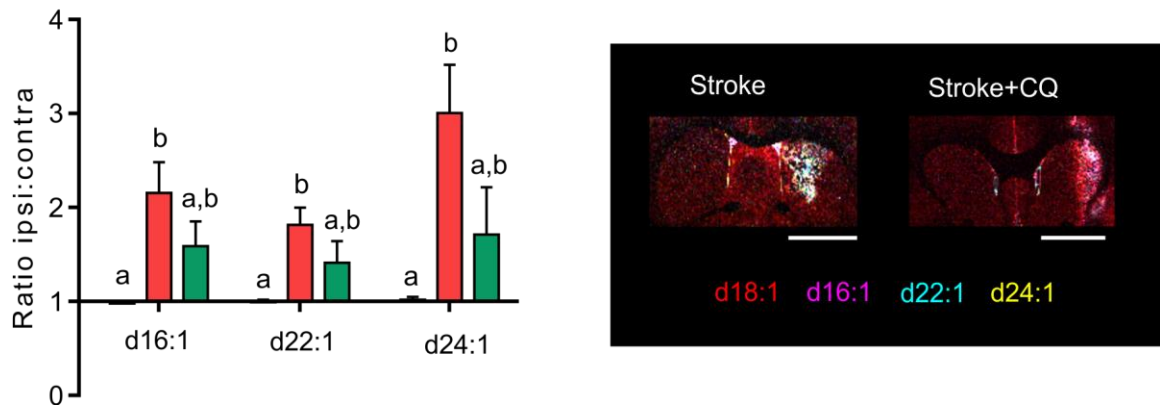
Appendix v: GM3 species with varied carbon length increase in response to stroke injury and are decreased with CQ treatment.

Several peaks corresponding to GM3 species with varied carbons in their ceramide moieties were detected along with the d18:1 and d20:1 species reported in Figures 5.2 and 5.3 of chapter 5. The masses of these GM3 species match what is reported in the Lipidmaps database for the d16:1 (m/z 1151), d22:1 (m/z 1234), and d24:1 (m/z 1262) species of GM3.

A. GM3 Species 3 d post-stroke



B. GM3 Species 21 d post-stroke



Appendix v: GM3 species with varied LCB increase in response to stroke injury and are decreased with CQ treatment. Quantification of MALDI IMS data along with representative MALDI images showing the abundance of GM3 species with 16, 22, and 24 carbons in control (left), stroke injured, and stroke injured CQ treatment groups 3 and 21 d post-stroke. (A) GM3 species were increased within the stroke region compared to control levels in stroke injured rats 3 d post-stroke. This significant increase was prevented with CQ treatment in stroke injured rats. (B) GM3 species remained significantly elevated compared to controls within the stroke region 21 d post-stroke, however, CQ treatment was associated with a reduction in this increase compared to stroke injury alone. Group with different letter represent a statistical difference with $p < 0.05$ via Two-way ANOVA, Tukey post-hoc.

Curriculum Vitae

Name: Sarah Caughlin

Post-secondary Education and Degrees:

The University of Western Ontario
London, Ontario, Canada
2008-2011 B.A. Psychology

The University of Western Ontario
London, Ontario, Canada
2008-2012 B.HSc. Health Sciences

The University of Western Ontario
London, Ontario, Canada
2012-2017 Ph.D. Anatomy and Cell Biology

Honours and Awards:

CIHR Strategic Training Program in Vascular Imaging
2013-2015

Ontario Graduate Scholarship
2015-2016; 2016-2017

Natural Sciences and Engineering Research Council (NSERC)
Doctoral Scholarship (PGS-D)
2016-2018

Related Work Experience

Teaching Assistant – Advanced Topics in Neuroscience
The University of Western Ontario
2013

Teaching Assistant - Histology
The University of Western Ontario
2013-2015

Teaching Assistant – Neuroanatomy, Physiotherapy Program
The University of Western Ontario
2013-2016

Teaching Assistant – Phys/Pharm Digestion and Lipid Metabolism
The University of Western Ontario
2016-2017

Publications:

Caughlin, S., Hepburn, J., Park, D.H., Jurcic, K., Yeung, K.C., Cechetto, D.F. & Whitehead, S.N. (2015). Increased expression of simple ganglioside species GM2 and GM3 detected by MALDI Mass Spectrometry Imaging in a combined rat model of A β toxicity and stroke. *PloS One*. 10(6): e0130364.

Weishaupt, N., **Caughlin, S.,** Yeung, K. K-C. & Whitehead, S.N. (2015). Differential anatomical expression of ganglioside GM1 species containing c-18 or c-20 sphingosine detected by MALDI Imaging Mass Spectrometry in mature rat brain. *Front. Neuroanat*. 9:155. doi: 10.3389/fnana.2015.00155.

Caughlin, S., Park, D.H., Yeung, K.K., Cechetto, D.F., Whitehead, S.N (2017). Sublimation of DAN Matrix for the Detection and Visualization of Gangliosides in Rat Brain Tissue for MALDI Imaging Mass Spectrometry. *J. Vis. Exp.* (121), e55254, doi:10.3791/55254.

Caughlin, S., Maheshwari, S., Weishaupt, N., Yeung, K-C., Cechetto, D.F. & Whitehead, S.N. (2017). Age-dependent and regional alterations in the long-chain base of simple and complex brain gangliosides observed using MALDI Imaging Mass Spectrometry. *Scientific Reports*. 7(1): 16135.

Caughlin, S., Maheshwari, S., Yeung, K-C., Cechetto, DF. & Whitehead, SN. Age and transgene differences in A-series ganglioside abundance of Fisher APP21 rats observed using MALDI Imaging Mass Spectrometry. *BBA General Subjects*. 1862(6): 1327-1338

Caughlin, S., Hepburn, J., Yeung, K-C., Cechetto, D.F. & Whitehead, S.N. Pathological and functional improvements associated with the restoration of ganglioside homeostasis after a severe neurodegenerative stroke injury using Chloroquine. *Neuroimage* (under review).